Swansea University
Prifysgol Abertawe

Alternative Formulations to Potentially Replace the Use of Hexahydrophthalic Anhydride in Coil Coatings

Christopher Paul Batchelor

Thesis submitted to Swansea University in fulfilment of the requirements for the Degree of Doctorate in Engineering

2021

If you have a bar on access, include the declarations below

Declarations

This work has not previously been accepted in substance for any degree and is not being concurrently submitted in candidature for any degree.

Signed..[redacted].....

Date.....20/03/2023.....

This thesis is the result of my own investigations, except where otherwise stated. Other sources are acknowledged by footnotes giving explicit references. A bibliography is appended.

Signed....[redacted].....

Date.....20/03/2023.....

I hereby give my consent for my work, if relevant and accepted, to be available for photocopying and for inter-library loans **after expiry of a bar on access approved by the University.**

Signed.....[redacted].....

Date.....20/03/2023.....

The University's ethical procedures have been followed and, where appropriate, that ethical approval has been granted.

Signed...[redacted].....

Date.....20/03/2023.....

Acknowledgements

First, I would like to thank my academic supervisors Prof David Worsley and Dr Ian Mabbett, both of whom provided invaluable advice on all aspects of the project and tips on maintaining a good work-life balance throughout my studies.

I would like to thank my Industrial supervisors Dr Chris Lowe, Mr. James Smith, and Catherine Vincent. Jim has provided me with many hours of support and training throughout my project, while Chris was always available for support and advice. Thank you both for the continued encouragement throughout my time working on this project. A special thanks to everyone in the Long-Term Development labs who helped me with my project and made me feel welcome.

I'd also like to thank Dr Francisco Martin-Martinez, his help and advice with computational chemical modelling have been invaluable to my project.

I would like to thank the Materials and Manufacturing Academy (COATED M2A) in Swansea University, Becker Group, Engineering and Physical Sciences Research Council (EPSRC via UKRI) (EP/L015099/1), and the European Social Fund via the Welsh Government (WEFO) for supporting the work described in this thesis.

Thanks to the team at the PMRC (Pilot Manufacturing Research Centre), without whom I would not have been able to set up the coatings lab or to keep the weathering cabinets operating. Thanks to all the staff and students that have shared an office with me over the years, everyone has been happy to lend a hand or give advice on how to approach problems for which I am very grateful, it has been a pleasure to share an office with such knowledgeable and welcoming people. Special thanks to Dr Chris Griffiths for proofreading some of my work and helping make the coatings lab a reality!

A huge thanks to my family, without your support and encouragement I would not have reached this point. Finally, I would like to thank my wife Andrea, her support, advice, and understanding have been invaluable throughout this endeavour.

I want to dedicate this thesis to my grandparents, John Boggins, Peter Batchelor, Margaret Batchelor, and Euphemia Boggins.

Cheers all.

Abstract

A study was performed to investigate degradation of clear coats exposed to aggressive environments via accelerated and natural weathering and periodically analysed for changes in gloss and colour alongside InfraRed analysis, performed with the drive to potentially replace HHPA (Hexahydrophthalic Anhydride) in future coating systems. It was found that HHPA containing systems provided superior weathering resistance compared to other coating systems, with CHDA (Cyclohexanedicaboxylic acid)-CHDM (Cyclohexanedimethanol) coatings being the second best performing and CHDA the worst. It can be concluded that it is more likely that a co-monomer-based system would have the greater potential to produce comparable weathering resistance to HHPA than a single monomer-based coating.

HHPA and CHDA containing pigmented systems were developed for weathering analysis, with the investigation showing that pigment addition did not influence coating performance, with CHDA still the poorer performing with regards to weathering.

Free-standing films were developed to investigate UV absorbance of HHPA and CHDA coatings, showing that the absorbance profiles within the UV region are very similar, with the crosslinker appearing to exert a greater influence over CHDA coatings.

An investigation was performed into the ability of HHPA and CHDA coatings to resist degradation in dark hydrolysis through immersion in water baths with IR, colour, and gloss analyses after 1,3, and 7 days. It was found that, in general, the CHDA containing coatings demonstrated worse performance than the HHPA variants, indicating a greater susceptibility to moisture related degradation.

Computational Chemical Modelling was performed to gain a greater degree of insight to the reasons behind the differences in weathering resistance offered by the different coating systems. Modelling aimed to calculate the reactivity of different structures within the coating systems when combined with HHPA or CHDA, in addition to identifying areas within the structures that were susceptible to electrophilic or nucleophilic attack. It was found that the CHDA containing models exhibited significantly more sites vulnerable to attack, particularly nucleophilic attack which suggests a greater weakness to moisture and moisture enhanced photodegradation.

From the research carried out, it has been shown that HHPA offers superior weathering resistance in coating systems compared to other similar cycloaliphatic monomers. This means that, at present, it has not been possible to identify a suitable replacement for HHPA within coatings and as such it would be unreasonable for HHPA to be classed as a Substance of Very High Concern (SVHC) by REACH, as it would result in instances of coatings with lower work life expectancy.

Contents

Table of Figures, Tables, and Equations

Chapter 1-Introduction, polymer breakdown and the prevention of polymer degradation

1.0 -Introduction

The body of work contained within this thesis focused on the development of novel resins and coating systems to investigate and compare the weathering performance of the novel resins against HHPA. These investigations led to studies into UV absorption values and how different coatings resisted hydrolytic interactions. Additionally, time was spent utilising computational chemical modelling to improve understanding into how HHPA coatings offer superior weathering compared to other cycloaliphatic based systems.

Polymeric coatings are used to protect the substrate and provide a more aesthetically agreeable product, in addition to other uses. Polymers are used in the development of resins, which are used as binders within coatings, with pigments and other components being dispersed within them. The mechanical and chemical properties of resins are known to dictate the properties of the final coating, which explains the large amount of research that has been performed in resin analysis.(1)

While there are many factors that need to be considered with regards to architectural steels, degradation resistance is arguably one of the more important. Degradation has many forms and will affect every structure, natural or man-made, in one form or another over a long enough period of time. It can be seen in the weathering of rocks, erosion of soil, the rusting of vehicles and the discolouration of coatings to name a few common examples. One of the issues with the slowing and prevention of Ultra-Violet (UV) induced degradation is that there is no "one size fits all" solution, with chemicals that are suitable in one area potentially resulting in increased damage in others.

Resisting UV degradation is an extremely important characteristic for an exterior coating, as degradation can compromise the structural integrity of the substrate, reducing its functional life. This is in addition to the discolouration that can occur, impacting on the aesthetics of the object. Degradation can also lead to corrosion mechanisms initiating due to decreased levels of protection of the underlying substrate from the coating, leading to additional damage to the object over time and further reducing the effective lifetime of the substrate.

With increased drives towards environmentally friendly products and legislation that bans or limits the use of many compounds that are major components of coatings and are capable of resisting UV degradation, it is crucial to develop alternative formulations that have comparable UV durability

capabilities but that lack the negative aspects that have been identified with some products currently in use. It may also be beneficial that they are compatible with Water-based and high-solid coatings which are being developed as alternatives to coatings containing high levels of Volatile Organic Compounds (VOCs).

As with many scientific fields, man-made UV shielding coatings seek to mimic behaviours observed in nature. Plants have developed sophisticated methods of minimising the damage caused by UV exposure which far surpass the techniques that are currently available for man-made materials. Plants have adapted to harvest sunlight to facilitate growth but have also been able to radically limit the damage that UV exposure is capable of. Plants are capable of utilising UV-absorbing species, free-radical scavengers and enzymes to absorb UV radiation, remove unwanted oxygen free radicals and decrease the number of oxidative reactions respectively. (2)

1.1-What is UV induced degradation and why is it harmful?

UV induced degradation is initiated due to the absorption of UV light.(3) Absorbance of UV radiation leads to the production of free radicals, which are generated within the coating that react with oxygen to form peroxides.

The breakdown of coatings is due to specific amounts (Quanta) of energy from UV radiation being absorbed by Oxygen molecules at the coating surface. The absorbed energy forces the Oxygen to move from their ‘‘normal’’ state to an ‘‘excited’’ state. The Oxygen atoms try to leave this state by reacting with functional groups or unsaturated (double) bonds within the polymer structure. This is known as photo-oxidation and causes the lowering of the molecular weight of the polymer (altering its properties in the process), and is also responsible for the generation of free radicals, which is known as secondary initiation. (4)

Free-radicals are damaging to coatings because they can fuel further oxidation reactions that produce additional free radicals, the free radicals also reform following their reaction, allowing them to react multiple times. This means that they are self-propagating and will be able to rapidly cause significant damage to the main polymer structure through chain scission, which results in a decrease of the molecular weight of the polymer. Chain scission is the breaking of the chain that makes up the backbone of the polymer, resulting in smaller chains. This structural damage can impact many characteristics of the polymer, from its gloss levels to mechanical and chemical properties. (4,5)

The propagation process of free radicals is shown in Reactions 1 and 2.

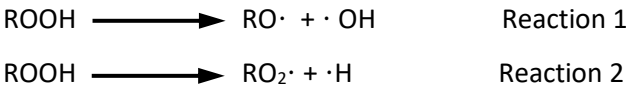

While two free radicals are formed in reactions 1 and 2, only $RO_2\cdot$ has the reactivity levels that are needed to break the C-H bonds that exist in the primary polymer chain.

In reaction 3 the free radical has reacted with the hydrocarbon backbone, forming a Carbon free radical in the process.

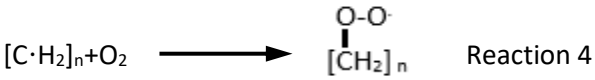

Reaction 4 shows that as the Carbon free radical reacts with the Oxygen molecule in an attempt to balance itself, it forms an Oxygen free radical, which allows for further breakdown of the polymer chain.(6,7)
UV lamps cannot supply enough energy to directly break Carbon to Carbon (C-C) or Carbon to Hydrogen (C-H) bonds, so the polymer backbone will remain unaffected for as long as free radical production can be prevented. Improving the coating resistance to UV induced degradation will result in an increased coating lifespan, and ultimately lower cost to the consumer.

1.2-Coil Coatings

The coil coating process is an industrial coating and curing process used to produce pre-painted metal for a wide range of end purposes, such as construction and appliances. Coil coating can take the form of forward or reverse roller coating, both of which have advantages and disadvantages over the other. These coating methods get their names from the direction in which the applicator roller(s) move relative to the direction that the substrate travels in. Forward roller coating is used in the application of low to medium thickness coating systems. The coating is transferred to the application roller from a storage reservoir, from which it is applied to the substrate. A doctoring roller is used to control the coating thickness, although the speed of the substrate and rollers also exert an influence over the final film thickness. Forward roller coating is the preferred method of application for primers. (8,9)

Reverse roller coating uses the same process as forward roller coating with the exception being the direction that the application roller moves in relative to the substrate, this results in a high shear force being applied to the coating and causes a better flow of the coating. Reverse roller coating is extensively used in the application of topcoats and some primer systems. (8,9)

1.3-Background

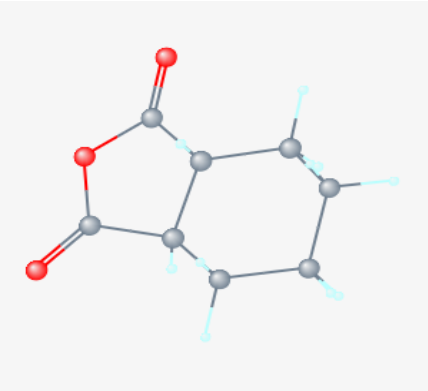

Figure 1.1-Structure of HHPA

Hexahydrophthalic Anhydride (HHPA) is an alicyclic anhydride that offers high levels of UV shielding with no impact to the desired colour of the overall coating, it is also transparent to UV light below 290 nm and as such is unlikely to partake in degradation initiation. The degree of shielding that is offered by HHPA is far more than that of other alicyclic anhydrides.

The diagram on the left represents the chemical structure of HHPA. The Oxygens are highlighted in red, the Hydrogens in cyan, and the Carbons are denoted in grey. (10)

Awasthi and Agarwal showed that cycloaliphatic compounds can have a significant effect on the properties of polymeric coatings, particularly polyurethane coatings. Polyurethane has been successful because of its ability to have high hardness in low stress conditions and higher flexibility and tensile strength when subjected to high stress conditions, whereas polyureas are known to be more rigid. Praw states that "*The combination of hardness and flexibility gives the polyurethanes the toughness that provides significant advantages over other thermoset chemistries such as polyureas and epoxies.*" (11) It was found that cycloaliphatic compounds impart physical properties on a level between aromatic and linear polyesters. Their investigation showed that cycloaliphatics offered better solubility during resin synthesis than both linear and aromatic aliphatics in addition to providing an intermediate level of chemical resistance and mechanical hardness. These results indicate that cycloaliphatics offer a good level of protection in a variety of environments and are able to be brought into solution faster, reducing production time for industrial processes. (11,12)

HHPA is commonly used as a hardener for epoxy resins and as an intermediate in polymer resins to improve flexibility, strength and prevent discolouration. It provides a clear coating that is able to resist the influence of UV exposure to a far greater degree than other alicyclic anhydrides and is typically employed in the production of durable, high gloss, weather resistant coatings. (10)

Resins are incredibly important within the coating field, pigment and extenders are dispersed within the resin to prevent their agglomeration and ensure an even distribution. As the resin solidifies it locks the pigments and extenders in place, preventing their movement. The chemical and physical properties of resins also dictate the overall properties of the finished film, determining their mechanical and adhesive strength, as well as the chemical and weather resistance offered by the coating. (1)

There have been health and environmental concerns over the use of HHPA, which has led to the chemical being classified as a Substance of Very High Concern (SVHC) by the European Chemicals Agency (ECHA) in 2012 due to the respiratory sensitising properties that it exhibits. This classification places limitations on how and where coatings containing HHPA can be applied. (13)

The report issued by ECHA states that there is scientific evidence showing that HHPA has the potential to induce occupational asthma, with other symptoms such as rhinitis, wheezing and coughing alongside nocturnal asthmatic symptoms over a period of several years. It is also claimed that HHPA can cause respiratory sensitivity during prolonged exposure, with 75% of an investigated workforce suffering from nasal and ocular symptoms while at the facility. (13)

Investigations by Nielsen et al. verify the potential for harm that HHPA can have on workers. A workforce of 154 who worked within a factory that utilised epoxy resins were investigated and any work-related symptoms of the eyes and airways were noted and compared to a control workforce of 57 who worked in mechanical industries within the same area but with no exposure to HHPA. The investigation took occupational and medical histories into account, having all participants fill in questionnaires, alongside the past and present tasks that each individual performed to determine exposure levels. It was found that the workers exposed to HHPA had far more instances of eye or airway symptoms than the non-exposed group, which can be observed in Table 1.1 (14):

Table 1.1 – *Breakdown of health problems related to HHPA exposure*

Symptoms	**Exposed workforce affected (%)**	**Non-exposed workforce affected (%)**
Nose problems	28	16
Eye problems	23	14
Lower airway problems	10	4
Nosebleeds	8	0
Total	69	34

From Table 1.1, it is possible to see that all symptoms were experienced in far greater amounts within the exposed group. While this may be due in part to the greater sample size of this group compared to the control, it is also strong evidence of the negative effects that can be experienced following continued HHPA exposure, particularly to the eyes and nose. The investigation was also able to find that HHPA levels in the urine increase alongside HHPA air levels. (14,15)

Following these reports, HHPA has been classed as a Class 1 skin sensitizer with the warning that it has the capacity to cause an allergic skin reaction, a Class 1 risk of eye damage or irritation that can cause

serious eye damage, and a Class 1 respiratory sensitizer that can cause allergy or asthma like symptoms alongside breathing difficulties if inhaled. (10,13,15)

1.4-Polymers and their degradation processes

The most commonly used resins within coil coating are polyester melamines, polyurethanes, polyvinylidene difluoride (PVdF), polyvinyl chloride (PVC) and epoxy resins.

1.4.1-PVC

PVC is generated through the suspension polymerisation of vinyl chloride in addition to radical chlorination to produce a product that is largely comprised of chlorine (65%). However, as this product tends to be poorly soluble, it is usually co-polymerised with small amounts of compounds such as vinyl acetate in order to increase the molecular weight and therefore improve solubility of the final compound. PVC is applied by being added to suitable plasticisers that have been pre-mixed with pigments, the amount of plasticiser relative to the PVC changes depending on the desired final flexibility. The PVC powder dissolves into the plasticiser during heating to create a thick thermoplastic material. There is typically a lower concentration of pigments in PVC compared to other polymer paints but is compensated for by the increased thickness of the final film. It is also common for mixtures of PVC resin powder to be used in combination, with finer powders making up the bulk of the addition, and coarser powders added to reduce the gloss of the final coating finish.

There are multiple degradation pathways for PVC, which limits its effectiveness in a variety of situations. It is possible for heat from the physical drying process to cause dehydrochlorination, the produced Hydrochloric acid then catalyses the reaction, accelerating the rate of degradation even further. The dehydrochlorination allows the formation of carbon-to-carbon double bonds (C=C) within the hydrocarbon backbone. A conjugated double bond system will then be able to develop, which is capable of absorbing electromagnetic radiation because the C=C bonds are chromophores. (1)

The first observable effect of degradation will be a yellowing of the coating, this yellowing will grow more pronounced as more C=C bonds are formed within the hydrocarbon backbone. Once there are 8 or more C=C bonds then it will be possible for the structure to absorb visible light, greatly increasing its rate of degradation.

If PVC absorbs UV radiation, then the supplied energy will be sufficient to break the present Carbon-Chlorine (C-Cl) bonds, creating free radicals and facilitating photooxidative degradation. (1)

PVC is an extremely formable polymer that offers good weather and corrosion resistance. One of the main limitations is the low temperature limit of 80^{o}C. Because of these characteristics, PVC can be applied to

aspects of internal and external architecture. Another issue is that line speeds have to be slower due to it being a high solid film, this results in longer production times and therefore an increased end cost.

1.4.2-PVdF

PVdF is a thermoplastic solid polymer with natural UV-stability, preventing chalking or discolouration from weathering. However, due to its poor mechanical strength, this polymer is usually restricted to use on wall cladding. It has been found that PVdF retains 58% of its gloss after 20 years of weathering exposure in Florida and 92% following 20,000 hours of exposure using an ATLAS weather-Ometer, this shows that that PVdF is suited for environments that involve long term UV exposure. (16)

To allow for colouration by pigment addition, PVdF is combined with acrylic resins. However, this can have a negative effect on the UV stability of the final coating. This is because while PVdF is stable because the strong Carbon-Fluorine (C-F) bond does not absorb within the UV component of the spectrum, acrylic resins are less stable and will begin to undergo photo-oxidation. The PVdF monomers have the capability to flow into the gaps created during photo-oxidation to prevent further degradation. This results in a product that suffers minor surface degradation before being arrested and exhibiting a lifetime similar to that of pure PVdF resin.

The main limitation of PVdF is its low level of abrasion resistance which limits its use to building materials that will not typically have to endure abrasive contact. This poor abrasion resistance means that the coating can be easily damaged, which will not only increase the rate of degradation due to an increase in surface area, but also potentially provide less protection for the substrate and will require re-application. A further limitation is that full gloss is impossible and that there is a limited colour palette, this is because of the UV transparency of PVdF. (1,16)

1.4.3-Polyester melamines

Polyester resins are one of the most versatile that are involved in coatings. They can be adapted to suit a wide range of applications through the modification of their hydrocarbon backbone structure, molecular weight, and functionality, the alteration of which determines their final properties.

There are constants between all polyester resins, such as the high viscosity that is exhibited when they are dissolved within organic solvents, which limits the obtainable operable solid content, with lower molecular weight mixtures providing softer finishes that give greater surface coverage but poorer mechanical performance.

An advantage to polyester resins is that they can be cross-linked to improve their protective qualities, it is common for derivatives of melamine to be used as they are cost effective and can provide high-solid

polyesters. The structure of polyester melamine structure determines the absorption potential of the structure.

Crosslinking gives the polymer chains anchoring points, which stop the chains from exhibiting excessive movement and keep them in their correct position within the network. The use of crosslinkers improves the stability of the coating system, solvent resistance, and affords a higher Glass Transition Temperature (T_g), in addition to improving resistance to solvent damage. (17)

The most commonly utilised melamine is hexamethoxymethylmelamine (HMMM), due to its relatively low cost and availability.(4,18,19)

Polyesters can also be developed through relatively environmentally friendly means, notably through the use of vegetable oils. (20)

The main limitation of polyesters is their level of UV stability, coupled with that when they absorb radiation, it is common for chain scission reactions to primarily focus at the ester linkage. This breakdown creates free radicals which, as mentioned previously, facilitate further degradation. However, this breakdown is more commonly observed in linear aliphatic polyesters and the addition of suitable compounds can cause a significant reduction in surface vulnerability. Polyesters also require a protective coating during processing, this additional step increases both production time and costs. (1,16)

One of the aspects of polyester monomers that influence the performance of a coating is if the monomer is saturated or unsaturated. An unsaturated polymer typically has poor weathering durability and as such are not typically seen within coating systems. Unsaturated polymers have poorer weathering capabilities as they have sites available to undergo chemical reaction in order to form saturated bonds, additionally due to the increased presence of double bonds within the system there is a greater probability that chromophores will be present within an unsaturated system.

It follows that saturated polyesters are desirable for coating systems, however there is further variation possible depending on if the polyester is linear or slightly branched, or if modifications have been added to the formulation. Linear polyesters are best utilised when flexibility is paramount, they are commonly applied as primer coatings, where high molecular weight linear resins have been shown to act as the best for primer resins. Slightly branched polyesters have higher molecular weights while retaining a high level of functionality. Modifications (or additives) such as siliconising have beneficial properties that bolster the performance of the coating.

While siliconising polyesters provide a beneficial improvement in weathering, they are increasingly being removed from the market due to their higher processing costs resulting from additional resin process steps to produce them.

One of the main drawbacks of polyester resins is that due to the high processing temperatures that are required it is expected that ether linkages will form within the resin. This compromises the weathering durability of the coating, reducing its effectiveness.

Melamine is greatly impacted by the Peak Metal Temperature (PMT), which is the temperature that the substrate reaches as it passes through a curing oven. Different temperatures resulting in variations in the size, degree, and dispersion of melamine self-condensation. A higher PMT will result in more instances of melamine self-condensation, but they will be smaller and greatly dispersed throughout the coating. Conversely, a lower PMT results in less dispersion and larger globules of melamine within the coating system.

The presence of melamine self-condensated agglomerations cause the coating system to be heterogeneous, which can cause degradation to occur at different rates across the coating. The impact of melamine self-condensation will be discussed within a later chapter.

Within the coil coating industry, there are two main crosslinker types that are utilised, these are melamine-formaldehyde resins and blocked isocyanates. The most popular crosslinker is hexamethoxy methylmelamine (HMMM). While other melamine crosslinkers are available that have lower amounts of methylation and/or butylation, this would cause an improved rate of reaction but will also result in increased melamine self-condensation which will cause a decrease in the flexibility of the generated coating system. The melamines with decreased methylation are also more susceptible to weathering damage, which limits their effectivity for external coatings.

Resins with less butylation, have also been reported to be less compatible with the resin system and have been found to have a tendency to move towards the air/coating interface, which increases the hardness of the coating. (21)

Melamine is susceptible to various forms of degradation, the majority of which involve the Hydrolysis of crosslink sites through the involvement of acid and water, which can be observed in Figure 1.2.

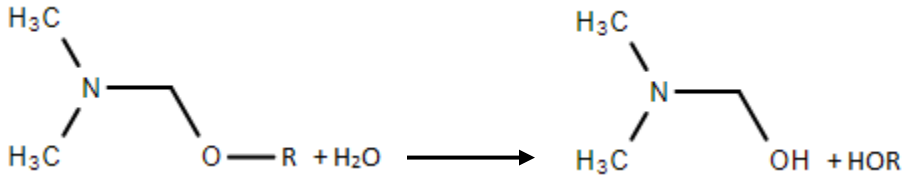

Figure 1.2- *Example of hydrolysis of melamine crosslinker*

It is also possible for melamine to be particularly susceptible to damage via UV light, which would result in the moiety in Figure 1.3.

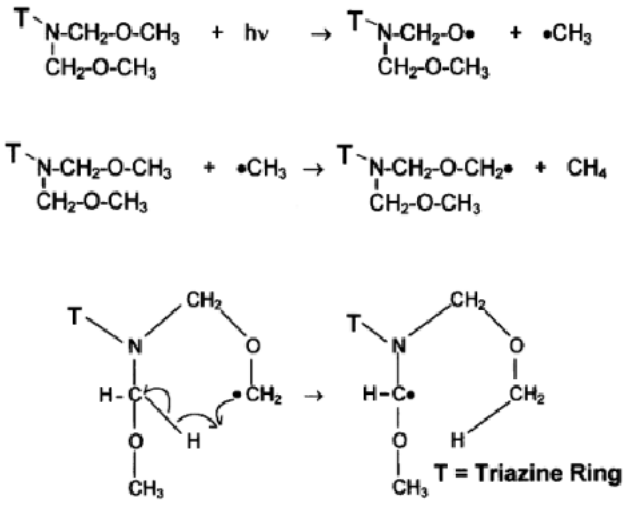

Figure 1.3- *Impact of UV absorption on melamine crosslinker*

The movement of the Hydrogen from a secondary Nitrogen to a primary Nitrogen on the Triazine ring has caused the compound to lose its ring structure, and therefore its activity.

When they are the only crosslinker used within a coating system, melamines are also susceptible to attack by free-radicals and become the first components to suffer damage from degradation.

1.4.3.1-Impact of melamine ratio on coating systems

Existing literature states that altering the ratio of melamine crosslinker can bestow mechanical advantages and disadvantages to the overall coating. Research performed by Radmila et al developed coatings with crosslinker ratios varying from 70:30 to 85:15, finding that the coating systems with increased melamine

ratios benefited from increased curing extent and improved hardness measurements, however it was also associated with diminished elasticity within the coating. Sorce et al also performed dynamic mechanical analysis on polyester coatings and found that generally the T_g and crosslink density increase in line with crosslinker content, further strengthening the connection between them. (22,23)

Recent research into the impact of melamine ratios has shown that while polyester-melamine coatings are susceptible to damage from both UV and moisture, they are particularly damaged by UV and moisture in combination. (24) Persson et al performed research showing that UV and moisture in combination resulted in larger degradation effects towards the air/coating interface but that a loss of melamine functionality was observed at depths up to 10μm. Their research also highlighted that using resins with lower hydroxyl numbers or coating systems with higher ratios of melamine content led to increased instances of melamine migrating towards the air/coating interface, while lower melamine ratios were associated with more uniform distribution of melamine throughout the entire coating system. Accelerated weathering tests were carried out according to BS EN ISO 11507:2007 standards. These took the form of repeated cycles of 60°C UV and 40°C Condensation for 4 hours each (referred to as STD UV-A weathering) or 8 hours of 80°C UV followed by 4 hours of 50°C Condensation cycles (referred to as HOT UV-A). (24)

From the exposure of samples in humid atmospheres, it is known that moisture can penetrate into PE:HMMM coatings , with the most damage occurring to the outermost parts of the coating and working inwards. It is also known that pigments can result in UV damage to be diminished, along with reducing moisture penetration. This occurs as long as the resin adheres to the pigments particles, but when the resin degrades then adhesion to the pigments will also fade, allowing for the generation of additional diffusion paths. (24)

1.4.4-Polyurethanes

Polyurethanes are formed through the addition polymerisation of isocyanates, hydroxyl functional groups and a suitable polyol such as polyethers. Due to their reactive nature, the isocyanates are blocked with the addition of specific compounds to prevent them from forming cross-linkages before the coating has been put in place. These blocking compounds then thermally degrade at various temperatures during the drying process, the different temperatures provide some control over the rate at which cross-linking occurs. (1) There are two general groups of isocyanates, aromatic and aliphatic, both with their own advantages and disadvantages. Aromatic isocyanates are the cheaper of the two and exhibit superior general performance in stability, gloss and colour retention compared to their aliphatic counterparts.

However, they also show poor protection of physical properties in external environments, causing aliphatic isocyanates to be the better choice when colour retention is a priority (such as with external architectural coatings). (11)

However, there have been concerns over the use of monomeric isocyanates as they have been shown to cause respiratory problems. It is more common for oligomers to be used, these also provide the added effect of blocking any free isocyanates, thereby preventing any premature cross-linkages from forming. Polyurethanes typically have a good level of formability coupled with high UV and thermal stability. Unblocked isocyanate trimers also see use in coatings, primarily within two-pack systems. (1,16)

1.4.5-Polymer degradation processes

There are several different degradation processes that can influence polymers and this chapter will focus on the chemical processes behind UV radiative decay and oxidative degradation as they have the potential to significantly impact all polymer structures, as well as the impact on the individual polymer structures that are commonly utilised within coil coating. oxidative degradation will be researched as most developed polymers will be used in environments in which oxygen is present.

Polymer degradation can occur through two main methods, chain scission and cross-linking. Chain scission results in the formation of low molecular weight separated chain segments referred to as moieties, whereas cross-linking causes the development of an insoluble and infusible networked structure. These two reactions usually occur in competition with each-other, so it is common for both to be observed to various degrees in degraded polymer structures. (25)

The energy required for the radiative decay of polymers can be supplied through UV radiation, which is shown in Figure 1.4.

UV radiation falls within the wavelength (λ) range of 100nm-400nm and supplies energy of between 3.1-12.4 eV. UV initiated degradation occurs because of the absorption of quantised energy by functional groups and the supplied energy is only able to excite an electron to moving to a higher energy state. (25) ionising radiation is any form of high energy, such as X-rays, electron beams or Gamma (γ) rays. Unlike UV radiation, which supplies specific energy to electrons to facilitate their movement into an excited state, ionising radiation directly transfers energy to all electrons within the path of the high-energy photons and can eject the electron from the molecule.(25)

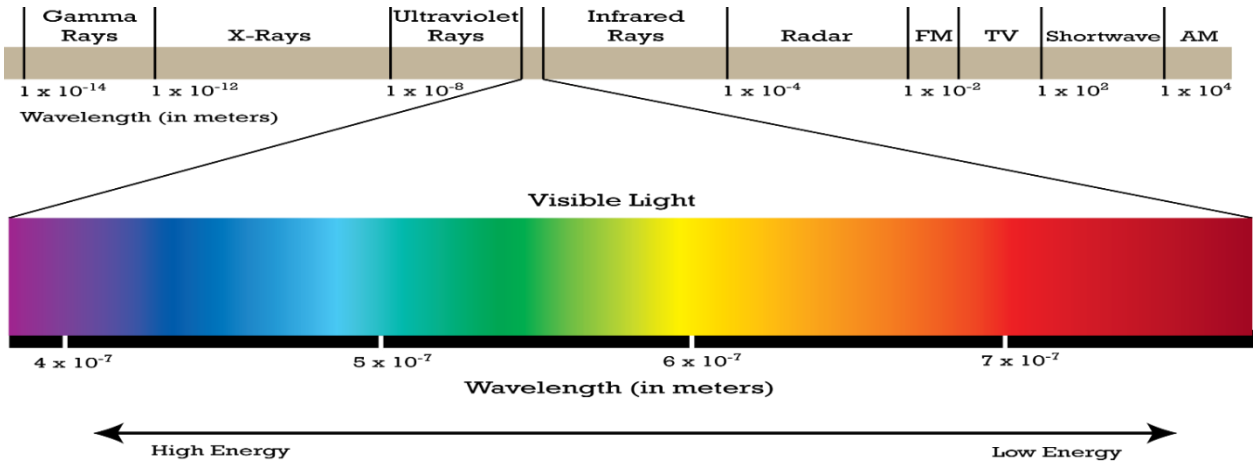

Figure 1.4- *Illustration of Solar spectrum*

The presence of Oxygen influences the degradation of polymers, as its presence allows for photo-oxidation to occur. Photo-oxidation is the primary cause of weathering in polymers and reduces the molecular weight, causing the polymer to become brittle and more susceptible to damage. Photo-oxidation also facilitates discolouration and an increase in the roughness of the surface. The presence of Oxygen can also affect the degree to which UV radiative decay occurs in two different initiation processes. The primary initiation method through which Oxygen (or Oxygen-substrate complexes) can affect UV radiative decay is by absorbing the energy supplied by the UV radiation to enter an excited state. It is also possible for the Oxygen to react with functional groups along the surface of the polymer to create charge-transfer complexes in areas of the hydrocarbon chain where double bonds or functional groups are located, this in turn leads to the formation of free radicals. This can fuel the photo-oxidation process with the development of active intermediates that yield further oxidation products, allowing the oxidation process to become self-propagating.

Secondary initiation occurs when the products of oxidation reactions of the substrate absorb UV radiation to produce free radicals, which then go on to propagate further oxidation reactions and cause further degradation of the substrate.

It is also important to note that the degradative processes initiated by UV can also be brought about by thermal initiation, with heat supplying the energy required to move Oxygen into an excited state.

The above initiation processes show the significant effect that Oxygen can have in exacerbating the issues that are associated with UV induced degradation, allowing additional chemical processes to occur and the formation of harmful free radicals and functional groups. While Oxygen does not have the ability to affect the initial degradation that is caused by ionising radiation, as ionising radiation is not affected by the

linkages connecting the atoms that it contacts, oxidation chains can still occur once a free radical has been formed and oxidation processes can occur in the same manner as UV radiative degradation. (25)

Different polymer structures have varying resistance to oxidative degradation. This is due to the differences in their chain stiffness and intermolecular forces that bind them. Polymers with larger intermolecular forces and chain stiffness generally have a relatively high degree of resistance to Oxidative degradation in addition to chemical and hydrolytic degradation. However, it is possible for the chain stiffness and intermolecular bonds to prevent the development of a regular, repeatable chain.(26)

Polymer stabilisation is of extremely high importance as unstable polymers will undergo slow aging when in contact with air, particularly in external environments. This is because, as mentioned above, UV radiation promotes the occurrence of Oxidation reactions.

While UV radiation can supply enough energy to bring about the breaking of most single covalent bonds, it cannot supply the required energy to allow an oxidation reaction to break the bond between two Carbon atoms (C-C) or a carbon and hydrogen atom (C-H). Instead, the bonds are attacked via the second initiation reaction that generates free radicals, the mechanism for which has previously been covered.

1.5-The development of polyester resins

Polyester resins are usually developed through condensation reactions between basic acids, esters, anhydrides and polyols. In the development of coating systems, the resin is of the utmost importance, as it makes up the majority of the final coating system and therefore the properties of the resin will exert the greatest influence over the properties of the final coating.

Resin systems have two major roles that they must be capable of fulfilling. Firstly, they must be capable of retaining a liquid form that can facilitate the suspension of pigments and other additives. Secondly, they must be capable of a second reaction whereby they form an insoluble film that binds the coating components to the substrate of choice. Polyester resins are typically formed through condensation reactions, with modern resins being the product of multiple raw materials and therefore have many chemical reactions occurring simultaneously during synthesis. All polyesters are formed through condensation reactions. Reaction temperatures can vary, but as a general rule, esterification is said to occur at 232°C, even though it can be observed at temperatures approaching this.

When the resin has been synthesised and the coating components added, they then have to formed into a coating system, this is achieved via the curing process and involves several mechanisms such as internal crosslinking, solvent evaporation and crosslinking with other reagents, with many polyesters crosslinked via carboxyl or hydroxyl functionality within the molecular structure. (27)

1.6-Factors affecting polymer stability

Backbone rigidity can affect many aspects of a polymer, not least its thermal stability, the importance of thermal stability will be covered later as an aspect of the Glass Transition Temperature. An important note is that polymers with cyclic structures are usually more resistant to deformation, which explains the widespread use of ring structured aliphatic anhydrides.

The addition of side chains can provide benefits and drawbacks for the polymer. While adding side chains to a cyclic structure can reduce the overall chain stiffness, it can also result in an increase of solubility, which is desirable from a formulation standpoint, this shows that, at times, a compromise in backbone rigidity can produce a more desirable final product, depending on the requirements of the final product.(26)

There are also significant differences between linear and branched chain polymers, for example, a linear polymer can form a crystalline phase because they are able to pack into a regular 3D pattern, whereas branched polymers are incapable of this because of the random branch lengths, which prevent regular packaging, showing that changes in crystallinity have a significant impact on many properties, including strength and optical clarity.

Hydrolysis has the potential to be a large contributor towards the degradation of a coating, this is because many links are sensitive to the process. Water can be especially damaging during processing, resulting in a shortening in chain lengths and influencing the final properties of the resin. Hydrolysis is so effective at degrading polymers that it has also seen use as a method of recycling polyesters and polycarbonates. At the most basic level hydrolysis is the reverse of the synthesis process of the polymer, as can be observed in Figure 1.5. (28)

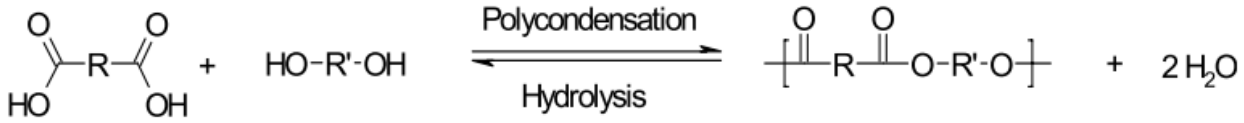

Figure1.5-*Showing most basic representation of hydrolysis*

There are eleven key interactions that can occur between the melamine crosslinker and a hydroxyl polymer during curing. Which reactions occur, and the degree to which they are performed depends on the degree of catalysis, the curing conditions, and the chosen melamine crosslinker, as the degree of crosslinker alkylation will strongly influence the reaction mechanisms that are possible. While all of the reactions are important, the 2 most prevalent reaction mechanisms can be found in Figure 1.6.

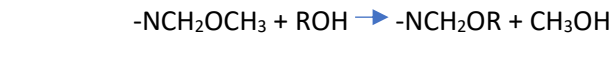

Figure 1.6 – *Overview of two prevalent hydrolysis mechanisms*

The first reaction mechanism describes the most prevalent mechanism that leads to the successful generation of polyester-melamine crosslinks. The second equation shows the process by which melamine self-condensate agglomerations are formed. (29)

Crosslinking can be critical in ensuring that the mechanical properties of polymers reach a level suitable for the intended use of the polymer. Crosslinking can take three forms, covalent (which is widely considered to be the most stable), ionic and physical crosslinking (which is made through Van der Waals forces, Hydrogen bonds and other similar interactions).(30)
Crosslinking also increases the glass transition temperature (T_g) by decreasing free volume within the polymer structure by causing chain segments to be more closely stacked. (31)
When deciding on the type of crosslinking, it is important to determine if it is reversible when exposed to certain conditions. While reversibility is a useful attribute from the perspective of recycling the polymer, it would have the potential to cause issues in long standing polymeric structures, such as polymer coatings for outside architecture, where longevity is highly important from a cost saving perspective. (30)
A consideration that needs to be made with crosslinking is the likelihood of homogeneous distribution of the crosslinker throughout the coating.

It is known that the melamine crosslinker tends to self-condensate during the curing stage of coil coatings. It is believed that these areas of self-condensation also impact the physical and chemical performance of the coating. Zhang et al studied the distribution of melamine through confocal Raman microscopy and found that melamine self-condensated areas are found towards both the coating/air interface and the coating/substrate interface, but that this distribution is somewhat random and not impacted by the choice of pigments within the coating. (32)

The presence of inhomogeneous zones was later verified by Nguyen et al, who developed a conceptual model of the hydrophilic domains that are formed within a crosslinked coating. (33) The impact of these lateral inhomogeneities was further explored by Makki et al, who found that the presence of these polar,

hydrophilic regions contributed to gloss loss through an increase of surface roughness. (34) It has also been documented by Rossi et al that melamine self-condensated agglomerations preferentially gather around polar areas. As the hydrophilic areas are polar, it stands to reason that melamine agglomerations may be attracted to these regions, which would in turn lead to vulnerability towards UV exposure and moisture ingress. (35)

Crosslinks are known to be susceptible to degradation through both photodegradation and hydrolysis, it has been found that the reaction between melamine and water progresses in the same manner as the reaction between melamine and the hydroxyl group of the polymer. (29) While hydrolysis can have a significant impact on the chemistry of the coating, it does not strongly influence its physical appearance. This is theorised to be due to the formation of melamine-melamine crosslinks as the polymer-melamine crosslinks undergo scission. It has also long been known that humidity plays a significant role in the degradation of melamine crosslinked coatings, with higher humidity leading to accelerated rates of degradation. The literature also states that, during natural exposure, it has been found that there was evidence for the hydrolysis of methoxy groups without polymer-melamine hydrolysis or melamine-melamine condensation being observed. They went on to claim that the accelerated methoxy group hydrolysis was caused by the formation of Carboxylic acid via photo-oxidative degradation of the coating. (29)

Photodegradation is caused by the exposure of a sample to UV radiation. The adsorption of UV radiation leads to photo-oxidative degradation, this in turn leads to the breakdown of the polymer backbone and the generation of free-radicals. Free-radicals are self-propagating, so when this stage is reached the polymer usually quickly degrades and loses its desirable properties. (3,16,25)
A smaller UV absorbance window decreases the range within which the monomer absorbs UV radiation, which would theoretically slow the rate at which photo degradation occurs and therefore would correspond to a lengthening of the life of the coating. This is corroborated by the connection between the faster rate of degradation experienced by aromatics compared to their cycloaliphatic counterparts, brought about by the fact that aromatics absorb closer to the visible region of the electromagnetic spectrum than cycloaliphatics.

There are several stages of mechanochemical degradation that affect polymers when they are heated, which are commonly referred to as the glassy region, transition region, rubbery plateau, rubbery flow and liquid flow. (25)

T_g (glass transition temperature) is the temperature at which the polymer moves from the glassy region to the Transition region, where the polymer chains begin to move and forces have the potential to cause alterations in the polymer chain formation and orientation. (25)

The higher the T_g then the more stable the polymer is within high temperature environments. However, the structure of the polymer has a significant impact on the final T_g value. It is a general rule that chains with a greater stiffness or more intermolecular interactions will have a higher T_g, this is because high stiffness results in lower mobility, so if they are present in the chain bulky groups prevent rotations at lower temperatures. (31)

However, it is also worth noting that increasing the chain length can cause a reduction in the T_g, this is because of increased chain mobility, enabling rotation around blocking groups. Longer chains and the addition of secondary chains also increase the free volume within the structure by affecting the way that the chains are packed together. (31)

Batista et al performed an investigation into the impact that the chemical structure of a polyester has on the stability of the coating during accelerated weathering. During this experiment, HHPA was combined in a co-monomer system with either terephthalic acid, phthalic anhydride, or CHDA. Their study found that HHPA combined with CHDA contributed the most significantly towards the overall polymer degradation. It is theorised within the paper that such a degradation was brought about as a result of the hydrogen atoms attached to the secondary and tertiary carbons within the structures, with HHPA exhibiting four secondary and two tertiary carbons, while CHDA contains six secondary and two tertiary carbons. These cause an impact on the polymer degradation due to the increased ease with which the hydrogens attached to these carbons can be abstracted, resulting in the formation of free radicals. (4)

1.7-The impact of pigments

The primary focus of pigments is to provide aesthetic appeal through the addition of colour and altering opacity. However, they also have the potential to influence the physical properties of the coating system. In order to understand how pigmentation of a coating can influence the system an in-depth understanding of pigments is required.

Pigments are particulates that are dispersed within the (otherwise clear) coating system. Pigments can be either crystalline or non-crystalline, showing that the atoms can be arranged in an ordered or random manner respectively.

The definition of a pigment states that they must be '…insoluble in, and essentially unaffected by the vehicle or substrate.' This means that for something to be considered a pigment it is required to be unreactive with the coating in addition to not being damaged by the binder and solvents within the coating system.

It is possible for unsuitable pigments to appear to be unreactive for some coating systems, in these cases there are several issues within the application and curing process that indicate that they are soluble within the system, which are blooming, plate out, bleeding, and re-crystallisation.

Blooming becomes evident if the pigment is soluble in the carrier medium, this causes the solvent to rise to the surface of the coating and evaporate during curing and leaves crystallised pigment particles on the coating surface as a fine powder. As solubility rises in line with temperature, higher curing temperatures lead to a more damaging effect.

If the pigment dissolves into the binder rather than the solvent then it forms a supersaturated solution and remains mobile following solvent evaporation, which allows the pigment to continually return to the surface during curing. Plate out has extremely similar properties to those mentioned above. However, they are known to only occur within plastics and powder coatings.

Bleeding can occur when a new coating is applied over the top of an already dried film. The pigments in the dried film dissolve within the solvents of the new coating, this can be especially problematic if the topcoat is of a different colour as the pigments have the potential to bleed through and stain the topcoat a different colour. This issue is made worse with elevated temperatures, such as those found on coil lines.

The final issue is pigment re-crystallisation, which has only become an issue since the introduction of beadmills. The heat that is produced during bead milling causes some of the pigment to dissolve, the coating is then able to pass through quality control as it forms a supersaturated solution with the dissolved pigment acting as a dye. As the coating cools, the pigment will begin to re-crystallise, this causes a decrease in the strength of the coating colour in some areas. Fortunately, this issue can be mitigated by controlling the temperatures reached during milling and using pigments that are insoluble in the presence of the solvents. (36)

A pigment of interest is TiO_2 (Titanium Dioxide), which sees wide use in coatings for multiple purposes. The concern with TiO_2 is that it is semi-conducting, meaning that it could facilitate photodegradation of the coating upon exposure to UV radiation.

TiO_2 receives such extensive use due to its desirable attributes such as a high refractive Index, good dispersibility, and photocatalytic stability. However, it is possible for TiO_2 to contribute to the breakdown of a coating through interactions between the TiO_2 and the light.

Exposure to short wave light causes the TiO_2 lattice to form an electron hole pair, which in turn would react with Hydroxyl groups and Ti^{4+} ions on the TiO_2 surface. From here the reaction between H_2O and an Oxygen molecule leads to the formation of Hydroxyl and Perhydroxyl free radicals, with these causing the breakdown of the coating.

1.8-Analysis of UV degradation prevention techniques and developments

It is clear to see that polymers are particularly susceptible to both thermal and UV induced degradation and require stabilisers and/or additives to negate these processes for an extended time.

Historically, varnish coats have been added via an additional step in order to diminish the rate of degradation, however unpigmented varnish was also observed to degrade rapidly through weathering exposure. (37)

Two of the methods that are used to improve the resistivity of polymeric coatings are through the inclusion of additives such as HALS, by changing the monomer(s) that are involved in the synthesis of the base resin, or by altering existing formulations to focus on different properties, such as the Glass transition temperature (T_g).

However, it is more common for additives to be added to the coating than for monomers to be changed. This is due to multiple reasons. As HALS have a known cost and efficiency, whereas using novel monomers has an inherent risk due to relatively unknown properties that may not become evident until after the resin has been synthesised, combined into a paint, applied to a substrate, and evaluated for degradation resistance. This requires a significant amount of time, which makes the process less desirable when compared with the adding of HALS to an existing coating formulation to improve it.

HALS are utilised to deactivate free radicals to prevent the degradation of the polymer backbone. UV absorbers can also be implemented to disperse UV radiation before it is able to cause harm to the polymer. It is also possible to use “Quenchers”, which are able to transfer energy from an excited molecule to prevent free radical production. (25,38)

Osswald and Menges agree with the use of HALS, quenchers, and UV absorbers, stating that stabilisers such as anti-oxidants or peroxide decomposers can slow the attack of double bonds by free radicals. However, they go on to stress that these measures do not stop degradation but are only capable of extending the amount of exposure/time required before degradation is observed. This is because that once the stabilisers have reacted they cannot be used again, eventually causing all the stabilisers to have been used, allowing degradation to continue at its normal pace. (39)

Cai further validates the use of HALS by stating that they can prevent oxidative degradation, discolouration, and cracking. Cai goes on to say that these abilities have generated a large amount of interest and research into HALS has facilitated rapid development, allowing them to become the primarily used light stabiliser in industry. (40)

Current research into HALS is leaning towards improving performance and functionality through the alteration of triacetonamine derivatives. The HALS obtained through these derivatives share many traits, such as high molecular weight, alkaline pH, capable of multi-functionality, and suitable to be combined with a polymer. The high molecular weight gives improved resistance to heat, folding of the polymer and washing, potentially extending the applications of the coated polymer. The alkaline pH means that there will be fewer H^+ ions present, limiting free radical excitation and therefore slowing the degradative process. Multi-functionality enables the HALS to exhibit multiple desirable attributes, an example being the Sunovin 5591 produced by the Shanxi Chemical Institute, which combines high levels of thermal resistance with light stability, preventing both thermal and photo-oxidative degradation. Finally, the polymer combination means that the HALS can be added directly to the polymer backbone, circumventing the issues that are associated with the transfer of the HALS and their compatibility with the substrate/polymer. (40)

Paine et al state that there have been disagreements over the chemical processes by which HALS provide such effective degradation resistance before stating that recent studies have shown that the aminoxyl radical harvests the free radicals generated through thermal/photo-oxidation and converts them into less reactive species through electron donation.

However, Paine et al go on to show that to gain an in-depth understanding of how HALS can suffer loss of action relies on gaining an understanding the chemistry of piperidinyl Nitrogen moieties that are present. This is because studies have shown that alterations to these moieties during curing or weathering can alter the physical characteristics and the chemical properties of the HALS, affecting its abilities as an antioxidant and stabiliser. (41)

UV absorbers are added to polymers in an attempt to slow the progression of degradation. Their role is to absorb radiation between 300nm-400nm and dissipate it in the least harmful way to the polymer. The absorption and dissipation of UV radiation prevents it from being absorbed by a sensitiser, which would initiate free radical generation and accelerated degradation. It is commonly thought that Carbon Black (CB) is the first man-made UV absorber, having been used since Ancient Egypt and remaining in regular use in current times. The development of UV absorbers as a science only began in 1960 with the development of the first benzotriazole based UV absorber. (2,7,42)

CB is still used to prevent coating degradation, Ghasemi-Kahrizsangi et al analysed its potential for slowing the degradation of epoxy coatings under accelerated UV exposure. Their experiment followed recognition of the effectiveness of CB when involved with other polymer coatings.

By comparing pure epoxy resins to those containing a CB dispersion, it was found that there was a significant decrease in the generated carbonyl groups in the coating containing CB. As carbonyl groups are generated during chain scission, it is possible to determine that CB has a dampening effect on UV degradation. It was found that CB acts as an antioxidant and free radical scavenger, capable of combining with free radicals as a single electron donor. (43)

However, it was also noted that the size and dispersion of the CB nanoparticles is critical for their efficiency. For CB to provide optimum UV protection it must be comprised of small nanoparticles that are evenly distributed. This can cause issues, as smaller particles tend to agglomerate and resist attempts at spreading. This would produce a coating that provides UV resistance in some areas only, so localised degradation would still be observed. The agglomeration can be prevented through the modification of CB nanoparticles by grafting them to the surface of the coating, preventing the potential for grouping. (43,44)

A limitation of UV absorbers is that they do not have universal applicative capabilities, the environment in which they will be placed requires consideration, as photoinduced instability can occur. From this it is possible for some UV absorbers to undergo structural changes, which in turn can alter their behaviours. An example of this is 4-tert-Butyl-4-methoxydibenzolmethane (BMDBM), which is a major component of sunscreens, preventing damaging UV-A radiation from being able to penetrate the skin. However, it has been found that BMDBM is altered from its enol form to a keto form, shifting its absorption range from UV-A to UV-C, therefore offering no protection to the substrate from UV-A radiation.

To prevent this from occurring, it is advised that another UV absorber be added alongside BMDBM to act as a quencher. Although this example is primarily of critical importance to the developers of sunscreen, it highlights the potential benefits that the implementation of quenchers can provide. (45)

As mentioned earlier, quenchers operate through the transfer of energy from the excited sensitiser to themselves, preventing the process that would lead to free radical formation. While HALS fall into the category of quenchers due to their mechanism of reacting with free radicals, it is possible for the role of the quencher to be fulfilled by the pigment component of coatings. (25)

It has been found that coatings that contain pigments tend to have better UV durability than transparent coatings, suggesting that the addition of pigments can significantly improve the resistive properties of the coating, however this is heavily dependent on the pigments chosen. The chemical quenching process removes the excited state of the donor molecule by transferring it to the excited state of the quencher molecule, which releases the energy via non-destructive pathways. This in turn causes a reduction in the fluorescence intensity of the donor molecule. Quenchers are often used in conjunction with photosensitisers, which increase the reaction rate or yield, but tend to decrease the overall stability of the coating. (16,46,47)

Quenchers are not without their limitations. Traditionally, they are sacrificial, only having a limited number of uses before being unable to function. They are also unable to prevent photo-oxidation, so surface degradation will still occur but at a reduced rate. These limitations mean that quenchers are most efficiently utilised alongside other preventive measures, such as UV absorbers and shielding.

Braig states that, in general, the efficiency of UV absorbers depends on the relative concentration used, the film thickness applied and on the specific molecules extinction coefficient. This is in stark contrast to HALS, which are not significantly impacted by the build of the applied film. (48)

Braig continues to speak of HALS, stating their main limitation as that they do not absorb light at frequencies over 250nm. This means that HALS alone are unable to provide adequate protection from degradation. The research on the limitations of HALS was continued by Paine et al, whose research showed that the N-CH_3 to N-H reaction, one of the main antioxidant processes of polymers, only occurs in the presence of UV light, making HALS useless for thermally induced degradation prevention. (41,48)

Cai speaks of the improvements in HALS technology in recent years, claiming that the improvement is due to the attention given to HALS due to their '…unique and excellent light protective performance…' which has made them the main light stabiliser products of choice in present day. (40)

Cai mentions the trends that new developments have yielded, such as increased molecular weight, making the components multi-functionalised, and more readily polymerisable. Higher molecular weights improve resistance to migration, folding and heat, therefore improving the durability of the final film. Making HALS multi-functionalised through the introduction of anti-oxidant groups also improves heat resistance and light stability. While making HALS more polymerisable allows the reactive groups to be introduced into

the polymer backbone during processing, improving the permanent light stability of the material, removing the issues of transference and compatibility when choosing which HALS to add to the coating. (40)

However, there are some issues with the claim that adding reactive groups into the polymer backbone will improve the permanent light stability of the polymer, as the HALS will still only be of limited use as they are unable to be replenished once used, eventually causing the polymer to retain no protective HALS, therefore reverting to its original light stability prior to the addition of HALS.

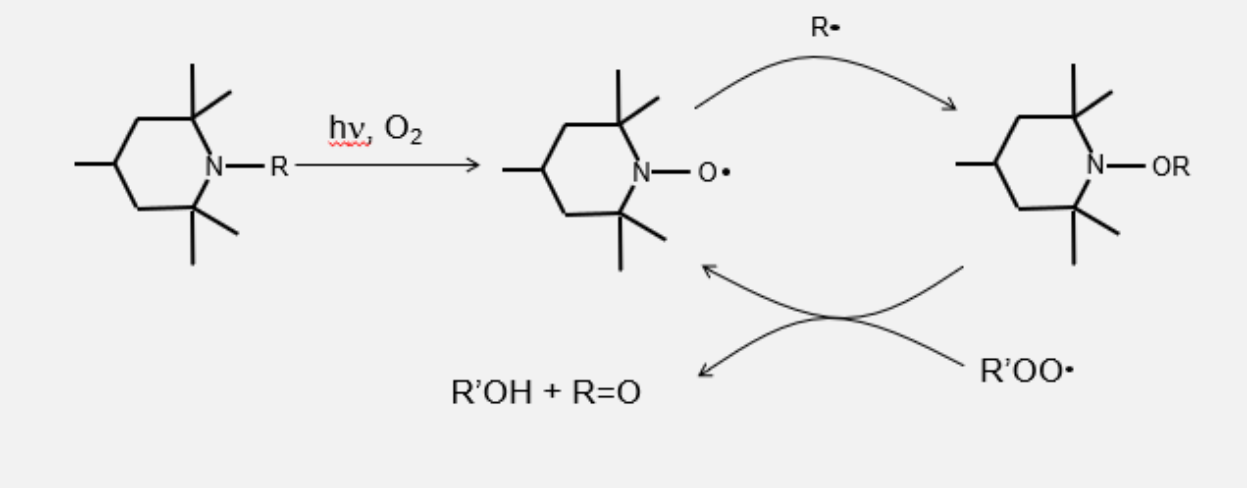

Figure 1.7-*Process through which HALS mop up free radicals* (49)

Figure 1.7 shows how HALS "mop up" radicals, in a process known as the Denisov Cycle. This cycle shows that the HALS can be used multiple times, reforming once they have interacted with radicals. However, they cannot carry out this process ad infinitum, as they are only able to recombine until the attached chain has been degraded. Hodgson et al claim that this is a simplified representation of the Denisov cycle, their research showing that there are multiple reaction pathways leading to more than 30 potential reactions which all contribute to the overall mechanism of free radical scavenging. The different reactions occur at different rates, which are influenced by the reaction temperatures. (50)

It is clear that both UV absorbers and HALS have strengths that are important for extending the service life of polymers and have been added in combination in recent years in an effort to utilise the strengths of both types of additives and bolster their respective weaknesses. However, these expectations have been exceeded as studies have made it apparent that combining HALS and UV absorbers have a synergistic effect, whereby the combined effect is greater than the sum of each of the individual additives. Shenoy et al found that the service life of coatings stabilised with combinations of UV absorbers and HALS exceeded that of coatings that only contained one or neither of the additives. (51)

Shenoy et al go on to explain that the reason that UV absorbers and HALS work well together is that they target different areas to prevent degradation. UV absorbers reduce the rate of the initial stages of polymer degradation; therefore, they provide the higher levels of resistance to yellowing. The HALS then scavenge the free radicals that are formed during polymer degradation. (51)

Guo et al performed a similar investigation into the effect of HALS and UV absorbers used in combination on plasticised Poly Vinyl Chloride (PVC). They found that PVC with HALS and UV absorbers outperformed PVC with HALS or UV absorbers and that the combination showed a significant amount of synergism which was attributed to the different stages of degradation at which the additives function, agreeing with the findings of Shenoy et al above. (51,52)

1.9-Analytical techniques for measuring degradation

There are many techniques available for the analysis of coating degradation, each with their own advantages and limitations. This chapter investigates these techniques to determine the most effective way that they can be used.

1.9.1-Weathering tests

One of the more crucial tests to determine degradation caused by UV radiation is via the accelerated testing offered by UV Accelerated Weather testing (QUV and ATLAS) apparatus. As the name suggests, the cabinet exposes samples to a limited range of UV radiation, allowing for long term effects of UV exposure to be analysed in a relatively short period. And can aid in determining the UV resistance of a coating under a variety of different environmental conditions. (53)

Laboratory based accelerated weathering tests do provide advantages, such as the potential to carry out simultaneous experimentation on a sample, prevention of contamination of sample, and results obtained much faster. However, the simulation of natural weathering is extremely difficult because of the many conditions such as temperature, humidity, and precipitation that can alter subtly over extremely small areas. This increases the difficulty in emulating these conditions within a laboratory environment. The British Standards Institute (BSI) published BS 7543:2015, which governs how to perform weathering tests in a laboratory setting by listing various variables (such as temperature, light exposure conditions, precipitation) that need to be considered. By taking the averages of these conditions and applying them to the laboratory experiment it minimises the potential for the laboratory exposed samples to undergo a different degradation pathway than if it were naturally exposed. (54,55)

If the real-world conditions are not considered, then there is the potential for the results of laboratory exposure to differ significantly from natural exposure. An example of this is the laboratory testing of

automotive coatings, which were irradiated with UV radiation while immersed in either a Hydrogen Peroxide solution or concentrated Oxygen and water vapour. While it was estimated that the team achieved an acceleration factor of 100, the conditions were extremely different to those that the coating would normally meet. This encourages different degradation pathways to be used, limiting the relevance of the laboratory results. (54)

The radiation source is of the utmost importance for accelerated UV exposure, as different lamps simulate different environments. UVA-340 bulbs provide the best mimicry of sunlight, but do not cover the full range of light types observed in sunlight, opting to focus on UV. UVA-351 bulbs are capable of simulating exposure of sunlight through a window, so a more diffuse light that causes less damage. UVB-313 bulbs are the most aggressive bulb type, offering levels of exposure that are not observed on the surface of the earth, so while this lamp will cause accelerated weathering, it is highly likely to cause additional damage to the sample that would not be otherwise observed. (54)

The strengths of the accelerated weather testing are that it can expose the sample to UV radiation at an accelerated temperature, making it possible to determine the degradation of years of exposure in a relatively short period, as well as able to mimic a wide range of environmental conditions and locations. However, there are several limitations with the process, such as the risk of unequal exposure if one of the bulbs fails. (53)

Wypych confirms these strengths and issues before continuing to state that it is not feasible for accelerated weathering to fully emulate the environment that the sample will be used in as there are too many variables that cannot be accurately predicted (such as minor alterations in humidity, precipitation, and heat). However, it is possible to use the results of accelerated testing to predict how the sample will behave in a real-world environment as the same degradation pathways are followed due to UV initiated excitation. Wypych shows that both real-time and accelerated weathering testing will reveal the sample with the lowest level of degradation, but that it is common for the sample subjected to accelerated testing to have suffered additional damage. The main advantage of accelerated weather testing is the rapid turnaround time of samples, allowing for samples to be subjected to weathering and the follow up analytical tests more rapidly, the results of which can be implemented into the design of second generation samples. (56)

Carmona-Quiroga et al validate this claim through their analysis of the ‘‘durability of anti-graffiti coatings on stone through natural and accelerated weathering’’ which provided visual evidence of the additional damage suffered by a sample following 2000 hours of UV exposure compared to one naturally exposed for 1 year. It was also found that the naturally exposed sample reached undesirable levels of degradation

in 9 months, whereas the accelerated testing sample reached the same point after only 500 hours' exposure. While some of this degradation may be due to the use of UV-B radiation for the accelerated sample, which is far more severe than the radiation that samples are exposed to on the earth's surface, the variation in the results must be remembered and taken into account when analysing samples from accelerated testing that the samples will have suffered more damage than if they were exposed naturally. (57)

The study concludes that the best practice would be to perform natural and accelerated weather testing on identical samples to gain more understanding into sample aging. QUV remains a staple of weathering analysis based investigations, due to its relative simplicity coupled with its modification friendly design, allowing for additional components to be added that facilitate other environmental factors, such as direct water spraying. (58)

It is worth considering at which point during a QUV cycle the samples suffer the most damage. This point is when the humidity cycle has finished, and the UV exposure has just started. This is the most damaging point due to the presence of water on the samples, which when combined with the energy supplied via UV lamps, initiate moisture-enhanced degradation. Moisture enhanced degradation will continue until the substrate is hot enough to evaporate the droplets from its surface. The presence of moisture adds a layer of complexity to the degradation process, as was noted by Nguyen et al during their investigation into the photodegradation chemistry of acrylic melamine coatings. (59) This builds on the work of Bauer et al, who showed that moisture enhanced degradation was more aggressive due to the increased numbers of free radicals produced via UV excitation. Nguyen et al go on to state that the rate of photooxidation is linear to the hydroperoxide (OH·) concentration. (59,60)

1.9.2-FTIR analysis

Fourier Transform-Infrared Radiation spectroscopy (FT-IR) is one of the better-known analytical techniques and can be used to characterise degradation processes and FT-IR microscopy can show areas of chemical difference on the surface of the sample, providing information on the rate of degradation as well as the chemical reactions that are occurring, facilitating additional understanding of how the sample is degrading. Qualitative analysis via FT-IR makes the rapid identification of resin and coating systems, as can the chemistry that is related to weathering degradation.

FT-IR exposes the sample to all Infrared (IR) frequencies simultaneously and measures the vibration of IR active bonds. It is also possible for FT-IR to produce results of a suitably high resolution to show the functional groups that are present within the sample, although high resolution spectra cannot be obtained with FT-IR. FT-IR can produce clear results for the changing dipoles of organic covalent molecules.

However, it can encounter issues identifying symmetric vibrations where the dipole moment does not change, as this sort of vibration is not very IR active. (61,62)

1.9.3-Raman spectroscopy

Like FT-IR, Raman spectroscopy can also provide spectroscopic analysis of the sample and its degradation processes. By identifying the functional groups that are present during analysis, it can be used to highlight the underlying chemical processes of the degradation. Raman spectroscopy has been utilised in recent studies to monitor the curing pathways of coatings, providing a real-world example of its applicability within coating analysis.(63)

Raman spectroscopy exposes the sample to monochromatic light and measures the resultant scattered light for small colour changes. Although most of the light will not have altered frequency, a small amount will have. This change in Stokes and Anti-Stokes lines is due to interactions with molecular vibrations during exposure and signals that the photon has undergone energy loss or gain. This change in frequency can yield information about the chemical structure of the sample. (64)

An advantage of Raman spectroscopy is that the results that it produces are complimentary to those produced by FT-IR, which means that in combination, the techniques can provide a clear representation of the chemical processes occurring within the sample and how they are altering its structure.

The limitations of Raman spectroscopy are that it relies on weak signal alterations, which have the potential to be missed if high levels of background noise are experienced. When used in 2D mode, it is very sensitive to the electronic structure of the sample, which could result in altered results. (64)(61)

1.9.4-Glass transition temperature

Understanding the T_g is of critical importance when considering how the rate of degradation can be affected by various environments. If the T_g is lower than the temperature of the environment, then the resin will become softer. This will cause issues with micro-hardness, as the resin will be easier to damage and remove, therefore providing less effective protection for the substrate.

An insufficient T_g can also result in the resin becoming "tacky" which is caused by the ambient temperature surpassing the T_g for the coating, causing it to begin to melt and flow. This can cause significant aesthetic issues in environments with large, airborne particulates, such as properties located near sand, as the sand could attach to the resin, decreasing the aesthetic nature of the coating in addition to its protective qualities.

A low T_g is also of concern in hot, humid environments due to the increased depth of water droplet penetration into the resin. It is known that water causes moisture enhanced photodegradation, therefore

the increased penetration allows additional exposure of the polymer chain to the moisture, resulting in more advanced degradation than would otherwise be seen.

Due to the degradation of the polymer backbone during exposure, it would be expected for the T_g to decrease following exposure. However, the limitation of T_g measurement is that it is destructive for the sample, as the resin layer will have to scrapped from the substrate. This means that there is potential for the sample to be contaminated by any underlying coats. However, the impact that such small quantities would have is minimal, the main concern would be having exposed areas of the substrate, which would allow for increased rates of degradation in further testing, skewing the final results of the investigation.

1.9.5-UV-Vis analysis

It is also important to understand the behaviour of the coating across the Ultraviolet-Visible (UV-Vis) light regions, as the degree and range to which the coating absorbs light within these regions has a significant impact on its susceptibility to weathering, as has been discussed previously within this chapter. The energy absorption leads to the excitation of electrons, causing them to move from the HOMO (Highest Occupied Molecular Orbital) to the LUMO (Lowest Unoccupied Molecular Orbital). However, for this electron transition to happen the absorbed energy must be the same as the gap in energy between the HOMO and LUMO.

Lowe agrees with this before continuing to discuss Allowed and Forbidden electronic transitions.

Forbidden transitions provide a small absorption peak, which is due to the transition from a singlet ground state to a triplet excited state.

Transitions are allowed if they are of the same symmetry, such as $\sigma \longrightarrow \sigma^*$ and the interatomic distance and nuclear kinetic energy must remain the same, following the Franck-Condon principle.

Singlet-Triplet (and Triplet-Singlet) transitions

Singlet states contain electrons that have opposite spins and are normally paired, whereas Triplet states contain electrons with the same spin and are therefore prevented from pairing. So triplet states are of lower energy than the singlet state for the same molecule due to electrons being in different areas of space or having a greater avoidance tendency than what is observed in singlet states.

In all compounds other than alkanes, several electronic transitions are possible at different bond energies, as can be seen below in decreasing order:

$\sigma \longrightarrow \sigma^*$ In Alkanes

$\sigma \longrightarrow \pi^*$ In Carbonyl compounds

$\pi \longrightarrow \pi^*$ In Alkenes, Carbonyl compounds, Alkyne compound

$n \longrightarrow \sigma^*$ In Oxygen, Nitrogen, Sulphur, and Halogen compounds

$n \longrightarrow \pi^*$ In Carbonyl compounds (Normally "Forbidden")

UV absorption occurs over a variety of wavelengths as molecules tend to have multiple possible modes of excitation. Absorption spectroscopy follows simple rules, in that the greater the number of molecules capable of absorbing light at a certain wavelength, then the greater the degree of absorption will be, and the more efficiently a molecule absorbs light at a specific wavelength then the greater the degree of light absorption will be.

It is also possible for substituent groups to influence the position and intensity of the absorption band. The influence of substituent groups can be divided into five different effects:

Auxochromic shift – Increase the intensity of the absorption

Bathochromic shift – A shift to a longer wavelength

Hypsochromic shift – A shift to a shorter wavelength

Hyperchromic shift – An increase in absorption intensity

Hypochromic shift -A decrease in absorption intensity

It is known that many compounds absorb very strongly within the UV regions, which can make analysis of the UV region difficult. Lowe argues that in order to obtain useful information the compounds must be analysed in weak solutions in order to obtain useful information. However, using solutions also bring with them their own issues, as many solvents contain chromophores which can influence the UV-Vis results that are obtained. Therefore, the best solvents to be used are those that contain chromophores that absorb at wavelengths lower than those of interest, such as water, Hexane, or Acetonitrile.

1.9.6-Gel permeation chromatography

Gel Permeation Chromatography (GPC), also known as size exclusion chromatography (SEC), is of great importance for the analysis of resins and is used to determine the size of the molecules that are formed during the polymerisation process. This is important because polymerisation doesn't create resins of

identical sizes, as some growing chains are able to ‘‘capture’’ more of the base monomer than other chains, meaning that a resin will contain polymer chains of a range of molecular weights.

GPC is a variation of the process used in High Performance Liquid Chromatography (HPLC) and uses a column packed with an inert, porous, and highly crosslinked gel as a substrate. This column is between 30 and 60cm long and of wider bore than those used in HPLC. The substrate contains pores of different sizes which only allow molecules below certain sizes into the pore, ensuring that the larger the molecule is then the lower its residence time will be as it would be unable to access as many pores. (65)

There are two common expressions for the molecular weight as measured through GPC, and they are calculated as follows:

Number average Molecular Weight (Mn)	$Mn = \sum_i n_i(Mn)_i / \sum_i n_i$
Weight average Relative Molecular Weight (Mw)	$Mw = \sum_i m_i(Mw)_i / \sum_i m_i$
Where m_i is equal to the mass of the component present	$(n_i * Mn_i)$

While it is not the only factor influencing market interest, the appearance of a coating is of great importance from an industrial standpoint, as a paint that has a low aesthetic appeal is unlikely to receive a large demand. However, the appearance of a coating is not simple, as there are multiple factors that exert an influence. The colour of a coating is governed by the spectral absorption and diffuse reflection of light by pigments within the coating system. The relationship between the physical structure of a material and the resulting optical properties is complicated. However, the property that most strongly impacts colour is selective absorption which occurs as light travels into and through the coating. The scattering of light occurs when the light interacts with interfaces between the resin and pigment particles.

1.9.7-Gloss analysis

Most coatings reflect some light from their surface, which is observed as gloss or haze. Gloss is commonly thought to be independent of colour, but it is possible for it to be influenced by the colour of the coating (due to the pigment size). This is because gloss can also be considered as a representation of the surface roughness, with a greater degree of surface roughness resulting in a lower gloss measurement and as larger pigments dispersed within a coating have the capacity to influence the roughness of a surface then they can impact the gloss levels. There are multiple factors that need to be considered when measuring gloss, it is a complex property and as such cannot be given on a linear scale.

Some of the factors that influence gloss are:

- The intensity of the specular reflection or brightness at or close to the specular angle.
- Distinctness of images, which is the amount of detail of a pattern that can be resolved on the surface of the coating.
- The grazing incidence sheen, which is a preferential reflection near the specular angle for light at near grazing incidence angle.

1.10-Reliability of laboratory tests

Batista et al investigated the effects of photooxidation on polyester-melamine coatings relating to coil coatings by investigating four different diacid monomers used in conjunction with a commonly used melamine. The polyester resins were formulated to 60% NVC (solid or Non-Volatile Content) and to have a Hydroxyl Value of 98. By ensuring that the only variations between the formulations was the diacid monomer, it allowed the degradation analysis to focus on the relative impact of the monomers, without influence from other aspects of the formulation. The monomers that were investigated were Isophthalic Anhydride (IPA), and mixtures of Hexahydrophthalic Anhydride (HHPA) with (i) Terephthalic acid(TA) , (ii) Phthalic Anhydride (PAN, (iii) 1,4 Cyclohexanedicarboxylic acid (1,4-CHDA). (4)

The results that Batista et al obtained are in line with the claims of previous literature that degradation occurs at different rates across the film, rather than in a uniform pattern. In addition, their results indicated that there was a self-catalysis occurring within the photooxidation reactions, this was inferred from the Photooxidation Index (POI) directly related to the number of degradation cycles that the samples had undergone. However, there are two issues with the investigation, the first will be discussed immediately, with the second issue investigated later in the text. The first issue is that although the aim was to investigate polyester-melamines as used with coil coatings, the coatings were applied to glass rather than metal sheets. This was done in order to 'enable the removal of the film for characterisation.'(4) It is possible that the substitution of glass in place of metal impacted the way that the coating was cured, potentially limiting heat transfer from the substrate to the coating and therefore impacting the chemical crosslinking process between the polyester and the melamine.

Batista et al obtained characterisation results using a glossmeter, Fourier Transform-InfraRed spectroscopy (FT-IR) and optical microscopy. FT-IR is only able to identify bonds that have a change in their dipole moment during vibration. This means that the structures need to be stretching asymmetrically to be identified via IR analysis. It has become common for Raman spectroscopy to be used alongside FT-IR as the techniques are complimentary, with each technique supplying information that the other is

incapable of recording. While it is not a requirement to examine samples using FT-IR and Raman spectroscopy, the additional information can assist in determining all of the chemical processes that occur as a result of exposure.(64) Zhang et al provide an example of the usefulness of Raman spectroscopy in the analysis of polyester-melamines through the study into the melamine distribution within the applied coating. It is possible for the melamine to self-condense within the coating, which results in areas of melamine enrichment. Zhang et al were able to study the melamine distribution in both clear and pigmented coatings using confocal Raman spectroscopy in a way that is not possible with surface scanning techniques, such as FT-IR and XPS. (32) Raman analysis showed four bands that related to bonds within the melamine, with a peak area ration being employed to calculate the amount of melamine present, the peak area ratio compared the band for the melamine ring against a strong polyester peak, allowing the relative amount of melamine within the coating to be calculated. (32) By not analysing samples via Raman spectroscopy, it is possible that Batista et al discounted an important factor as a large amount of melamine self-condensation can affect the performance of the coating. (32)

The use of Raman alongside IR analysis is well documented, with Young et al stating that 'Raman spectroscopy complements IR in that band vibration modes that are IR active tend to be weak or inactive in IR spectroscopy and vice versa.' (66)

It is possible that applying the coating to glass impacted the end results of the investigation, as it impacted the second issue with the investigation. Batista et al cured the coated samples in an air circulated oven at 265^{o}C for 160 seconds, which resulted in the samples reaching a measured temperature of 241^{o}C. The paper claims that the process was performed this way to simulate real world coil coating and curing conditions using a high speed and high temperature process. Sander states that 'Typical temperatures and times for the fast coil coating process are 240^{o}C and some 30 seconds…' before continuing to say that over-curing can result in brittle films, poor adhesion properties and, in extreme cases, yellowing of the film. (1)

In a study that investigated the distribution of melamine within four polyester-melamine formulations for coil coating, Zhang et al coated metal substrates, stating 'All samples were prepared using a standard coil coating simulation method.'(32)

The samples were cured in an electric oven for 30 seconds, this enabled the substrate to reach a peak metal temperature (PMT) of 232^{o}C before being quenched in tap water and air dried. This follows a more real-world procedure for what the coating would be subjected to on a coil coating line. By exposing the samples to quenching and drying procedures, which have the potential to influence the coating, Zhang et al were able to produce samples that more accurately mimicked the structure of a large-scale industrial

process. By comparison, Batista et al make no mention of any quenching process, likely due to their choice of substrate being unsuitable for rapid temperature fluctuations, giving further evidence that the substrate they chose was unfit for purpose as it did not provide the same characteristics of a metal substrate. (1,4,32)

This could potentially explain some of the damage that Batista et al observed during their investigation, with some samples exhibiting severe cracking following exposure.(1,4) It is also worth mentioning that the removal of the coating was not essential for characterisation, as film thickness could have been determined through cross-sectional analysis of punches taken from a metal substrate that had the coating applied.

Batista et al also failed to naturally expose samples, choosing instead to rely entirely on accelerated UV exposure in the form of an ATLAS weather-Ometer using a Carbon electrode as the UV light source. (4) Batista et al are not alone, many investigations rely solely on accelerated weathering machines, such as Hwang et al, who studied 'Scratch resistant and Transparent UV protective coatings on polycarbonate' by exposing samples to 3600 hours of UV exposure using a Xenon flash lamp. (67) Katangur et al also relied on accelerated weathering for their UV exposure during their study of 'Nanostructured Ultraviolet resistant polymer coatings', opting for a Q panel UV weather-Ometer for cycles of 4 hours of UV and 4 hours of condensation. (68)

Accelerated exposure does have advantages, as results can be obtained much faster than via traditional exposure and contamination is less of a concern. However, it does not provide the same level of information that a naturally exposed sample will. Cocuzzi and Pilcher, in a joint study between the ASTM and the National Coil Coatings Association, looked at the variation between the durability of samples exposed naturally for 10 years with those exposed in accelerated weathering devices. Cocuzzi & Pilcher exposed samples for 10 years, obtaining data at 2,3,5, and 7-year intervals in addition to the final 10-year sample, within this period they also ran accelerated weathering tests using Xenon arc, UV-B 313nm and UVA 340nm UV sources and found that no accelerated method can correlate with 10 years of real world exposure, and that the most reliable method of anticipating the results of 10 years of natural exposure is 7 years of natural exposure. The recommendation of the investigation was to expose samples as quickly as possible using natural exposure to build up exposure levels and aid future predictions. (69)

Wypych agrees with the findings of Cocuzzi and Pilcher, continuing to state that 'We want to perform studies in the minimum possible time and under well controlled, repeatable conditions. It is not reasonable to expect that accelerated weathering conditions will simulate natural weathering conditions.'(56) Wypych follows this with the claim that the results obtained from natural exposure can

also be extremely misleading, as '…Testing materials in a tropical climate…does not expose them to the proper natural conditions if the material will be used in Alaska.'(56) This raises the point that it is difficult to predict how a material would react in any environment without placing a sample in that environment. This is due to local fluctuations in pollution, light intensity, rain, pH, humidity, and numerous other factors, all of which have the potential to influence the rate of degradation. Smith has also reported on this, stating that results can be very specific to specific locations, due to variations in the levels of these factors. Smith also agrees that QUV A testing shows poor correlation with 2 years of natural exposure and that there was a large amount of variation between different natural exposure sites, with some correlating with each other and others showing little similarity despite relative proximity to each other. (49)

Wypych claims that the most important characteristics to look for when choosing an accelerated weathering method are to have the highest accelerating factor and initiate the same major degradation mechanisms that would cause the sample to degrade during natural exposure. Both Wypych and Cocuzzi & Pilcher show that accelerated weathering tests cause a greater degree of degradation than is observed through natural exposure, but that the most severe degradation is caused by Carbon arc and UVB sources. (56,69)

Katangur et al used UVB-313 bulbs as the UV source of UV light for accelerated exposure.(68) Wypych concedes that UVB lamps subject samples to radiation that they would not otherwise come into contact with, before going on to mention a study comparing accelerated exposure of UVB lamps with natural exposure in Brisbane. This study found that the natural exposure was more severe than that of the accelerated exposure, with both resulting in the same degradation product, which is indicative of the same degradation mechanisms being followed. This result was explained by the high temperatures that the natural samples were exposed to, which is believed to have had an effect on the dehydrochlorination rate of the samples. (56) This provides evidence for the importance of considering the other influences that a sample is subjected to during natural exposure that are absent in accelerated laboratory tests. It is accepted by Wypych and others that it is best practice to have samples exposed via natural exposure alongside those exposed via accelerated weathering tests. This allows for the determination of the main methods of degradation, and ensuring that they are the same via both methods, giving more validity to the accelerated weathering studies. (56)

An example of this good practice has been exhibited by Carmona-Jacobs et al, who were studying the durability of anti-graffiti coatings on stone via both natural and accelerated weathering methods. While this method doesn't relate strongly to coil coats other than that anti-graffiti coats can also be applied it does provide a working example of good practice, with samples being exposed for 1 year at a site in the

South of England while simultaneously, samples were exposed in a QUV chamber for 2000 hours. The investigation monitored changes in colour, gloss, water-repellence, roughness and micro-structure periodically during the experiment.(57)

To summarise, accelerated and natural weathering tests used in conjunction with IR, Raman, gloss and colour measurements make it possible to identify and track the major degradation pathways of coating systems and allow for the identification of which coating systems demonstrate poorest levels of weatherability.

1.11-Potential areas of research and studies within the field

The following section will focus on the areas and drives of current research in UV degradation prevention, in addition to any of their limitations, and potential avenues of further research within the field.

1.11.1-UV resistive coatings utilising additives

In 2003, Hwang et al performed an investigation into a novel scratch and UV resistant coating to be applied to polymers that retained effective adhesion during thermally initiated expansion. This coating was developed through the combination of acetyl acetone chelated silanes and modified nano-titanium sols, which were utilised as the UV protective materials through the generation of Sol-gels. A network was formed by the controlled hydrolysis and condensation of Methyl Tri Methoxy Silane (MTMS) and Di-Methyl Di-Methoxy Silane (DMDMS). Titanium Dioxide (TiO_2) was then dispersed within the coating to improve UV resistance. The produced sols are then modified via 3-glycidoxypropyl-trimethoxysilane (GPTMS). The improved adhesion during thermal expansion was obtained through plasma treatment, meaning that an additional step was required to make the coating fit for purpose, increasing production time. (67)

By analysing samples coated with the novel coating against non-coated polycarbonate samples following 3600 hours of accelerated UV exposure, it was possible to see that the novel coating provided significantly improved resistance to scratching and discolouration with increased volumes of the coating applied that varied by altering the amount of GPTMS used to modify the sol-gel, as can be seen in Table 1.2.

Table 1.2-*Influence of altering GPTMS on coating characteristics*

GPTMS content (wt.%)		0	5	10	20
Property	**Pencil Hardness**	5H	6H	5H	5H
	Abrasion Hardness	1.3	1.7	1.8	2.5
	Yellowing resistance	1.6	1.9	3.6	5.6
	Crack presence	Yes	No	No	No

Table 1.2 shows that there is a general improvement in the desirable attributes of the coating with increasing amounts of GPTMS, the only exception being the increase of the Pencil Hardness at 5%wt to 6H, before dropping back to 5H for the higher amounts. This was not explained, and the paper states that the highest pencil hardness attained was 5H, so the higher result was potentially discounted as anomalous.

It was found that the GPTMS modified coating suffered a slower rate of yellowing than the uncoated film, but a higher rate of yellowing than the coated film that had not been modified. This indicates that the resistance to yellowing is not an outcome of the GPTMS modification, and was attributed to the presence of the TiO_2 nanoparticles that were dispersed into the sol-gel prior to modification. (67)

The conclusions of this investigation stated that TiO_2 has the potential to act as a UV blacking material to prevent degradation and that the addition of GPTMS modification allows for the film to remain crack free following extending UV exposure. (67)

Katanguer et al have also utilised the UV resistive properties of TiO_2 throughout their investigation into nanostructured UV resistant polymer coatings. The aim of their investigation was to design and develop acrylic coatings with high UV absorption and very low levels of light dispersion to prevent material degradation using Zinc Oxide and Titanium Dioxide nanoparticles. (68)

The investigation involved the testing of the mechanical and chemical properties of coated and non-coated Kevlar fabric following 1 day and 1 week of exposure via strip and tear tensile testing, UV, Visible + IR spectroscopy and wide/small angle X-ray analysis.

This investigation was novel because most additives, like free radical quenchers, were unsuitable for use as they had the potential to have a negative effect on the chemical and physical properties of the fabric. Chemical UV stabilisers were also unsuitable due to their relatively short lifetime, which would make them unsuitable for a product that is expected to have long lasting durability and strength retention.

The nanoparticles had a size range of 15 – 70 nm and the final film thicknesses ranged from 10-20μm on the Kevlar fabric. The coatings were applied via the wire bar technique, which enabled uniform coating depth to be applied to the small samples.

The mechanical tests showed that without the addition of nanoparticles the Kevlar only retained 67% of its strength after a week of exposure, whereas with 10%wt nanoparticles the fabric lost 19% after 1 day of exposure and 20% after a week, showing 80% retention. The 20%wt nanoparticle coating showed a loss of between 3-5% following a day and a week of exposure. These results indicate that the nanoparticles have a significant effect on the improvement of the longevity of the substrate.

The absorption spectra of all the nanoparticle embedded films behaved similarly, with no or negligible observed changes after a week of UV exposure. This indicates that the nanoparticles retain their ability to absorb UV following extended exposure, so can provide protection to the substrate for an extended period. This is an advantage over other UV absorbers, which tend to lose their efficiencies over time.

The FT-IR analysis of the Kevlar fabric provided significant results, giving information on the degradation of the amide linkages, which is caused by free radical attacks. The absorbance peak that corresponded to the amide linkages was located at 1632 cm^{-1}, analysis of neat Kevlar gave a value of 0.374, which decreased to 0.200 after a week of UV exposure, showing a decrease of roughly 46%, which is believed to have been caused by amide linkage degradation. The average absorbance decrease in the 10μm coatings was 10%, and 5% decrease for the 20μm coatings. This indicates that the use of nanoparticles has a significant effect in the prevention of photo-oxidation and free radical attack. (68)

This investigation yielded significant results, indicating that nanoparticles such as TiO_2 can be used to extend the life of substrates in situations where other UV stabilisers may be unsuitable.

The drawback of the above investigation has been the chosen method of UV degradation, QUV via UVB 313 and UVA 350 bulbs. This bulb combination is inappropriate for simulation of the environments that the material would be used in, this is because UVB 313 bulbs emit a significantly harsher type of radiation than is typically found on Earth, this results in a significantly higher degree of degradation to the coating than would be observed in a real-world environment. In addition to this, UVA 350 bulbs are adequate at simulating natural light through a diffuse medium such as windows but are not the best UV bulb for the simulation of natural light. To have validated these results the team could have also produced samples that were exposed to natural light for an extended time, this would indicate whether the same degradation pathways were followed and shown that the accelerated exposure produced results that were indicative of real-world events. (56)

Another drawback is the way that the results have been described for the tear strength retention. The initial tear strength of neat Kevlar is recorded in the text, whereas the tear strength of the coated samples is only referenced in graph form. The information could have been more clearly laid out in tabular form and eliminated the potential for confusion.

Mahltig et al utilised the UV absorption properties of TiO_2 in conjunction with organic UV absorbers through the Sol-Gel technique. This investigation hoped to utilise the fact that different UV absorbers have absorption bands within different wavelengths and that, by combining multiple absorbers into one coating, a coating that offered a greater range of UV protection might be produced.

The ideal UV absorber is one that absorbs across the entire UV spectrum while remaining invisible in the visible region and converting the absorbed UV light energy into heat. They go on to state that a combination of UV absorbers is required as no single UV absorber can achieve full absorption of UV light while retaining no visibility within the visible region.

Combining only organic UV absorbers would not yield the desired effect because they will only be able to absorb within specific bands, this is due to the absorption bands of the molecules. It is far more common for inorganic UV absorbers such as TiO_2 or ZnO to be used as pigments or a pure oxide layer but are only able to absorb light of a higher energy than that of their bandgap energy values. Combining inorganic and organic UV absorbers also provides a benefit for the inorganics, as through the sol-gel technique it is impossible for inorganic coatings to not suffer from high transmission within the Near InfraRed (NIR) region but introducing organic absorbers can circumvent this issue if they have absorbance bands within this region.

The coatings were developed in several steps, the organic UV absorbers Tinuvin 213™/CIBA (Organic Absorber A) and SEMA20163™/Sema GmbH Coswig (Organic Absorber B) could be applied without purification or preparation steps, while the inorganic coatings were prepared via the sol-gel technique.

The Sol-gel technique was used as it is a long-established method for the preparation of inorganic coatings (having also been used by Katanguer et al), three separate inorganic sol-gels were produced. Sol-gel 1 only contained the inorganic absorber TiO_2, sol-gel 2 contained both TiO_2 and SiO_2 and the final sol gel contained only SiO_2. Following production, Organic absorbers A and B were dissolved into the prepared solutions (the sol gels having been diluted with ethanol), Organic absorber A in the range of 1.0-7.0 %wt and Organic Absorber B in the range of 0.1-1.25 %wt. Following this, the substrates where then dip coated at 30cm/minute before being dried at room temperature and thermally treated for 1 hour at 120°C.

The individual coatings were analysed, as were coatings that were comprised of combinations of the organic and inorganic coatings. Sample analysis showed that Organic Absorber B must be embedded in

lower quantities to prevent chalky formations, for a clear coating to be formed, a maximum of 0.1%wt of Organic Absorber B can be used. However, up to 1%wt can be used in conjunction with acetonic PMMA solution. The low concentration of Organic Absorber B means that a high transmission (T) of more than 20% was observed for wavelengths (λ) below 300nm, indicating that Organic Absorber B is unable to provide sufficient UV protection in this region to be viable, whereas Organic Absorber A is capable of lowering T to lower than 6% in the region λ< 350nm.

The TiO_2 layer reduced T<10% for λ<275nm, which can be moved towards 325nm by increasing the TiO_2 coating thickness, which correlates with the findings of Katanguer et al, that increasing the thickness of the coating layer results in improved UV degradation resistance. This behaviour was also observed in the TiO_2:SiO_2 sol-gel, with increasing levels of UV protection resulting from decreasing SiO_2 levels. (68,70)

The best results were obtained through the combination of Organic Absorber A and TiO_2 sol-gel, whereby the amount of UV transmission decreases with increasing levels of the absorber. At 1%wt Organic Absorber A and 110nm film thickness produces almost no transmission in the UV region and has significantly better UV absorbance than 0.5%wt, as shown in Figure 1.8. (70)

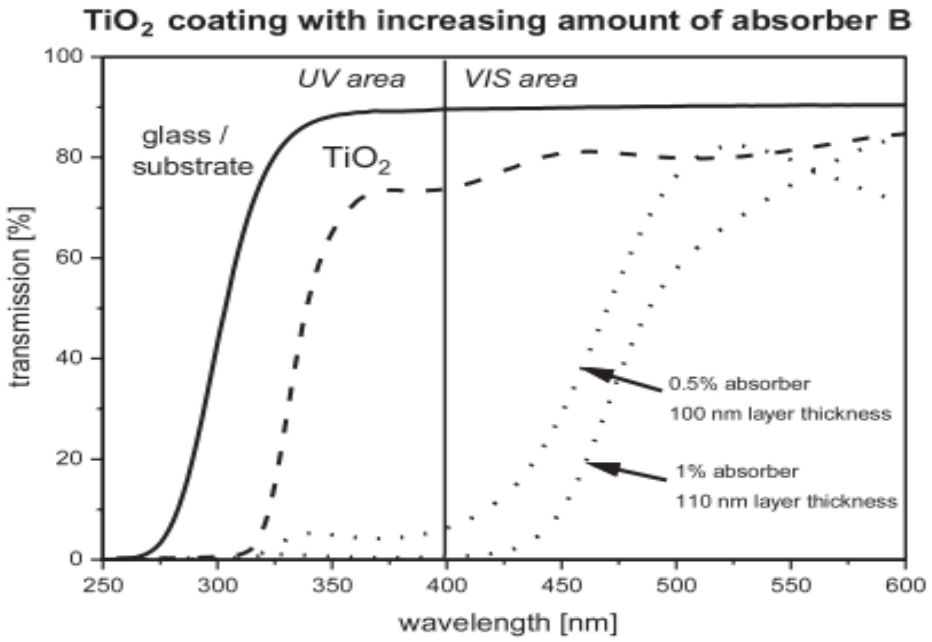

Figure 1.8- *Influence of absorber percentage and layer thickness on transmission* (70)

From Figure 1.8, it is possible to see that the 1%wt sample does allow for slightly higher transmission at the high end of the visible region than its 0.5% wt counterpart, however the levels of transmission do not increase further than that of TiO_2 or of the uncoated substrate. It also shows the significant difference in

transmission spectra between a lone TiO_2 sol-gel coating, and one that has been combined with Organic Absorber A. TiO_2 coating alone allows a transmission of over 70% at roughly 360nm, the corresponding transmission for the Organic/Organic Sol-gel combination was approximately 1% or lower. At no point within the UV region does the Inorganic/Organic coating allow more than 5% transmission, it also allows for significantly lower transmission within the visible region, although the transmission levels rise to equal TiO_2 at 600nm.

This paper concluded that an inorganic and organic combination coating can provide significant reduction of UV transmission, but also causes a decrease in the transmission of visible light, and as such other coatings may be preferable. While this may be the case for clear plastic or glass coatings that high visible transmission is desirable, it may be possible that the lower Vis transmission will allow this coating to be a viable choice for the resin components of paints.

To summarise

1.11.2-UV resistive coatings using different monomers

All the above areas of research attempt to bolster the coating to counteract the limitations of the pure coating. The most effective method of improving the UV resistance of the polymer coating is to alter the chemical structure of the coating. An example of an addition to the coating is HHPA but, as has been discussed above, there are significant health effects relating to its use.

Batista et al attempted to determine the most effective polyester:melamine coating in 2010. The investigation showed that the greater the number of Hydrogens at these locations, the greater the potential for Hydrogen removal via photo-oxidation reactions, which in turn can lead to faster free radical generation.

The conclusions of this investigation are extremely useful, especially when applied to the continued development of polymeric coatings. By confirming that the number of Hydrogens is indirectly related to the rate of photo-oxidation and degradation, it promotes a new avenue of compound combination development in the prevention of UV degradation through the development of monomer combinations that provide high levels of UV resistance while having the minimum levels of Hydrogen atoms, lowering the amounts of Hydrogens that can be removed via photo-oxidation reactions to produce free radicals. (4)

1.12-The use of computational chemical modelling

Computational chemical modelling has seen a sharp increase in use within the last 2 decades led by the continued advancement of computer systems and the development of multiple computational chemical modelling programs, such as ORCA and Avogadro. Computational modelling can serve as an aid to traditional experimental research, particularly by offering insights into the system that would otherwise be unknown. This is highlighted in research performed by Akbulatov *et al*, who performed model studies into the kinetics of ester hydrolysis under stretching forces. By combining computational calculations with experimental data they were able to determine that stretching ether group containing polymers does not impact on its hydrolysis kinetics. (71) Another examples is identified through the work of Rossi *et al*, who worked on MARTINI coarse grained modelling of a thermoset polyester coatings and successfully presented a coarse grained model of a typical polyester resin through combining the results of thermodynamic and mechanical tests into coating properties with molecular dynamic simulations. (35)

However, computational modelling is not without its limitations. They rely on multiple approximations and assumptions, this in turn can make it difficult to determine the uncertainty factor for obtained results. It is also possible for errors to combine in unanticipated ways and cause total errors within the model, which is observed in DFT (Density Functional Theory). (72)

As mentioned above, the MARTINI method is used to develop coarse-grained models, these models work by grouping atoms together into interaction sites, causing the model to focus on the more prominent features while generalising less important regions. However, these generalisations can cause several issues, such as the potential for the size of the ‘‘bead’’ (group of atoms) to risk generating artificial free-energy barriers. This is known to occur where beads of different sizes interact together through a reduction in the LJ (Lennard-Jones) parameter. (73)

ORCA is a popular and free to use ab initio quantum chemistry program for computational modelling, it facilitates the use of methods such as DFT, many-body perturbation, and semi-empirical quantum chemistry. A factor that limits the use of ORCA is the lack of GUI (graphical user interface), as such it requires the user to access the programme through the command line, which demands a certain level of computing literacy on the part of the user. (74,75)

Computational chemistry has another drawback, in that many of the calculations can become quite computationally expensive and require either large amounts of time, resources, or a combination of the two in order to complete the calculations. Fortunately, the continued improvement in computational

abilities and their widespread use has led to the development of such projects as Supercomputing Wales, which is a programme designed to provide university researchers with access to extremely powerful computing capabilities on a remote basis. The Supercomputing Wales project utilises "clusters", which are high-performance computing systems comprised of high specification computers interconnected to work as one unit, greatly increasing processing power compared to a stand-alone computer. (76) Ensuring access to a powerful computer system or supercomputer project is a necessity for many computational chemical programmes as, if the calculation that the user wishes to run has too high a computational cost for their ordinary system, then the calculation will fail, potentially resulting in a large amount of wasted time.

DFT has strongly influenced the development of quantum chemistry over the years and has provided the basis for the development of computational methodologies for gaining a greater insight into the structure and properties of atoms and molecules with a much lower computational cost compared to other techniques. (77)

All of the calculations were performed through the use of the Fukui function. The Fukui function describes the electron density of a molecule after the addition or removal of an electron, analysis of the electron density following these changes in electron number made it possible to see where the most electrophilic or nucleophilic sites are. The dual descriptor combined the Fukui function for electron removal with the one for electron addition, and made it possible to visualise the local chemical reactivity of the two Fukui functions within the same molecule at the same time.

Computational chemical modelling was brought into the project in the final stages to improve understanding into the causes of the differences in performance observed between HHPA and the other monomer based coating systems. The potential benefits of utilising computational modelling were only realised later on in the project, with the correlations made from computational studies made within this thesis only being possible as a consequence of the large amount of experimental work carried out throughout the studies, with a large amount of the computational modelling work being performed during the COVID lockdowns.

1.13-Aims of the research to be carried out

The aim of the research carried out and repeated, in the following Chapters was to determine if there would be an alternative to HHPA that is not hazardous and capable of producing coatings with comparable properties.

The research would be performed via a series of steps. The first step would be to produce a selection of polyester-melamine coatings that contain different cycloaliphatic components with and without HALS. These coatings would then be evaluated for efficacy through a combination of accelerated and real-world weathering tests with periodic analysis to determine the impact that weathering has on the various coating systems and highlight which, if any, exhibit comparable coatings to coating systems based on HHPA. Computational modelling would also be performed to add further understanding behind the processes that would be occurring within the coatings and to potentially derive alternative routes that future research may take.

1.14-References

1. Sander J. Coil Coating. First. Hanover: Vincentz Network; 2014. 69–90 p.
2. Wypych G. Introduction. In: Handbook of UV Degradation and Stabilization. Second. ChemTec Publishing; 2015. p. 1–7.
3. Yousif E, Haddad R. Photodegradation and photostabilization of polymers, especially polystyrene: review. Springerplus. 2013;2(1):398.
4. Batista MAJ, Moraes RP, Barbosa JCS, Oliveira PC, Santos AM. Effect of the polyester chemical structure on the stability of polyester-melamine coatings when exposed to accelerated weathering. Prog Org Coatings [Internet]. 2011;71(3):265–73. Available from: http://dx.doi.org/10.1016/j.porgcoat.2011.03.009
5. Feldman D. Polymer Weathering : Photo-Oxidation. J Polym Environmnet. 2002;10(4).
6. Hall C. Chemical properties. In: Polymer materials: An introduction for technologista and scientists. Second. Hong Kong: Macmillian Education LTD; 1989. p. 131–4.
7. Van Krevelen D., Hoftyzer P. Degradation. In: Properties of Polymers: Correlations with Chemical Structure. First. Amsterdam: Elsevier Publishing Company; 1972. p. 347–50.
8. G.P.A Turner. General industrial paints. In: Lambourne R, Strivens T, editors. Paint and Surface Coatings: theory and practice. Second. Cambridge: Woodhead Publishing Limited; 1999. p. 502–28.
9. The coil coating process. European Coil Coatings Association. 2021.
10. Hexahydrophthalic Anhydride. National Center for Biotechnology Information. 2016.
11. Praw M. Polyurethane coatings: A brief overview. J Prot Coatings Linings. 2013;30(8):34–9.
12. Awasthi S, Agarwal D. Influence of cycloaliphatic compounds on the properties of polyurethane coatings. J Coatings Technol Res. 2007;4(1):67–73.
13. Agreement of the Member State Committee of the classification of HexaHydroPhthalic Anhydride as a Substance of Very High Concern. 2012.
14. Nielsen J, Welinder H, Jönsson B, Axmon A, Rylander L, Skerfving S. Exposure to hexahydrophthalic and methylhexahydrophthalic anhydrides - Dose-response for sensitization and airway effects. Scand J Work Environ Heal. 2001;27(5):327–34.
15. Rosqvist S, Nielsen J, Welinder H, Rylander L, Lindh CH, Jönsson BAG. Exposure-response relationships for hexahydrophthalic and methylhexahydrophthalic anhydrides with total plasma protein adducts as biomakers. Scand J Work Environ Heal. 2003;29(4):297–303.
16. Wypych G. Uv Degradation & Stabilization of Polymers & Rubbers. In: Handbook of UV Degradation and Stabilization. 2015. p. 177–292.
17. Cowie JM. (University of S. Polymers: Chemistry & Physics of Modern Materials. Stead K (University of E, editor. London: International textbook Company Limited; 1973. 283 p.
18. Lukey CA, Hill DJT, Pomery PJ. UV photolysis of melamine formaldehyde crosslinkers. Polym Degrad

Stab. 2002;78(3):485–90.

19. Gamage NJW, Hill DJT, Lukey CA, Pomery PJ. Factors affecting the photolysis of polyester-melamine surface coatings. Polym Degrad Stab. 2003;81(2):309–26.

20. Karak N. Biopolymers for paints and surface coatings. Biopolymers and Biotech Admixtures for Eco-Efficient Construction Materials. 2016. 333–368 p.

21. Pilati F, Toselli M, Messori M, Van Dijk H, Yeates S., Petterson B, et al. Waterborne & Solvent Based Saturated Polyesters and their End User Applications. Sanders D, editor. Brisbane: Wiley & Sons; 1999.

22. Radičević RZ, Jaroslavak BS. The effects of alkyd/melamine resin ratio and curing temperature on the properties of the coatings. J Serbian Chem Soc. 2005;70(4):593–9.

23. Sorce FS, Ngo S, Lowe C, Taylor AC. The effect of HMMM crosslinker content on the thermal-mechanical properties of polyester coil coatings. Prog Org Coatings [Internet]. 2019;137(September):105338. Available from: https://doi.org/10.1016/j.porgcoat.2019.105338

24. Persson D, Heydari G, Edvinsson C, Sundell PE. Depth-resolved FTIR focal plane array (FPA) spectroscopic imaging of the loss of melamine functionality of polyester melamine coating after accelerated and natural weathering. Polym Test [Internet]. 2020;86(November 2019):106500. Available from: https://doi.org/10.1016/j.polymertesting.2020.106500

25. Reich L, Stivala S. Various types of Polymer degradation. In: Elements of Polymer Degradation. New York: McGraw-Hill; 1971. p. 16–35.

26. Reich L, Stivala S. Factors Affecting Polymer Stability. In: Elements of Polymer Degradation. First. New York: McGraw-Hill; 1971. p. 294–341.

27. Amoco. How to Process Better Coating Resins with Amoco PIA and TMA. 1992.

28. Yoshioka T, Grause G. Hydrolysis of Polyesters and Polycarbonates. In: Nakano Y, Yamashita H, editors. polyester: Properties, Preparation and Applications. New York: Nova Science Publishers; 2019. p. 1–32.

29. Bauer D. Melamine/Formaldehyde crosslinkers: Characterization, Network formation and Crosslink Degradation. Prog Org Coatings. 1986;14(3):193–218.

30. Tillet G, Boutevin B, Ameduri B. Chemical reactions of polymer crosslinking and post-crosslinking at room and medium temperature. Prog Polym Sci [Internet]. 2011;36(2):191–217. Available from: http://dx.doi.org/10.1016/j.progpolymsci.2010.08.003

31. Painter P, Coleman M. Fundamentals of Polymer Science. First. Lancaster: Technomic; 1994. 274–287 p.

32. Zhang W, Smith R, Lowe C. Confocal Raman microscopy study of the melamine distribution in polyester-melamine coil coating. J Coatings Technol Res. 2009;6(3):315–28.

33. Nguyen T, Gu X, Vanlandingham M, Byrd E, Ryntz R, Martin JW. Degradation modes of crosslinked coatings exposed to photolytic environment. J Coatings Technol Res. 2013;10(1):1–14.

34. Makki H, Adema KNS, Hendrix MMRM, Peters EAJF, Laven J, Van Der Ven LGJ, et al. Weathering of a polyester-urethane clearcoat: Lateral inhomogeneities. Polym Degrad Stab [Internet].

2015;122:180–6. Available from: http://dx.doi.org/10.1016/j.polymdegradstab.2015.10.022

35. Rossi G, Giannakopoulos I, Monticelli L, Rostedt NKJ, Puisto SR, Lowe C, et al. A MARTINI coarse-grained model of a thermoset polyester coating. Macromolecules. 2011;44(15):6198–208.

36. Abel A. Pigments for Paint. In: Lambourne R, Strivens T., editors. paint and surface coatings theory and practice. Second. 1991. p. 91–165.

37. Jeffs R, Jones W. Additives for paint. In: Lambourne R, Strivens T., editors. Paint and Surface Coatings: theory and practice. 2nd ed. Woodhead Publishing Limited; 1987. p. 194–5.

38. Stabilizers. Sigma-Aldrich Company website. 2017.

39. Osswald T, Menges G. Mixing of Polymer blends, Solution and additives. In: Materials science of Polymers for Engineers. First. Cincinnati: Hanser Publishers; 1995. p. 133–73.

40. Cai J. Recent progress on hindered amine light stabilizers (Hals). Pop Plast Packag. 2016;61(1):26–8.

41. Paine MRL, Barker PJ, Blanksby SJ. Characterising in situ activation and degradation of hindered amine light stabilisers using liquid extraction surface analysis-mass spectrometry. Anal Chim Acta [Internet]. 2014;808:190–8. Available from: http://dx.doi.org/10.1016/j.aca.2013.09.039

42. Owen E. Photodegradation of Polyvinyl chloride. In: Labana S, editor. Ultraviolet Light Induced Reactions in Polymers. First. Washington D.C: American Chemical Society; 1976. p. 208–17.

43. Ghasemi-Kahrizsangi A, Neshati J, Shariatpanahi H, Akbarinezhad E. Improving the UV degradation resistance of epoxy coatings using modified carbon black nanoparticles. Prog Org Coatings [Internet]. 2015;85:199–207. Available from: http://dx.doi.org/10.1016/j.porgcoat.2015.04.011

44. Ghasemi-Kahrizsangi A, Shariatpanahi H, Neshati J, Akbarinezhad E. Degradation of modified carbon black/epoxy nanocomposite coatings under ultraviolet exposure. Appl Surf Sci [Internet]. 2015;353:530–9. Available from: http://dx.doi.org/10.1016/j.apsusc.2015.06.029

45. Kikuchi A, Oguchi-Fujiyama N, Miyazawa K, Yagi M. Triplet-triplet energy transfer from a UV-A absorber butylmethoxydibenzoylmethane to UV-B absorbers. Photochem Photobiol. 2014;90(3):511–6.

46. Wypych G. Effect of Additives on Weathering. Handb Mater Weather. 2013;547–79.

47. Wypych G. Photochemistry. Handb Mater Weather. 2013;27–48.

48. Braig A. Light Stabilization Toolbox. Paint Coatings Ind. 2010;(March):22–8.

49. Smith J. Natural and Accelerated UV degradation of coatings - some like it Hot. In: European Coatings Show Conference 2017 (ECS conference). Nurnberg: European Coatings; 2017.

50. Hodgson JL, Coote ML. Clarifying the Mechanism of the Denisov Cycle: How do Hindered Amine Light Stabilizers Protect Polymer Coatings from Photo-oxidative Degradation? Macromolecules. 2010 May;43(10):4573–83.

51. Shenoy MA, Marathe YD. Studies on synergistic effect of UV absorbers and hindered amine light stabilisers. Pigment Resin Technol. 2007;36(2):83–9.

52. Guo C, Zhou L, Lv J. Synergistic Effect of Hindered Amine Light Stabilizers/ Ultraviolet Absorbers on

the Plasticized PVC During Photo-Irradiation. J Appl Polym Sci. 2012;3376–84.

53. Woods R. Weathering and Stability Assessment of Coatings. Swansea; 2017.

54. Wypych G. Laboratory Degradation Studies. Handb Mater Weather. 2013;153–87.

55. BSI. BRITISH STANDARDS INSTITUTION. BS 7543: Guide to durability of buildings and buildings elements, products and components. 2015;

56. Wypych G. Artificial Weathering Versus Natural Exposure. Handb Mater Weather. 2013;231–44.

57. Carmona-Quiroga PM, Jacobs RMJ, Martínez-Ramírez S, Viles HA. Durability of anti-graffiti coatings on stone: Natural vs accelerated weathering. PLoS One. 2017;12(2):1–18.

58. Wade R. Accelerated Weatherings of Wood Coatings by QUV-A With Direct Water Spray. Paint Coatings Ind. 2009;25(October):30–6.

59. Nguyen T, Martin J, Byrd E, Embree N. Relating laboratory and outdoor exposure of coatings: II. J Coatings Technol. 2002;74(9):65–80.

60. Bauer D., Mielewski D., Gerlock J. Photooxidation kinetics in crosslinked polymer coatings. Polym Degrad Stab. 1992;(38):57–67.

61. Koenig J. Spectroscopy of Polymers. First. Washington D.C: American Chemical Society; 1991.

62. Lowe C (Becker ICL. INFRARED SPECTROSCOPY. In: Characterisation and measurement of polymeric materials : Volume 1 - Analytical methods for Surface Coatings. SITA technology; 2002. p. 61–87.

63. Sugimoto T, Yamaguchi K, Higashiyama Y, Nomura N. Detection of paint curing by surface potential of painted layer charged by corona discharge. IEEE Trans Ind Appl. 2014;50(6):4239–44.

64. Renishaw. Raman Spectroscopy. www.Renishaw.com.

65. Lowe C (Becker ICL. GEL PERMEATION CHROMATOGRAPHY. In: Characterisation and measurement of polymeric materials : Volume 1 - Analytical methods for Surface Coatings. 2002. p. 209–19.

66. Young R, Lovell P. Introduction to Polymers. Third Edit. Boca Raton: CRC Press; 2011.

67. Hwang DK, Moon JH, Shul YG, Jung KT, Kim DH, Lee DW. Scratch resistant and transparent UV-protective coating on polycarbonate. J Sol-Gel Sci Technol. 2003;26(1–3):783–7.

68. Katangur P, Patra PK, Warner SB. Nanostructured ultraviolet resistant polymer coatings. Polym Degrad Stab. 2006;91(10):2437–42.

69. Cocuzzi DA, Pilcher GR. Ten-year exterior durability test results compared to various accelerated weathering devices: Joint study between ASTM International and National Coil Coatings Association. Prog Org Coatings [Internet]. 2013;76(6):979–84. Available from: http://dx.doi.org/10.1016/j.porgcoat.2012.10.018

70. Mahltig B, Böttcher H, Rauch K, Dieckmann U, Nitsche R, Fritz T. Optimized UV protecting coatings by combination of organic and inorganic UV absorbers. Thin Solid Films. 2005;485(1–2):108–14.

71. Akbulatov S, Tian Y, Kapustin E, Boulatov R. Model studies of the kinetics of ester hydrolysis under stretching force. Angew Chemie - Int Ed. 2013;52(27):6992–5.

72. Simm GN, Proppe J, Reiher M. Error assessment of computational models in chemistry. Chimia

(Aarau). 2017;71(4):202–8.

73. Alessandri R, Souza PCT, Thallmair S, Melo MN, De Vries AH, Marrink SJ. Pitfalls of the Martini Model. J Chem Theory Comput. 2019;15(10):5448–60.

74. ORCA forum. phpBB. 2020.

75. Neese F. Software update: the ORCA program system, version 4.0. WIREs Comput Mol Sci. 2018 Jan;8(1).

76. Supercomputing Wales. Data Innovation Research Institute. 2021.

77. Geerlings P, De Proft F, Langenaeker W. Conceptual density functional theory. Chem Rev. 2003;103(5):1793–873.

Chapter 2-Experimental

2.0-Introduction

This chapter focuses on the experimental processes that were employed in the development of the novel resin and coating systems that were then used for testing and analysis in determining the viability of providing a suitable replacement to the widely used HHPA (Hexahydrophthalic Anhydride).

2.1-Substrates

All experiments were carried out using chromate primed coil coated steels. All steel was provided by Beckers Group. This steel was used as it is the most popular substrate of choice for architectural steels.

2.2-General method for the synthesis of novel resins

The generation of a resin takes place over several stages: formulation, charging, melting, distillation, and reflux.

The formulation of a resin is arguably the most important stage, as this is where the product is tailored to ensure that it can meet the requirements for its desired end purpose. A formulation spreadsheet aids in this customisation, giving an insight into the resulting hydroxyl value, molecular weight, straight chain percentage, solid content and other important information following each alteration to the existing formula.

The formulation of a resin can be broken up into the addition of acids and polyols.

Acids can either be aromatic, aliphatic, or cycloaliphatic and each influences the properties of the resin in different ways. Aromatics will provide a higher T_g, whereas aliphatics give greater flexibility and a reduction in the likelihood of crystallisation. Polyol choice can be broken down into di-functional and tri-functional, with individual polyols within each group providing a wide range of benefits such as improvements in flexibility, increasing Non-volatile content (NVC) or lowering the chances of crystallisation.

Three of the most important parameters that require consideration during the formulation of a novel resin are the T_g, molecular weight, and the OH content. The T_g is determined by the monomers that make up the backbone, by using different percentages in co-polymer systems the T_g can be increased or decreased. By increasing the percentage of aromatics used the T_g raises, which additionally provides a greater degree of moisture resistance. Raising the amount of aliphatics improves the flexibility of the finished resin. The molecular weight of a resin strongly influences its mechanical properties. The molecular

weight of a resin is determined during the resin synthesis process. To ensure that the resin does not overshoot its desired molecular weight, it is regularly tested during the Reflux stage via GPC (Gel Permeation Chromatography).

The OH content directly influences the crosslink density of the final coating system (alongside the crosslinker concentration) and, as such, requires careful monitoring throughout the synthesis process to ensure that the optimum crosslink density can be attained.

It is during the formulation stage that Patton's gelation constant is determined, as shown in equation 2.1. This equation is used to verify the amount of hydroxyl excess required for the formulation. In addition, the calculation indicates the likelihood that the resin has of gelling during processing as it approaches the target acid number. However, in practice the likelihood of gelling is altered during synthesis depending on the volume of glycol lost.

$$K = \frac{\text{Moles Hydroxyl material} + \text{Moles Carboxyl material}}{\text{Eq. Carboxyl material}}$$

Eq 2.1-*Calculating K value*

Charging the kettle is the addition of the raw materials to the mixing vessel. During this stage, it is important to add the liquid glycols first as this prevents charring of the components during the mixing process. Once the charging process has been completed, the vessel is gently heated in order to "melt out" the solid components and aid mixing. Once all the components have become liquid and the stirrer is free to move, a catalyst can be added if desired (typically 0.1% of the total yield), then the distillation stage can begin.

During the distillation stage a packed column is used, and the head temperature carefully monitored. The packed column is used to minimise potential glycol loss, this is a concern as some glycols have a boiling point only slightly above that of water. This is also why the head temperature must be carefully monitored to ensure that it remains high enough to cause water to be given off while low enough to prevent undesired glycol losses.

As the components react and esterification occurs, water is given off. This can be accelerated by using faster stirring, increasing the nitrogen flow, or by increasing the reaction temperature. The temperature can be increased up to a maximum of 220^{o}C while ensuring that the head temperature does not exceed 100^{o}C. However, increasing the temperature also has the potential to cause discolouration of the resin, limiting its potential uses.

The liquid (assumed to be only water) that is given off is periodically recorded, the refractive index (RI) is also measured to verify that water is the only liquid given off during distillation. Glycols have an RI value of 1.4, whereas water has an R.I value of 1.33, so visual analysis is suitable for determining the presence of glycols.

Once the temperature has been brought up to 220^{o}C, the reaction system is left to ensure that no more water can be boiled off and a sample is obtained to determine the acid value. If the acid value is below 30, then the apparatus can be cooled and transferred to the Reflux stage. The purpose of the Reflux stage is to remove the final 10% of water that is present within the reaction mixture, this is commonly the most time-consuming part of the synthesis process.

During the Reflux stage the packed column is replaced with a Dean and Stark apparatus, which is half filled with water with the water level marked. The rest is made up with xylene until it reaches a high enough level to begin to flow into the vessel. Additional xylene is then added to the kettle via the Dean and Stark apparatus. At the Reflux stage, the temperature is started at 180^{o}C before being slowly increased up to 220^{o}C. The purpose of the Reflux stage is to maximise the amount of water removed from the kettle.

This stage of the synthesis is measured via acid value, solid content, and viscosity tests every hour, with occasional tests via Agilent Gel Permeation Chromatography (GPC) to monitor the molecular weight to ensure that it remains within desired levels. As the Reflux process continues, and the resin approaches its desired endpoint, the testing is performed every 30 minutes. As soon as the resin is close to its endpoint it is cooled, this is done to prevent the resin from overshooting and ending up with a molecular weight outside of acceptable limits. The resin is then decanted from the kettle into an appropriate container and weighed to determine its quantity. Knowing the quantity and the NVC makes it possible to calculate the correct amount of Solvesso: Butyl Glycol blend that is required to bring the resin down to the desired solid content. Hydroxyl testing is performed at the end of resin synthesis to ensure that the value is within the desired range, it is not commonly carried out during processing due to the time required to perform this step which would mean that the reaction would have progressed further.

It cannot be overstated the care that must be taken when synthesising resins as there are a multitude of ways through which the processing can be affected, leading to a final resin that may lack the properties required for its target end use.

As previously mentioned, the acid Value is tested throughout the duration of the synthesis. The acid value is determined through the weighing of a sample of the resin into a conical flask. The sample is then

dissolved using a xylene solvent blend and titrated against 0.1M potassium hydroxide (KOH) with phenolphthalein as an indicator. When the solution turns from colourless to pink, the titration is stopped, and the acid value is calculated as shown in equation 2.2. The monitoring of Acid Value is of extreme importance, as it gives an indication of the sum of acidic components within the resin. In addition to this it is (along with viscosity) a useful guide for quality control of the resin, this is due to the rapid manner in which results can be obtained compared against molecular weight or Hydroxyl values, which require a long time frame in order to generate results.

$$Acid\ value = \frac{Titre\ (cm^3) * 56.1 * 0.1}{Sample\ weight\ (g)}$$

Equation 2.2 – *Calculating Acid value during resin synthesis*

The viscosity was measured by taking a resin sample that was assumed to be at 95% and diluting it to 65% NVC in xylene. The resulting solution was placed into a bubble tube and left in a water bath (set at 25°C) to acclimatise. It was then tested against bubble viscometer standards, which provide known viscosity levels with samples at 25C working via the principle that viscosity is inversely proportional to the speed that the bubble travels at. Comparison was made by holding the unknown and standardised tubes together and inverting them at the same time. Each tube contains an air bubble and the speed at which this bubble moved from the bottom of the tube to the top is monitored. While this method does invite some inaccuracies (temperature of the lab, length of time out of the water bath, if the tube has been inverted fully or not) it provides a useful estimation of the viscosity of the resin. Once the viscosity had been measured, the experimental sample was then used to determine the NVC of the diluted solution which indicates the NVC of the resin being synthesised. If it was discovered that the diluted sample was not 65% NVC, then the assumed NVC of the processing resin would be adjusted accordingly during the next set of tests.

Monitoring the Acid Value and Viscosity is extremely important as the Acid Value changes rapidly at the beginning of the synthesis and slows as the viscosity begins to change. Care must be taken once the Acid Value decreases to roughly 5, as it is liable to gel if it drops much lower than this.

The Hydroxyl value was monitored towards the end of the first stage of the synthesis and throughout the second stage until the target OHV was met. A large sample (roughly 9-10g) was taken from the kettle and allowed to cool. 3 x 150cm^3 glass jars were used, approximately 3g of the sample placed into each jar and the weight carefully recorded. 15cm^3 ethyl acetate was added to each of the jars, which were then stirred

and warmed until the resin completely dissolved. A further 3 jars were used as blanks, they undergo all processes and chemical additions with the exception that they did not contain any of the resin sample.

Once all the samples had dissolved then 5cm^3 acetylating solution was added to all jars. To track the potential introduction of errors, the actual amount added to each jar via a dispensator was weighed and recorded. All jars were then placed back onto a hotplate and stirred for a further 15 minutes. A pyridine:water blend (10cm^3:5cm^3) solution was then added via another dispenser before the jars placed back onto stirrer for another 20 minutes. Following this heating, they sat at room temperature for at least 30 minutes, after which they were titrated against 0.5M KOH solution (with phenolphthalein as the indicator) until a colour change was observed.

The average titre for the blank samples was established and used in equation 2.3, which is repeated for all samples.

$$In\ process\ OHV = ((Blank\ titre - Sample\ titre) * 56.1 * 0.5))\ /sample\ weight$$

Equation 2.3- *Calculating Hydroxyl value of in process resins*

Three sample results were then compared and if they were very close (within 1 OHV) then they were accepted. If one of the results was different, then it was excluded as an outlier. However, if all results differed significantly then the results were assumed to be erroneous and discarded with the hydroxyl test repeated to establish an accurate result for the resin. All components involved in the testing of resin systems were supplied by Becker LTD resin development labs as part of their standard testing procedures and were to an analytical standard.

It cannot be overstated how carefully the synthesis process should be monitored as there are many potential issues that can significantly alter the resin. The four most common issues are thermal degradation, ether formation, glycol loss within the packed column, and over processing of the resin.

Thermal degradation occurs when the heating rate is set too high, it can cause a decrease in viscosity and can cause a yellowing or ‘‘burning’’ of the resin, which could impact its end use viability. Ether formation can be prevented using some catalysts, ethers within the formulation influence many of its properties through altering the monomer ratios in addition to increasing the likelihood of the resin gelling. Glycol loss within the packed column occurs when the heating rate of the kettle is too high and/or the column is poorly packed. Over processing of a resin can cause the target solid content and viscosity levels to be unattainable, if this happens then the resin synthesis process must be restarted.

While all the above issues are serious, the most commonly occurring is glycol loss, as even relatively small levels of glycol loss influence Patton's gelation constant [Eq 2.1] by lowering the K value to a point that gelation becomes more likely as a low acid number is reached.

Although glycol loss can be minimised, due to the prevalent use of low boiling point glycols, it should be anticipated for there to be some level of glycol loss and preparations made for the inclusion of additional glycol into the kettle through determining how much glycol left the system. There are multiple methods to calculate how much glycol (if any) has been distilled off. The simplest method is to establish how much liquid has been given off during the reaction and subtract the theoretical water produced from the formulation. However, this method requires the reaction to be near completion before the result can be reliable which may be too late to prevent the resin from gelling.

The preferred industrial method is determining if glycol is present through analysis of the Refractive Index (RI) of the distillate. The RI value is then compared against published percentage glycol in water graphs to uncover the percentage of glycol in the distillate. The total glycol lost can be calculated as shown in Equation 2.4.

Lost Glycol = (Percentage glycol in distillate) (Charge Wt – Y')

Where Wt - Y' represents the base charge of the raw materials.

Equation 2.4 – *Calculating glycol loss during resin development*

It is also possible to cause the formation of ethers during processing, this can lead to gelling, alters the monomer ratios and causes the end resin to be more susceptible to weathering degradation. Glycol loss is a common issue if the head temperature exceeds 100°C, if the glycol levels are not adjusted then the resin is liable to gel.

Confirming the final NVC content of a resin is more in-depth than the method used during processing. Three samples are taken from the resin and weighed into pre-weighed metal dishes, the aim being to add between 0.5g-1.0g of resin to each dish. The dishes are then placed into an oven at 165°C for 90minutes. The dishes are then weighed again once cool, the data then being used to calculate the final NVC percentage as shown by Equation 2.5.

$$\frac{Total\ weight\ after\ heating\ [g] - Empty\ tub[g]}{Amount\ of\ Resin\ added\ [g]}$$

Equation2.5-*Calculating final solid content of resin system*

2.2.1-Developed resins and associated issues

Multiple resins were formulated in order to obtain those optimised in order to be most likely to provide the greatest amount of information during analysis. The resins displayed in Table 2.1 show the total resins that have been synthesised and used to develop coating systems during the project. The resins BK001, BK003, and BK004 were proprietary resins obtained from Becker Group and were used in the production of initial clear coat systems, the purity and company of origin of the major components was previously discussed in Chapter 2.

All resins were synthesised within the Becker LTD resin development laboratory, utilising their small-scale resin synthesis equipment. The raw materials used to produce the resins described throughout this thesis can be found in Table 2.1, with a break-down of the supplier, component purity, and chemical formula. The resins developed from these chemicals are laid out and discussed in Chapter 3.

Table 2.1-*Breakdown of components used during resin synthesis, their purity*

Chemical name	**Purity (%)**	**Supplier**	**Chemical structure**
Hexahydro phthalic anhydride	99.0	Sigma-Aldrich	$C_8H_{10}O_3$
Cyclohexane dicarboxylic acid	99.0	Sigma-Aldrich	$C_6H_{10}(CO_2H)_2$
Cyclohexane dimethanol	99.0	Sigma-Aldrich	$C_6H_{10}(CH_2OH)_2$
Perhydro bisphenol A	90.0	Sigma-Aldrich	$(CH_3)_2C(C_6H_{10}OH)_2$
Adipic acid	99.0	Sigma-Aldrich	$HOOC(CH_2)_4COOH$
1,6 Hexanediol	99.0	Sigma-Aldrich	$HO(CH_2)_6OH$
Neopentyl glycol	99.0	Sigma-Aldrich	$(CH_3)_2C(CH_2OH)_2$
Trimethylol propane	98.0	Sigma-Aldrich	$CH_3CH_2C(CH_2OH)_3$
Ethylene glycol	99.8	Sigma-Aldrich	$HOCH_2CH_2OH$

Table 2.2-*Breakdown of generated resin systems*

Resin Code	Main component(s)	Ratios of contents (if appropriate)	Used in further testing? (Y/N)
BK001	HHPA	N/A	N
BK003	CHDA	N/A	N
BK004	CHDA:CHDM	N/A	N
LSBS-STD	HHPA	N/A	Y
LSBS-33	CHDA	N/A	Y
LSBS-34	Perhydro Bisphenol A	N/A	N
LSBS-37	CHDA:CHDM	1.28 : 1	N
LSBS-38	CHDA:CHDM	1 : 1.04	N
LSBS-37-R	CHDA:CHDM	1.28 : 1	Y
LSBS-38-R	CHDA:CHDM	1 : 1.04	Y
LSBS-39	CHDA:CHDM	1 : 1.57	Y
LSBS-40	CHDA:CHDM	2 : 1	Y
LSBS-41	CHDA:CHDM	4 : 1	Y

The synthesis of novel resins was not completed without encountering issues, chief amongst them being gelation of the resin. While the synthesis of resins described above is a relatively straightforward process, the reaction must be carefully monitored, as the rate at which the reaction occurs differs significantly from resin to resin depending on the base monomers used.

Table 2.2 shows all the resins that were developed utilising the previously described method, it also shows which resins were selected for further testing, which will be covered in greater detail later in the chapter. Three resins were not selected for further testing, LSBS-34, LSBS-37, and LSBS-38.

LSBS-34 utilised Perhydro Bisphenol A as the monomer base. However, LSBS-34 did exhibit issues with a lack of reactivity and re-crystallisation. The poor reactivity was evidenced during the final GPC testing, which indicated that there may be some unreacted monomer remaining within the resin and would likely have caused the resin to be more susceptible to weathering degradation.

The greatest issue with this resin was the re-crystallisation. If a resin re-crystallises, it is common practice for it to be gently heated up to 41°C, it is important for the temperature to not rise past this as glycol will begin to be lost which would influence the properties of the final coating. Unfortunately, LSBS-34 remained in a crystalline state even at higher temperatures, making it unsuitable for use without compromising the desired properties of the resin.

LSBS-37 and LSBS-38 both experienced the same issue, where they progressed through the first stage of resin synthesis extremely quickly and with GPC analysis showing an average molecular weight of between 30,000-35,000 which was more than double the target molecular weight. As such, repeat resins were synthesised (LSBS-37R and LSBS-38R respectively) without the inclusion of a catalyst, these replacements resulted in the synthesis of resins that met the ideal requirements that had previously been determined. Repeating the synthesis without the addition of a catalyst was anticipated to greatly decrease the rate of the reaction and leading to a longer synthesis time, but this was only the case for LSBS-38R. LSBS-37R reacted faster without a catalyst and was ready to move on to the Reflux stage within an hour of processing, with the reasons behind this accelerated reaction being unknown.

2.3-Development of Coating systems

The coating systems were generated at Swansea University using a Becker LTD proprietary formulation, they were mixed using a ball mill and ceramic beads to grind the pigments. All coating components and pigments were supplied by Becker Group, with a breakdown supplied in Table 2.3.

Table 2.3-Breakdown of coating components

Coating component	**Purity (%)**	**Supplying company**
Resin of choice	NA	As described in Table 2.1
Komelol MM90GE	NA	Supplied by Becker Group
Disperbyk 170	NA	BYK
Solvesso 150	NA	Supplied by Becker Group
Estasol	NA	Supplied by Becker Group
Aerosil R972	NA	Evonik
Ferro Yellow PK10406	NA	Ferro pigments
Bayferrox 130M	NA	Bayferrox
Bayferrox Black 303T	NA	Bayferrox
n-Butanol	NA	Supplied by Becker Group
50% Disparlon solution	50%	Kusumoto
Shamrock SN 381 (40% solution)	40%	Supplied by Becker Group
AMP Blocked p-TSA	NA	Supplied by Becker Group
Syloid ED44	NA	Supplied by Becker Group

It was decided that the colour of the coatings would be chocolate brown. This colour was chosen due to the low amount of Titanium Dioxide (TiO_2) within the formulation. TiO_2 was avoided as it has the capacity to influence the apparent weathering durability of the coating, this is because it can either cause the reflection of some light and give the appearance of superior weathering durability, or aid in the absorbance of light, which would result in accelerating the rate of degradation exhibited by the coating system.

The ceramic mixing vessel was cleaned with ethanol and deionised water and once dry, the container had the raw materials for paint manufacture weighed directly into it. The mixture was then stirred at 1000rpm using a small shear mixer while the required pigments were added, once all pigments had been added stirring continued for an additional 15 minutes to ensure an even distribution throughout the mixture.

The full coating mixture then had ceramic mill beads added and was then mixed using a Retsch PM100 planetary ball mill at 500rpm for 120 minutes with a pause every 15 minutes for 5 minutes. This pause

was required to allow the mixture to cool and prevent overheating. Overheating was a significant concern due to the desire to avoid re-crystallisation issues in the final coating film. When the mixing cycle was completed the paint was tested using a Hegman grind gauge, if the coating provided a result in excess of 10µm then it was placed back into the bead mill for an additional hour following the same procedure before being retested.

Pre-filter components were then added to the mixture, which was then stirred using the Dispermat shear mixer for 5 minutes at 1000rpm. The mixture was then filtered through a 250µm filter and into a paint tin whose empty weight had already been recorded. This made it possible to calculate the percentage paint that had been transferred and therefore determine the adjusted quantities of components to add, after which point, the paint was stirred using the shear mixer for 10 minutes at 500rpm.

The next step in paint generation was gloss testing and lowering to the desired range. A paint curing oven was calibrated to ensure that it provided a PMT of 232^{o}C for a dwell time of 35 seconds, measured using RS pro temperature strips. At this point, a sample was coated, cured, and had its gloss levels analysed. If the gloss level was higher than desired, then a matting agent was added to reduce the gloss value. The paint would then be mixed using a shear mixer at 500rpm for 15 minutes before being left to settle for a further 15 minutes. The settling stage provided additional time for the matting agent to expand throughout the system, if this stage was to be ignored then it would be possible for the gloss level to gradually decrease while in storage.

Viscosity testing was then performed with a Ford F4 flow cup with the paint at 21^{o}C with a timer used to measure how long it took for the cup to empty. The target time was between 90-100 seconds and if the coating was unable to meet this parameter, then Solvesso and Estasol would be added in a 1:1 ratio, stirred for 5 minutes at 500rpm and the temperature of the paint measured before testing the viscosity again. Once the viscosity reached the desired level then another empty tin was weighed, into which half of the generated paint was transferred. The amount of paint transferred was then used to calculate the correct quantity of HALS to add to ensure that it remained at 1% of the paint formulation. Following this method ensured that the paint systems were identical except for the presence of HALS in one of the coatings, minimising the potential for variables requiring consideration during later comparison stages.

The first and second stage materials were measured into a mixing vessel. These were then mixed at 1500rpm using a Dispermat shear mixer while the third stage materials (pigments) were added, after this point, mill beads were added to the vessel and a milling impeller was used to grind the pigments at

3000rpm for an initial time of 35 minutes. Due to the heat generated during this process the vessel was secured into a water container throughout this stage in order to minimise thermal damage to the paint.

Following milling, the coatings were tested on a Hegman (20µm - 0µm) gauge to ensure that the pigments had been ground down to a fine enough size. If the Hegman test showed pigments of a greater size than 10µm then milling was resumed for a further 15 minutes, this process would be completed as many times as required until the pigments reached the desired size. If additional milling time was required, then the water containing vessel would require re-filling in order to remain able to keep the paint cool.

Pre-filter components were added and mixed at 1000rpm for 5 mins before being filtered through 190µm filter cloth into a clean paint tin whose empty weight was already known. Once filtering finished, the percentage paint that was transferred was calculated as shown in Equation 2.6.

$$\left(\frac{Paint\ after\ filtering\ (g)}{Total\ amount\ of\ components\ added\ \ (g)}\right) * 100 = percentage\ paint\ transferred$$

Equation 2.6-*Calculating percentage paint transferred during filtering*

The remaining components were then recalculated using the percentage paint transferred in order to maintain the required ratios within the coating. The post filtering components were then added, mixed, and the coating prepared for gloss analysis which was performed as described in Chapter 3.

The coatings were applied onto chromated steel panels using a 28K drawdown bar and cured in an industrial paint oven for 35 seconds in order to reach a PMT (Peak Metal Temperature) pf 232^{o}C.

The decision was made to primarily focus on the more common PE:HMMM ratios of 70:30, 80:20, 85:15, and 90:10 coatings throughout the investigation. While these ratios have been covered in work by others, it was decided to investigate these polyester-melamine ratios as they see common use within industrial coil coatings.

2.3.1-Developed coating systems and associated issues

Table 2.4-*Breakdown of developed clearcoat and pigmented coating systems*

New coating code	Resin base	Polyester : Crosslinker Ratio	HALS? (Y/N)	Pigmented? (Y/N)
HH8020	BK001	80:20	N	N
HH8515	BK001	85:15	N	N
CHDA8020	BK003	80:20	N	N
CHDA8515	BK003	85:15	N	N
CHDADM8020	BK004	80:20	N	N
CHDADM8515	BK004	85:15	N	N
HH8020Br	BK001	80:20	N	Y
HH*8020Br	LSBS-STD	80:20	N	Y
HH*8020BrH	LSBS-STD	80:20	Y	Y
HH*8515Br	LSBS-STD	85:15	N	Y
HH*8515BrH	LSBS-STD	85:15	Y	Y
CHDA*8020Br	LSBS-33	80:20	N	Y
CHDA*8020BrH	LSBS-33	80:20	Y	Y
CHDA*8515Br	LSBS-33	85:15	N	Y
CHDA*8515BrH	LSBS-33	85:15	Y	Y
CHDA1.3DM8020Br	LSBS-37R	80:20	N	Y
CHDA1.3DM8020BrH	LSBS-37R	80:20	Y	Y
CHDA1.3DM9010Br	LSBS-37R	90:10	N	Y
CHDA1.3DM9010BrH	LSBS-37R	90:10	Y	Y
CHDA1.0DM8020Br	LSBS-38R	80:20	N	Y
CHDA1.0DM8020BrH	LSBS-38R	80:20	Y	Y
CHDA1.0DM9010Br	LSBS-38R	90:10	N	Y
CHDA1.0DM9010BrH	LSBS-38R	90:10	Y	Y
CHDA0.6DM8020Br	LSBS-39	80:20	N	Y

CHDA0.6DM8020BrH	LSBS-39	80:20	Y	Y
CHDA0.6DM9010Br	LSBS-39	90:10	N	Y
CHDA0.6DM9010BrH	LSBS-39	90:10	Y	Y
CHDA2.0DM8020Br	LSBS-40	80:20	N	Y
CHDA2.0DM8020BrH	LSBS-40	80:20	Y	Y
CHDA2.0DM9010Br	LSBS-40	90:10	N	Y
CHDA2.0DM9010BrH	LSBS-40	90:10	Y	Y
CHDA4.0DM8020Br	LSBS-41	80:20	N	Y
CHDA4.0DM8020BrH	LSBS-41	80:20	Y	Y
CHDA4.0DM9010Br	LSBS-41	90:10	N	Y
CHDA4.0DM9010BrH	LSBS-41	90:10	Y	Y
HH*8020	LSBS-STD	80:20	N	N
HH*8515	LSBS-STD	85:15	N	N
HH*9010	LSBS-STD	90:10	N	N
CHDA*8020	LSBS-33	80:20	N	N
CHDA*8515	LSBS-33	85:15	N	N
CHDA*9010	LSBS-33	90:10	N	N
HH*7030Br	LSBS-STD	70:30	N	Y
HH*9010Br	LSBS-STD	90:10	N	Y
CHDA*7030	LSBS-33	70:30	N	Y
CHDA*9010	LSBS-33	90:10	N	Y

Most generated coatings were completed without issue. However, several coatings encountered unexpected difficulties during the mixing process. The coatings in which these issues appeared shared resin bases that required extended periods of time to "melt out" and undo the crystallisation that occurred following resin synthesis, as previously mentioned. The primary issue that became evident during coating development was solidification during the filtration process, brought about by cooling of the coating. This issue required circumvention in order to maximise the final yield in addition to ensuring that a full coating mixture was generated as a product and was solved through continuous gentle heating during the filtration process with a hair dryer.

Care needed to be taken to ensure that the coating did not reach too high a temperature in order to prevent the coating from overheating as this would potentially cause a loss of Glycol components and exert an influence over the final coating.

2.4-Exposure and Analysis of Coatings

2.4.1-Weathering exposure

The previous chapter highlighted the importance of weathering durability when designing novel coating systems, which was particularly true for those systems determined for external use. As such it was decided that a combination of exposure techniques would be utilised to test the developed coatings.

Sample panels were cut to size and exposed to accelerated weathering tests according to BS EN ISO 11507:2007. The cycles used were 8 hours UVA exposure at 80°C followed by 4 hours condensation at 50°C (referred to as HOT-UVA), or 4-hour cycles of 60°C UVA exposure and 40°C condensation (referred to as STD-UVA), with the gloss of each coating measured after every 500 hours, where metal punches were also taken from each sample at the same time as gloss measurements were performed to allow IR (Infrared) analysis to be performed. As well as the accelerated testing, panels were also exposed south facing angle of 45° to the vertical in Florida with the gloss, colour, and metal punches taken every 12 months. All accelerated weathering tests were performed using Q-Lab QUV accelerated weathering cabinets equipped with Solar Eye.

Natural weathering and accelerated weathering were used in combination to combat the limitations of each method. Accelerated weathering does not contain all of the factors that influence degradation (biological growth, pollution, etc) but does cause the coating to break down at a faster rate due to the intensity of UV radiation and temperatures that are applied, allowing more information to be obtained about the susceptibility of a coating to photodegradation and moisture enhanced photodegradation. Whereas the limitation of natural weathering is time and location, as it requires years of exposure before any meaningful results can be obtained, but it exposes samples to the full gauntlet of factors that have the capability of influencing the rate of degradation.

Samples exposed to natural weathering were exposed in Florida for 2 years, with half of the panel being washed and the other half unwashed. (1)

2.4.2-Infra-Red analysis

All Infra-Red (IR) analysis was performed at Swansea University with a Perkin Elmer Spectrum 2 with a SPECAC ATR crystal with a scan range of 4000cm^{-1} – 400cm^{-1} and with 4 scans performed per measurement.

There are multiple areas of interest in IR analysis, as laid out in Table 2.5.

Table 2.5-*Overview of IR bands of interest*

Band position (cm^{-1})	**Corresponding bond**
3560-3160	O-H stretch
3000-2800	CH_2 + CH_3 stretch
1730	C=O Stretch
1545	In plane Deformation of Triazine ring
1475	
1450	Triazine ring + CH_2+CH_3 Bending
1375	CH_3 Bending
1350	C-H bending
1310	C-O of O=C-O-C
1240	C-O-C from O=C-O-C
1155	C-O-C from O=C-O-C
1110	C-O stretch
1070	CO-O-CO Anhydride stretch
1030	C-O stretch from O-CH
1000	
875	C=C Bending
815	Out of plane Triazine ring deformation
755	CH_2 rocking

2.4.3-Raman analysis

Raman analysis was carried out using a Renishaw inViva Raman Microscope with a Renishaw CCD Camera as an area locator. Scans were run at 5% power for 1 second. These settings were chosen through a trial-and-error approach, where longer exposure times or higher power percentages resulted in burning of the samples. It was possible to identify clearly separate areas through microscopic analysis, white, yellow and green regions. (2,3)

2.4.4-Gloss and colour measurements

Gloss measurements were obtained using a handheld GM1 Gloss meter with a 60° contact angle with an error value of +/- 1.2 gloss units. Five (5) measurements for each sample were obtained and an average was calculated to determine the average Gloss measurement for the coating.

Colour measurements were taken using an X-rite Gretag MacBeth colour Spectrolino in reflectance mode with a 2° Observer angle and utilising D65 illusion to generate CIELab76 measurements. These measurements were, in turn, used to calculate Δ E as in Equation 2.7. (4)

$$\Delta E = \sqrt{(L_1 - L_0)^2 + (a_1 - a_0)^2 (b_1 - b_0)^2}$$

Where:

L_1 is the L measurement following exposure — L_0 is the L measurement prior to exposure

a_1 is the a measurement following exposure — a_0 is the a measurement prior to exposure

b_1 is the b measurement following exposure — b_0 is the b measurement prior to exposure

Equation 2.7-*Calculating* ΔE

2.4.5-Depth profiling

All coating depth measurements were performed using the Erichsen paint borer 518 using a number 2 drill bit and analysed with the associated software. A standard wedge cut method was utilised, meaning that samples would be cut at a specific angle, utilising this known angle and the circumference of the drilled profile it was possible to obtain coating thicknesses for all coatings within the tested system.

2.4.6-UV-Vis analysis

All UV measurements were performed using a Perkin Elmer UV-Vis-NIR Lambda 950 with a 150nm integrating sphere, which measured from 200nm to 2500nm at increments of 10nm in transmission mode.

The coatings were developed using proprietary formulations, after which free films were generated.

Each coating was applied to a PTFE treated sheet and then cured in an oven set to 265°C for 35 seconds in order to reach a Peak Metal Temperature (PMT) of 232°C. Once cooled, the samples were peeled away from the PTFE treated sheet to produce a free film.

A complete breakdown of the coatings is shown in Table 2.6.

Table 2.6-*Breakdown of produced coating systems including monomer base and PE:HMMM ratio*

Coating code	Resin code	Monomer base	PE:HMMM ratio
HH8020	BK001	HHPA	80:20
HH8515	BK001	HHPA	85:15
CHDA8020	BK003	CHDA	80:20
CHDA8515	BK003	CHDA	85:15
HH*8020	LSBS-STD	HHPA	80:20
HH*8515	LSBS-STD	HHPA	85:15
HH*9010	LSBS-STD	HHPA	90:10
CHDA*8020	LSBS-33	CHDA	80:20
CHDA*8515	LSBS-33	CHDA	85:15
CHDA*9010	LSBS-33	CHDA	90:10

The primary focus was analysis of absorbance of the free films in the visible and UV-A region (740-380nm and 400-320nm respectively), although the UV-B (315-280nm) and UV-C (280-100nm) region were also investigated as the range of interest was from 780nm to 200nm.

As the measurements were performed in transmission mode, a conversion calculation was required to change the results to show the Absorbance profile, as shown in Equation 2.8.

$$Absorbance = 2 - log\%Transmittance$$

$$Absorbance = Extinction\ Coefficient * Concentration * Length$$

$$Absorbance = A * \varepsilon * l$$

Equation 2.8-*Calculating Absorbance from Transmission values*

2.4.7-Hydrolytic activity analysis

Novel resins were developed using proprietary formulations, utilising either HHPA (Hexahydrophthalic Anhydride) or CHDA (CycloHexane Dicarboxylic Acid) as the sole monomer resin base containing the same additives in the same quantities, with a proprietary HHPA resin used as a reference. Table 2.1 gives a breakdown of the resins while an overview of the coatings used within this investigation is given in Table 2.5.

All resins were developed with two key guidelines in place, a Hydroxyl value (OHV) of 50, and a molecular weight of approximately 2200. All resins were developed using methods that are well documented within the literature of resin synthesis. (5)

The resins were then used as the bases for pigmented coating formulations, with each resin being used in the development of 80:20 and 85:15 ratios with HMMM (Hexamethoxymethyl Melamine) to develop full Polyester:Melamine coating systems. Table 2.7 gives a breakdown of the coatings and the codes that will be referred to going forward.

Table 2.7-*Overview of coatings used in hydrolysis investigation*

Resin Code	Coating code	Primary Monomer Base	Polyester: Melamine Ratio
BK001	HH8020Br	HHPA	80:20
LSBS-STD	HH*8020Br	HHPA	80:20
LSBS-STD	HH*8515Br	HHPA	85:15
LSBS-33	CHDA*8020Br	CHDA	80:20
LSBS-33	CHDA*8515Br	CHDA	85:15
LSBS-STD	HH*7030Br	HHPA	70:30
LSBS-STD	HH*9010Br	HHPA	90:10
LSBS-33	CHDA*7030Br	CHDA	70:30
LSBS-33	CHDA*9010Br	CHDA	90:10

The coatings were generated using a proprietary coating formulation from Beckers group in a 7-stage process.

The first and second stage materials were measured into a mixing vessel. These were then mixed at 1500rpm using a Dispermat while the stage 3 materials (pigments) were added, after this point, mill beads were added to the vessel and a milling impeller was used to grind the pigments at 3000rpm for an initial time of 35 minutes. Due to the heat generated during this process the vessel was secured into a water container throughout this stage in order to minimise thermal damage to the paint.

Pre-filter components were added and mixed at 1000rpm for 5 mins before being filtered through 190µm filter cloth into a clean paint tin whose empty weight was already known. Once filtering was completed, the percentage paint that was transferred was calculated in the formula given in Equation 2.6.

$$\left(\frac{Paint\ after\ filtering\ (g)}{Total\ amount\ of\ components\ added\ \ (g)}\right) * 100 = percentage\ paint\ transferred$$

Equation 2.6 – *calculated percentage paint transferred during filtering*

The remaining components were then recalculated using the percentage paint transferred in order to maintain the required ratios within the coating. The post filtering components were then added, mixed, and the coating prepared for sample generation, which was done via application to a steel panel using a 28k drawdown bar and curing in an industrial oven for 35 seconds to reach a PMT (Peak Metal Temperature) of 232^{o}C. (6)

The coatings were then cut to approximately 70mm x 25mm panels, and then had baseline IR spectra obtained. Three investigations were then carried out, with 2 samples of each coating type per investigation.

2.4.7.1-Hydrolysis investigation

30 Samples were submerged in distilled water (with 2 samples of each coating type for each submersion time) and covered in order to prevent contact with sunlight. Samples were submerged for either 1, 3, or 7 days, once they reached their submersion time they were removed and allowed to air dry before an IR spectrum was obtained for each sample. (7,8)

2.4.7.2-Temperature enhanced hydrolysis

30 Samples were submerged in distilled water (with 2 samples of each coating type for each submersion time) in a beaker, which was then placed into a water bath set to 40^{o}C. Samples were submerged for either 1, 3, or 7 days, once they reached their submersion time they were removed and allowed to air dry before an IR spectrum was obtained for each sample.

2.5-Computational Chemical calculations

One of the objectives of this project was to improve understanding behind the weathering durability of HHPA containing and CHDA containing coatings. To reach this objective, Computational Chemical Modelling was utilised.

After literature research and meeting with experts in the field, a plan to investigate the kinetics between both HHPA and CHDA when attached to NPG (Neopentyl Glycol) was developed. The calculations would primarily focus around Density functional theory (DFT) which is a versatile calculation method that is based around quantum mechanics and the solution of Schrodinger's wave equation, useful for improving understanding the molecular and electronic structure of atoms, molecules, clusters, and solids. It can not only calculate the molecular properties of the species of interest, but also provides a better understanding of the chemical reactivities of the investigated system.

The development of the chemical structures was performed with use of the open-source molecular editing program Avogadro. Once the 2D structures were developed, Avogadro was able to optimise the structure within 3D space. Avogadro also allows an optional plug-in (component that adds a specialist feature) that allows the generation of ORCA input files directly from the Avogadro GUI (Graphical User Interface). (9)

ORCA is an ab-initio, DFT, and semi-empirical computational package that can perform complex chemical calculations in a short time frame. ORCA does not have a GUI, so must be summoned, and controlled through the command line. Due to this, the actual instructions for the calculations that are desired must be included within the input file itself. (10)

The first step would be to perform DFT calculations with a focus on geometry optimisation on NPG, HHPA, CHDA, HHPA-NPG, and CHDA-NPG structures, in addition to having the base monomer structures reacted with other key resin components, such as TMP (Trimethylol propane) and BEPD (Butyl Ethyl propanediol). This would provide information into the positions of the HOMO (highest occupied molecular orbital) and the LUMO (lowest unoccupied molecular orbital) as well as the energy that would be required to cause the movement of an electron from the HOMO to LUMO. (11)

The next step was to quantify the BSSE (basis set superposition error), which are commonly observed in DFT calculations. (12) BSSEs are serious problems that impact the calculation of interactions between different entities using molecular orbital calculations. The BSSE is brought about because the energy of each molecule is artificially decreased by the basis functions of the other molecules. (13) Following this it became possible to produce .cube files for the HOMO and the LUMO, which are then multiplied against each-other to produce a file that can be opened through VMD for the purpose of visualising areas of the compounds that would be susceptible to electrophilic and nucleophilic attack. Identifying areas vulnerable to attack.

The interactions of the chosen monomers were investigated as stand-alone components, in addition to when reacted with Neopentyl Glycol (NPG), Trimethylolpropane (TMP), and Butyl Ethyl propanediol (BEPD). The structures were designed using the program Avogadro, which also allowed the structures to be optimised for 3 dimensional space as well as generating an ORCA input file.(9) The program ORCA was then used to carry out DFT (Density Functional Theory) geometry optimization calculations using the basis set def2-TZVPP and the B3LYP functional.

From the output files, it was possible to identify the HOMO and LUMO of the different structures, as seen in Table 6.1. Once the energies for the HOMO and LUMO were identified, it was possible to calculate the Mulliken electronegativity through the calculation laid out in Equation 2.7. The larger the resulting electronegativity is, the more resistive the structure will be to chemical change, making it possible to determine the inherent reactivity of the structures with a greater positive number implying a more reactive structure.

Following this, Gaussian cube calculations were performed to identify the areas within the molecules that would be most susceptible to electrophilic and nucleophilic attack. These calculations also made it possible to visualise these areas. The isosurface for all structures was set to 0.01 and -0.01 to show electrophilic and nucleophilic susceptibility respectively. Setting the isosurface at these values made it possible to represent all the areas susceptible to electrophilic and nucleophilic attack without obscuring the overall model.

$$\frac{(I + A)}{2}$$

Equation 2.7-*Electronegativity calculation*

Where: I = HOMO (Ionisation energy) *A= LUMO (Electron affinity)*

2.6-Use of factorial design

In retrospect, factorial experimental design would have been a beneficial approach as it would have allowed each component to have been investigated for its impact on the overall weathering resistance of the coating systems and made it possible to reduce time demands and resource requirements.

However, as each stage of the investigation was heavily influenced by the results of the preceding stage, it was not possible to lay out the required framework required for factorial design and due to time constraints, it was not possible to retroactively insert the obtained data into a factorial design style framework.

2.7-References

1. Nichols ME. Paint weathering tests. Second Edi. Handbook of Environmental Degradation of Materials. Elsevier Inc.; 2005. 387–404 p.

2. Zhang WR, Zhu TT, Smith R, Lowe C. A non-destructive study on the degradation of polymer coating II: Modelling of degradation depth profiles. Polym Test [Internet]. 2012;31(8):1100–4. Available from: http://dx.doi.org/10.1016/j.polymertesting.2012.08.008

3. Greunz T, Lowe C, Bradt E, Hild S, Strauß B, Stifter D. A study on the depth distribution of melamine in polyester-melamine clear coats. Prog Org Coatings. 2018;115:130–7.

4. Verma G. Weathering, salt spray corrosion and mar resistance mechanism of clay (nano-platelet) reinforced polyurethane nanocomposite coatings. Prog Org Coatings [Internet]. 2019;129(May 2018):260–70. Available from: https://doi.org/10.1016/j.porgcoat.2019.01.028

5. Amoco. How to Process Better Coating Resins with Amoco PIA and TMA. 1992.

6. Liu Y, Zhang C, Du Z, Li H. Preparation and curing kinetics of bisphenol a type novolac epoxy resins. J Appl Polym Sci. 2006;99(3):858–68.

7. Makki H, Adema KNS, Peters EAJF, Laven J, Van Der Ven LGJ, Van Benthem RATM, et al. Quantitative spectroscopic analysis of weathering of polyester-urethane coatings. Polym Degrad Stab [Internet]. 2015;121:280–91. Available from: http://dx.doi.org/10.1016/j.polymdegradstab.2015.09.019

8. Lee WK, Nowak RW, Gardella JA. Hydrolytic degradation of polyester blend monolayers at the air/water interface: Effects of a slowly degrading component. Langmuir. 2002;18(6):2309–12.

9. Avogadro. 2018.

10. ORCA forum. phpBB. 2020.

11. Craig B, Skylaris CK, Schoetz T, de León CP. A computational chemistry approach to modelling conducting polymers in ionic liquids for next generation batteries. Energy Reports [Internet]. 2020;6:198–208. Available from: https://doi.org/10.1016/j.egyr.2020.03.025

12. Simm GN, Proppe J, Reiher M. Error assessment of computational models in chemistry. Chimia (Aarau). 2017;71(4):202–8.

13. Kobko N, Dannenberg JJ. Effect of basis set superposition error (BSSE) upon ab initio calculations of organic transition states. J Phys Chem A. 2001;105(10):1944–50.

Chapter 3-Resin Development

3.1-Introduction

It is known that the resin exerts a significant influence over the final coating, with a more detailed explanation of resins, their impact, and the associated chemistries can be found in Chapter 2.2, but at the most basic level the formation of a polyester requires a dicarboxylic acid and a diol, these react together to form an ester bond and water.

Multiple resins are utilised for use in the development of coatings, with different coatings providing a wide variety of properties that suits an application site. One of the advantages of resin formulation is that the resin can be tailored to fit the desired use by the end-user.

It is also well recorded in the literature that different monomer bases provide different qualities to the end product, due to their structure and chemical composition. (1) This is covered in more detail in Chapter 1.

HHPA is known to be a popular monomer that is associated with health concerns, leading it to be considered as a Substance of Very High Concern (SVHC) by REACH, a more in-depth discussion on this can be found in Chapter 1, sub-section 1.3.

Other popular monomers that see regular use include 1,4-CHDA (CycloHexane Dicarboxylic Acid) and CHDM (CycloHexane DiMethanol). An interesting feature of CHDM is that it is not a suitable candidate as the sole monomer in a resin formulation due to its inability to mix adequately. CHDM remains a monomer of interest for this in replacing HHPA, but it will require investigating through the development of Co-monomer resin systems, which will be covered in more detail later within the chapter.

The development of novel resins is a complex balancing act to ensure the development of a resin that exhibits high enough levels of all required qualities to be fit for their end purpose.

There are many components that can go into the production of a polyester resin, including diacids (such as Adipic acid or HHPA), polyols, glycols (e.g. Neopentyl Glycol), solvents, catalysts, and antioxidants. These components heavily influence different aspects of the final coating, with the T_g controlled by the chosen monomer, the molecular weight being influenced by process control and the relative percentage of tri-functional monomers within the formulation.

The resins that will be discussed within this chapter were all formulated with architectural coil coating processes in mind as the end purpose. As such the resins were used as the based for pigmented coating systems following their successful synthesis.

The first stage of the investigation involved the generation of two Polyester resins with identical characteristics, with the exception that one would be developed with HHPA as the base, and the other being primarily CHDA containing. This would enable the impact that the monomers have on the final coating properties to be investigated without influence from other components within the resin formulation.

The resins are monitored in terms of K value, percentage yield, Hydroxyl Value, molecular weight, percentage solid (Non-Volatile) Content, and the straight chain percentage. The K value of a resin aids in predicting the likelihood of gelation during processing, while other factors such as glycol loss and equipment used in processing play a role in the real-world gelation probability. The calculations and processes utilised to determine these values in-process are covered in-depth in Chapter 2.

The percentage yield indicates how much of the final resin will be produced as value from the raw materials. While this is not of critical importance in terms of the immediate research, any produced resin would also be desired to be cost effective when being considered for scaled up processes such as coil coating.

Hydroxyl Value is related to the hydroxyl excess, which is used in the curing process of the coating film, with a larger number corresponding to a more densely crosslinked coating. Resin formulation produces a theoretical OHV that can be used as a guide.

The theorised molecular weight is used as an indicator of the probable viscosity of the resin and can provide an estimate of the amount of solvent required. The percentage solid (non-Volatile) content is an indicator of the amount of material remaining once the solvent has been removed via heating.

Straight chain percentage records the presence of straight chain molecules within the resin as a whole. Monitoring the percentage presence of straight chain molecules within the formulation can be used to give an indication of how well the resin will behave following exposure to UV light compared to other resins. It is known that the greater the straight chain percentage of a resin, then the poorer the final coating system will be able to resist degradation compared to resins with a lower presence of straight chains.

3.2-Initial Resin Development

Thegeneral process of resin development has been laid out in great detail within Chapter 2. The Resins were developed in 5ltr processing kettles or a specially designed small-scale Resin synthesis apparatus located within the Becker Group Resin Labs. Periodically during resin synthesis Equation 3.1 and Equation 3.2 were used to track the change in Acid and Hydroxyl values.

$$\text{Acid value} = \frac{\text{Titre } (\text{cm}^3) * 56.1 * 0.1}{\text{Sample weight (g)}}$$

Equation 3.1-*Acid value calculation*

$$\text{In process OHV} = ((\text{Blank titre} - \text{Sample titre}) * 56.1 * 0.5)) \text{ /sample weight}$$

Lost Glycol = (Percentage glycol in distillate) (Charge Wt – Y')

Where Y' represents the base charge of the raw materials.

Equation 3.2-*In process hydroxyl value calculation*

3.2.1-Standard HHPA based Resin

The first resin to be developed was primarily HHPA containing. A breakdown of the formulation is shown in Table 3.1, showing the theoretical targets for K value, percentage yield, Hydroxyl Value, molecular weight, percentage solid content (%NVC), as well as the straight chain percentage.

Table 3.1-*Breakdown of LSBS-STD resin system formulation*

Component Code	Component Name	Weight to be added	Acid/Diol
HHPA	Hexahydro phthalic anhydride	62	Acid
TMP	Trimethylol propane	5	Diol
NPG	Neopentyl glycol	16	Diol
EG	Ethylene glycol	11	Diol
HD	1,6 hexanediol	7	Diol
% Yield	92.8		
OHV	52.6		
Molecular weight	2224		
% Straight chain	17.8		
K value	1.03		
% NVC	68		

The Standardised HHPA resin was developed over a 5-day period due to a slow rate of reaction within the first stage of synthesis, giving off a total of 83cm^3 of water. The synthesis process was carried out using a 5ltr resin system at the Resin Labs within the Becker Industrial Coatings Liverpool facility.

Table 3.2 shows the final Acid Value, hydroxyl value, and solid content of the LSBS-STD resin

Table 3.2 -*Showing Final values of LSBS-STD resin*

Resin Code	Final Acid Value	Final in OHV	Final Solids content (%)
LSBS-STD	0.93	37.9	71

3.2.2-CHDA Trial Resin

The resin shown in Table 3.3 was developed to be primarily CHDA containing and to be a comparable resin to the one illustrated within Table 3.1. This was done with the intention of comparing the weathering resistance capabilities of coatings based on HHPA and CHDA monomers with the minimum influence from other components. The CHDA resin required 66.5 CHDA by weight compared to the 62 HHPA by weight to achieve a similar molecular weight and hydroxyl value. The CHDA resin exhibits a slightly smaller percentage yield and molecular weight compared to the HHPA containing resin, but also shows a slightly greater hydroxyl excess. The CHDA resin also has a slightly smaller straight chain percentage, this is important as a greater straight chain percentage is linked towards an increased rate of degradation in the final coating systems.

Table 3.3-*Breakdown of CHDA containing LSBS-33 resin system formulation*

Component Code	Component Name	Weight to be added	Acid/Diol
CHDA	Cyclohexane dicarboxylic acid	66.5	Acid
TMP	Trimethylol propane	5	Diol
NPG	Neopentyl glycol	16	Diol
EG	Ethylene glycol	10	Diol
HD	1,6 hexanediol	7	Diol
% Yield	86.7		
OHV	53.7		
Molecular weight	2208.5		
% Straight chain	16.3		
K value	1.03		

Table 3.4-*Showing Final values of LSBS-33 resin*

Resin Code	Final Acid Value	Final in OHV	Final Solids content (%)
LSBS-33	1	59.31	71

Table 3.4 breaks down the final values for LSBS-33. It can be seen by comparing Table 3.4 with Table 3.2 that LSBS-33 has slightly higher acid and hydroxyl values compared to LSBS-STD, but that they have equivalent final solid contents of approximately 71%.

3.2.3-PerHydro Bisphenol A Trial Resin

LSBS-34 was initially formulated to be based on Perhydro Bisphenol A (PHBA), which is the cycloaliphatic equivalent of the aromatic Bisphenol A, with the hope being for PHBA to offer similar weathering resistance to degradation as the aromatic BPA without the negative health-based side effects that have been recorded. However, during formulation it was found that a resin based solely on PHBA was unable to reach the desired theoretical values for mol wt, OHV, and NVC%. To investigate the potential benefits of PHBA within a resin system it had to be implemented alongside CHDA and adipic acid. A breakdown of the formulated resin properties can be found in Table 3.5.

Table 3.5-*Breakdown of formulation of LSBS-34 resin system*

Component Code	Component Name	Weight to be added	Acid/Diol
CHDA	Cyclohexane dicarboxylic acid	13	Acid
AA	Adipic Acid	39	Diol
NPG	Neopentyl glycol	7	Diol
TMP	Trimethylol propane	6.5	Diol
PHBA	Perhydro Bisphenol A	62	Diol
% Yield	90.32		
OHV	53.3		
Molecular weight	2249.1		
% Straight chain	30.59		
K value	1.04		
% NVC	72.36		

Table 3.6-*Showing Final values of LSBS-34 resin*

Resin Code	Final Acid Value	Final in OHV	Final Solids content (%)
LSBS-34	0.57	51.2	62

During processing, the PHBA resin experienced multiple instances of foaming and partial crystallisation. It was also observed to be difficult to "melt out" after solidifying overnight, which was only rectified through the addition of greater levels of solvent than initially anticipated, causing a corresponding decrease in the final solid content of the resin as shown in Table 3.6.

3.2.4-Summary and observations of Developed Stage 1 Resins

Tables 3.10-3.12 give a breakdown of the properties of the resins that were developed in this stage. One of the more significant differences between the resins produced is the final solid content and viscosity values, while LSBS-STD and LSBS-33 both have similar values, those obtained for LSBS-34 are markedly lower both in solid content and in final viscosity value as shown in Tables 3.7-3.8. This is due to the significantly greater volume of solvent that was required to remove the coating from the vessel and continuing processing.

Table 3.7- *Solid content for comparison (%)*

LSBS-STD	LSBS-33	LSBS-34
64	63.55	81.91
65	65.78	71.63
65	65.61	70.72
65	66.78	70.29
65.3	74.69	67.86
63.25	70.75	63.03
66.86		62.39
66.31		
71.8		
70.23		

Table 3.8-*Viscosity values for comparison (Stokes)*

LSBS-STD	LSBS-33	LSBS-34
2.9	3.1	170
3.2	5.4	80
3.9	7.8	46
4.4	9.1	34
5.1	70	
4.1	45	
9	45	
9.8		
52		
43		

Table 3.9-*Final breakdown of key components of developed resin systems*

Resin Code	Main Component	Final NVC %	Final OHV	Mn	Mw	Viscosity
LSBS-STD	HHPA	71	38	4082	17575	43
LSBS-33	CHDA	71	63.44	4212	16846	45
LSBS-34	CHDA + PHBS	62	50	2197	21184	34

Table 3.9 gives a breakdown of the main targets of interest during resin development. Table 3.10 shows the final solid content of the resins, with LSBS-STD and LSBS-33 showing very similar values, while LSBS-34 exhibiting a significantly lower solid content value of 62% It is possible to see that LSBS-34 differs significantly in many of these areas, including Solid content, Viscosity and Molecular weight.

The synthesis of the Perhydro Bisphenol A based resin encountered several complications. This was partially due to the combination of monomers that were chosen as well as it being synthesised in a different scale set-up compared to the other resins, which utilised a jacketed oil-based heating system as opposed to the more traditional electrical heating mantle. Stirring was also shown to produce excessive foaming which in turn led to fluctuations in head temperature. It was found that increasing the flow of N_2 gas into the kettle limited foam production and aided in maintaining the desired head temperature of 100^{o}C.

Due to the small size of the kettle, it was subject to greater influence of cooling from ambient air movement. To circumvent this issue both the kettle and condenser column were swaddled to provide an insulative barrier. However, wrapping these components resulted in immediate and severe bubble propagation which required a higher flow of N_2 and a slower stirring speed to circumvent. This in turn led to parts of the resin solidifying within the kettle while processing was still ongoing, which required significant solvent addition to return the resin to a processable state.

Due in part to the smaller size of the kettle the second stage of the reaction progressed much faster than other resin generations. GPC (Gel Permeation Chromatography) analysis indicated that there were unreacted components within the final resin, which also drove the reaction to completion faster. The

presence of unreacted components may have also been a contributing factor in why reflux was observed to occur at a significantly lower temperature than anticipated.

The unreacted components within the resin were also possibly responsible for the resin being particularly viscous at the target of 65% solid, as such the resin had to be decreased to 62% solid to meet viscosity targets. Unfortunately, the resin became crystalline when cooled and quickly returned to this state following any attempt at melting out, making it unsuitable for inclusion within a pigmented coating system.

Table 3.9 shows that LSBS-34 holds final properties that are significantly different to the target parameters. However, LSBS-33 and LSBS-STD also fail to match the target for the final Hydroxyl values highlighted during the formulation process. LSBS-STD was unable to reach the final OHV whereas LSBS-33 exceeded it. The reason for this is that other parameter targets were not reached at the same time as the OHV, with GPC indicating the presence of unreacted components for longer in the case of LSBS-33.

3.3-Development of second Generation of Resins

Following analysis of the first generation of pigmented coating systems that were generated from the first generation of resin systems subjected to accelerated and natural weathering (covered in greater detail in Chapter 4) it was found that coatings based on CHDA: CHDM blend resin provided overall superior resistance to weathering degradation compared to coatings based on CHDA resins. While the weathering performance was poorer than that exhibited by HHPA coatings, it was decided to investigate the ratio at which these co-polymer blends provided the greatest degree of weathering resistance, with further testing into physical and mechanical properties of the coating that is determined to provide the greatest levels of weathering resistance. The ratios of CHDA to CHDM were altered in each resin, however this caused a change in other target values. As such, other components were needed to be added to bring the resin properties back on target. When the amount of CHDA was decreased, Adipic acid was used while 1,6-Hexanediol was utilised when CHDM was lowered while all other components were kept at the same value.

3.3.1-Formulation of Co-Monomer resin systems

A total of 5 resins were initially formulated, with the initial resin (LSBS-37) being used as the "Jumping off Point", with the subsequent resins containing lower levels of either CHDA or CHDM, as shown in Table 3.10.

Table 3.10-*Breakdown of main component of Second Generation of Resins*

Resin Code	CHDA Level	CHDM Level	Adipic Acid/Hexanediol added?	Amount added (g)
LSBS-37	40	31.3	No	0
LSBS-38	30	31.3	Adipic Acid	8.6
LSBS-39	20	31.3	Adipic Acid	17.1
LSBS-40	40	20	1,6 Hexanediol	9.2
LSBS-41	40	10	1,6 Hexanediol	17.3

The addition of either Adipic acid or 1,6-Hexanediol was required to maintain the Hydroxyl values, molecular weights, and solid contents within the desired limits. The negative consequence of these additions was an increase of the straight chain percentages, which have the potential to influence the overall weathering capabilities of the coating and as such required consideration during the analysis of the coating systems. This is potentially due to a lowering of the T_g, which is explored in more depth in Chapter 4.

Tables 3.11-3.15 give an in-depth breakdown of the coatings and clearly show the changes that are brought about through manipulating the levels of CHDA or CHDM. As mentioned previously, the addition of Adipic acid in the case of lowering CHDA or 1,6 Hexanediol when lowering CHDM levels resulted in an increase of the straight chain percentage. However, this rise was unavoidable if the other key targets were to remain as close as possible and was determined to be the addition of necessary variables.

Table 3.11 – *Breakdown of components of LSBS-37 resin*

Component Code	Component Name	Weight to be added	Acid/Diol
CHDA	Cyclohexane dicarboxylic acid	40	Acid
TMP	Trimethylol propane	3	Diol
CHDM	Cyclohexanedimethanol	31.3	Diol
% Yield	88.7		
OHV	30.8		
Molecular weight	3511.1		
% Straight chain	0		
K value	1.01		
% NVC	59.9		

Table 3.12-*Breakdown of components of LSBS-38 resin*

Component Code	Component Name	Weight to be added	Acid/Diol
CHDA	Cyclohexane dicarboxylic acid	30	Acid
AA	Adipic Acid	8.6	Acid
CHDM	Cyclohexanedimethanol	31.3	Diol
TMP	Trimethylol propane	3	Diol
% Yield	88.5		
OHV	30.2		
Molecular weight	3632.2		
% Straight chain	11.8		
K value	1.01		
% NVC	59.4		

Table 3.13- *Breakdown of components of LSBS-39 resin*

Component Code	Component Name	Weight to be added	Acid/Diol
CHDA	Cyclohexane dicarboxylic acid	30	Acid
AA	Adipic Acid	17.1	Acid
CHDM	Cyclohexanedimethanol	31.3	Diol
TMP	Trimethylol propane	3	Diol
% Yield	88.2		
OHV	30.8		
Molecular weight	3618.4		
% Straight chain	23.9		
K value	1.01		
% NVC	58.9		

Table 3.14- *Breakdown of components of LSBS-40 resin*

Component Code	Component Name	Weight to be added	Acid/Diol
CHDA	Cyclohexane dicarboxylic acid	40	Acid
TMP	Trimethylol propane	3	Diol
CHDM	Cyclohexanedimethanol	20	Diol
HD	1,6 hexanediol	9.2	Diol
% Yield	88.4		
OHV	30.9		
Molecular weight	3566.5		
% Straight chain	12.7		
K value	1.01		
% NVC	59.2		

Table 3.15- *Breakdown of components of LSBS-41 resin*

Component Code	Component Name	Weight to be added	Acid/Diol
CHDA	Cyclohexane dicarboxylic acid	40	Acid
TMP	Trimethylol propane	3	Diol
CHDM	Cyclohexanedimethanol	10	Diol
HD	1,6 hexanediol	17.3	Diol
% Yield	88.1		
OHV	30.5		
Molecular weight	3695.5		
% Straight chain	24.6		
K value	1.01		
% NVC	58.5		

Tables 3.11 – 3.15 give a breakdown of the different co-monomer resins and their components, showing that the resins with the largest straight chain percentages are Tables 3.13 and 3.15. All resins demonstrated a final percentage yield of 88%, a hydroxyl value between 30-31, and a theoretical molecular weight of between 3500-3700.

3.3.2-Synthesis of Co-Monomer Resins

The second generation of resins were developed as described above, with a detailed account available within Chapter 2.

Initial issues were experienced with LSBS-37 and 38, both of which reacted extremely quickly, moving to the secondary reflux stage within 6 hours and completing synthesis with molecular weights of between 30,000 and 35,000, which was approximately 10x the theorized target.

It was believed that the resins were more susceptible than anticipated to the catalyzing agent that was used, therefore the synthesis was repeated with the omission of the catalyzing agent. However, this was seen to have the opposite effect for LSBS-37, which required moving to the reflux stage within 30 minutes of beginning stage 1 processes and the resin completed within 1 day. Conversely, LSBS-38 required a much longer reaction time without the catalyst addition, taking a total of nearly 10 days to fully react. All the other resins were developed without incident and completed synthesis within 3-5 days. Table 3.17 shows that all of the second generation of resins demonstrated approximately equivalent hydroxyl values.

3.4.1-Results

As has been previously mentioned GPC (Gel Permeation Chromatography) is an important component of the analysis of resins as it is utilised to determine the molecular weights of the resin systems. It is known that the molecular weight of the resin has a significant impact on several characteristics, such as flexibility. As the desired area of interest was the inherent abilities of the monomer every effort was made to ensure that all developed resins exhibited as close to the same molecular weights as possible. GPC analysis was performed every 30 minutes during the reflux stage of resin generation, due to the rapid turnover required it was necessary to perform GPC at a rate of 0.8ml/minute, this introduced a greater potential for error within the results. To compensate for this, the final GPC analysis was performed at the slower rate of 0.3ml/minute. The final molecular weights of the first three resins that were developed are shown in Table 3.16.

Table 3.16-*Breakdown of first generation of resins*

Resin Code	Main Component	Mw
LSBS-STD	HHPA	17575
LSBS-33	CHDA	16846
LSBS-34	PBPA	21184

The difference in molecular weight of LSBS-34 from the other two resins aids in explaining why the solid content had to be lowered, as the larger molecular weight led to a greater disposition for gelling during processing. This was highlighted during the coating generation process (explained in greater detail in Chapter 4) when it became evident that LSBS-34 had crystallised. While it is not uncommon for resins to crystallise while in storage, this can usually be rectified through gentle heating at no higher than 41°C. Heating is limited to a ceiling of 41°C due to it being possible for Glycol to be lost at temperatures greater than this, which would in turn negatively impact the quality of the final resin and their associated properties. These reasons prevented full coating systems from being generated using the LSBS-34 resin.

Table 3.17-*Breakdown of characteristics of second generation of resins*

Resin Code	Contents		Straight chain percentage	OHV (mgKOH/g)
LSBS-37R	CHDA:CHDM	Trimethylol propane	0	30.9
LSBS-38R	CHDA:CHDM	Trimethylol propane, Adipic acid	11.8	30.2
LSBS-39	CHDA:CHDM	Trimethylol propane, Adipic acid	23.9	30.8
LSBS-40	CHDA:CHDM	Trimethylol propane, 1,6 Hexanediol	12.7	30.9
LSBS-41	CHDA:CHDM	Trimethylol propane, 1,6 Hexanediol	24.6	30.5

One of the limitations of the second generation of resins was their tendency to crystallise when removed from the heating vessel. This made the resins difficult to characterise as the viscosities could not be compared against standards, nor could samples be run through the GPC which prevented accurate final Mn and Mw measurements from being obtained. This failure to obtain final values for viscosity, Mn, and Mw will be problematic when considering scale up. However, if the resins can be utilised to determine the optimum co-monomer ratio then further research can then be performed on the optimum resin to improve its other characteristics for larger scale work.

3.5-Conclusions

Initial testing and resin development clearly showed that Perhydro Bisphenol A was unsuitable for use in developing a coating system due to the remnants of unreacted monomer within the resin in addition to the resin remining crystalline at temperatures above 41°C, making it impossible to "melt out" the resin without risking the loss of glycol and therefore changing the composition of the resin system. This would prevent the resin from being used to generate a coating system. The other resins were found to be suitable

for continued use and as such were used in the development of pigmented coating systems, which are covered in greater detail in Chapter 4.

This chapter has shown that while novel resins can be formulated with great accuracy in terms of desired target values, processing can cause unanticipated issues, such as glycol loss and foaming. Processing can also identify other issues, such as rapid reactivity.

Several issues were encountered while synthesising the second generation of resins, this included rapid reaction rates of LSBS-37 and LSBS-38 which resulted in final Mw of between 30000-35000, approximately 10x the intended final value. Repeating the synthesis yielded more appropriate results within the desired rages for OHV and NVC. The greatest issue with the second generation of resins was the inability to accurately measure their final Mw and Mn values due to their propensity to crystallise when removed from heating vessels. Following consultation with the head of the Resin lab it was decided to utilise the resins for the generation of coatings as, while the Mw may differ from resin to resin, the main targets of Hydroxyl value and NVC were within acceptable range which allowed for the differences between the CHDA:CHDM ratios to be investigated. An in-depth analysis of the behaviour of the resins within full coating systems can be observed within Chapter 4, which shows the behaviour of full coating systems during accelerated and natural weathering analysis.

Following synthesis, the resins contained within this chapter were used to generate novel coating systems for analysis, a comprehensive breakdown of which can be found in Chapter 4. By analysing the results obtained through analysis of LSBS-STD, LSBS-33, and LSBS-34 based coatings, it is easy to identify which gives superior performance.

LSBS-34 continued to experience solidification issues and required melting out, unfortunately it required temperatures in excess of 46^{o}C to begin to "melt out", as this would significantly alter the resin composition through glycol removal the decision was reached for LSBS-34 to be removed from further testing. Comparing LSBS-STD and LSBS-33 (HHPA and CHDA containing respectively) it became clear that LSBS-STD provided superior weathering durability in terms of colour stability, gloss retention, and changes in hydrolytic activity.

Analysis of the exposure results from coatings based off the second generation of resins produced interesting results. In terms of poor performance, CHDA4.0DM provided the highest increase of hydroxyl activity and greatest change in perceived gloss retention, with the only exception being change in hydroxyl activity for 90:20 ratio coatings, where CHDA2.0DM performed more poorly. In terms of colour retention,

the poorest performing coatings under standard UV-A were CHDA0.6DM for 80:20 and 90:10 ratios, while CHDA1:3DM showed the most significant colour change during HOT UV-A weathering.

LSBS-37R provided the best performing coating system in terms of gloss retention for 80:20 and 90:10 samples exposed to UV-A STD accelerated weathering, as well as 90:10 coatings for Hot UV-A, additionally, the resin provided the smallest changes in hydroxyl activity for UV-A for 80:20 and 90:10 UV-A STD and 80:20 Hot UV-A. LSBS-38R provided the best gloss retention for 80:20 UV-A STD samples, 80:20 colour retention for STD and Hot UV-A, the lowest increase in hydroxyl activity for 90:10 samples in Hot UV-A and naturally exposed 80:20 coatings. Finally, LSBS-41 provided the best colour retention for 90:10 Hot UV-A samples.

In terms of poor performance, we can see that LSBS-41 more readily provided coatings that were more susceptible to harm, suggesting that lowering the CHDM composition of the coatings causes significantly poorer performance than lowering the CHDA contribution. This could be due to 1,6 hexanediol being more susceptible to degradation than adipic acid or it could be due to CHDM having better weathering durability properties than CHDA. The coating with the best performance tends to be CHDA1.3DM, which is comprised of CHDA and CHDM with no additional straight chain additions, and it can be assumed that this is due to the lack of straight chain percentage components within the formulation preventing the coating systems from failing as rapidly as others.

From the observations made within this chapter, further research would be well suited to optimising the LSBS-37R and LSBS-38R formulations, as while they did not show superior weathering performance in all areas, they are consistently responsible for the coatings that are least damaged from exposure.

3.6-References

1. Amoco. How to Process Better Coating Resins with Amoco PIA and TMA. Amoco Chemical Company; 1992.

2. Siyab N, Tenbusch S, Willis S, Lowe C, Maxted J. Going Green: making reality match ambition for sustainable coil coatings. Journal of Coatings Technology Research. 2016;13(4):629–43.

3. Agreement of the Member State Committee on the identification of MethylHexahydrophthalic Anhydride as a substance of Very High Concern. [Internet]. 2012. Available from: https://echa.europa.eu/documents/10162/7183371/agreement_hhpa_en.pdf/8a707077-bf1c-462d-bf25-dd58ffa14cf8

4. Rosqvist S, Nielsen J, Welinder H, Rylander L, Lindh CH, Jönsson BAG. Exposure-response relationships for Hexahydrophthalic and methylHexahydrophthalic anhydrides with total plasma protein adducts as biomakers. Scandinavian Journal of Work, Environment and Health. 2003;29(4):297–303.

5. Kristiansson MH, Lindh CH, Jönsson BAG. Correlations between air levels of Hexahydrophthalic anhydride (HHPA) and HHPA-adducted albumin tryptic peptides in nasal lavage fluid from experimentally exposed volunteers. Rapid Communications in Mass Spectrometry. 2004;18(14):1592–8.

6. Nielsen J, Welinder H, Jönsson B, Axmon A, Rylander L, Skerfving S. Exposure to Hexahydrophthalic and methylHexahydrophthalic anhydrides - Dose-response for sensitization and airway effects. Scandinavian Journal of Work, Environment and Health. 2001;27(5):327–34.

Chapter 4-Development and analysis of Coating systems

4.0-Introduction

Coil coatings are used in a wide range of outside applications, such as machinery, cladding and automotive parts. This means that the coatings are exposed to environmental conditions that contribute to weathering degradation, including temperature variations, humidity, and strong sunlight, which have the potential to impact both the aesthetic appearance and protective capabilities of the coating which would lead to substrate damage. A more in-depth description of the influence of weathering on coating systems can be found in Chapter 1.

This chapter will outline the development, generation, and examination of three generations of coatings which differ in the components and relative concentrations of components, with the end aim being to determine how and why they degrade in the manner that they do in addition to understanding which monomer resin base provides the greatest level of protection from weathering degradation and why.

As has been mentioned in Chapters 1 and 2, natural weathering is the preferred testing method for coatings. However, the drawback of this type of testing is the time required to obtain meaningful data. As such, accelerated testing methods are utilised. It is accepted that these accelerated tests do not provide a true assessment of the weathering capabilities of the coating, as they focus on specific types of exposure (UV, Salt spray, etc) and tend to be more severe than natural testing methods. (1)

One of the physical tests that is of the greatest interest is gloss retention. Coatings lose gloss over time from an increased degree of surface roughness. Makki et al state that increased surface roughness arises from "…the lateral inhomogeneity of degradation processes" with areas of the coating surface being removed via interactions with water in the presence of oxygen. (1)

The findings of Makki et al support the work by Nguyen et al, who analysed samples via Atomic Force Microscopy (AFM) and Fourier Transform InfraRed (FT-IR) Spectroscopy to propose a model through which the inhomogeneous degradation occurs. They proposed that there are nanoscale hydrophilic areas within the coating comprised from unreacted and polar molecules. Nguyen et al go on to propose that these hydrophilic areas are dispersed randomly alongside highly crosslinked areas. When exposed to moisture, these hydrophilic areas are removed through interactions with water to create small craters within the coating that then act as ingress points for further degradation. (2)

In addition to indicating the best resin base for weathering resistance, this work will also investigate the influence that differing melamine ratios exert over the ability of a coating to resist photodegradation, the literature for which was discussed in Chapter 1, Section 1.4.3.1.

4.1-Initial coating development (Clear Coats)

Clearcoats are designed to be resistant against environmental stresses such as high temperatures, water, and UV exposure. Clearcoats see extensive use in both coil coating and automotive coating industries, therefore it is imperative that these coatings have weathering resistance as a key aspect of their design. Analysing clearcoats for their weathering resistance gives a truer measurement of the weatherability of the resin base, as there is no influence from pigments, which could act to hinder or accelerate the rate of degradation due to their own UV absorption characteristics.

4.1.1-Formulation and Generation

Based on the information discussed above and within the previous literature review chapter, the decision was made to analyse several different cycloaliphatic coatings via FT-IR, Raman, Gloss, and Colour analysis after every 500 hours of exposure to accelerated UV/Condensation weathering cycles.

Six clear coatings were developed using proprietary formulations from Becker industrial Coatings Ltd as discussed in Chapter 2. Clear coatings were chosen for initial generation and analysis due to their simplicity, which made it possible to gain experience in coating generation in addition to allowing analytical testing to have minimal input from components other than the base resin. The base resin controls the general properties of the coating and in turn is controlled by the monomers that are utilised in the synthesis of the resin. This made it possible to gain an insight into the behaviour of HHPA, CHDA, and CHDA/CHDM* containing coatings during accelerated weathering testing cycles. While these components were not the only ones contained within the resins, they made up a large percentage by weight and would be anticipated to have the most significant impact over the properties of the final resin. A more in-depth breakdown of the components of the resin system are found within Table 4.1.

A total of six coatings were produced at the Beckers Long Term Development facility using proprietary formulas. Two coatings were generated from each resin, as can be seen in the Table 4.1. The melamine used was Hexamethoxymethylmelamine (HMMM).

Table 4.1-*Breakdown of clear coats*

Sample code	Monomer resin base	Polyester: melamine ratio
HH8020	(44%) HHPA, Succinic acid, Sebacic acid	80:20
HH8515	(44%) HHPA, Succinic acid, Sebacic acid	85:15
CHDA8020	(42%) 1,4-CHDA, Succinic acid, Sebacic acid	80:20
CHDA8515	(42%) 1,4-CHDA, Succinic acid, Sebacic acid	85:15
CHDADM8020	(12%) 1,4-CHDA and (36%) CHDM, Succinic acid, Sebacic acid	80:20
CHDADM8515	(12%) 1,4-CHDA and (36%) CHDM, Succinic acid, Sebacic acid	85:15

A full description of the coating generation and analysis process can be found in Chapter 2.

4.1.2-Testing

4.1.2.1-Gloss measurements

Gloss measurements were obtained using a handheld gloss meter with a 60^{o} contact angle. Five measurements were obtained for each sample and an average was calculated to determine the average Gloss measurement for the coating.

4.1.2.2-Colour analysis

Colour analysis was performed with the use of a Colour Spectrolino, which measures L*, A*, B* and density of coatings. As the first generation were clearcoats, the observed colour change was far more likely to represent the primer layer beneath. However, colour change was still a useful measurement to take, as the primer layer would not exhibit a change in colour from UV light if the clear coat was performing effectively.

4.1.2.3-FTIR analysis

Fourier Transform-InfraRed (FT-IR) analysis was carried out via UATR PerkinElmer FTIR, scanning from 4000cm^{-1} to 400cm^{-1}. Following acquisition of a background spectra, each punched coupon (obtained as previously stated) was placed over the UATR crystal and clamped down to ensure adequate contact was made before the spectra were obtained.

The spectra were then analysed to determine common peaks between the samples. Table 4.2 shows the bands that were focused on during the investigation, as well as the bonds that they correlate to.

Table 4.2-*Breakdown of IR peaks of interest*

Band position (cm^{-1})	**Corresponding bond**
3560-3160	O-H stretch
3000-2800	CH_2 + CH_3 stretch
1730	C=O Stretch
1545	In plane Deformation of Triazine ring
1475	
1450	Triazine ring + CH_2+CH_3 Bending
1375	CH_3 Bending
1350	C-H bending
1310	C-O of O=C-O-C
1240	C-O-C from O=C-O-C
1155	C-O-C from O=C-O-C
1110	C-O stretch
1070	CO-O-CO Anhydride stretch
1030	C-O stretch from O-CH
1000	
875	C=C Bending
815	Out of plane Triazine ring deformation
755	CH_2 rocking

Of the bands described above, several were of interest. The peaks that corresponded to a triazine ring (both in and out of plane) deformation were monitored as a way of investigating the fate of the HMMM, which was the only triazine ring containing component of the coating.

4.1.2.4-Raman analysis

Raman analysis was carried out using a Renishaw inViva Raman Microscope with a Renishaw CCD Camera as a detector, a 90mW 532nm excitation laser, and a 50 × 0.5 NA objective lens which led to a spot size of 1.2 μm. Analysis of the primer layer was performed utilising 5% power for 5 seconds, however, this could not be replicated with the clear coat samples due to experiencing sample degradation through burning, so scans of the clear coat samples were run at 5% power for 1 second for 3mW power.

It was possible to identify clearly separate areas through microscopic analysis, and separated through Raman microscopy as white, yellow, and dark green/black regions. As the samples being analysed are clear coats it would be reasonable to assume that all colouration arises from the primer coating beneath,

which was shown to be true through comparing primer images against those obtained from the clear coated samples.

Analysis of a primed panel without a clear coat showed that the primer layer exhibits the same topographic structures, indicating that the environments shown in the images obtained from the Raman microscope are largely representative of the primer layer rather than the clear coats themselves.

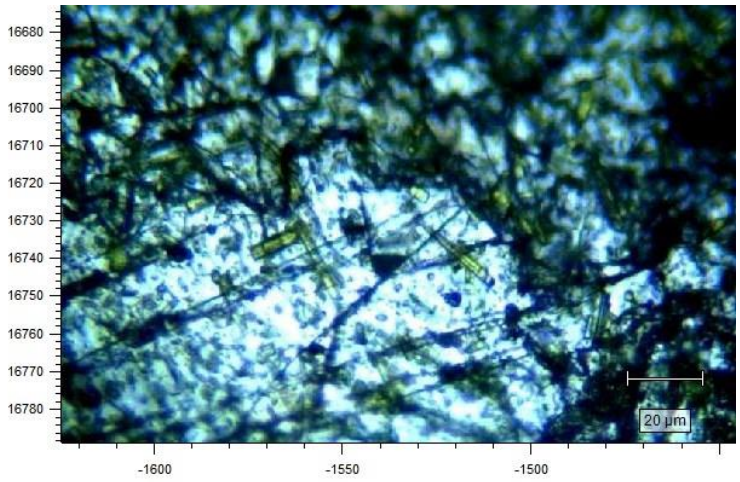

Figure 4.1-*Raman microscopy image*

Analysis of the different topographic regions yielded spectroscopic differences, which have been broken down and shown in Table 4.3 and Figures 4.2-4.13. The spectra in these figures were baseline corrected and smoothed in order to minimise the impact of noise that was brought about through the short laser excitation time and allow peaks of interest to be identified through the analysis software.

Table 4.3-*Raman frequencies of common chemical functional groups* (6)

Peak correspond to:	**Peak location (Raman shift cm-^{1})**
Lattice vibrations	74
Lattice vibrations	92
Aliphatic chain	374
C-O-C	864
Carboxylic acid	892
Aliphatic ring	1001
Aliphatic ring	1449
C=N	1612
Carboxylic acid	1724

From comparing the spectra obtained for the same regions with and without the clear coats it can be seen that there is a difference both in peak intensities and in the peaks that can be identified. The intensity of the spectra obtained from clear coats were weaker in all instances, most significantly when analysing the white regions, where a maximum count of 11,600 was obtained when analysing the primer, and 2800 when looking at the clear coated samples.

From analysing the spectra from the different coating systems against that obtained from the primer layer alone has shown that there are differences in the peaks observed. Comparing Figures 4.2-4.5 show significant differences in the obtained spectra for the dark regions of the system as shown in Figure 4.1, not just between the primer and the clear coats, but between the different coating systems. Most peaks were identified from the primer, with 864cm^{-1} and 892cm^{-1} showing the greatest intensity. The HH8020 coating shows peaks corresponding to lattice vibrations, an aliphatic chain, C-O-C and carboxylic acid, with the latter 2 peaks again showing the greatest intensity. Figures 4.4 and 4.5 show extremely similar spectra, this would be expected as both coatings contain CHDA. The most intense peak in both instances was for the lattice vibrations at 74cm^{-1}, while other peaks showed minor differences in intensities. It is possible that the bands at approx. 850cm^{-1} could be assigned to the chromate of the strontium chromate that comprises the primer, these are able to show up even when focussed on top coating surface due to light passing through the clear coat and exciting the molecules within the primer. (7)

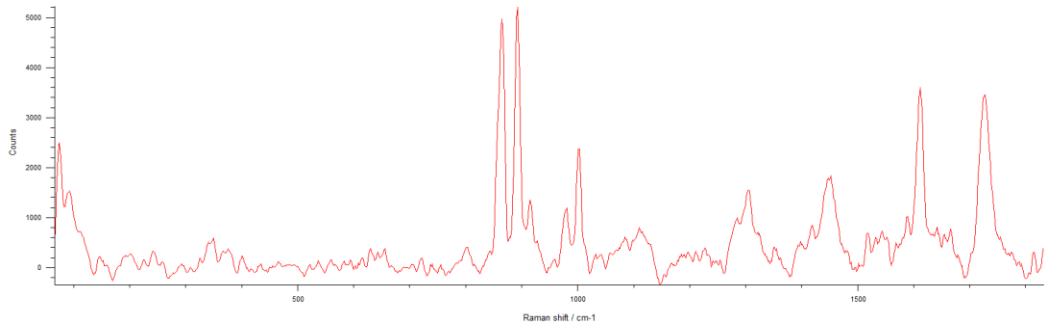

Figure 4.2-*Raman spectra of Dark region from primer*

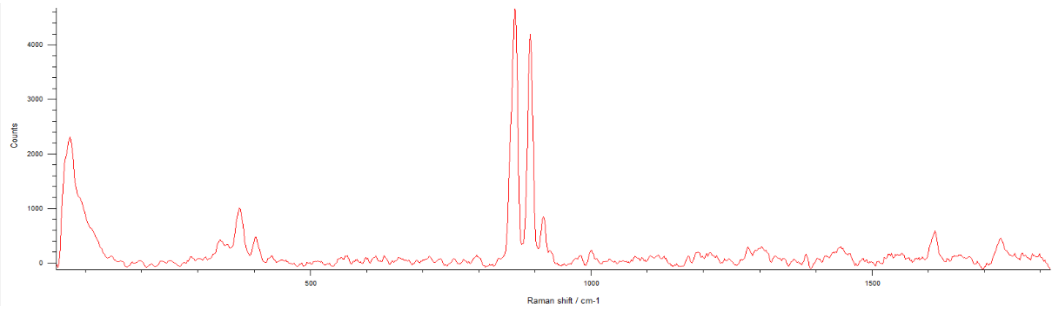

Figure 4.3-*Raman spectra of Dark region from HH8020*

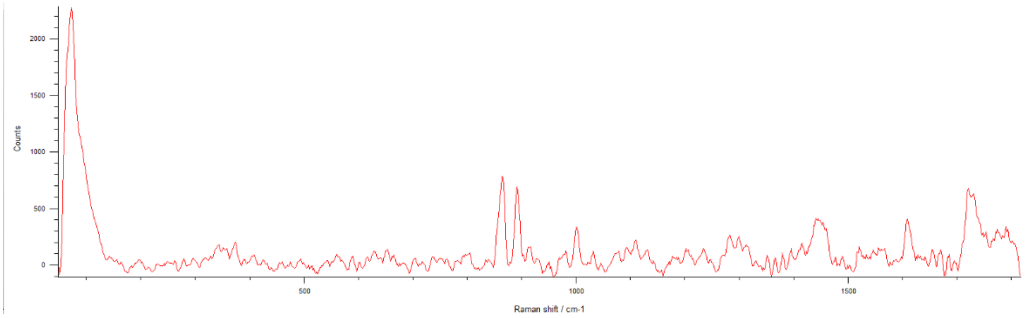

Figure 4.4-*Raman spectra of Dark region from CHDA8020*

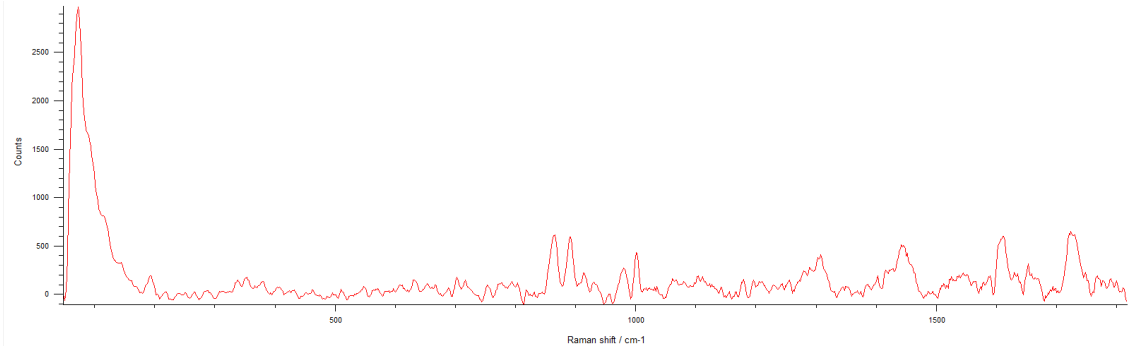

Figure 4.5-*Raman spectra of Dark region from CHDADM8020*

Figures 4.6-4.9 illustrate the Raman spectra from the primer and all coating systems at the yellow crystalline regions shown in Figure 4.1. The most intense peaks in all of the spectra correspond to C-O-C bonds and carboxylic acid. HH8020 shows a large peak for lattice vibrations, followed by a peak for the Aliphatic chain. Figure 4.8 shows that CHDA8020 primarily shows peaks at 864cm^{-1} and 892cm^{-1}, with small levels of activity for regions indicating the aliphatic chain and lattice vibrations. The CHDADM8020 spectrum shows the same peaks as the CHDA8020 spectrum but with greater intensities for all, with the exception of the lattice vibrations, which were the same in both.

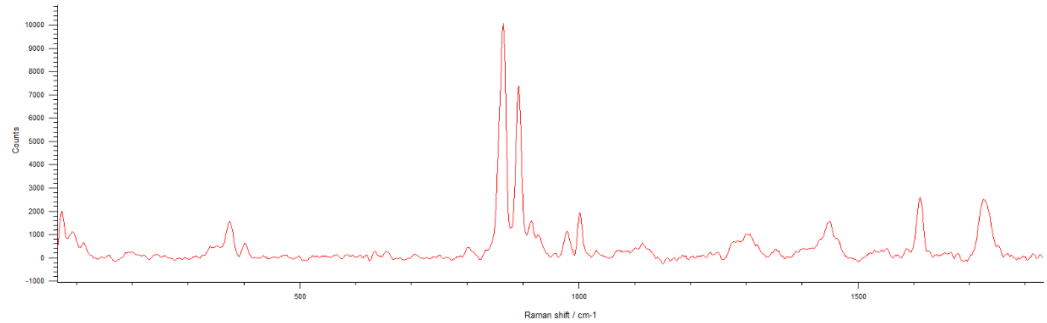

Figure 4.6-*Raman spectra of yellow crystal like regions from primer*

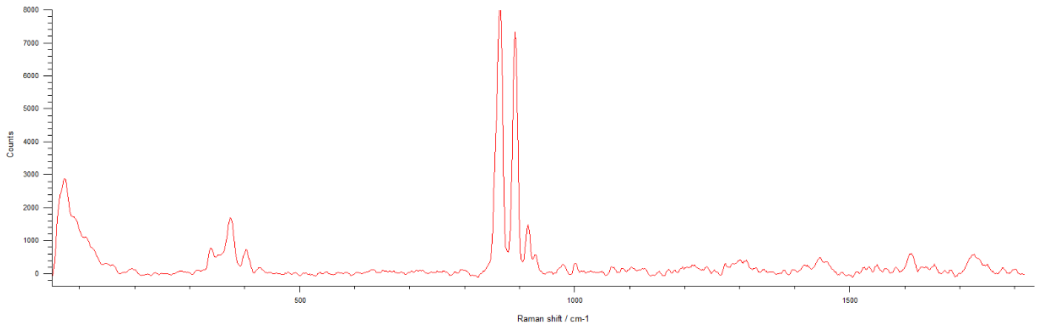

Figure 4.7-*Raman spectra of Yellow crystal like regions from HH8020*

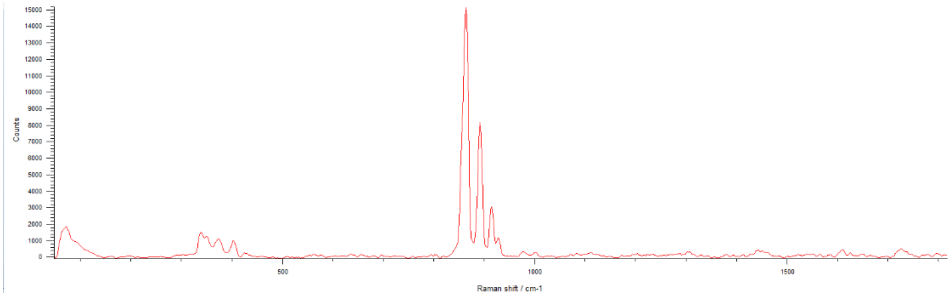

Figure 4.8-*Raman spectra of Yellow crystal like regions from CHDA8020*

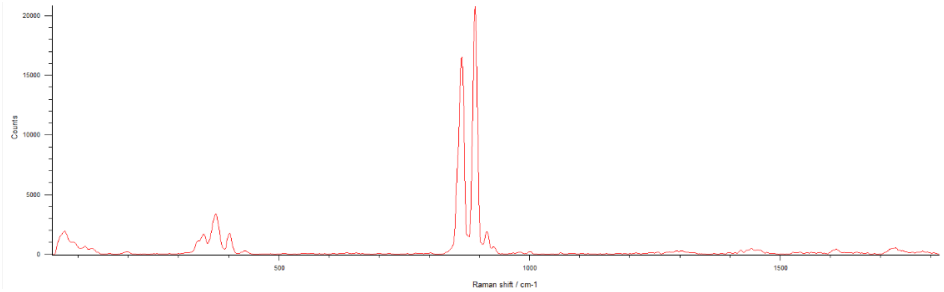

Figure 4.9-*Raman spectra of Yellow crystal like regions from CHDADM8020*

The spectra for white regions (as identified in Figure 4.1) taken from the primer and various coating systems can be seen in Figures 4.10 – 4.13. It can be seen that for all the coating systems the most prominent peak related to lattice vibrations, with low intensity peaks in other areas relating to aliphatic rings, C=N bonds and carboxylic acid.

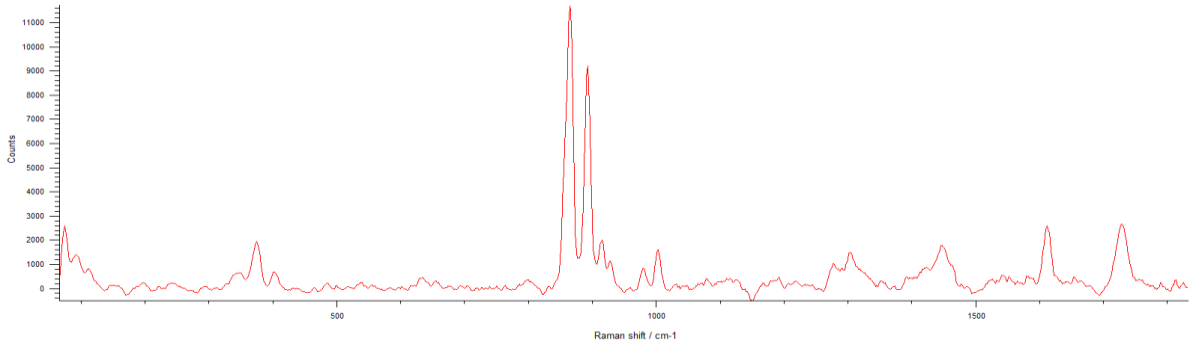

Figure 4.10-*Raman spectra of White regions from primer*

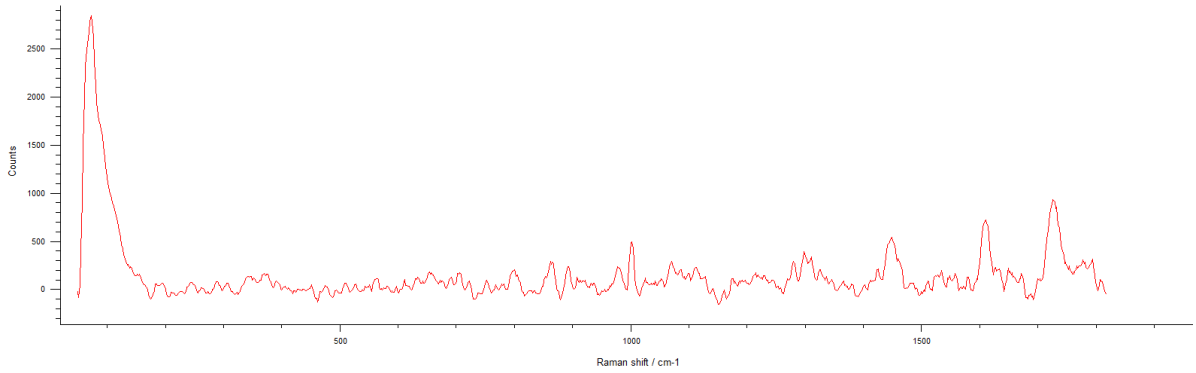

Figure 4.11-*Raman spectra of White regions from clear coat HH8020 sample*

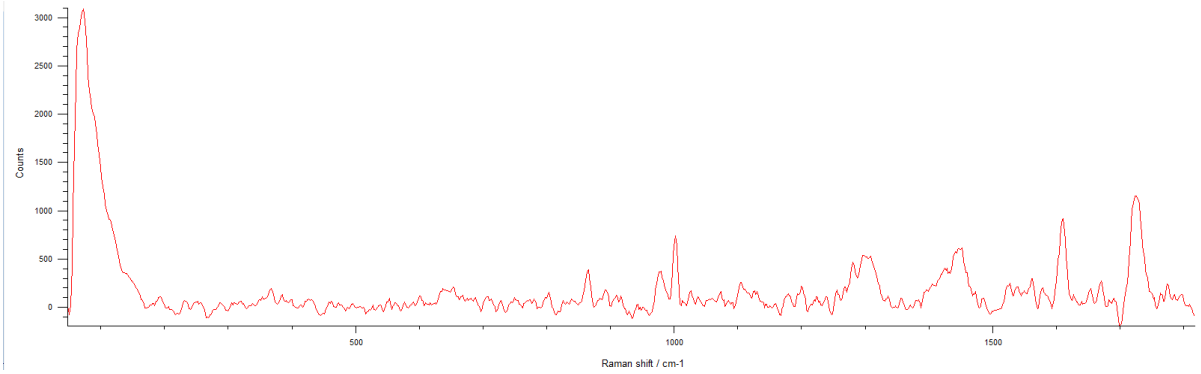

Figure 4.12-*Raman spectra of White regions from clear coat CHDA8020 sample*

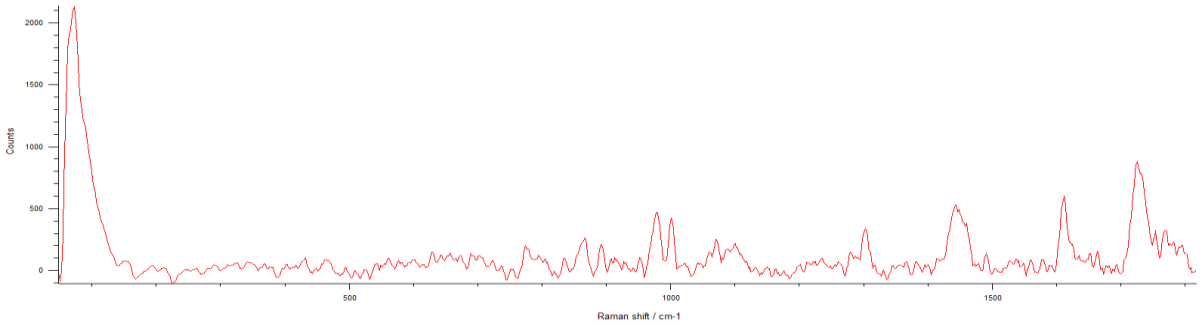

Figure 4.13-*Raman spectra of White regions from clear coat CHDADM8020 sample*

From analysing the different Raman spectra, it becomes possible to see that the different coating systems demonstrate peaks of different intensities and at different Raman shift positions. This could be indicative of the underlying primer layer influencing the top clear coat in different ways depending on the chemistry of the coatings, with CHDA and CHDA+CHDM coatings sharing the greatest level of similarities due to the presence of CHDA within both coating systems.

4.1.2.5-Thermal gravimetric analysis

Thermal Gravimetric Analysis (TGA) was also performed on the coating systems to determine their Glass Transition Temperatures (T_g). Understanding the T_g is crucial in gaining a clearer overall picture of all the factors that influence the weathering durability of the coating systems. A breakdown of the T_g values of clear coat systems is provided in Table 4.6.

4.1.2.6-Gloss retention

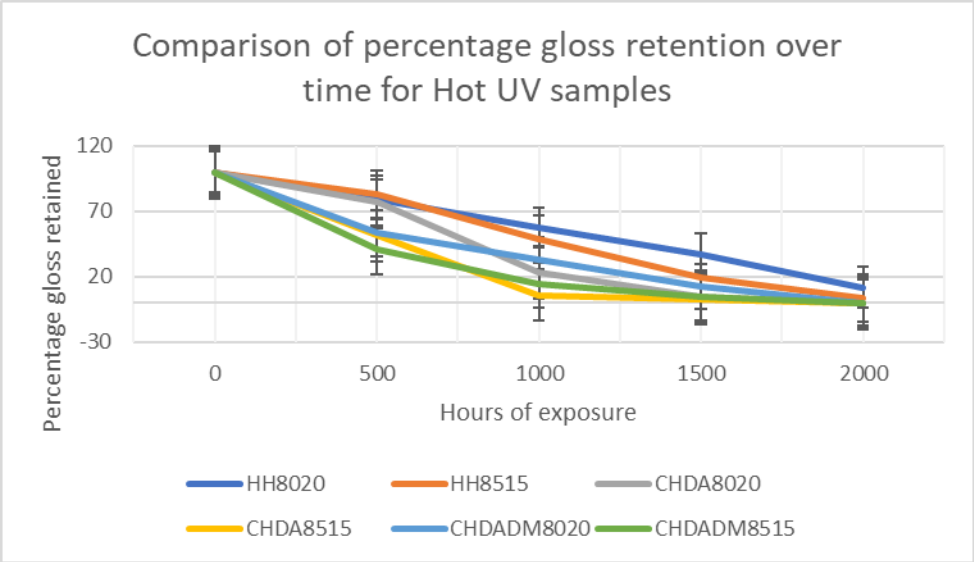

Figure 4.14-*Comparison of changes in percentage gloss values over time of samples subjected to HOT UV-A weathering*

Analysis of percentage gloss change over time for samples exposed to Hot UVA accelerated weathering (Figure 4.14) showed that all the 85:15 ratio coatings performed worse than their 80:20 counterparts. It should also be noted that even when removed at 2000 hours for excessive degradation, the coatings containing HHPA retained a higher percentage of gloss than any of the other coatings, which were removed after 1500 hours due to significant damage and flaking away from the substrate. The 85:15 ratio CHDA coating performed the worst by retaining the lowest percentage of gloss.

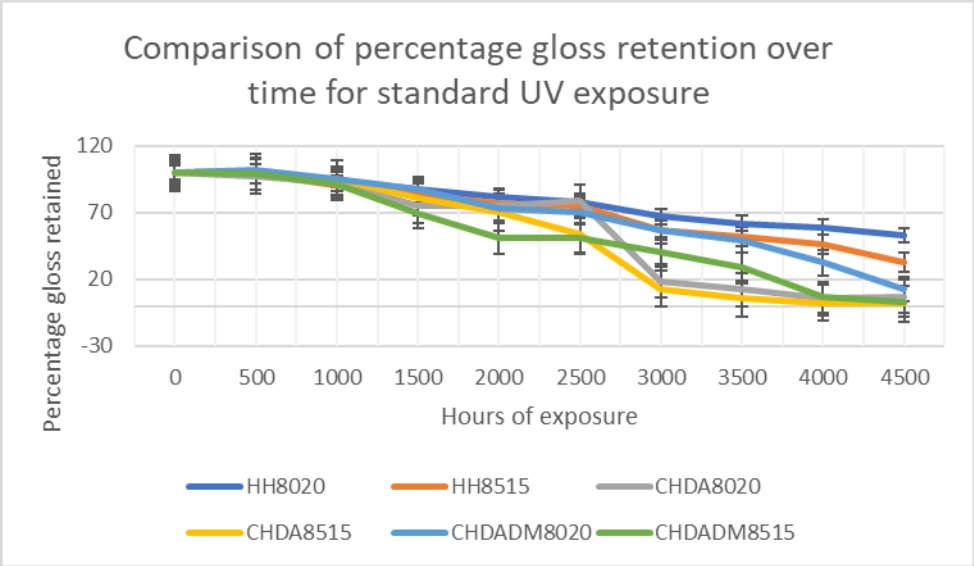

Figure 4.15-*Comparison of changes in percentage gloss retention over time of samples subjected to STD UV-A weathering*

Figure 4.15 shows that samples exposed through STD UV-A accelerated weathering cycles for a longer period, once again showed that the coatings containing provided the highest levels of gloss retention with the 80:20 ratio coating surpassing the 85:15 coating. The trend of the 85:15 ratio coatings exhibiting poorer gloss retention was also continued with those exposed through standard accelerated weathering. The CHDA containing coatings were the poorest performing in both the 80:20 and 85:15 ratios.

4.1.2.7-Colour analysis

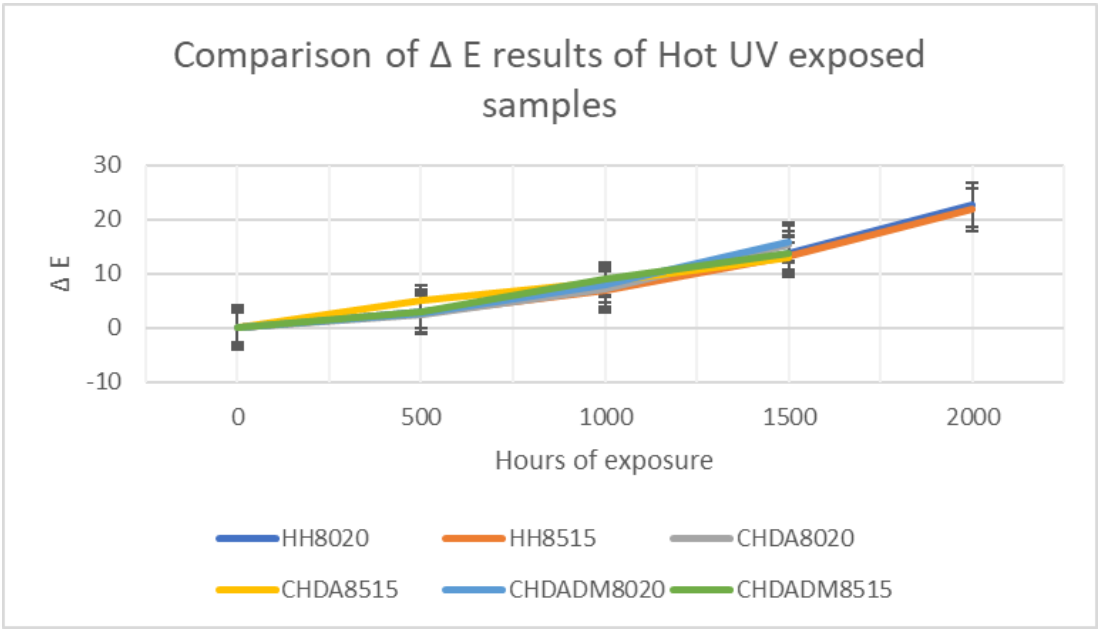

Figure 4.16-*Comparison of ΔE measurements over time of samples subjected to HOT UV-A weathering*

ΔE was calculated via repeated CIELab67 L*A*B* colour measurements to assess how the coating colour changed over time before ocular examination would indicate a change in colour. Analysis of the results for the samples that were exposed to Hot UVA accelerated weathering cycles showed similar behaviour to the samples discussed above, with CHDA containing coatings being the poorest performing and with 80:20 coatings showing the greatest degrees of colour change within the primer, indicating that the clear coat offered greater levels of protection. After 1500 hours, the same pattern was observed from the CHDA:CHDM coating containing as well. All CHDA and CHDA:CHDM containing samples were removed from Hot exposure after 1500 hours due to the significant damage that had befallen the coatings. The HHPA containing coatings remained the best performing until the point of their removal after 2000 hours of exposure, although at the point of the final measurement the 85:15 coatings showed slightly less colour change of the primer when compared to the 80:20 samples.

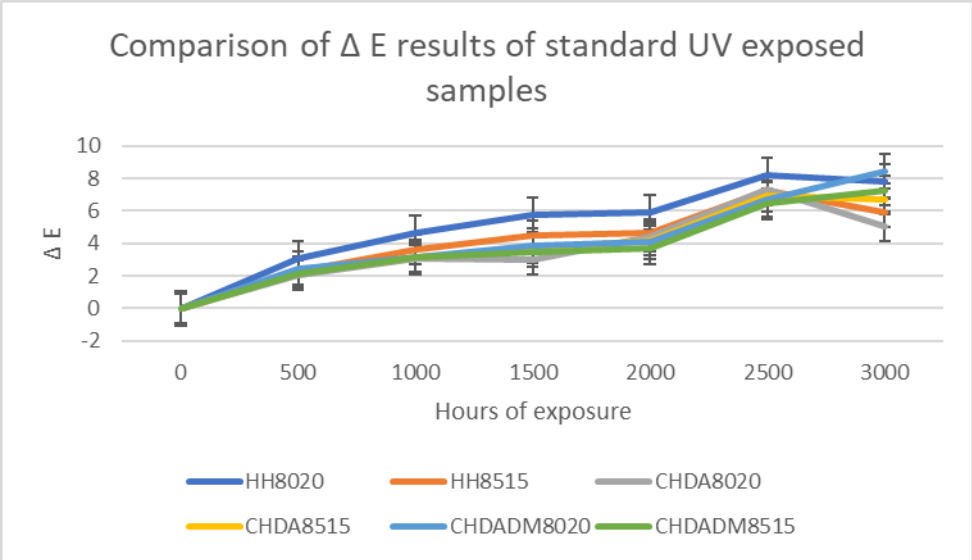

Figure 4.17-*Comparison of ΔE measurements over time of samples subjected to STD UV-A weathering*

As expected, coatings exposed through Standard UV-A accelerated weathering exhibited significantly lower levels of colour change of the primer layer than the Hot UV-A samples.

The patterns that were exhibited previously were largely observed within the samples exposed to standard cycles, with the 85:15 coatings exhibiting lower levels of colour change than their 80:20 counterparts. At the end of exposure (4000 hours), the worst performing coating in terms of colour retention was CHDADM8020, with the second poorest performing coating being CHDADM8515. The best performing coating after 4000 hours of exposure was observed to be CHDA8515.

4.2.1.8-FTIR analysis change in hydroxyl activity

The area of greatest interest during weathering tests is the hydroxyl area (3800 cm^{-1} - 2040cm^{-1}), as increases within this region are attributed to the production of hydroxyl free radicals that are generated as photodegradation products. An example spectrum is shown in Figure 4.18.

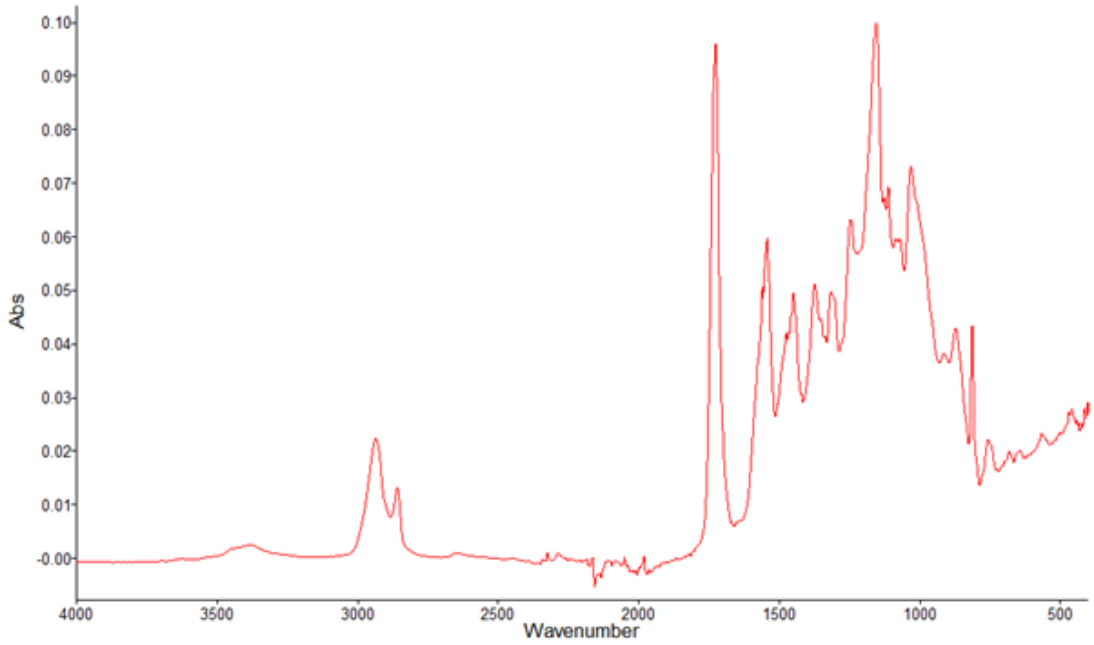

Figure 4.18-*Example baseline spectrum from HH8020*

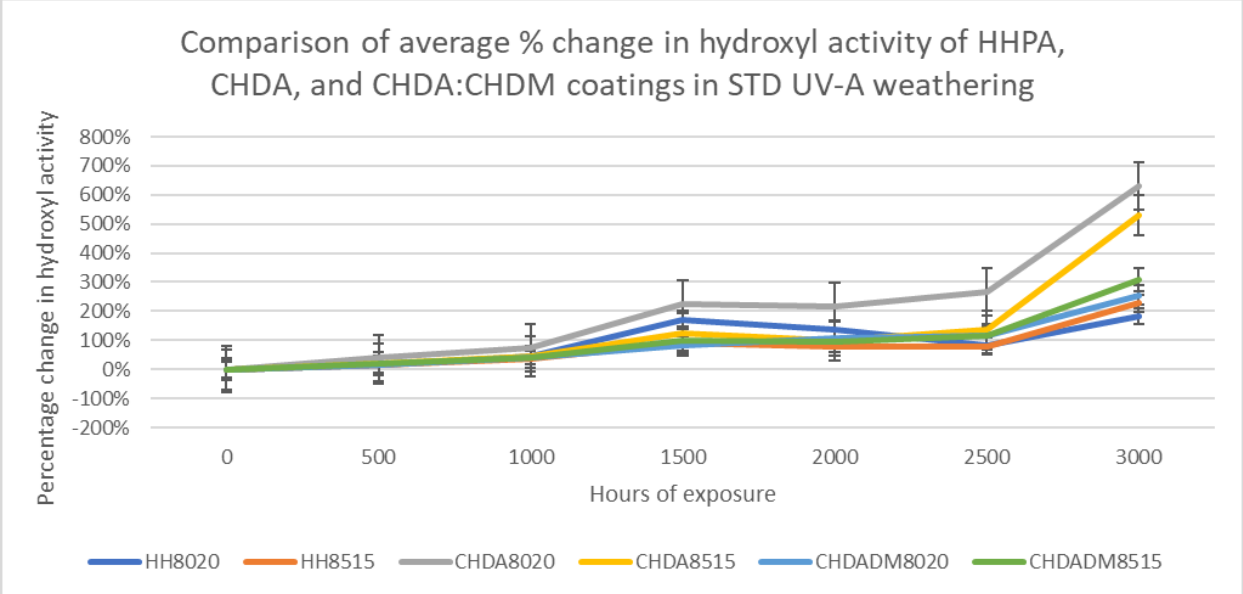

Figure 4.19-*Comparing the average percentage change in hydroxyl activity over time for samples subjected to STD UV-A weathering cycles*

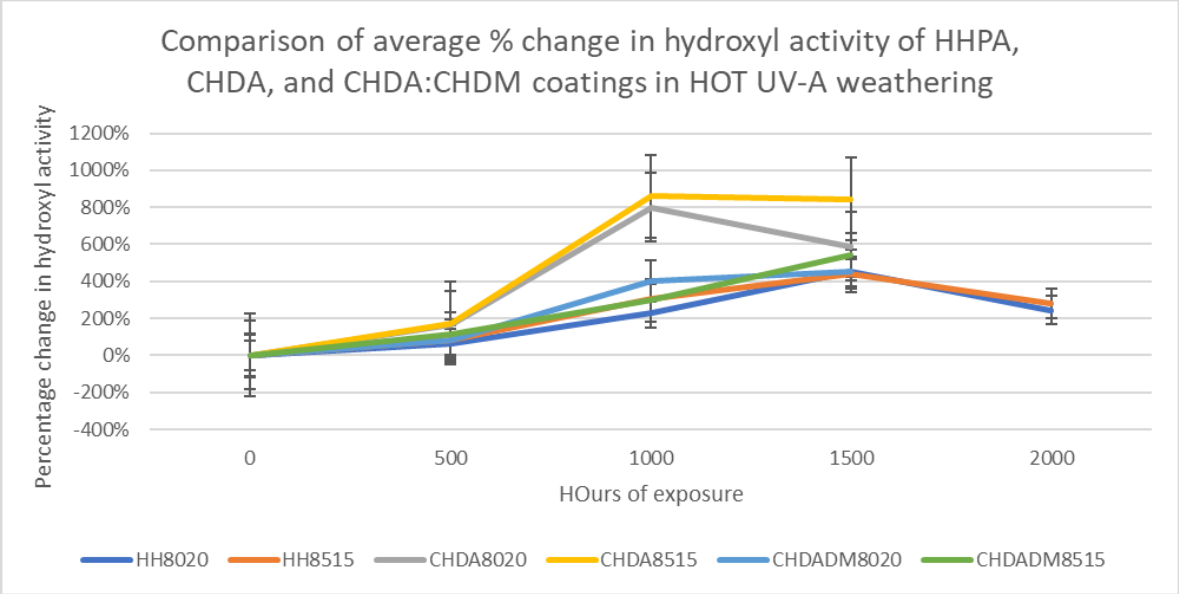

Figure 4.20-*Comparing the average percentage change in hydroxyl activity over time for samples subjected to HOT UV-A weathering cycles*

Figures 4.19 and 4.20 give a breakdown of the percentage changes in hydroxyl activity during STD UV-A and Hot UV-A weathering cycles. In both instances the CHDA coatings showed the greatest increase in hydroxyl activity. In Figure 4.19 it is only CHDA8020 that shows a greater increase in hydroxyl activity than its 8515 variant. In Figure 4.20, two peaks can be observed, one at 1000 hours which impacted CHDA8020, CHDA8515, CHDADM8020, and CHDADM8515, followed by the second at 1500 hours that affects HH8020, and HH8515. The decrease in hydroxyl activity following these peaks indicates that the coatings were beginning to fail, this was corroborated through visual inspection and resulted in the coatings being removed from testing following the next exposure cycle (1500 hours and 2000 hours respectively).

Raman microscopy allowed images to be obtained that tracked the physical degradation of the coating layers, as can be observed in the images from 80:20 ratio CHDA samples subjected to HOT UV-A, illustrated in Figures 4.21 - 4.24. It is believed that the observed damage occurred in the clear coat layer (at least initially) as if the damage were localised to the primer layer beneath then spectroscopic analysis of the area would indicate the presence of the topcoat.

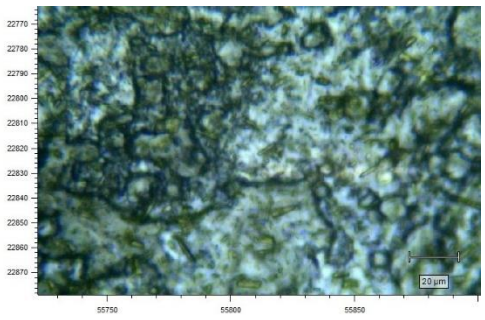

Figure 4.21-*CHDA8020 0 hours*

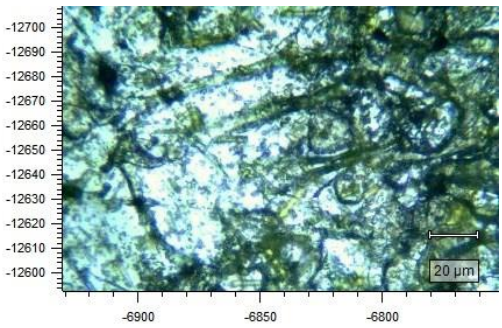

Figure 4.22-*CHDA8020 500 hours*

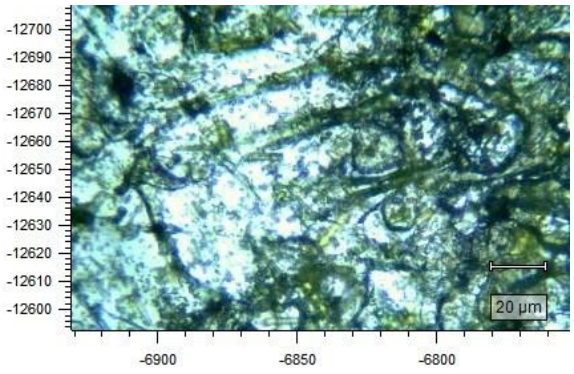

Figure 4.23-*CHDA8020 1000 hours*

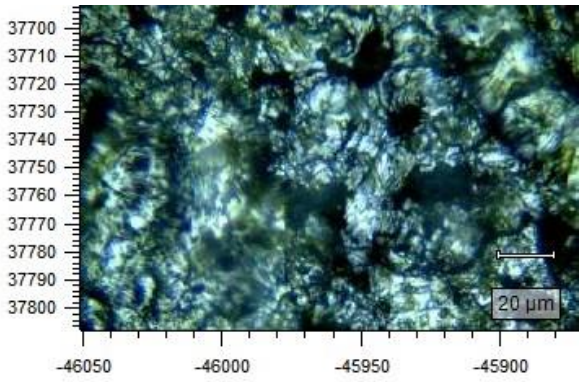

Figure 4.24-*CHDA8020 1500 hours*

Figures 4.21-4.24 show the propagation of degradation across the coating in the form of the dark areas, which have been identified in the red circles. When Raman microscopy is used to attempt to gain a spectrum of these dark regions, it only returns noise, which indicates that there is no coating present, suggesting that the areas are holes. Before the coating was exposed it did not show any areas of degradation, after 500 hours there was one clear area of degradation, this increased to two large areas of degradation and several smaller areas after 1000 hours and finally after 1500 hours of exposure areas of degradation had propagated throughout the coating. It should be noted that the holes that were observed were of a greater size than required to cause an impact in gloss readings.

Raman microscopy has previously been used to study the distribution of melamine within polyester-melamine coating systems. It is known that melamine enrichment can be observed towards to the coating/air interface following high temperature curing, as shown by Hirayama et al. While there are several differences between the coatings in the make up on their resin bases, the primary monomer (HHPA, CHDA, or CHDA & CHDM) is the most significant difference between them, which suggests that the monomer with the greatest percentage weight within the base resin can exert an impact over the

distribution and degree of melamine agglomeration throughout the coating, with the HHPA containing resin facilitating lower instances of melamine agglomeration throughout the coating.

As has been mentioned previously, T_g is an important consideration when determining how practical a coating will be in different environments. Figure 4.25 and Table 4.4 give a breakdown of the T_g of the clear coats.

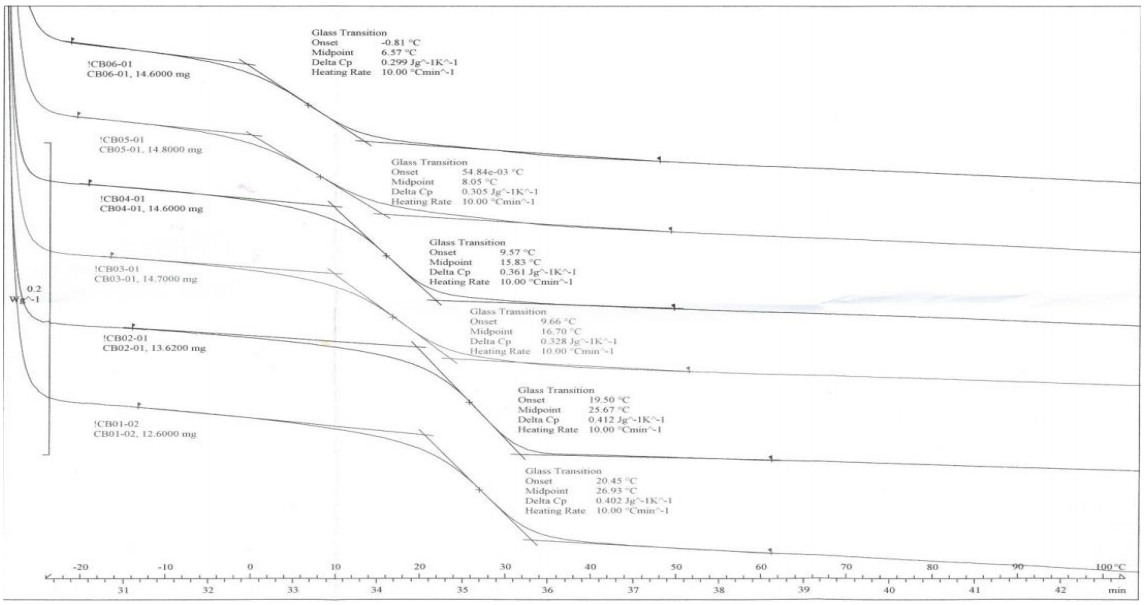

Figure 4.25-*T_g results for clear coats*

Table 4.4-*Breakdown of the T_g of the clear coats and their PE:HMMM ratios*

Sample Code	Midpoint T_g value (°C)	PE:HMMM Ratio
HH8020	27	80:20
HH8515	26	85:15
CHDA8020	17	80:20
CHDA8515	16	85:15
CHDADM8020	8	80:20
CHDADM8515	7	85:15

The T_g of the samples analysed within this section can be seen in Table 4.4 and Figure 4.25. The T_g of the samples show that most are not particularly suitable for architectural use, with only HH8020 and HH8515 showing satisfactory T_g levels, this is because temperatures in most environments can exceed those required for the coatings to reach their T_g. However, if any of the coatings show a suitably high level of degradation resistance, then further research can be undertaken to determine if the T_g can be improved without altering the properties of the coating to a significant degree.

The T_g of the coatings impacts the environments that they are suitable for use in, with HH8020 being the most suitable for warmer environments with a transition temperature of 27°C, and CHDADM8515 having the lowest T_g, with a result of 7°C. These low T_g results had the potential to contribute to lower weathering durability.

The low T_g measurements that were obtained for CHDADM8020 and CHDADM8515 aid in explaining how an increase in gloss was obtained during exposure. The low T_g made re-flow possible, which is often accompanied by an increase in the gloss level by the coating smoothing out as the top moves from a solid state to a liquid state and filling in some of the crevices that developed through interactions with water and photodegradation. As gloss decreases with increasing surface roughness, the act of smoothing out the coating leads to apparent increases in gloss despite the continued degradation of the coating.

From observing the T_g of the clear coats it is possible to see that diminishing the ratio of crosslinker within the formulation results in a decrease in the measured T_g. It has also been observed that HHPA based coatings give the highest T_g, followed by CHDA containing coatings, with the CHDA-CHDM co-monomer containing coatings recording the lowest T_g values.

4.1.3-Conclusions

In terms of gloss and colour retention HHPA containing clear coats perform in a superior manner compared to their CHDA, or CHDA:CHDM counterparts. The behaviour of the CHDA and CHDA:CHDM containing clear coats is interesting, as while there is some variance in the early stages of exposure, it has generally been observed that CHDA containing coatings provide poorer gloss and colour retention towards the latter exposure cycles.

While CHDADM8020 and CHDADM8515 showed a rapid decrease in gloss retention during initial weathering cycles, this slowed significantly as exposure continued. It is possible that this apparent gloss retention was actually a consequence of reflow of the coating surface that occurred due to the low recorded T_g values. Reflow would have undone some of the damage caused by photodegradation and caused a decrease in surface roughness, which directly impacts the observed gloss value.

As previously discussed, Raman analysis has shown that some melamine structures can reach a significant size, identified to be more than 20μm in length. The dry film thickness of polyester-melamine coatings is limited to 20μm, so it is possible that providing the structures are in the correct orientation, melamine crystals could breach the surface of the coating. Crystals breaching the surface would provide areas of weakness and potentially lead to moisture entering the coating system and reaching to the

coating/substrate interface, where significant damage, such as delamination of the coating from the substrate, could occur. Figure 4.26 illustrates the lateral inhomogeneities that could occur across the surface of the coating.

It has also been observed that melamine has a predisposition to be attracted to the coating-substrate interface. Raman analysis (as discussed previously) has shown that there are melamine crystals in excess of 20μm long, which makes it feasible that if the crystals are orientated in the correct way, they can travel from the coating-substrate interface and reach the coating-air interface. This would provide additional nucleation points for degradation, as well as easier ingress points for moisture which would lead to additional moisture enhanced photodegradation. Work by W.Zhang *et al* showed that melamine agglomerations have a tendency to develop at the surface of aliphatic polyester coatings, where they degrade first, leaving holes in the coating. (8–10)

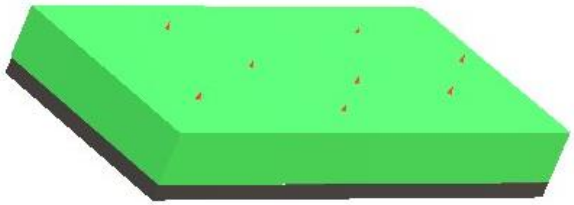

Figure 4.26-*Illustration of melamine crystals breaching the coating surface following curing*

It is clear that in terms of clear coats, the HH8020 and HH8515 coatings outperform both the CHDA and CHDA:CHDM counterparts, with the CHDA containing coatings being the poorest performing overall.

4.2-Second Generation coating Development

4.2.1-Formulation

Of the first generation of novel resin systems, two were of a suitable standard for use in the development of the second generation of full coating systems. As it is very uncommon for architectural coatings to be clear coats, it was decided to develop a pigmented coating system. The HHPA containing coatings (HH*8020Br, HH*8020BrH, HH*8515Br, HH*8515BrH) were developed from the LSBS-STD resin which was covered in detail in Chapter 3. These coatings acted as the standards against which all other coatings in this section were measured as they represented a primarily HHPA containing coating system against which the CHDA containing coatings could be compared against. It was also decided to include a pigmented

variant of HH8020 (HH8020Br) to compare the weathering resistance of primarily HHPA based coatings and a HHPA containing one.

The chosen colour of the coating system was ‘‘chocolate brown’’. This colour was picked due to the relatively small amount of TiO_2 (Titanium Dioxide) that would be present within the formulation. While TiO_2 lends beneficial properties to coatings, it can cause an increase in initial degradation sites across the coating surface due to its semi-conductive nature, which in turn would alter the rate that the coating would degrade during exposure. More detail is given on the potential negative impacts of the inclusion of TiO_2 is set out in Chapter 1.

4.2.2-Generation

The coatings were developed within the resin and coatings laboratory within Swansea University before being applied to chromate primed steel with a 28k wire wound bar to result in a dry film thickness of 20μm. A detailed description of the coating generation process is available in Chapter 2.

4.2.3-Testing

Pigmented samples were analysed for changes in both gloss and colour change, as well as IR spectroscopy and glass transition temperature as described previously within this chapter.

It was initially planned to analyse pigmented samples via Raman microscopy with the same settings that were used for the clear coat samples above (Scans were run at 5% power for 1 second). However, it was not possible to analyse the pigmented samples using Raman microscopy due to their colouring, as it caused extreme degradation of the samples even during the briefest exposure and lowest energy levels.

4.2.4-Results

Figure 4.27 shows the results of the percentage gloss retention 3000 hours of accelerated weathering under 80^{o}C UV / 50^{o}C Condensation cycles (8Hr/4Hr). The CHDA containing coatings have significantly poorer performance compared to their HHPA containing counterparts. With the 80:20 coatings outperforming their 85:15 ratio versions for each monomer. It is also interesting to note that the control coating has a poorer final performance compared to the other HHPA containing coatings. This has been theorised as being due to the other components within the resin base that were not present within the novel resins generated for this investigation. Table 4.5 gives a breakdown of the resin components within the HHPA containing control coating, as well as the novel HHPA and CHDA containing coatings.

Table 4.5-*Breakdown of major resin components of second-generation coatings*

	Resin code	**Resin components**
Control coating	BK001	HHPA, Succinic acid, Sebacic acid, TriMethylol Propane, NeoPentyl Glycol, Ethylene Glycol, Hexanediol
Novel HHPA coating	LSBS-STD	HHPA, TriMethylol Propane, NeoPentyl Glycol, Ethylene Glycol, Hexanediol
Novel CHDA coating	LSBS-33	CHDA, TriMethylol Propane, NeoPentyl Glycol, Ethylene Glycol, Hexanediol

Figure 4.28 shows a similar situation, with all 80:20 coatings outperforming their 85:15 counterparts and with HHPA based coatings showing significantly greater percentages of gloss retention compared by the CHDA containing coatings. CHDA containing coatings give the appearance of being impacted to a greater degree by STD UV-A accelerated weathering cycles than the HHPA containing alternatives. This is observed through the faster decrease in retained gloss percentage.

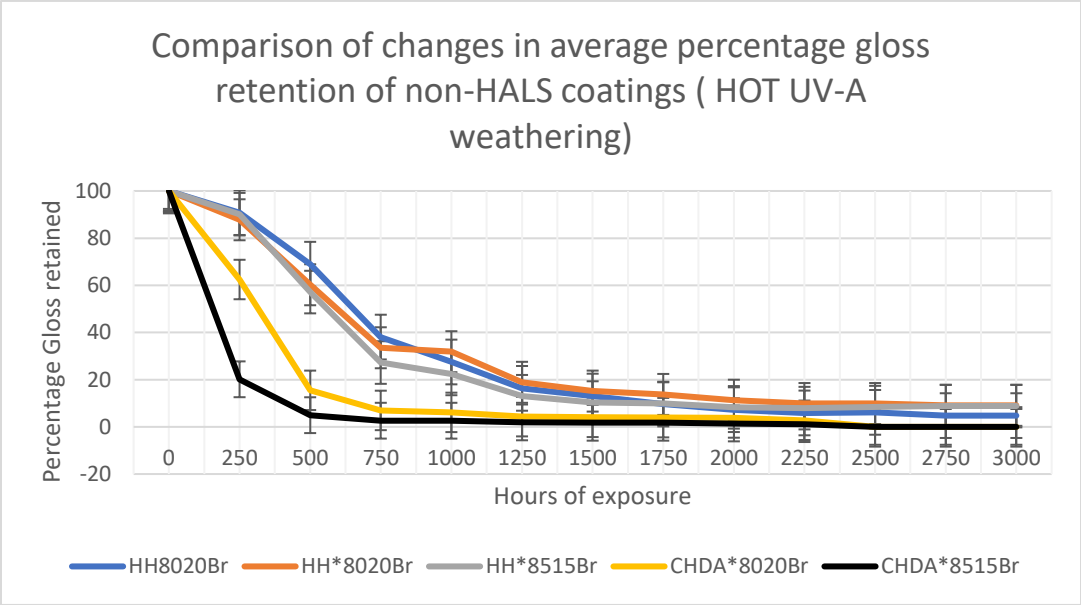

Figure 4.27-*Comparison of change in percentage gloss values of non-HALS coatings subjected to HOT UV-A weathering cycles*

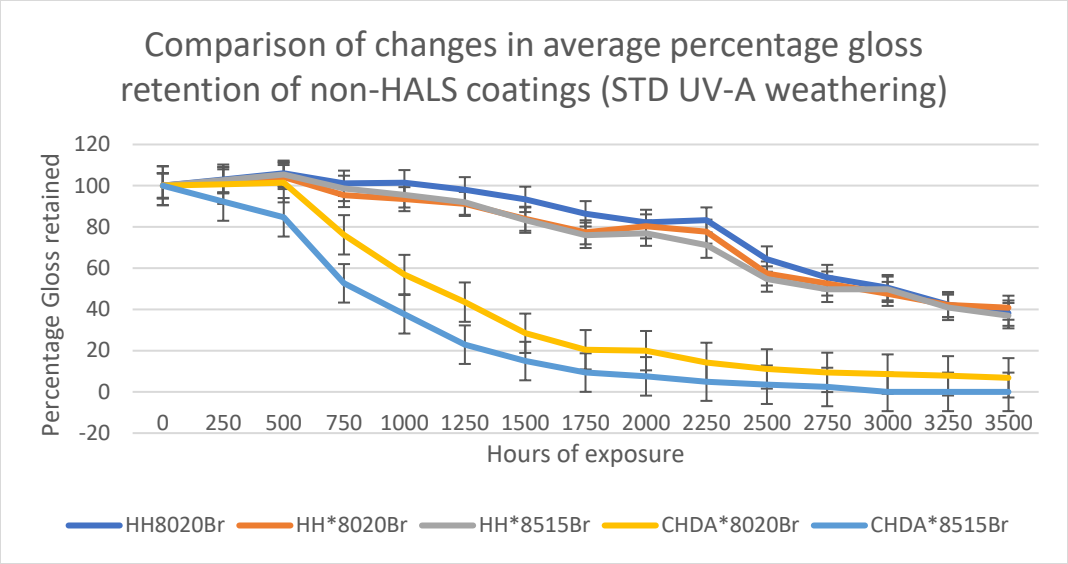

Figure 4.28-*Comparison of change in percentage gloss values of non-HALS coatings subjected to STD UV-A weathering cycles*

The average change in Δ E is representative of the change in colour during exposure. It is interesting that Figure 4.29 shows a relatively small increase in Δ E value for all coatings which give very similar values, despite the accelerated weathering conditions being the most severe and the CHDA based coatings requiring early removal due to their highly degraded state. Figure 4.30 gives a breakdown of HALS containing HHPA and CHDA coatings subjected to Hot UV-A, which show a greater degree of colour retention compared to the non-HALS variants, with CHDA*8020BrH showing the largest change in Δ E for all HALS coatings.

Figure 4.31 shows a greater increase in Δ E values, with CHDA containing coatings showing significantly greater change than their HHPA containing counterparts. The 85:15 CHDA containing coating displayed a higher Δ E value compared to the 80:20 CHDA containing coating whereas the HHPA containing coatings showed extremely similar values. Figure 4.32 gives a breakdown of the change in Δ E of the HALS containing coatings that were subjected to STD UV-A weathering, with all HALS coatings showing a smaller change in Δ E than the non-HALS variants. Additionally, the HHPA containing coatings exhibit significantly smaller colour changes than the CHDA containing coatings, showing that CHDA containing coatings are more susceptible to photodegradation to the point that the sacrificial HALS are used up at an accelerated rate, with CHDA*8515Br demonstrating significantly poorer performance.

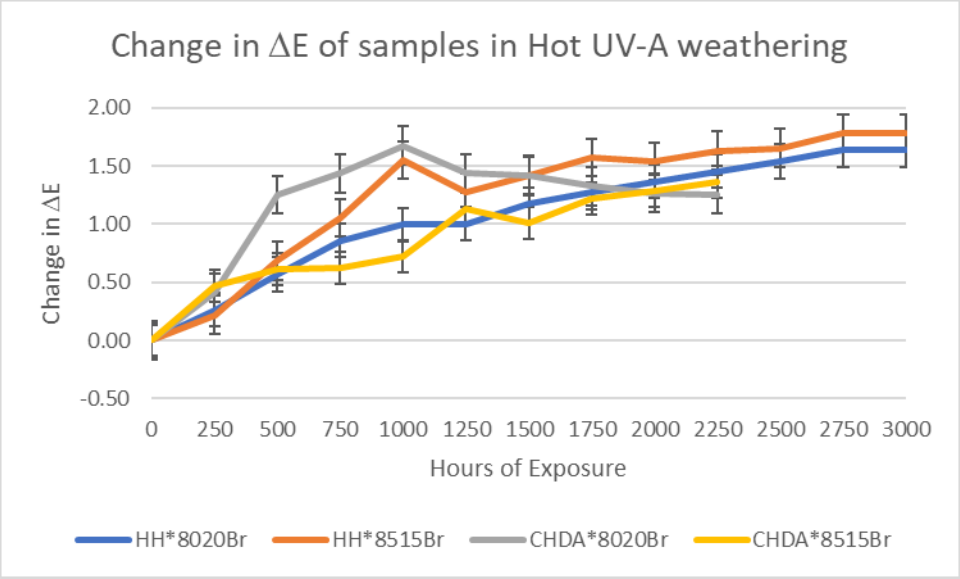

Figure 4.29-*Comparison of ΔE values over time of non-HALS coatings subjected to Hot UV-A weathering cycles*

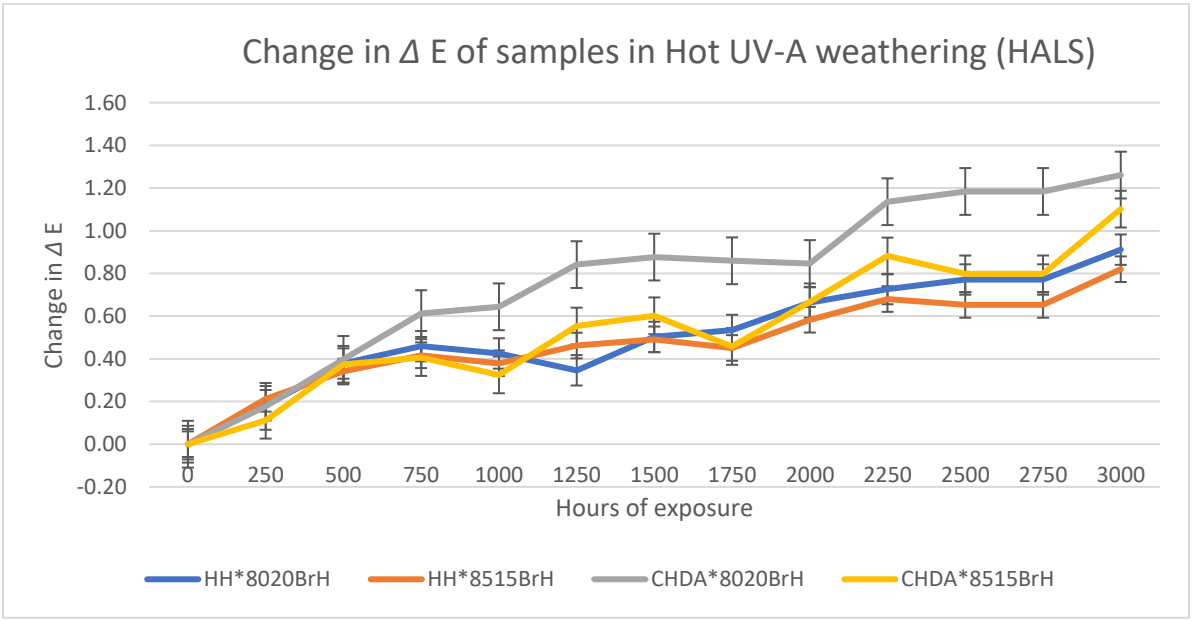

Figure 4.30-*Comparison of ΔE values over time of HALS coatings subjected to Hot UV-A weathering cycles*

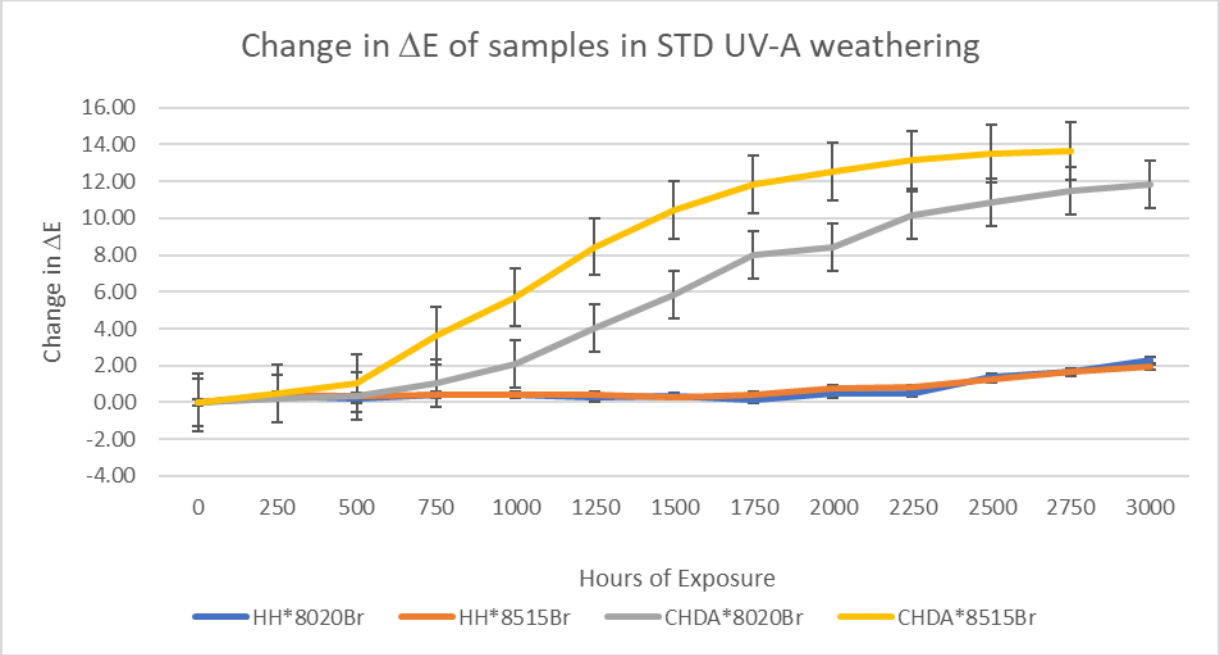

Figure 4.31-*Comparison of ΔE values over time of non-HALS coatings subjected to STD UV-A weathering cycles*

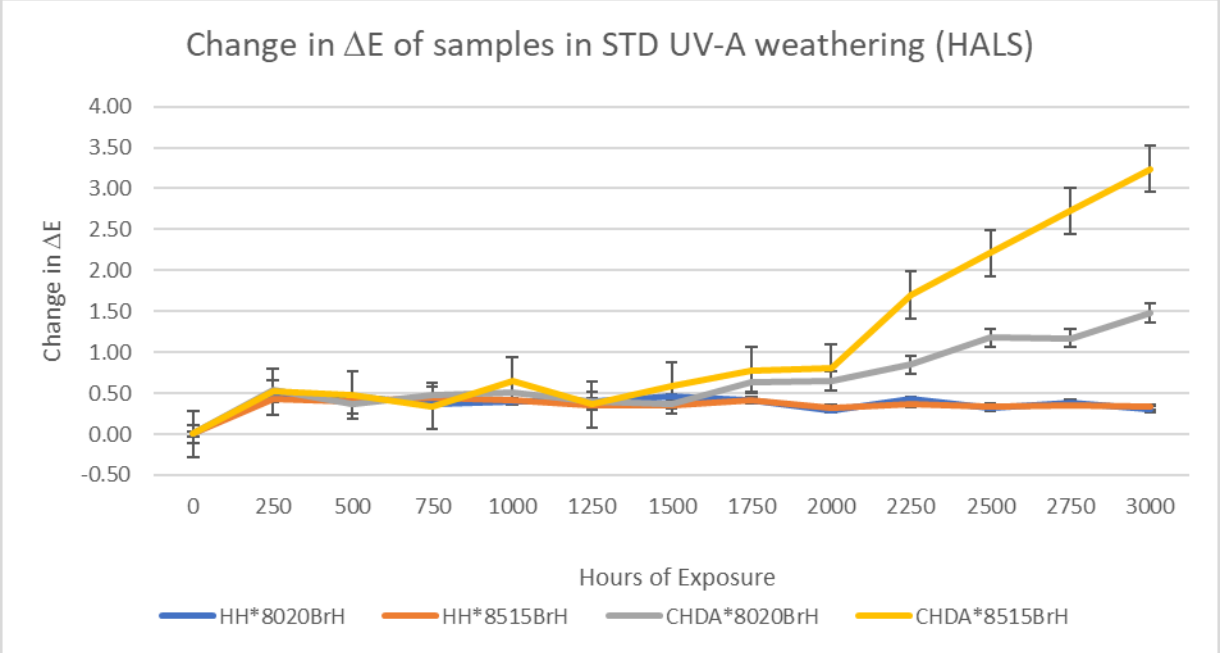

Figure 4.32-*Comparison of ΔE values over time of HALS coatings subjected to STD UV-A weathering cycles*

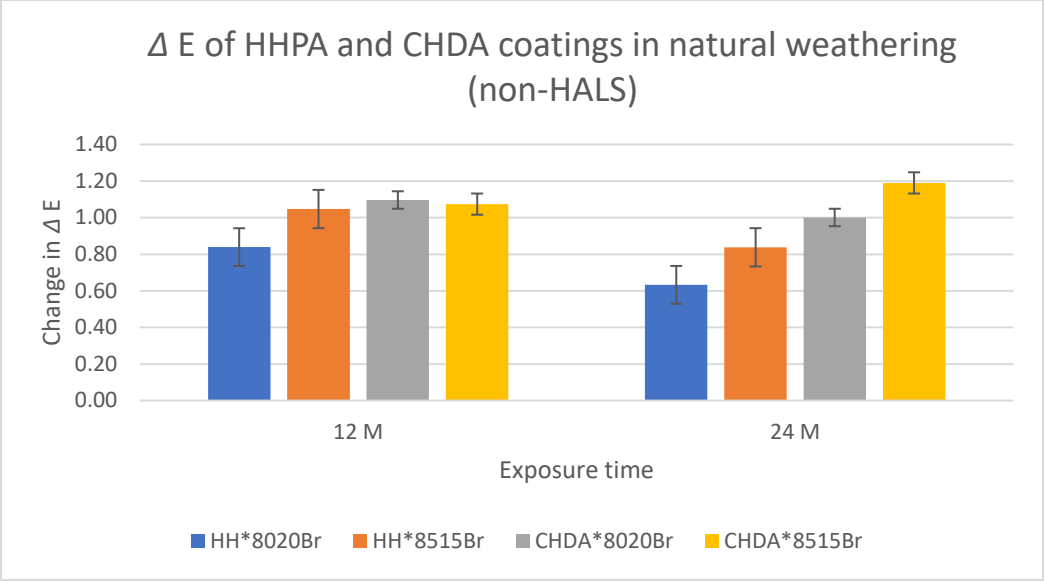

Figure 4.33-*Comparison of ΔE values over time of non-HALS coatings subjected to natural weathering in Florida*

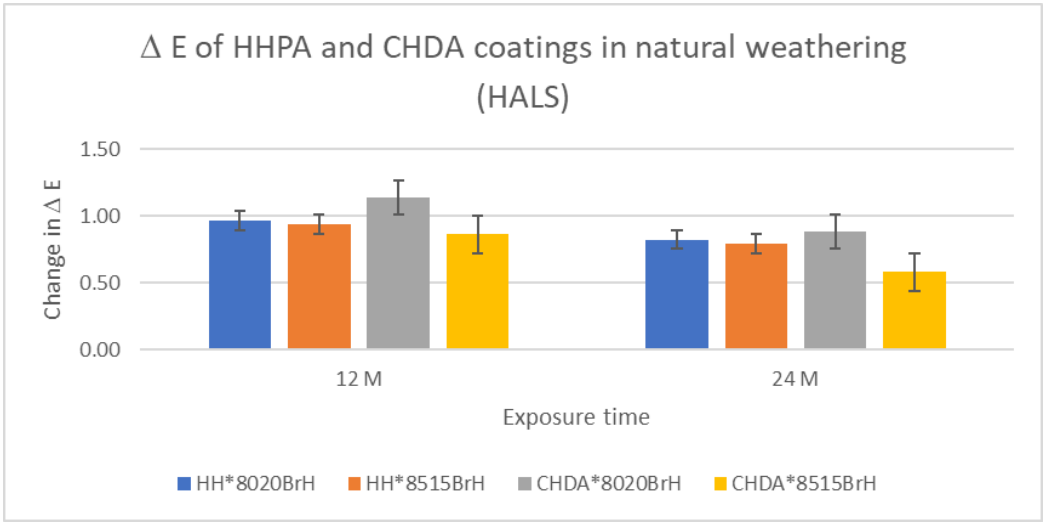

Figure 4.34-*Comparison of ΔE values over time of HALS coatings subjected to natural weathering in Florida*

Figures 4.33 and 4.34 show the change in Δ E from natural weathering of non-HALS and HALS containing samples respectively. While there is an increase in Δ E following 24 months of exposure, the greatest change is observed after 12 months. As these samples are periodically washed throughout their exposure time, the fluctuation in the results can be a consequence of when the samples were last washed prior to being analysed for colour change. The greatest change in Δ E was observed in coatings subjected to STD UV-A weathering cycles, with the smallest change being shown by naturally weathered samples. The decrease in ΔE from 12 to 24 months can be explained from the chalking of the coating, which was then removed via washing, allowing the topcoat to be gradually reduced over time.

The hydroxyl activity of coatings was measured through IR analysis and normalised against the CH_2+CH_3 band that represents the hydrocarbon backbone. The OH band is very important as an increase in hydroxyl activity is commonly associated with coating degradation and the formation of free radicals.

Figures 4.35-4.38 give a breakdown in the change in hydroxyl concentration for both non-HALS and HALS HHPA and CHDA containing coatings exposed to Hot UV-A and Standard UV-A accelerated weathering cycles. HH8020Br is an example of an in-service coating system and has been included to all graphs to serve as a reference, it is also the pigmented form of HH8020 that was covered in Section 4.2.

Figure 4.35 illustrates the change in percentage hydroxyl activity of non-HALS samples that were exposed to Hot UV-A weathering cycles (HOT UV-A). CHDA*8020Br is seen to exhibit the greatest increase in percentage hydroxyl activity (356%), followed by CHDA*8515Br (322%), HH*8020Br (269%), HH8020Br (256%), and finally HH*8515Br (246%). The significant difference between CHDA and HHPA coatings also explains why the CHDA coatings were removed from testing following 2000 hours, as the larger production of photodegradation products would have led to the rapid degradation of the coating system that was observed. For both CHDA and HHPA, the 85:15 ratio coating variant experienced a smaller increase in percentage hydroxyl activity compared to the 80:20 counterparts, this indicates that the coating systems with a lower crosslinker excess are less susceptible to large increases in hydroxyl activity.

All CHDA coatings were removed from Hot UV-A testing cycles following 2000 hours of exposure due to the severe damage that they exhibited, with the primer showing through in several places.

When HALS (Hindered Amine Light stabilisers) are added to the coating formulations (shown in Figure 4.36) there is a smaller increase in percentage hydroxyl activity compared to the non-HALS containing variants discussed previously. This is to be expected, as the sole purpose of HALS is to extend the working life of a coating. The CHDA coatings still suffer from a greater increase in percentage hydroxyl activity compared to the HHPA coatings.

However, the CHDA*8515Br coating shows the greatest increase in hydroxyl activity, compared to with non-HALS, where CHDA*8020Br showed a greater increase. This suggests that, with CHDA coatings, the HALS are used up faster when there is a lower crosslinker concentration. This is not observed with the HHPA coatings, where HH*8020Br shows a greater increase in hydroxyl activity than HH*8515Br, at least within the confines of Hot UV-A weathering testing.

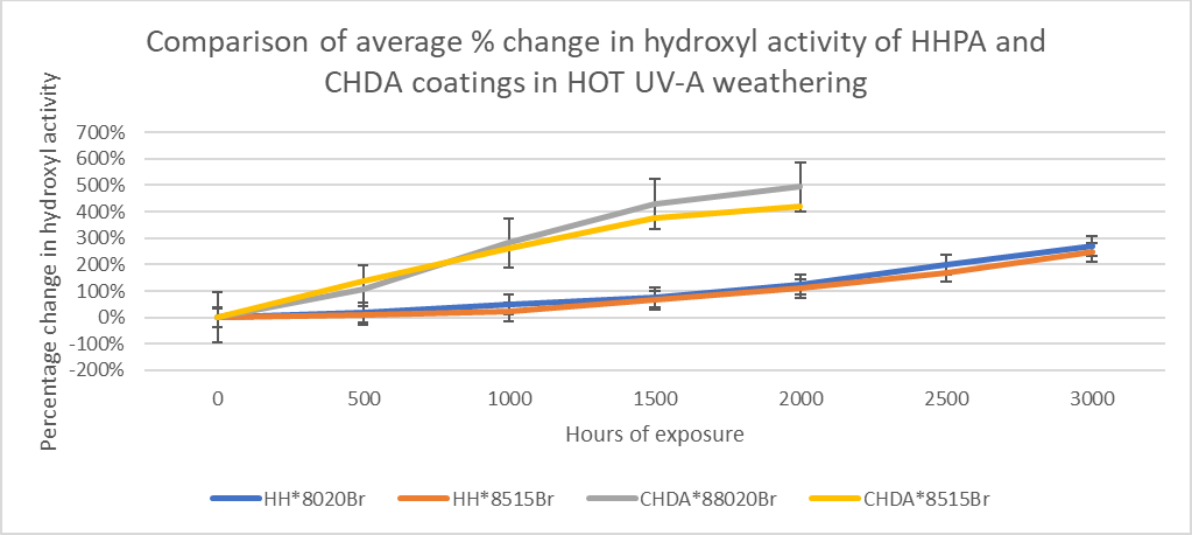

Figure 4.35-*Comparison of percentage change in hydroxyl activity of non-HALS coatings subjected to Hot UV-A weathering*

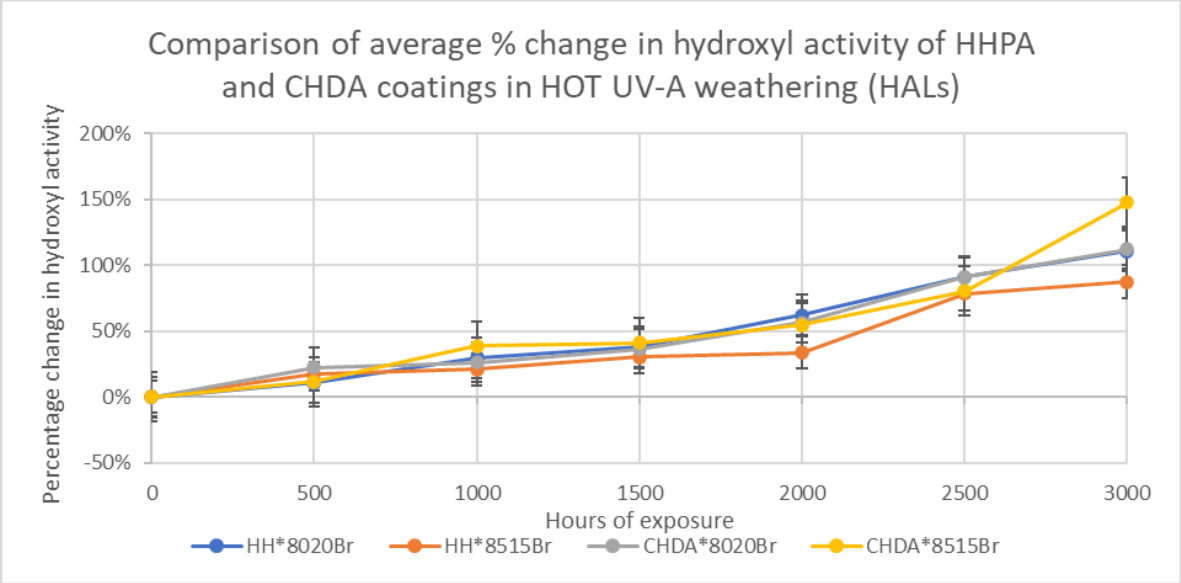

Figure 4.36-*Comparison of percentage change in hydroxyl activity of HALS coatings subjected to Hot UV-A weathering*

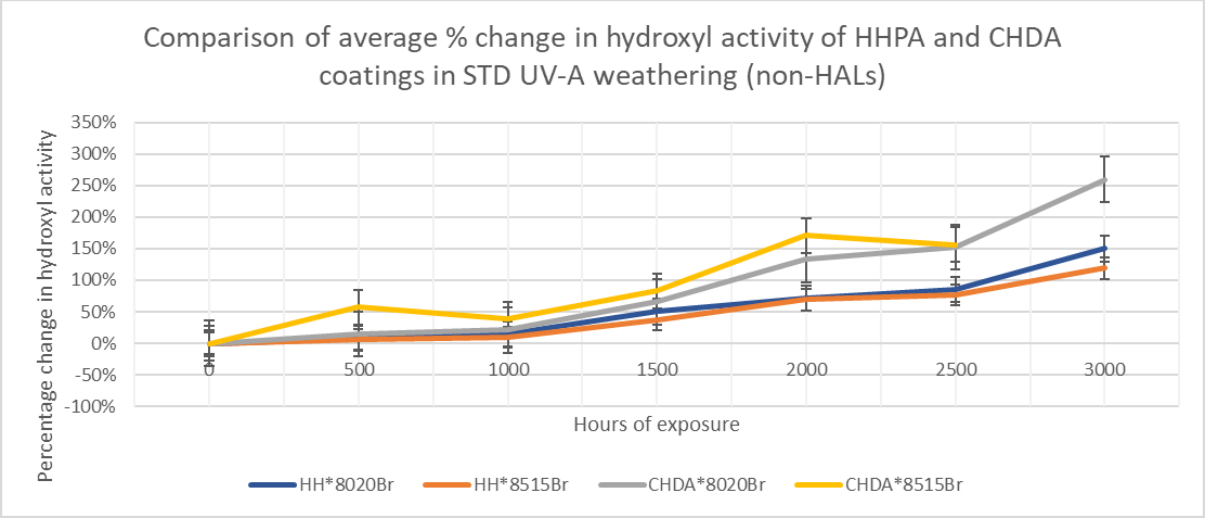

Figure 4.37-*Comparison of percentage change in hydroxyl activity of non-HALS coatings subjected to STD UV-A weathering*

With the non-HALS coatings that were exposed to STD UV-A (Figure 4.37), the CHDA containing coatings show a larger increase in normalised hydroxyl content compared to the HHPA coatings. CHDA*8020Br (257%) and CHDA*8515Br (152%) showed extremely similar increases in percentage hydroxyl activity up to 2500 hours of exposure, at which CHDA*8515Br had to be removed due to high levels of degradation seen during visual analysis. Once again, the HH*8515Br (75%) coating showed the lowest change in hydroxyl content after 3500 hours of exposure, outperforming both HH8020Br (80%) and HH*8020Br (116%), with the latter exhibiting the largest increase in hydroxyl activity of all HHPA coatings.

The HALS containing coatings exposed to STD UV-A weathering are shown in Figure 4.38. As expected, all samples show smaller increases in normalised hydroxyl activity than their non-HALS counterparts, with the 85:15 ratio coatings once again showing smaller increases in hydroxyl activity than their 80:20 counterparts.

While CHDA*8020Br again shows the largest increase in hydroxyl activity, it is followed by HH*8020Br, then HH*8515Br, with CHDA*8515Br showing the smallest increase in percentage hydroxyl activity of all the coatings.

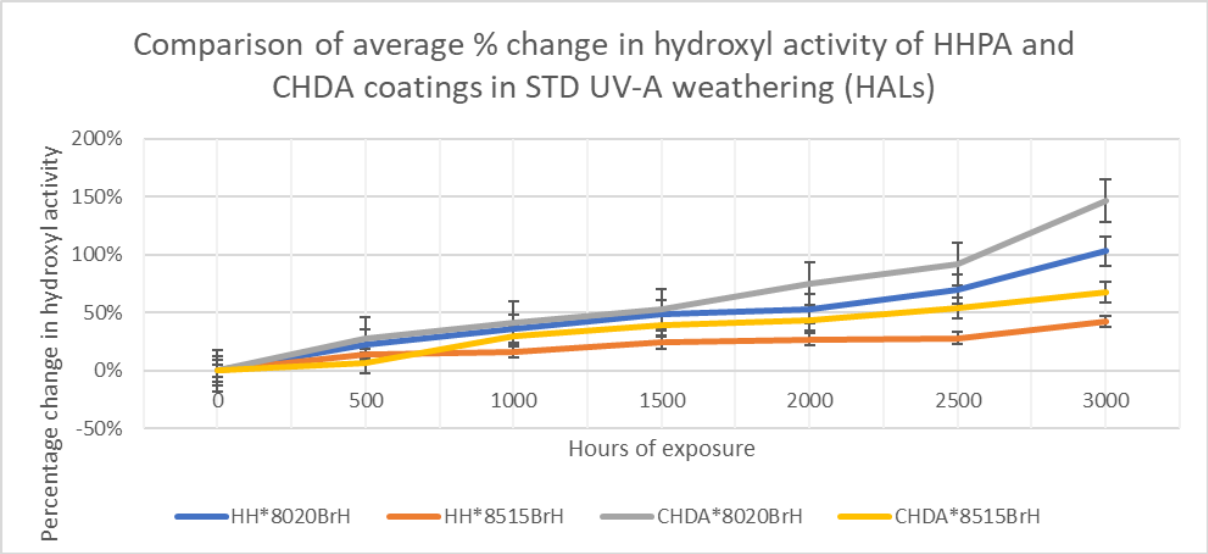

Figure 4.38-*Comparison of percentage change in hydroxyl activity of HALS coatings subjected to STD UV-A weathering*

Figures 4.39 and 4.40 show the percentage change in hydroxyl activity for the samples subjected to natural weathering in Florida over 2 years. For the non-HALS containing samples (Figure 4.39), the CHDA coatings show a larger increase in hydroxyl activity than the HHPA coatings. The coating with the largest increase in hydroxyl activity after 24 months was CHDA*8515Br, with HH*8020Br exhibiting the smallest increase in activity.

Figure 4.40 shows the HALS containing samples, which have a significantly smaller change in Δ E than the non-HALS containing versions. The coating with the smallest change in Δ E is HH*8515BrH, with the poorest performing coating being CHDA*8020BrH which after 24 months of exposure had a change in Δ E that matched the value of CHDA*8020Br after 12 months of exposure.

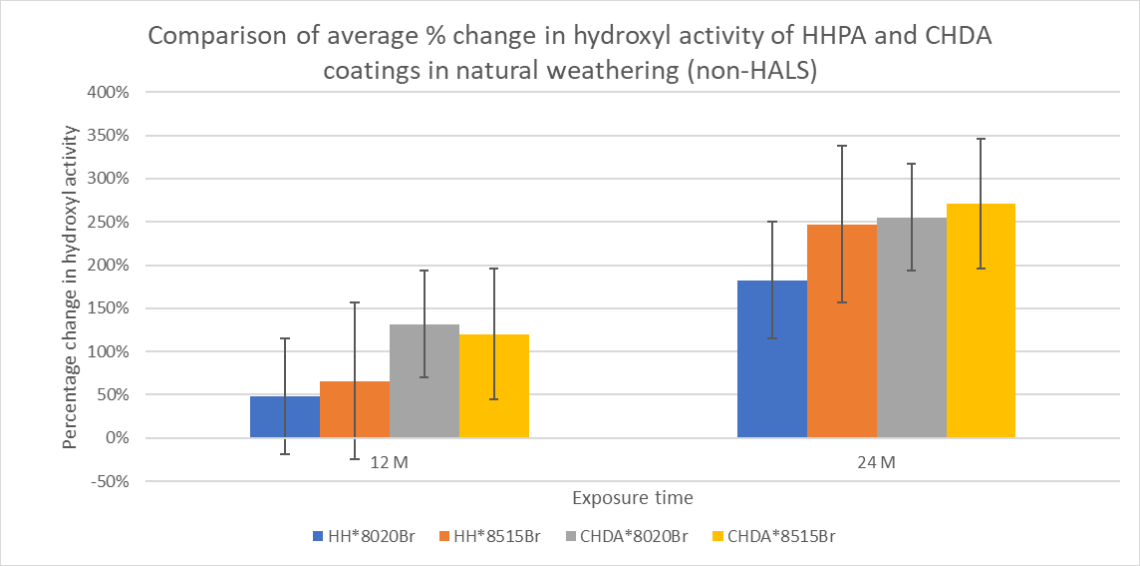

Figure 4.39-*Comparison of percentage change in hydroxyl activity of non-HALS coatings subjected to natural weathering*

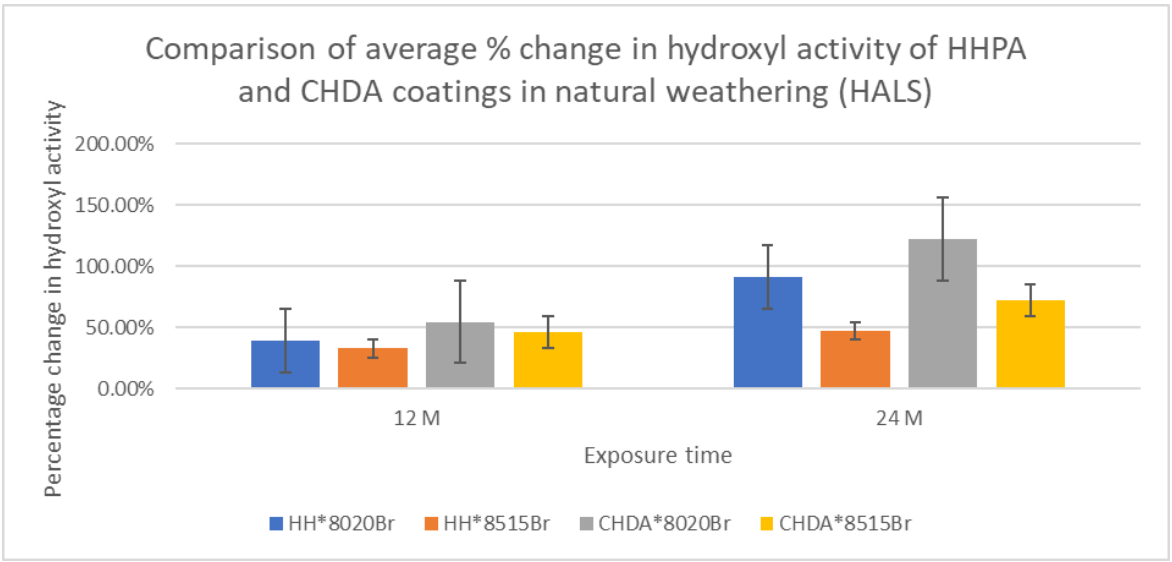

Figure 4.40-*Comparison of percentage change in hydroxyl activity of HALS coatings subjected to natural weathering in Florida*

Table 4.6 gives a breakdown of both non-HALS and HALS pigmented coatings. Analysis of the T_g of the coatings shows that the addition of HALS to the coating formulation does not impact the T_g, demonstrated as all coatings only showing a difference in T_g of between 1-2°C, with no observable pattern behind the behaviour.

Table 4.6-*Breakdown of coating systems illustrating glass transition temperature, HALS content, resin base and PE:HMMM ratio*

Coating code	**Resin base**	**Ratio**	**HALS? (Y/N)**	**Midpoint T_g (°C)**
HH8020Br	BK001	80:20	N	28
HH*8020Br	LSBS-STD	80:20	N	32
HH*8020BrH	LSBS-STD	80:20	Y	31
HH*8515Br	LSBS-STD	85:15	N	29
HH*8515BrH	LSBS-STD	85:15	Y	31
CHDA*8020Br	LSBS-33	80:20	N	29
CHDA*8020BrH	LSBS-33	80:20	Y	30
CHDA*8515Br	LSBS-33	85:15	N	29
CHDA*8515BrH	LSBS-33	85:15	Y	27

4.2.5-Conclusions

It can be seen that in terms of gloss and colour retention, that CHDA based coatings (CHDA*8020Br + CHDA*8515Br) show significantly poorer performance than the HHPA based equivalent coatings across accelerated and natural weathering exposure. It is also accepted that 2000 hours of accelerated weathering exposure is roughly equivalent to 2 years of natural weathering, with the standard BS EN 10169-2 stating this equivalency. In terms of change in hydroxyl activity, neither the non-HALS coatings exposed to std or Hot UV-A correlate with the percentage change in hydroxyl activity shown by the naturally weathered samples after two years.

When considering non-HALS containing coatings, those based on CHDA also exhibited significantly greater increased in percentage hydroxyl activity than those based off HHPA as seen in Figures 4.35,4.37, and 4.39. This aids in explaining the poor gloss and colour retention observed in CHDA based coatings, as while CHDA and HHPA coatings are both hydrolysing, the CHDA coatings are doing so at a significantly faster rate.

It can be seen by looking at the Δ E values for the non-HALS coatings, that the coatings subjected to STD UV-A weathering showed a significantly greater change in Δ E than samples exposed to Hot or natural weathering. This could be due to the increased number of cycles between UV and condensation which resulted in more instances of chalking of the coatings.

The poorest performing coating across all tests, with the exception of the Hot UV-A exposure of HALS containing samples, was CHDA*8020Br or CHDA*8020BrH (as appropriate). The poorest performing HALS

coating exposed to Hot UV-A weathering was CHDA*8515BrH. However, by looking at Figure 4.36 it can be seen that the percentage change in hydroxyl value for CHDA*8020BrH peaks at 2500 hours and slightly declines towards 3000 hours. This indicates that the coating had suffered significant damage and the primer layer was beginning to show through (hence the decrease in hydroxyl activity) whereas CHDA*8515BrH continued to decrease. This suggests that while CHDA*8515BrH shows the greatest change in percentage hydroxyl activity, that it may not have been the poorest performing coating.

The work performed by Persson et al can also go towards explaining the observation that HHPA coatings were superior to their CHDA counterparts within this section. Persson noted that it is possible for the addition of pigments to a coating system to reduce the impact of UV and moisture, but that it is heavily dependent on the resins adhering effectively to the pigments. The lower T_g values exhibited by the CHDA coatings may have facilitated re-flow and given the appearance of better gloss retention, but the same low T_g value may have weakened the adhesion between the resin and the pigments, allowing for greater permeation of moisture throughout the coating, which in turn would lead to additional sites of degradation and free radical production.

From the analysis carried out during this section it can be confirmed that CHDA based coating are more sensitive to photodegradation and moisture enhanced photodegradation than HHPA coatings, and while the addition of HALS has a beneficial effect on the longevity of the coatings, the sacrificial additives do not cause a larger increase in performance in CHDA coatings, causing them to continue to fail faster than the HHPA coatings once the HALS have been used.

4.3-Third Generation coating development

4.3.1-Formulation

From the information obtained through analysing the clear coats and first generation of pigmented coatings it was decided to focus on pigmented co-monomer blend coatings. This was due to the superior performance that the CHDA;CHDM blend clear coats exhibited compared to the CHDA coatings.

The coatings were required to use a co-monomer base as CHDM is very unreactive as a stand-alone monomer. Due to this requirement the decision was also make the coatings using resins with different ratios of CHDA to CHDM in order to identify the optimum ratio for superior weathering performance.

The resins were formulated to meet the same criteria, with Hydroxyl Values (OHV) of 30, number average molecular weights between 3500-5000, and an acid value of below 10.

These ratios were obtained by beginning with a formulation containing a 40:30 (CHDA:CHDM) by weight, then decreasing either the CHDA or CHDM to reach the desired ratio. To ensure that the OHV and molecular weight remained within acceptable levels for appropriate comparison, the formulations were compensated with adipic acid in the case of lowering CHDA, and 1,6 hexanediol when lowering CHDM. A full description of the resin and coating generation process can be found within Chapter 2.

One of the issues that became apparent during the coating generation process involved LSBS37-R. This was due to the resin solidifying and requiring heating to melt out for coating development. The issue reoccurred during the paint generation process, where coatings based off the LSBS37-R resin solidified when stored below 20^{o}C. In order to rectify this problem, additional solvent needed to be added to the coating formulation, this resulted in significantly more solvent being added to the coating system which in turn lowered the solid content from the target value.

4.3.2-Testing

Pigmented samples were exposed to accelerated weathering cycles, with periodic analysis for changes in gloss and colour change, as well as IR spectroscopy and glass transition temperature as described previously within this chapter.

4.3.3-Results

Comparing the T_g of non-HALS coatings with their HALS containing counterparts laid out in Table 4.8, it is clear to see that in general the addition of HALS has a plasticising effect on the coatings, which results in a lower T_g value. Of the 10 HALS coatings, 7 were found to have lower T_g values, two had the same values and 1 exceeded the T_g of the non-HALS variant. This is in line with the results that were discovered during T_g analysis of the first generation of pigmented coatings and is a factor that would require consideration during long term exposures as while the HALS may prevent photodegradation in the short term, in hot environments once the HALS have been used up then the lower T_g values could contribute to a rapid degradation of the coating.

Table 4.7 and Figure 4.40 illustrate the change in colour of samples subjected to HOT UV-A accelerated weathering tests for 80:20 and 90:10 coatings. Within 80:20 coatings the coating with the poorest colour retention is CHDA4.0DM8020Br, which also contains the smallest amount of CHDM, this was followed by CHDA0.6DM8020Br (with the lowest amount of CHDA), then the jumping off formulation (CHDA1.3DM8020Br), with CHDA1.0DM8020Br being the best novel coating. However, all the novel coating formulations were significantly outperformed by HH8020Br.

The 90:10 formulations suffered much greater initial colour change, except for CHDA1.3DM9010Br, which shows the same rate of colour change as its 80:20 counterpart. It is interesting to note that while it was initially the poorest performing coating, CHDA4.0DM9010Br showed the lowest degree of colour change following 2000 hours of exposure, whereas its 80:20 counterpart showed the greatest degree of change.

Table 4.7-*Comparing straight chain % and ∆ E of non-HALS coatings during HOT UV-A weathering*

Coating code	Change in ∆E after 2000 hours exposure	Straight chain percentage
CHDA1.3DM8020Br	13.60	0
CHDA1.3DM9010Br	13.55	0
CHDA1.0DM8020Br	10.25	12
CHDA1.0DM9010Br	13.97	12
CHDA0.6DM8020Br	13.63	24
CHDA0.6DM9010Br	13.12	24
CHDA2.0DM8020Br	12.93	13
CHDA2.0DM9010Br	13.58	13
CHDA4.0DM8020Br	14.07	25
CHDA4.0DM9010Br	11.40	25

Straight chain percentage by weight was determined during resin development through addition of the straight chain components that were added to the formulations in order to keep hydroxyl value and Mw within the desired range.

Comparing the results contained within Table 4.7 gives an explanation for the order in which the coatings suffered from colour fade.

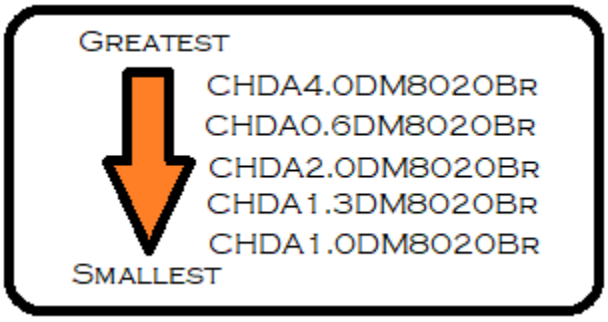

Figure 4.41-*Illustration of coating ranks from worst to best colour retention*

The worst performing coating in Figure 4.41 in terms of colour retention was CHDA4.0DM8020Br, while the coating with the greatest degree of colour retention was CHDA1.0DM8020Br. A full breakdown of the

ranks of the coatings in terms of colour retention can be found in Figure 4.40. CHDA4.0DM8020Br and CHDA0.6DM8020Br have the highest straight chain percentages of 24.61% and 23.95% respectively, CHDA2.0DM8020 has a lower straight chain percentage (12.74%) and provides superior colour retention, this suggests that as the straight chain percentage of a coating increases, so does its susceptibility to degradation. However, CHDA1.0DM8020Br has a straight chain percentage of 11.78% and provides greater colour retention that all other novel coatings, including CHDA1.3DM8020Br which does not contain any straight chains. This in turn suggests that the negative impact of an increased straight chain percentage can be offset by a decreased ratio of CHDA within a coating but only up to a point after which the negative impact of straight chains within the coating offset any measurable advantage of diminishing the CHDA content. It can also be observed that lowering the amount of CHDA in the coating provides superior weathering protections than coatings where the CHDM content was decreased by the same amount.

Table 4.8-*Breakdown of coating systems, T_g, and straight chain percentages*

Coating code	Resin base	PE:HMMM Ratio	HALS? (Y/N)	T_g (°C)	Straight chain (%)
HH8020Br	BK001	80:20	N	28	N/A
CHDA1.3DM8020	LSBS-37R	80:20	N	53	0
CHDA1.3DM8020H	LSBS-37R	80:20	Y	50	0
CHDA1.3DM9010	LSBS-37R	90:10	N	47	0
CHDA1.3DM9010H	LSBS-37R	90:10	Y	43	0
CHDA1.0DM8020	LSBS-38R	80:20	N	35	11.797
CHDA1.0DM8020H	LSBS-38R	80:20	Y	35	11.797
CHDA1.0DM9010	LSBS-38R	90:10	N	32	11.797
CHDA1.0DM9010H	LSBS-38R	90:10	Y	32	11.797
CHDA0.6DM8020	LSBS-39	80:20	N	20	23.95
CHDA0.6DM8020H	LSBS-39	80:20	Y	19	23.95
CHDA0.6DM9010	LSBS-39	90:10	N	13	23.95
CHDA0.6DM9010H	LSBS-39	90:10	Y	14	23.95
CHDA2.0DM8020	LSBS-40	80:20	N	34	12.74
CHDA2.0DM8020H	LSBS-40	80:20	Y	31	12.74
CHDA2.0DM9010	LSBS-40	90:10	N	30	12.74
CHDA2.0DM9010H	LSBS-40	90:10	Y	27	12.74
CHDA4.0DM8020	LSBS-41	80:20	N	12	24.609
CHDA4.0DM8020H	LSBS-41	80:20	Y	10	24.609
CHDA4.0DM9010	LSBS-41	90:10	N	9	24.609
CHDA4.0DM9010H	LSBS-41	90:10	Y	7	24.609

Figures 4.42-4.43 show the average percentage gloss retention of the non-HALS containing coatings subjected to STD UV-A weathering cycles for 80:20 and 90:10 coating systems respectively. Some of the coatings suffered extreme gloss loss following 250 hours of accelerated weathering exposure, notably CHDA0:6DM9010, CHDA2.0DM9010, and CHDA4.0DM9010, all of which dropped to below 10% of original gloss values. Two of the novel coatings (CHDA1.3DM8020Br and CHDA1.0DM8020Br) were the only coatings to continually outperform the control coating across all 2000 hours of exposure. These were both 80:20 PE:HMMM ratio coatings. It is possible to see that during Hot UVA weathering the 80:20 ratio coatings all outperformed their 90:10 counterparts significantly.

The superiority of the 80:20 coatings is further highlighted in Figure 4.43, which shows the gloss percentage retention of the HALS containing coatings and demonstrates that the 80:20 coatings provided greater gloss retention than their 90:10 counterparts in Figure 4.44.

Figures 4.42 and 4.32 illustrate the percentage change in obtained gloss value for 80:20 and 90:10 non-HALS coatings respectively while being compared against a standard 80:20 PE:HMMM HHPA containing coating. In Figure 4. it can be seen that the HHPA coating outperformed all others with the exception of CHDA1.3DM8020Br. The poorest performing coating was CHDA4.0DM8020Br, followed by CHDA0.6DM8020Br, this poor performance can be due to the large presence of straight chain components within the base resin formulations and also indicating that either 1,6-Hexanediol is more susceptible to photodegradation than Adipic acid, and that CHDA has poorer inherent weathering capabilities compared to CHDM which is demonstrated through the coating with the largest ratio of CHDA to CHDM being the poorer performing of the two systems.

Figure 4.40 shows that the 90:10 PE:HMMM coatings suffer significantly higher levels of percentage gloss loss, with CHDA1.3DM9010Br being the best performing co-monomer based coating, and CHDA4.0DM9010Br being the worst performing by the end of exposure. With all 90:10 coatings demonstrating poorer performance than the standard HHPA coating, as well as suffering increased gloss loss compared to their 80:20 counterparts, it strongly suggests that a higher crosslinker concentration can have favourable effects over the retention of physical characteristics during accelerated weathering.

Figure 4.43 demonstrates the change in average percentage gloss retention for HALS containing 80:20 coatings subjected to STD UV-A weathering. As anticipated, the HALS coatings outperform the non-HALS variants, due to the sacrificial protective nature of the HALS. There are some similarities between the

coatings, with CHDA1:3DM8020BrH being the best performing coating in terms of gloss retention and CHDA0.6DM8020BrH exhibiting the poorest levels of gloss retention.

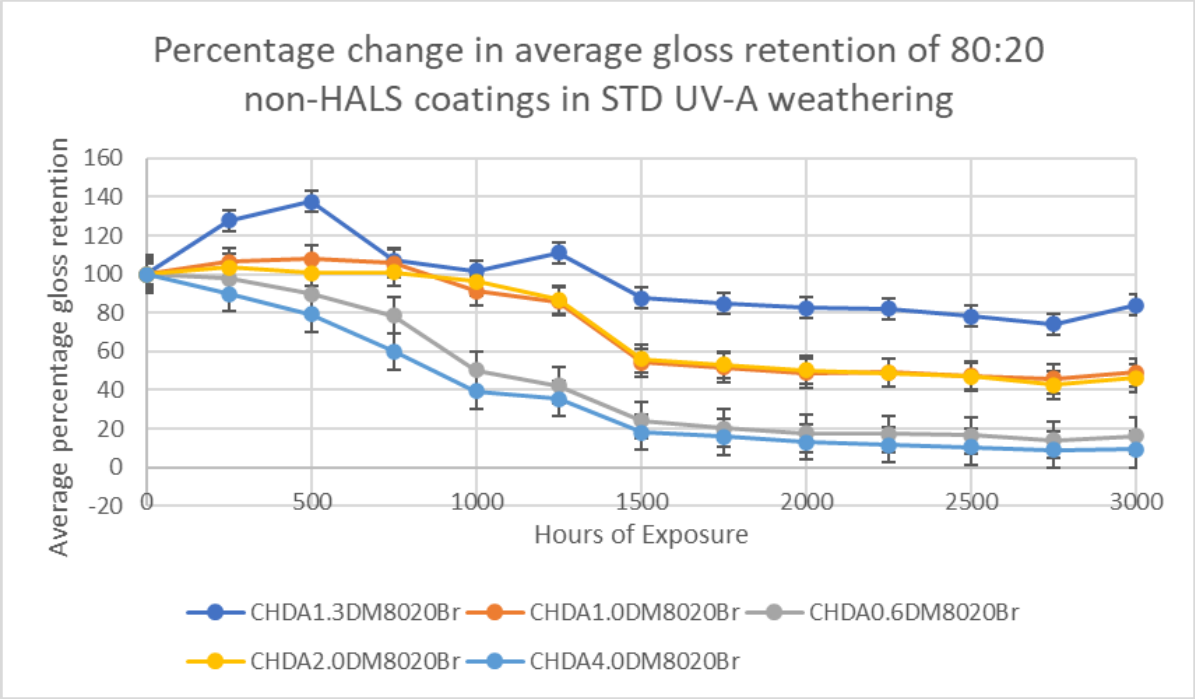

Figure 4.42-*Comparing change in percentage gloss for 80:20 non-HALS containing coatings exposed to STD UV-A weathering cycles*

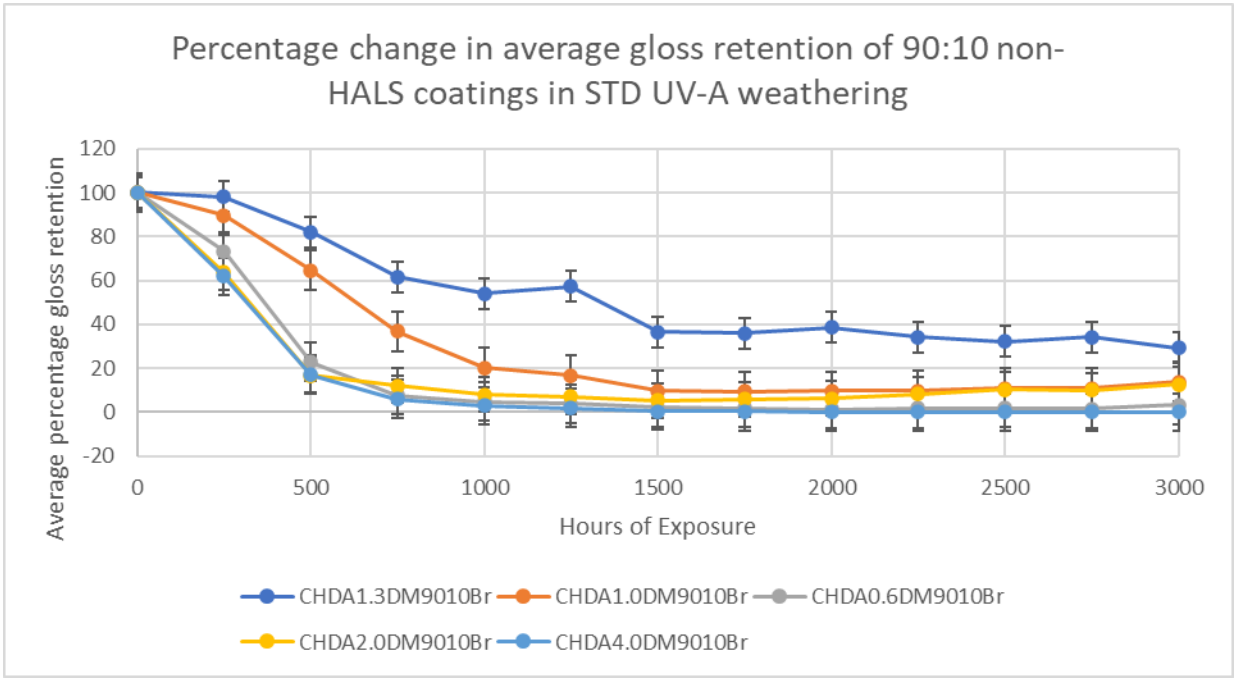

Figure 4.43-*Comparing change in percentage gloss for 90:10 non-HALS containing coatings exposed to STD UV-A weathering cycles*

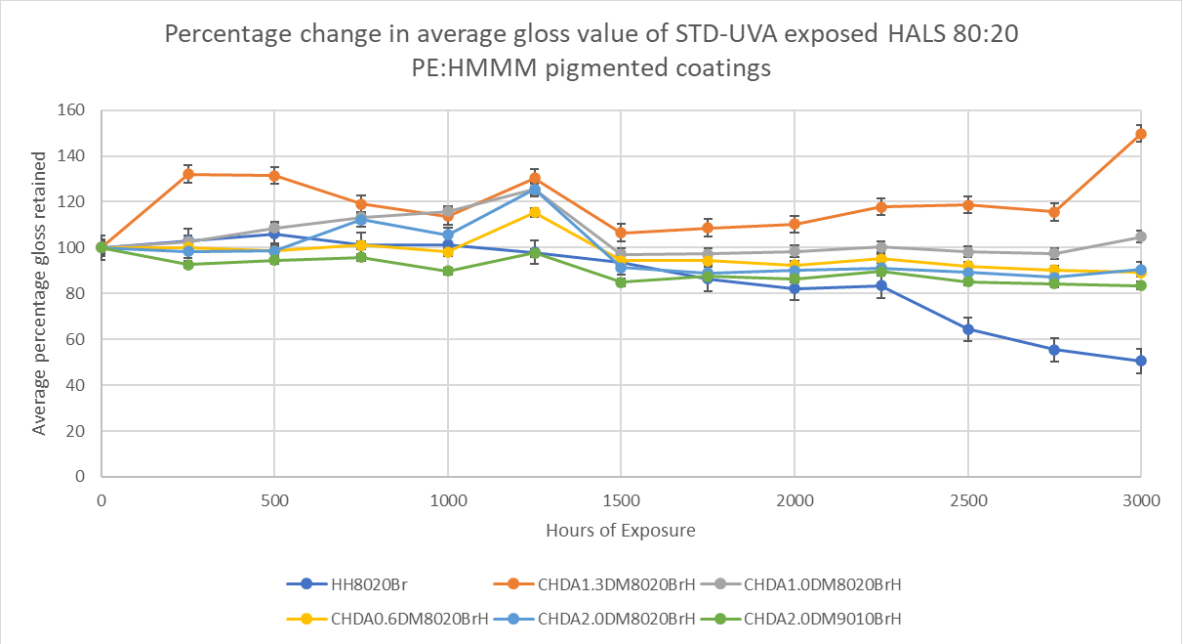

Figure 4.44-*Change in percentage gloss values of STD UV-A exposed HALS containing 80:20 PE:HMMM pigmented coatings*

Figures 4.43-4.44 show the impact of HOT UV-A weathering on the change in percentage gloss values for 80:20 and 90:10 non-HALS coatings respectively. The coating that exhibited the greatest level of gloss retention of the 80:20 coatings was CHDA1.0DM8020Br, with CHDA4.0DM8020Br showing the lowest levels of gloss retention. CHDA1.0DM8020Br, CHDA1.3DM8020Br, and CHDA2.0DM8020Br all outperformed the standard HHPA containing coating, which demonstrated gloss retention on an equivalent level to CHDA0.6DM8020Br. This is the first instance of CHDA1.0DM8020Br outperforming CHDA1.3DM8020Br, and it could be explained that a small addition of straight chain components provides beneficial properties to the coating system when exposed to the elevated temperatures found during HOT UV-A weathering.

The best performing co-monomer based 90:10 non-HALS coating system was CHDA1.3DM9010Br, with the second-best coating being CHDA1.0DM9010Br and CHDA4.0DM9010Br exhibiting the greatest rate of gloss loss of all coatings.

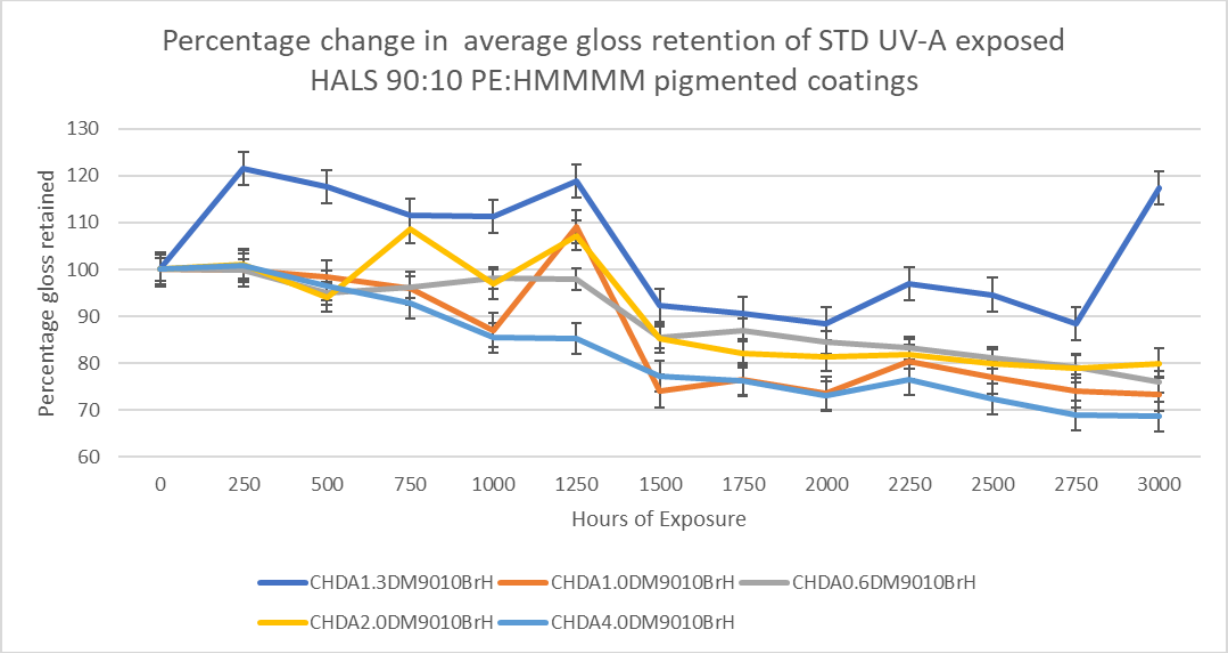

Figure 4.45-*Change in percentage gloss retained of STD UV-A exposed HALS containing 90:10 PE:HMMM pigmented coatings*

The sample that demonstrated the greatest percentage gloss retention of 90:10 HALS containing coatings subjected to STD UV-A weathering was CHDA1.3DM9010BrH, with all HALS coatings outperforming the 80:20 non-HALS HHPA containing standard coating (HH8020Br). Comparing Figures 4.42 and 4.44 demonstrates the impact that the addition of HALS has on coating performance for 90:10 coatings. As anticipated, the HALS coatings outperform the non-HALS variant. While CHDA1.3DM9010 remains the best performing coating and CHDA2.0DM9010 remains the worst, there is some variation in the behaviours of the middle-ranked coatings. It is interesting to note that CHDA1.0DM9010 performed worse than CHDA0.6DM9010, which due to the higher straight chain percentage would be anticipated to be the poorer performing coating of the two. This could suggest that the straight chain percentage exerts an influence over the distribution of HALS throughout the coating system.

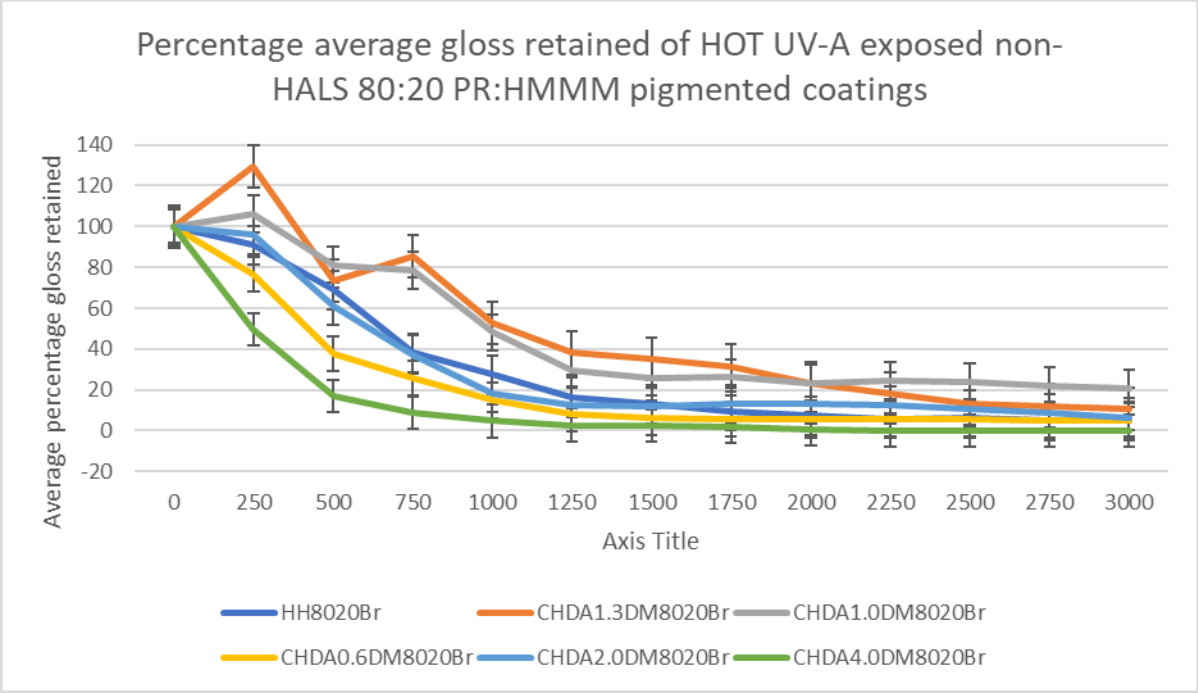

Figure 4.46-*Change in percentage gloss retention of HOT UV-A exposed non-HALS containing 80:20 PE:HMMM pigmented coatings*

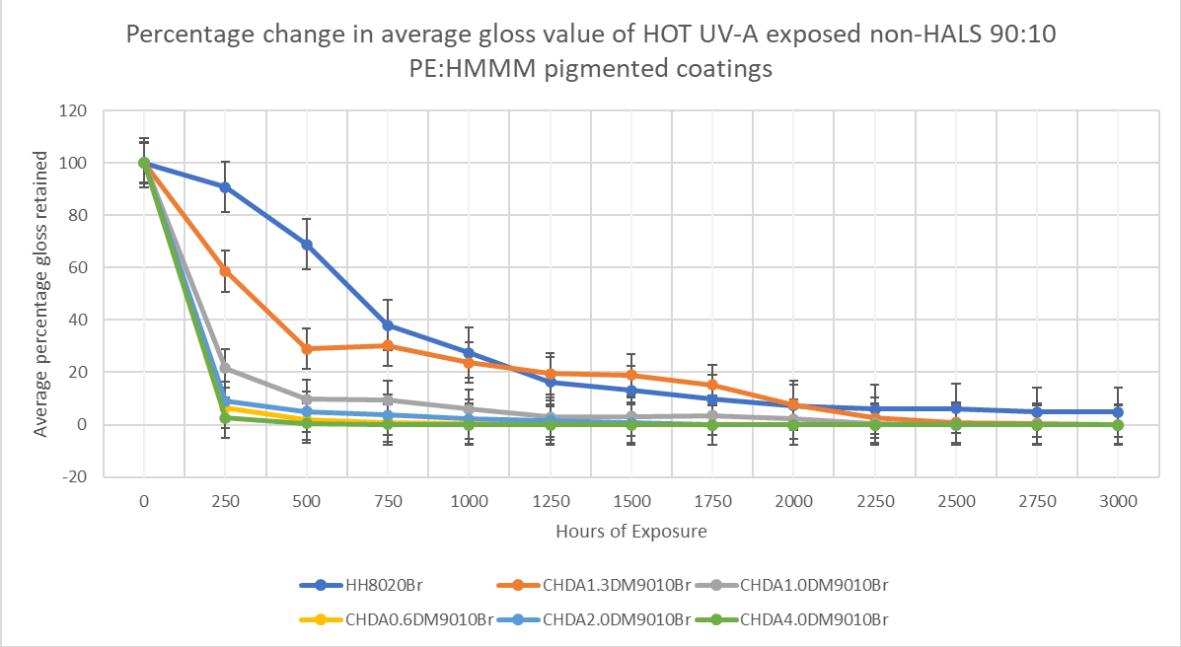

Figure 4.47-*Change in percentage gloss retained of HOT UV-A exposed non-HALS containing 90:10 PE:HMMM pigmented coatings*

The percentage change in average gloss value for 80:20 HALS containing coatings subjected to HOT UV-A weathering, as with the majority of the gloss investigations made within this section, CHDA1.3DM8020BrH

exhibits the greatest gloss retention, while CHDA4.0DM8020BrH demonstrated the poorest gloss retention for the co-monomer based coatings. CHDA1.0DM8020BrH exhibits better gloss retention than CHDA2.0DM8020BrH, which may be due to the greater amount of CHDM within CHDA1:0DM8020BrH, or that Adipic acid is less susceptible to photodegradation than 1,6-Hexanediol. The same results are observed in Figure 4.49, which highlights the percentage gloss retention of 90:10 HALS containing coatings subjected to HOT UV-A weathering.

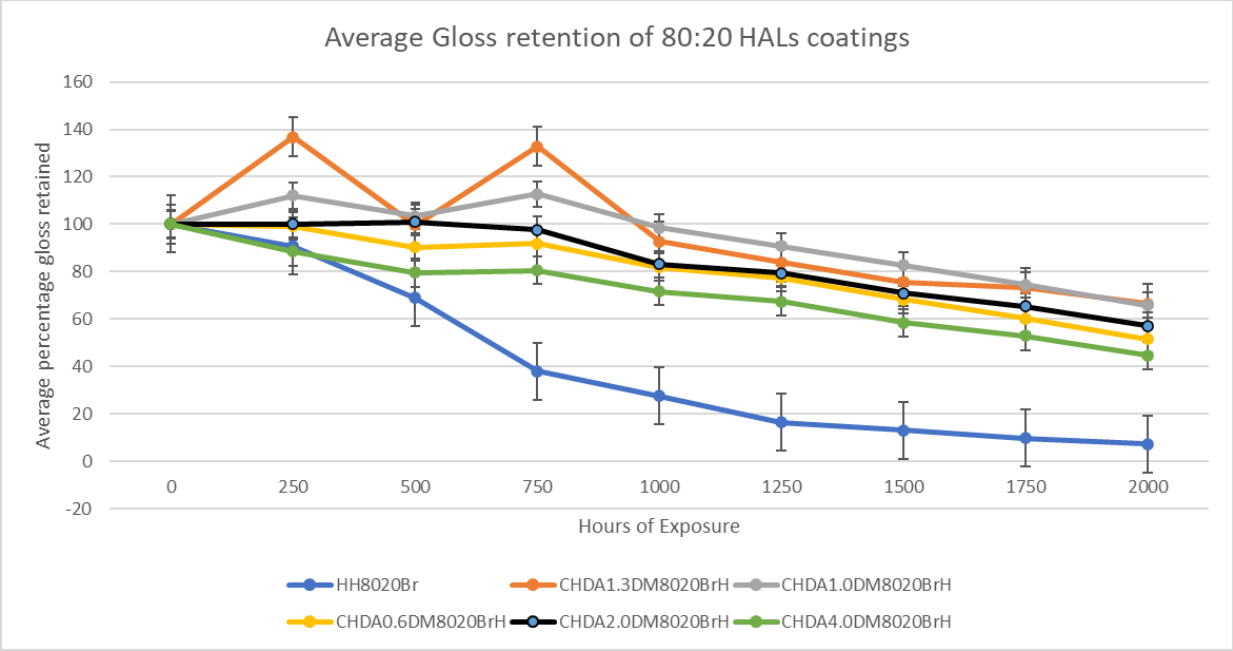

Figure 4.48-*Change in percentage gloss retained of HOT UV-A exposed HALS containing 80:20 PE:HMMM pigmented coatings*

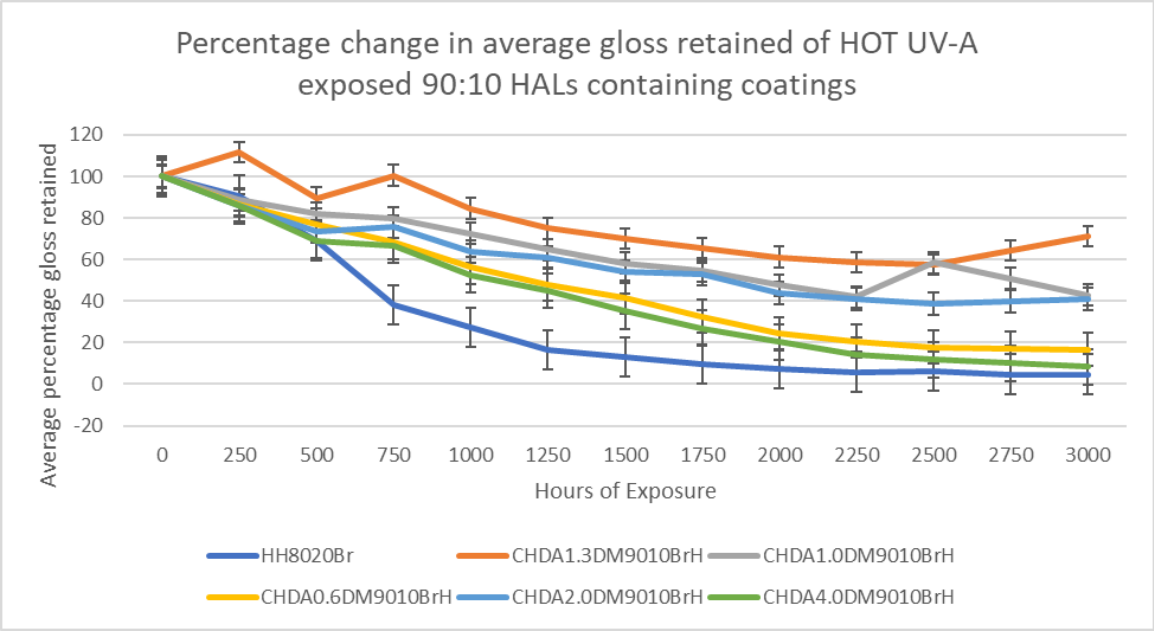

Figure 4.49-*Change in percentage gloss retained of HOT UV-A exposed HALS containing 90:10 PE:HMMM pigmented coatings*

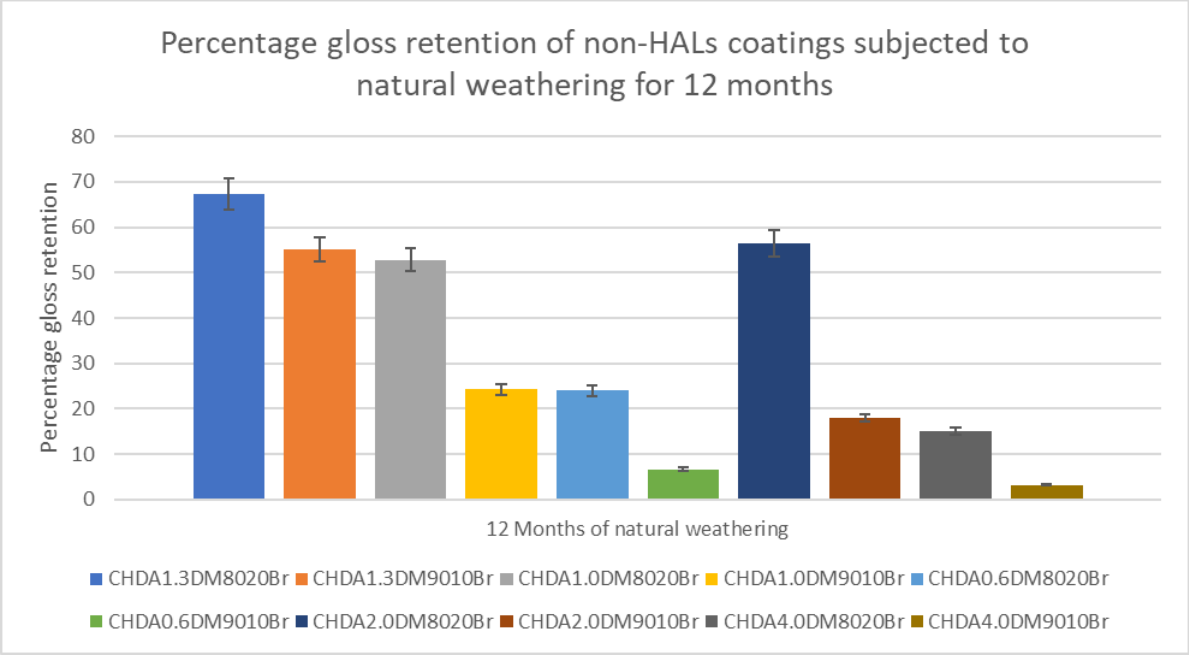

Figure 4.50-*Change in percentage gloss retained of naturally exposed non-HALS containing pigmented coatings*

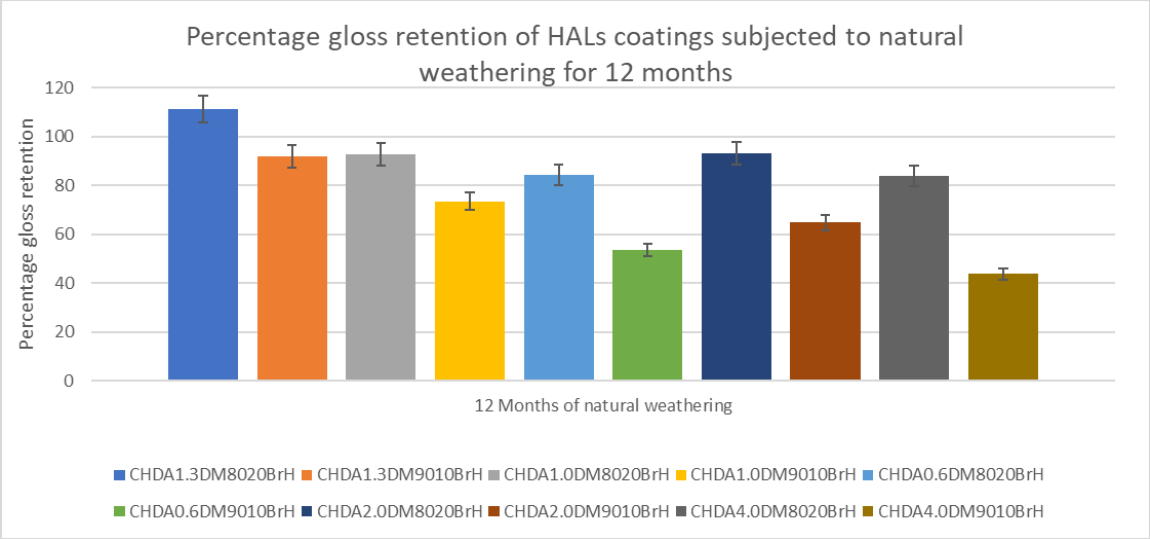

Figure 4.51-*Change in percentage gloss retained of naturally exposed HALS containing pigmented coatings*

Figure 4.50 shows the percentage gloss retention following 12 months of natural weathering exposure. It can be observed that CHDA1.0DM retains the greatest amount of gloss for 80:20 and 90:10 coating systems, while CHDA4.0DM illustrates the lowest levels of gloss retention for both. It can also be seen that in all instances the 80:20 coating variants outperformed the 90:10 coatings in terms of gloss retention, which indicates that a lower melamine content does not exert a positive effect on gloss retention in real world exposure situations.

Figure 4.51 shows the gloss retention for the HALS containing coatings exposed to natural weathering. By comparing the results to Figure 4.49 it can be clearly seen that all of the HALS containing coatings outperformed the non-HALS variants.

A breakdown of the changes in ΔE for 80:20 non-HALS coatings subjected to STD UV-A weathering is demonstrated in Figure 4.52. The poorest performing coating was CHDA4.0DM8020Br, with CHDA0.6DM8020Br being the next poorest. While CHDA1.3DM8020Br exhibited the smallest change in ΔE for the majority of the exposure time, it was outperformed by both CHDA1.0DM8020Br and CHDA2.0DM8020Br after 3000 hours of exposure, which suggests that the addition of a small amount of straight chain monomer into the base resin system may provide some benefits for colour retention such as improved pigment retention or increased chemical stability. The change in ΔE for the 90:10 non-HALS coatings subjected to STD UV-A weathering are shown in Figure 4.53, where it can be seen that CHDA1.3DM9010Br is the best performing coating while CHDA0.6DM9010Br is the poorest performing.

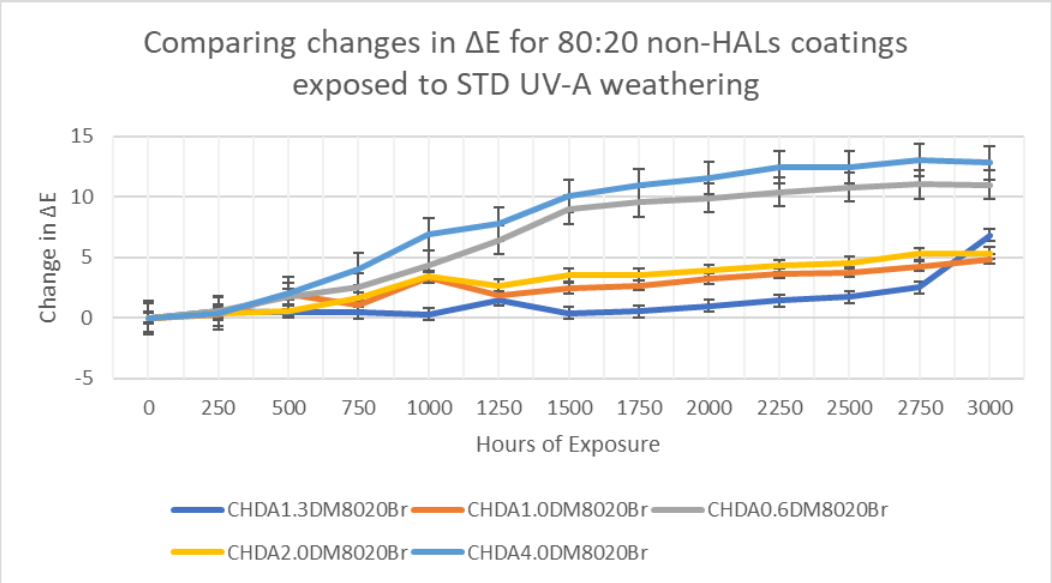

Figure 4.52-*Comparing changes in ΔE for STD UV-A exposed 80:20 non-HALS containing coatings*

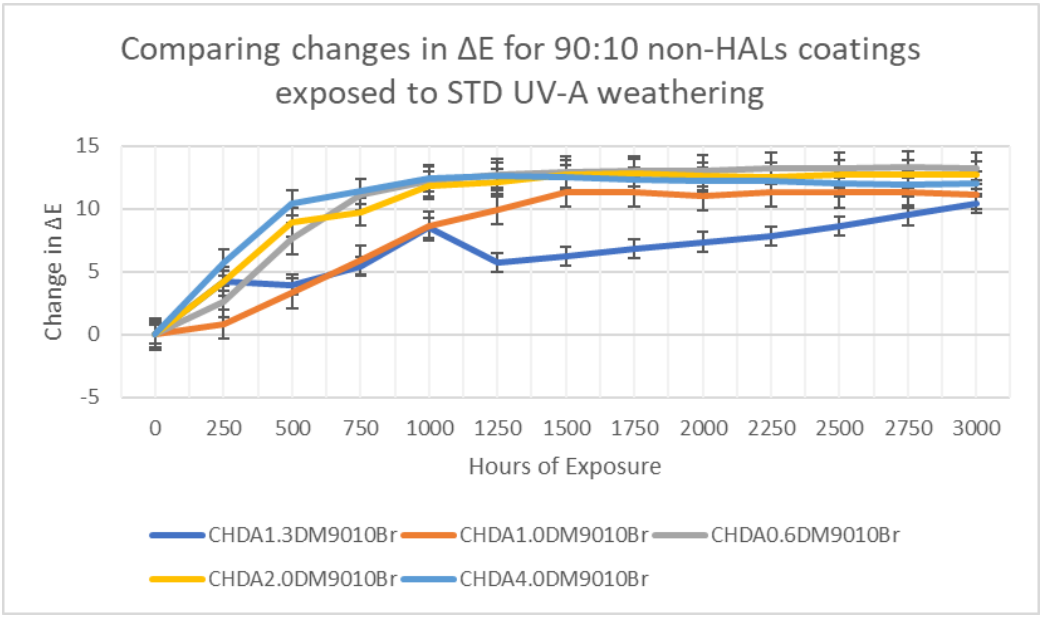

Figure 4.53-*Comparing changes in ΔE for STD UV-A exposed 90:10 non-HALS containing coatings*

Figures 4.54 and 4.55 show the impact of weathering on the ΔE of 80:20 and 90:10 HALS coatings in STD UV-A weathering respectively. In both instances, it can be seen that the CHDA1.3DM coating exhibits the greatest colour change, suggesting that straight chain additions could provide a benefit in the distribution of HALS throughout the coating system, or a reduction in the degree of pigment removal through interactions with water during weathering.

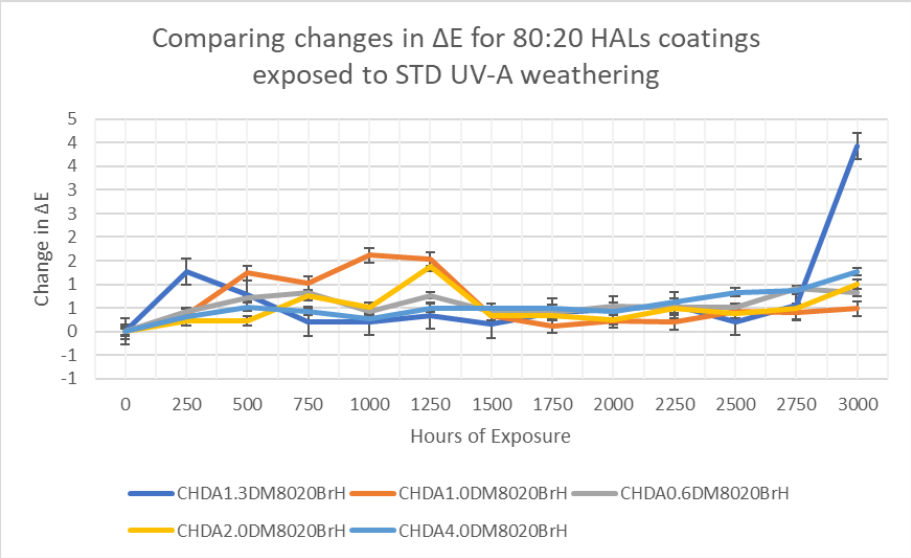

Figure 4.54-*Comparing changes in ΔE for STD UV-A exposed 80:20 HALS containing coatings*

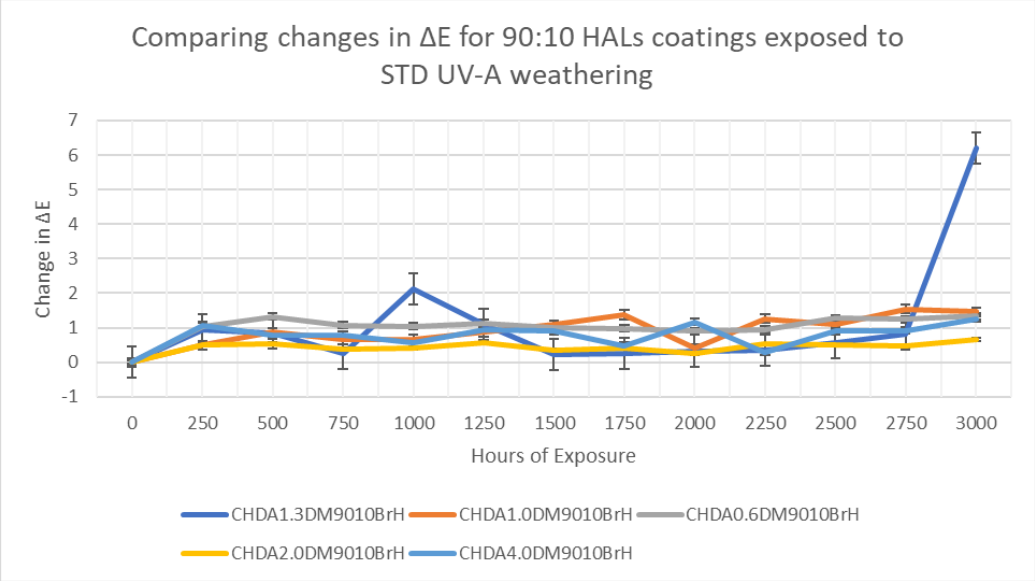

Figure 4.55-*Comparing changes in ΔE for STD UV-A exposed 90:10 HALS containing coatings*

Figures 4.56-4.59 illustrate the ΔE of coatings subjected to HOT UV-A weathering cycles. The ΔE of 80:20 non-HALS containing coatings are shown in Figure 4.56. It can be seen that CHDA1.3DM8020Br demonstrates the greatest degree of colour change, while CHDA1.0DM8020Br shows the smallest. By comparing Figure 4.56 against 4.52 it can be shown that all coatings exposed to HOT UV-A weathering saw greater colour change than those subjected to STD UV-A cycles.

Figure 5.57 shows the ΔE of 90:10 ratio coatings subjected to HOT UV-A cycles, where CHDA1.3DM9010Br is the worst performing and CHDA4.0DM9010Br shows the smallest colour change. The majority of

coatings demonstrated a significant colour change following 250 hours of UV-A cycles which then largely levelled off. The diminishing rate of colour change can be explained as the initial colour change was very severe that there was little pigment left to be damaged or removed via interactions with water.

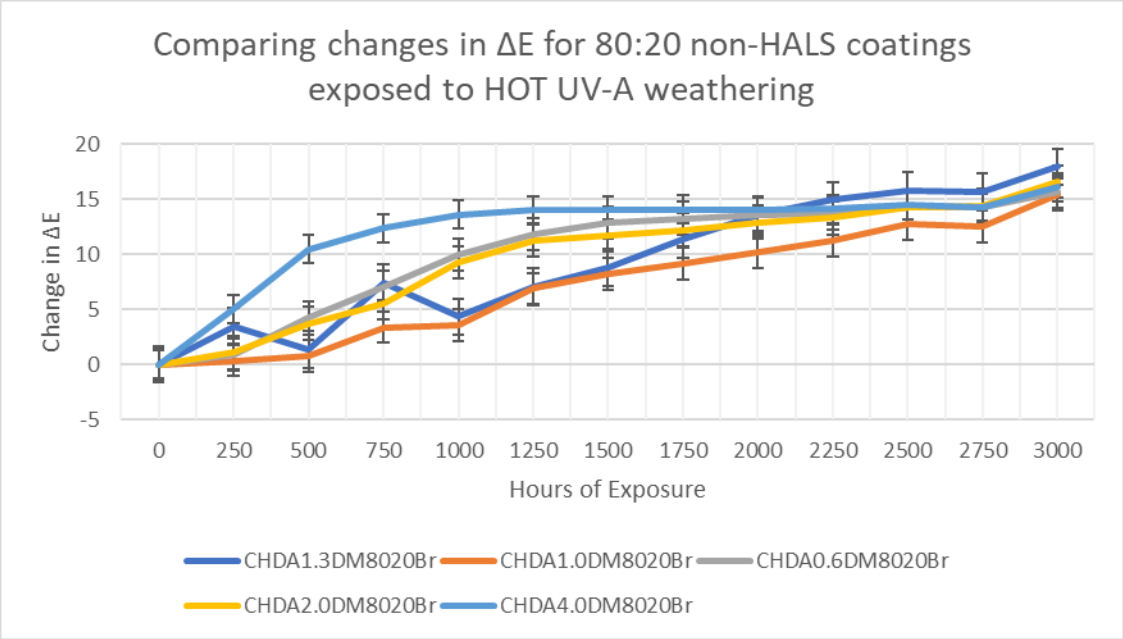

Figure 4.56-*Comparing changes in ΔE for HOT UV-A exposed 80:20 non-HALS containing coatings*

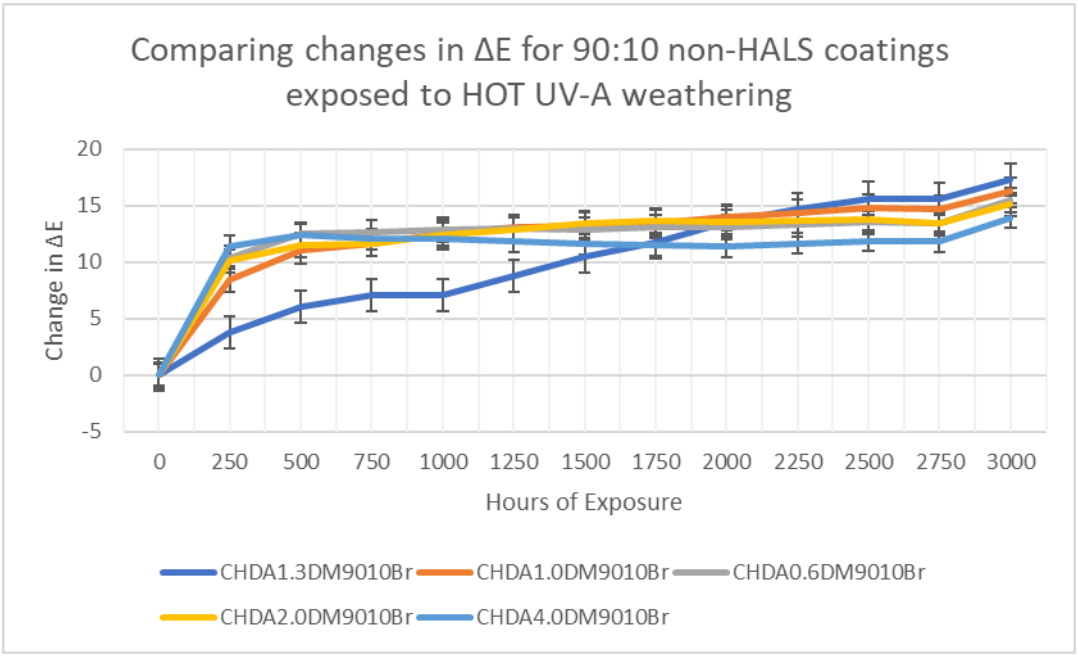

Figure 4.57-*Comparing changes in ΔE for STD UV-A exposed 90:10 non-HALS containing coatings*

Figures 4.58 and 4.59 show the colour change of 80:20 and 90:10 HALS containing coatings respectively. By comparing Figure 4.58 against Figure 4.56 it becomes apparent that while CHDA1.3DM8020Br demonstrates the greatest degree of colour change and CHDA1.0DM8020Br shows the smallest, that all coatings suffer a reduced level of colour change, which is due to the presence of the sacrificial HALS. All coatings see a sharp rise in ΔE following 2750 hours of weathering exposure, which indicates that this is the point where the majority of the HALS within the coating formulation had been spent causing the coatings to rely on their own inherent weathering resistance. Figure 4.60 shows the ΔE of 90:10 HALS coatings subjected to HOT UV-A weathering. It can be seen that CHDA4.0DM9010BrH shows the greatest change, followed by CHDA0.6DM9010BrH, which are the coatings with the greatest straight chain percentage. This indicates that at lower melamine ratios the level of straight chain in the formulation plays a more significant role in the degradation of the coating system.

By comparing Figure 4.58 and 4.60 together it can be seen that CHDA4.0DM9010BrH and CHDA4.0DMBr reach the same ΔE value following 3000 hours of HOT UV-A weathering. This is the only instance of a HALS containing coating demonstrating equal performance when compared to its non-HALS variant. This in turn suggests that higher values of CHDA and Hexanediol in a formulation, combined with a low melamine content cause the development of a coating that has poor properties in terms of colour retention.

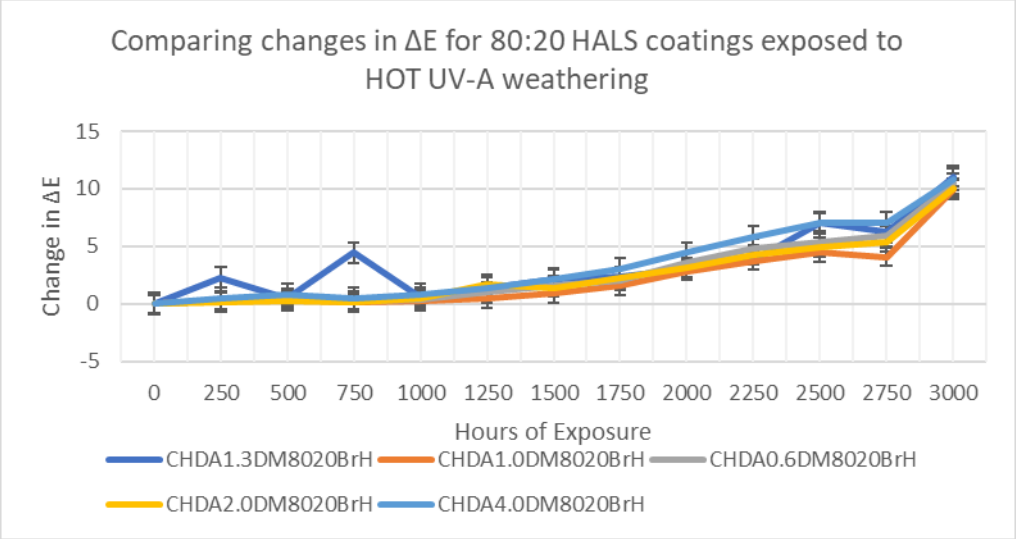

Figure 4.58-*Comparing changes in ΔE for HOT UV-A exposed 80:20 HALS containing coatings*

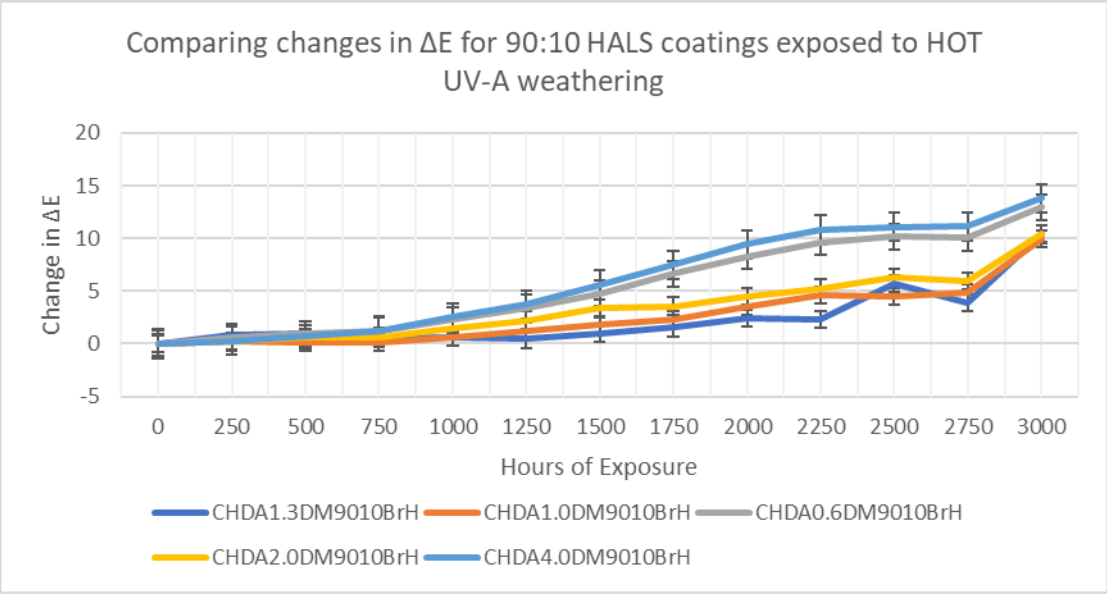

Figure 4.59-*Comparing changes in ΔE for HOT UV-A exposed 90:10 HALS containing coatings*

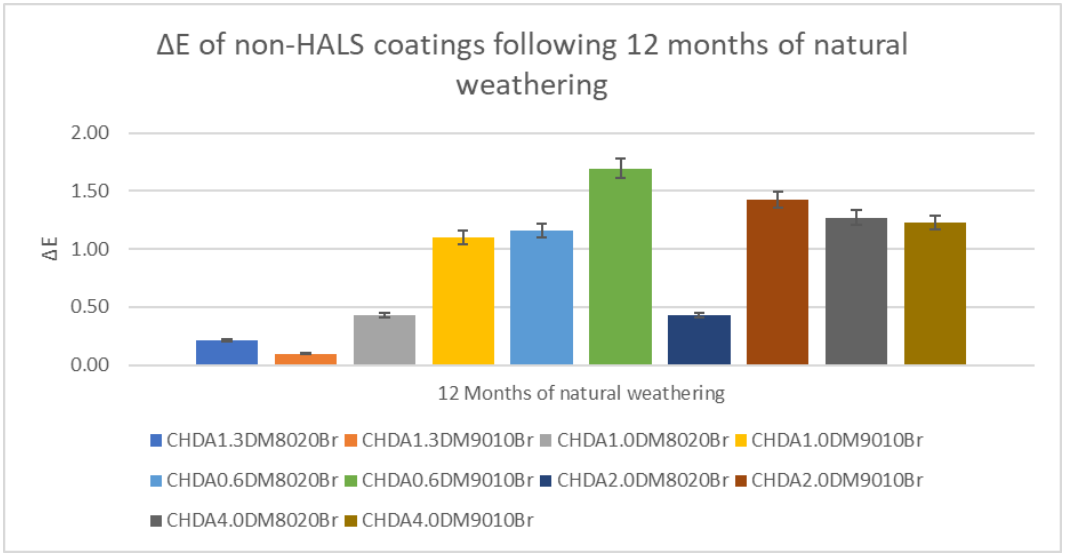

Figure 4.60-*Comparing changes in ΔE for naturally exposed non-HALS containing coatings*

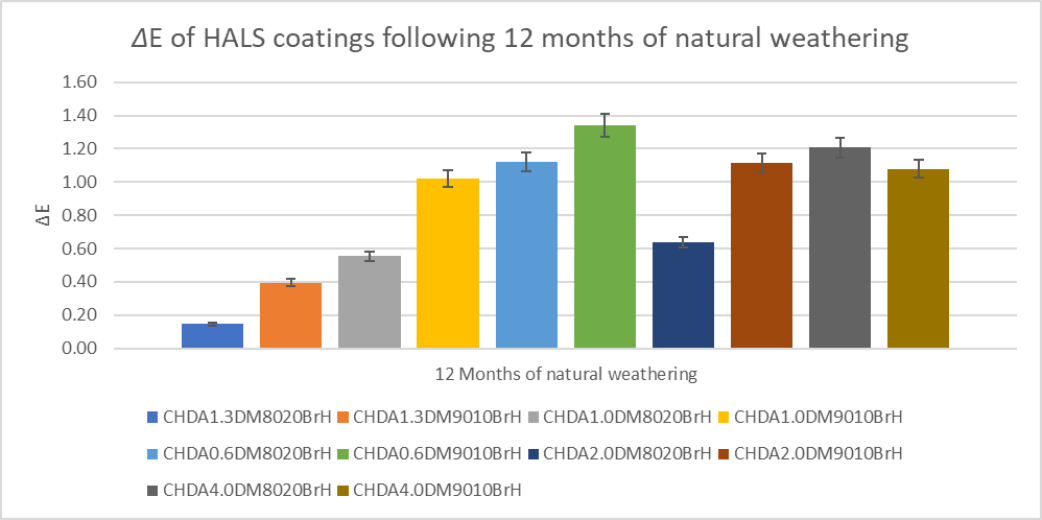

Figure 4.61-*Comparing changes in ΔE for naturally exposed HALS containing coatings*

Figure 4.60 shows the change in ΔE for naturally exposed non-HALS coatings. By comparing Figure 4.60 with previous ones within this section it can be seen that the non-HALS coatings exhibit a reduced degree of colour change compared to samples subjected to accelerated weathering tests. This could be in part due to the exposure time and the fact that the naturally exposed samples were washed periodically, which could have removed the chalking that occurs over time and influenced the apparent colour retention.

Figure 4.61 shows the ΔE of HALS containing coatings after 12 months of natural weathering. When comparing this with Figure 4.60 it is interesting to see that there are some instances where the non-HALS containing coating demonstrated a lower ΔE value than the HALS counterpart. This is notably the case for CHDA1.3DM9010Br, CHDA1.0DM8020Br, and CHDA2.0DM8020Br. It is unusual for a HALS containing coating to exhibit poorer weathering durability compared to a non-HALS containing coating. However, if aspects of the colour change were brought about through interactions with water (such as pigment removal) then the addition of HALS to the coating system would not be beneficial.

Analysis of the normalised change in hydroxyl activity also yielded significant information. It can be observed in Figure 4.62 that the coating with the lowest normalised increase in hydroxyl content was CHDA1.3DM8020Br, whereas the highest change in activity was demonstrated by CHDA4.0DM8020Br after 3000 hours of accelerated weathering. The coating with the smallest increase in hydroxyl activity (CHDA1.3DM8020Br) is the only coating that does not contain straight chain components, whereas the two poorest performing coatings (CHDA0.6DM8020Br and CHDA4.0DM8020Br respectively) had the highest straight chain percentages, with the coating with the larger CHDA ratio (CHDA4.0DM8020Br) being the poorest performing. This indicates that in the case of STD-UVA weathering of 80:20 PE:HMMM

coatings that higher ratios of CHDA within the coating system likely contribute towards an accelerated rate of degradation, with increased levels of straight chain percentages also negatively impacting the weathering durability of the coating systems.

A similar pattern is observed during HOT-UVA exposure of 80:20 PE:HMMM coatings, with CHDA1.3DM8020Br showing the smallest increase in hydroxyl activity and CHDA4.0DM8020Br the largest, as shown in Figure 4.63.

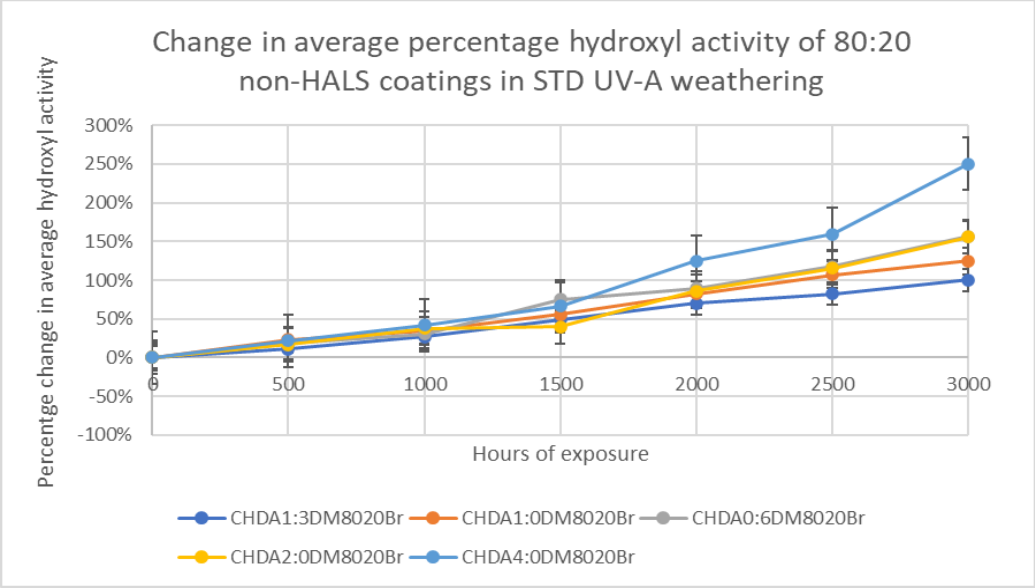

Figure 4.62-*Change in average percentage hydroxyl activity for 80:20 non-HALS coatings exposed to STD UV-A weathering*

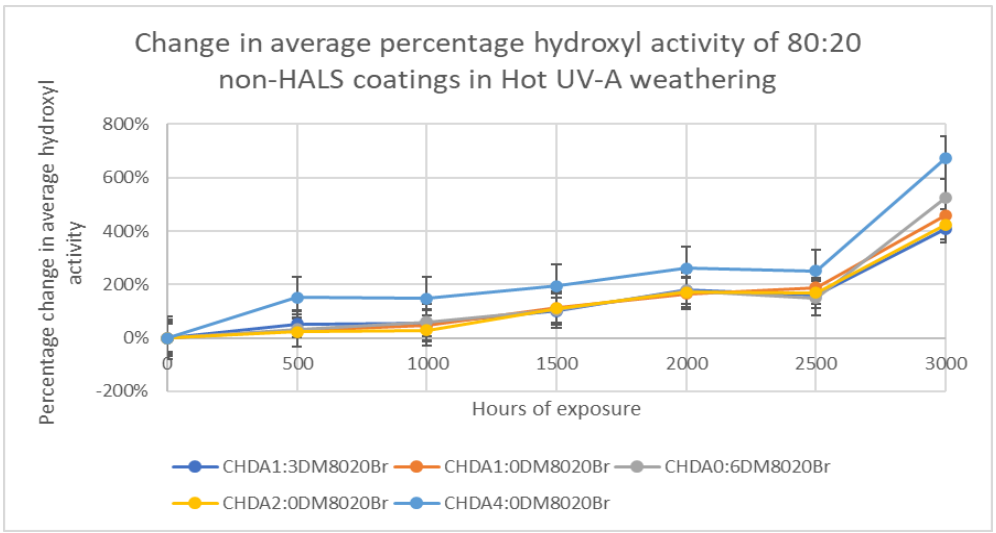

Figure 4.63-*Change in average percentage hydroxyl activity for 80:20 non-HALS coatings exposed to HOT UV-A weathering*

Figures 4.64-4.65 show the change in percentage average hydroxyl activity for HALS containing 80:20 coatings during Standard and HOT UVA weathering exposure respectively. In Figure 4.64 it can be observed that the measured hydroxyl levels increase and decrease as exposure progressed by a small amount, which could be due to experimental error through contact with the ATR crystal during FT-IR analysis. As the IR measurements were taken from coupons obtained from the sample, the fluctuations in hydroxyl level can be explained by the knowledge that coatings are not homogeneous and the possibility that the HALS was not evenly distributed throughout the coating surface. The heterogeneous nature of the coatings can also explain the overall decrease in normalised hydroxyl activity of CHDA1.3DM8020BrH. While CBDA4.0DM8020BrH continues to exhibit the greatest increase in hydroxyl activity, there is variation in the other coatings. This indicates that the addition of HALS into coating systems will not increase the durability of the coatings by a uniform amount. An example of this is CHDA2.0DM8020BrH, which exhibits an increase in hydroxyl activity approximately equivalent to CHDA4.0DM8020BrH, whereas the non-HALS equivalent (Figure 4.62) exhibited a significantly lower increase in hydroxyl activity compared to the poorest performing coating.

Figure 4.64 shows that CHDA1.3DM8020BrH exhibits the greatest change in hydroxyl activity after 3000 hours of weathering cycles. This is in opposition to previous results, where CHDA1.3DM8020Br coatings demonstrated the smallest changes in OH activity, which may suggest that CHDA1.3DM8020BrH is more susceptible to degradation at higher temperatures than other HALS containing coatings.

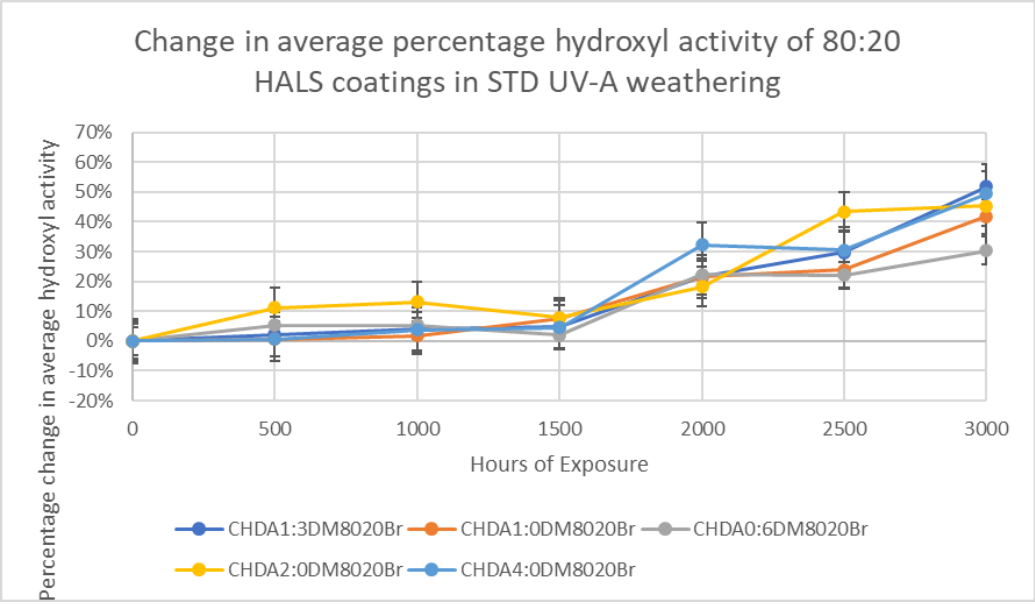

Figure 4.64-*Change in average percentage hydroxyl activity for 80:20 HALS coatings exposed to STD UV-A weathering*

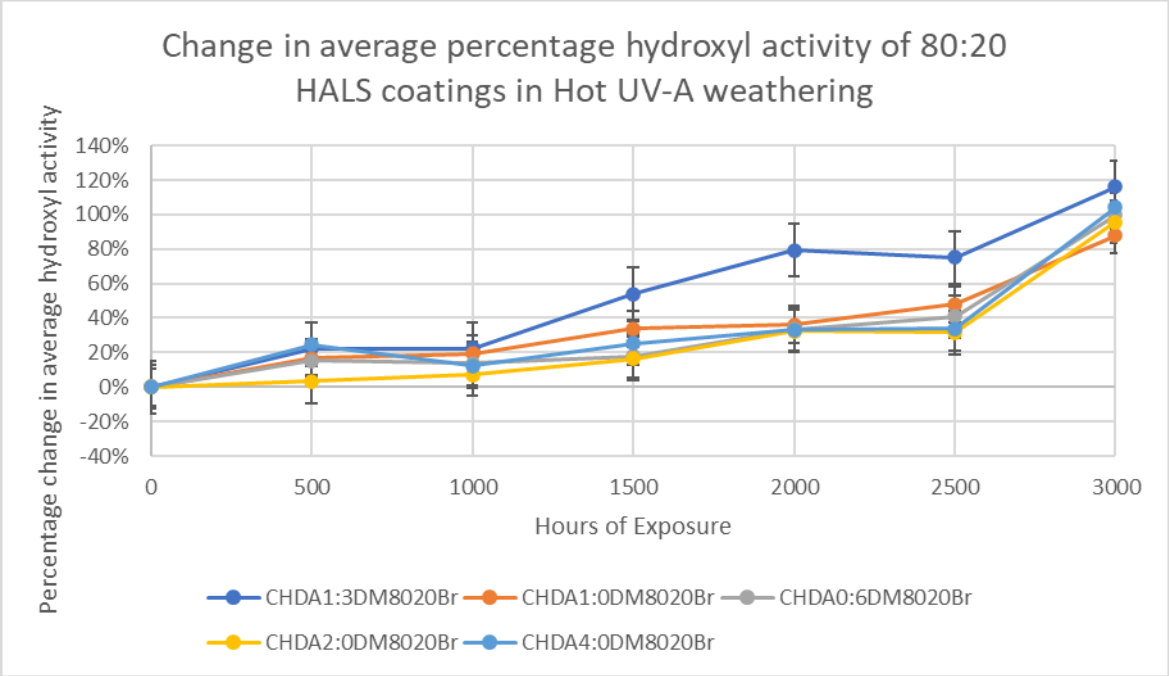

Figure 4.65-*Change in average percentage hydroxyl activity for 80:20 HALS coatings exposed to HOT UV-A weathering*

Figure 4.66 shows that CHDA1.3DM9010Br shows the smallest increase in hydroxyl activity, with CHDA4.0DM9010Br demonstrating the second smallest and CHDA2.0DM9010Br exhibiting the most significant change in hydroxyl activity.

There are several differences between the 90:10 coatings and their 80:20 counterparts in Figure 4.65. While the majority of the 90:10 PE:HMMM coatings exhibited greater increases in hydroxyl activity compared to the 80:20 variants, this was not the case for CHDA4.0DM9010Br, which showed an increase of 178% while CHDA4.0DM8020Br had an increase of 225%. This suggests that a larger crosslinker ratio within the coating formulation does not guarantee increased weathering durability.

Figure 4.67 breaks down the changes in hydroxyl activity for 90:10 non-HALS coatings exposed to HOT-UVA weathering. It is clear that the coatings subjected to HOT weathering demonstrated a greater increase in hydroxyl activity compared those exposed to standard-UVA. Comparing the results with those of 80:20 coatings in Figure 4.58 show several interesting results. CHDA4.0DM8020Br and CHDA4.0DM9010Br exhibit very similar increases in hydroxyl activity (674% and 678% respectively). It is interesting to note that for the coatings with a higher relative ratio of CHDM (CHDA1.0DM and CHDA0.6DM) the 90:10 coatings exhibit a smaller final increase in hydroxyl activity than their 80:20 counterparts, while the inverse is true for coatings where CHDA is more prominently featured.

Figures 4.66 and 4.67 show the changes in hydroxyl activity for 90:10 HALS containing coatings for standard-UVA and HOT-UVA weathering, respectively. Comparing Figures 4.65 and 4.66 show that the samples exposed to HOT-UVA weathering exhibit larger changes in hydroxyl activity than those in Std-UVA.

Comparing Figures 4.63 and 4.67 show that, except for CHDA1.3DM, the 80:20 HALS containing coating variants demonstrate a larger increase in percentage hydroxyl activity than the 90:10 counterparts.

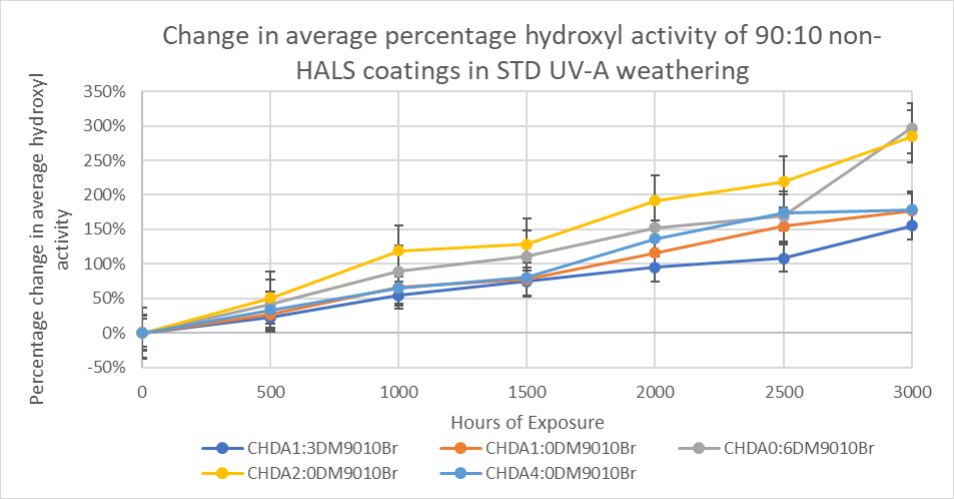

Figure 4.66-*Change in average percentage hydroxyl activity for 90:10 non-HALS coatings exposed to STD UV-A weathering*

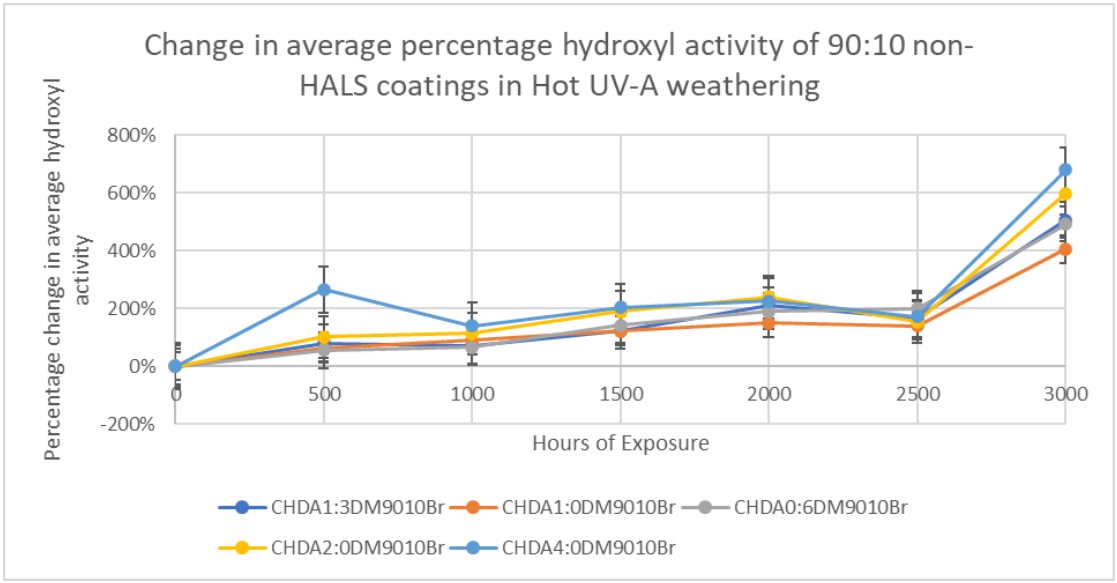

Figure 4.67-*Change in average percentage hydroxyl activity for 90:10 non-HALS coatings exposed to HOT UV-A weathering*

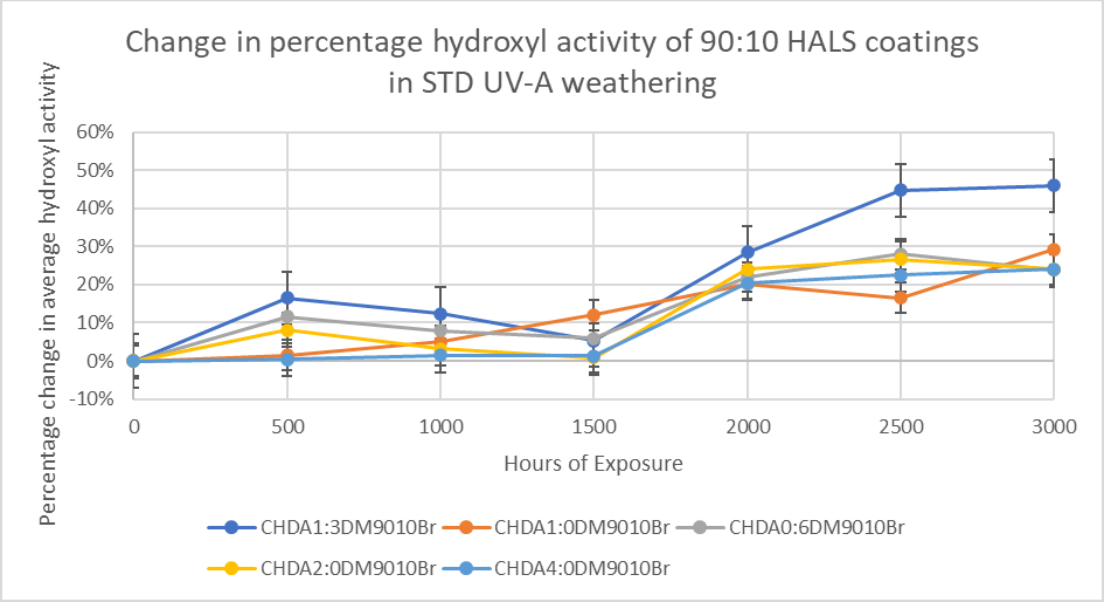

Figure 4.68-*Change in average percentage hydroxyl activity for 90:10 HALS coatings exposed to STD UV-A weathering*

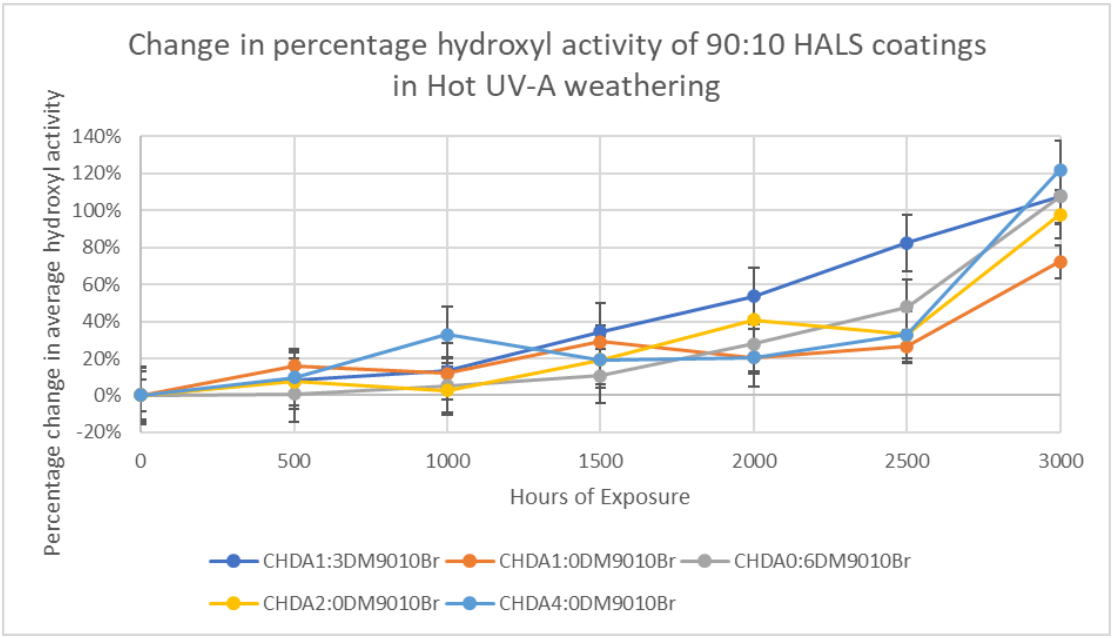

Figure 4.69-*Change in average percentage hydroxyl activity for 90:10 HALS coatings exposed to HOT UV-A weathering*

Figures 4.70-4.71 demonstrate the percentage changes in hydroxyl activity of CHDA:CHDM samples that were subjected to natural weathering. Unfortunately, it was not possible to obtain sample coupons after 6 months of exposure due to the unforeseen circumstances related to the COVID-19 global pandemic. The coating that demonstrated the greatest increase in hydroxyl activity in Figure 4.70 was

CHDA4.0DM8020Br, with an increase of 128% after 12 months, and 160% after 18 months of exposure. All coatings show a continued increase in hydroxyl activity between 12 and 18 months, with CHDA1.0DM8020Br showing the smallest increase in hydroxyl activity with 42% after 18 months.

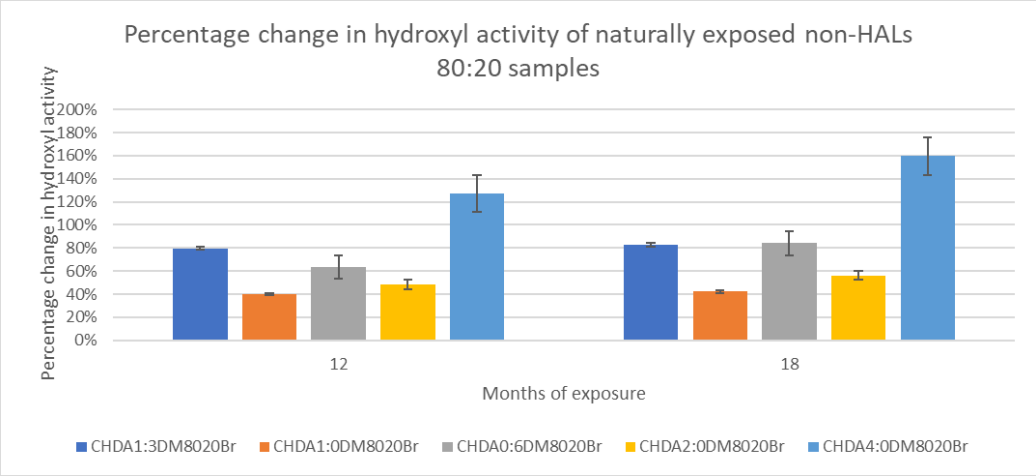

Figure 4.70-*Percentage change in average hydroxyl activity of naturally exposed 80:20 non-HALS coatings*

Figure 4.71 shows the change in hydroxyl activity for the HALS containing 80:20 coatings after 12 and 18 months of exposure. The most obvious result is from CHDA1.0DM8020BrH, which shows the greatest increase in hydroxyl activity. Another interesting result is demonstrated by CHDA2.0DM8020Br, as while it shows an increase in activity after 18 months of 1.3%, after 12 months it demonstrated a larger increase of 13%. This could be indicative of the removal of coating layers during weathering.

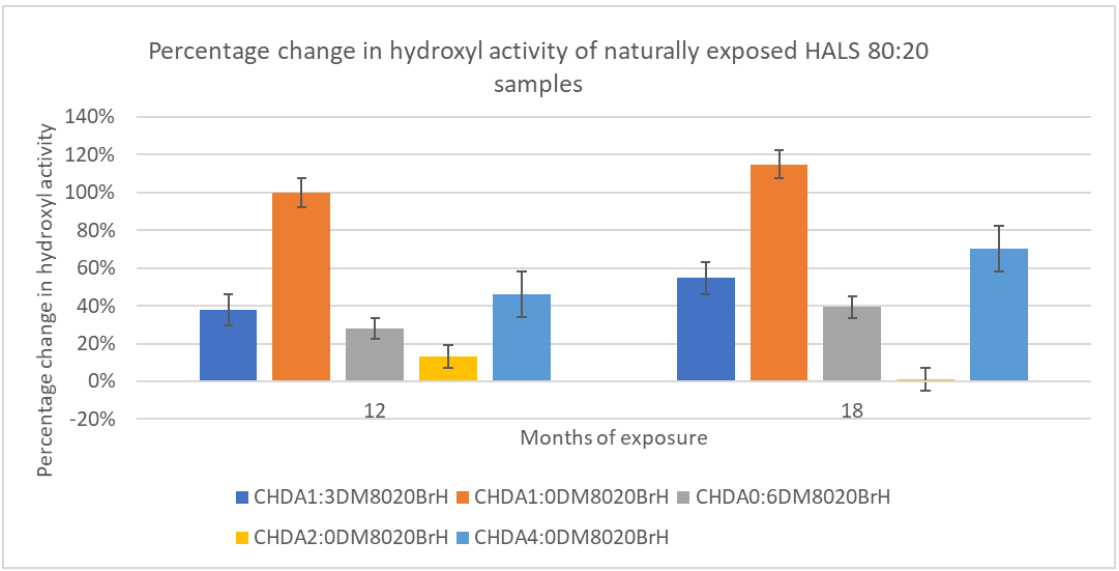

Figure 4.71-*Percentage change in average hydroxyl activity of naturally exposed 80:20 HALS coatings*

Figure 4.72 demonstrates the change in percentage hydroxyl activity of the 90:10 non-HALS naturally weathered coatings. As with the 80:20 non-HALS coatings, CHDA2.0DM9010Br shows the greatest increase in hydroxyl activity with an increase of approximately 300% after 18 months. CHDA0.6DM9010Br exhibits the smallest increase of hydroxyl activity, with a final value of 60%. Comparing the results from Figures 4.71 and 4.72 it can be seen that CHDA0.6DM9010Br shows a very similar increase in hydroxyl activity to its 8020 counterpart.

The HALS containing 90:10 ratio coatings outperform the non-HALS variant, with CHDA2.0DM9010Br again demonstrating the most significant increase in hydroxyl activity after 18 months of exposure as shown in Figure 4.73.

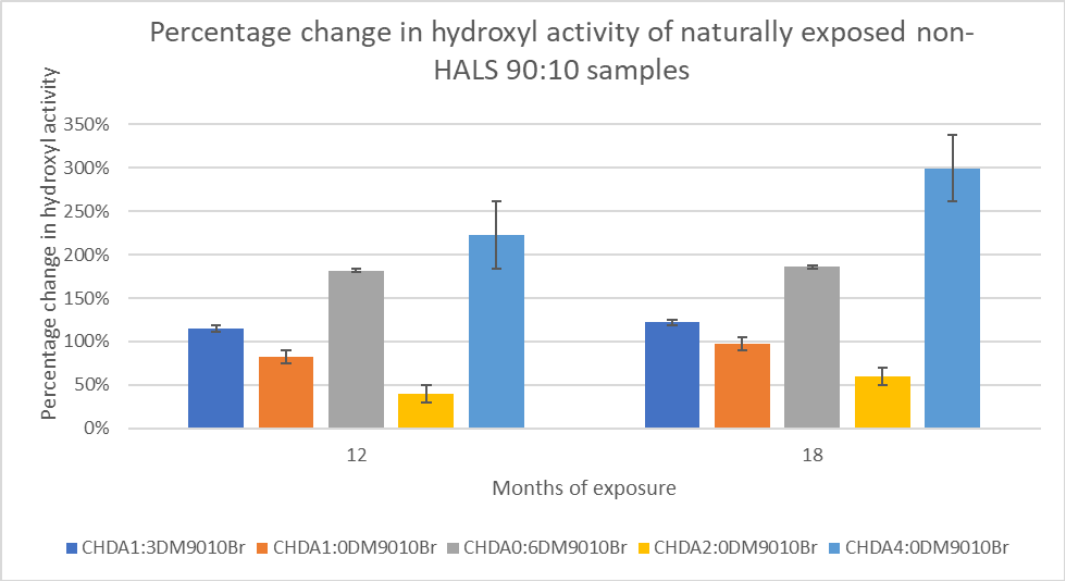

Figure 4.72-*Percentage change in average hydroxyl activity of naturally exposed 90:10 non-HALS coatings*

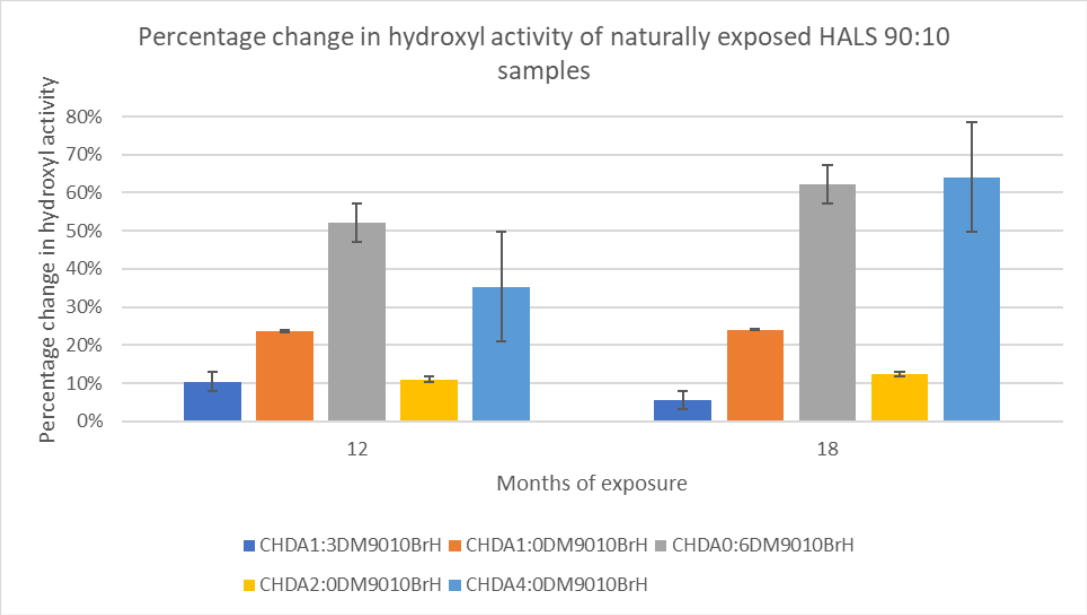

Figure 4.73-*Percentage change in average hydroxyl activity of naturally exposed 90:10 HALS coatings*

4.3.4-Discussion

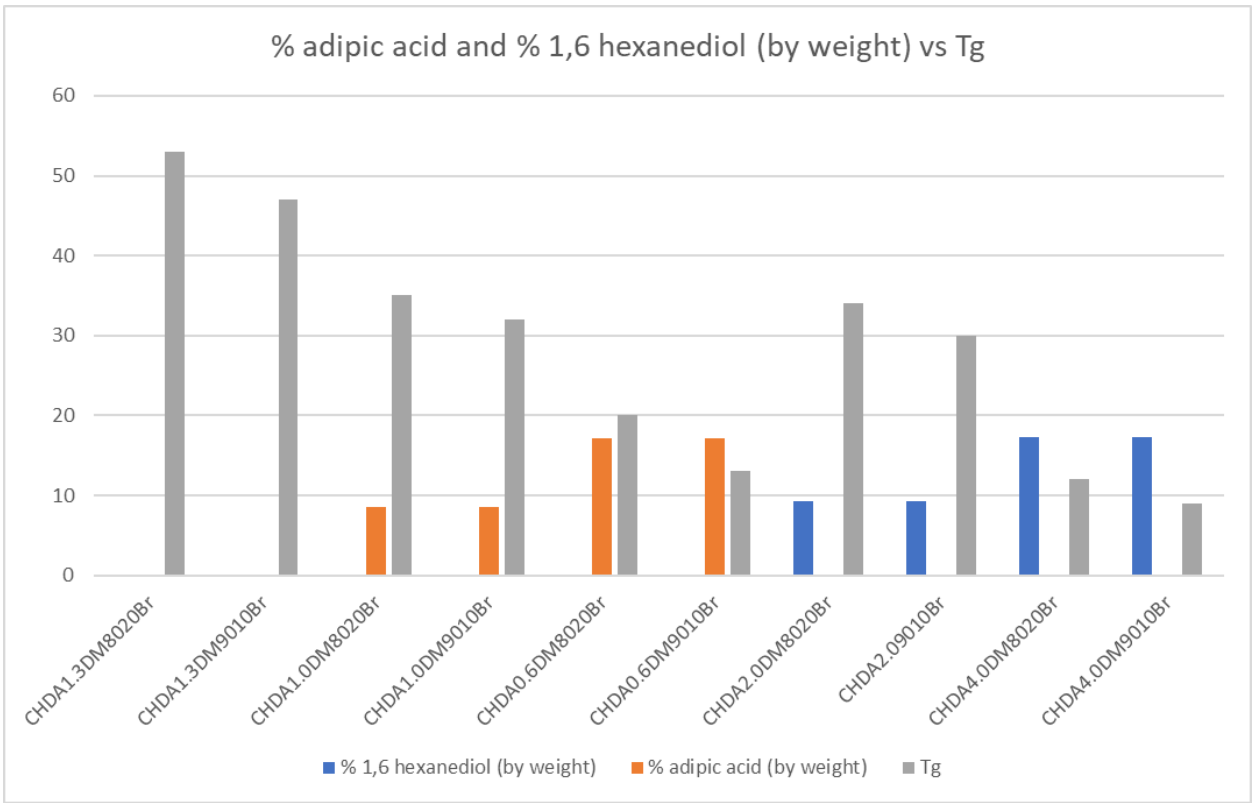

Figure 4.74-*Comparing percentage composition of Adipic acid and 1,6 Hexanediol against T_g*

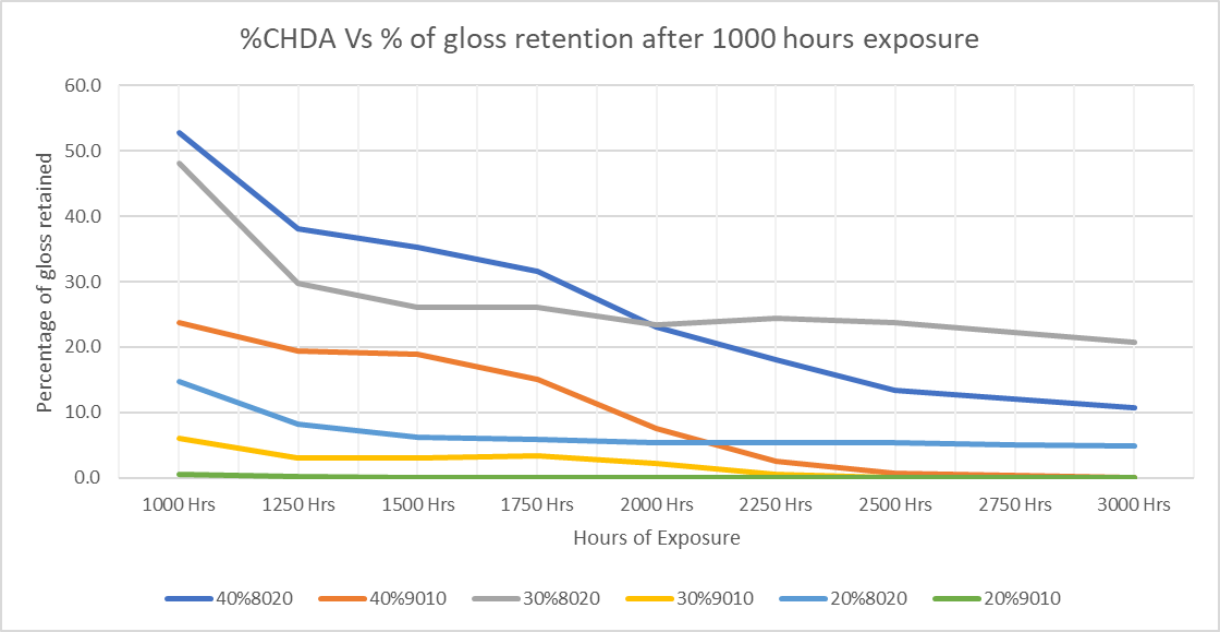

Figure 4.75-*Comparing percentage CHDA against percentage gloss retention from 1000-3000 hours of exposure*

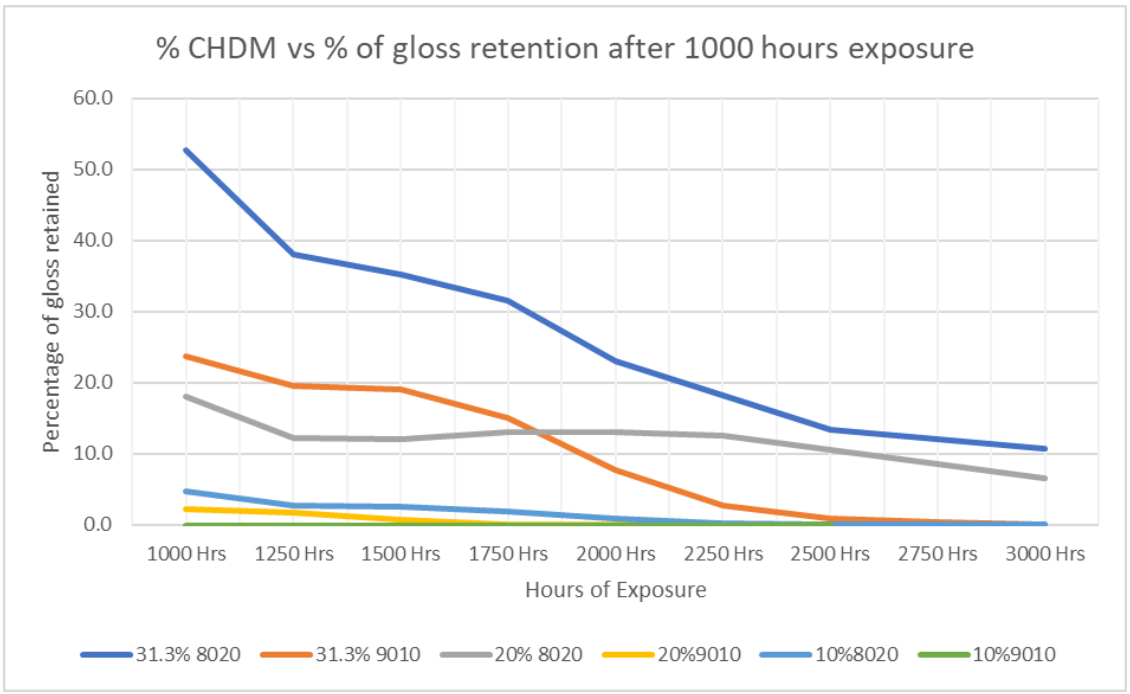

Figure 4.76-*Comparing percentage CHDM against percentage gloss retention from 1000-3000 hours of exposure*

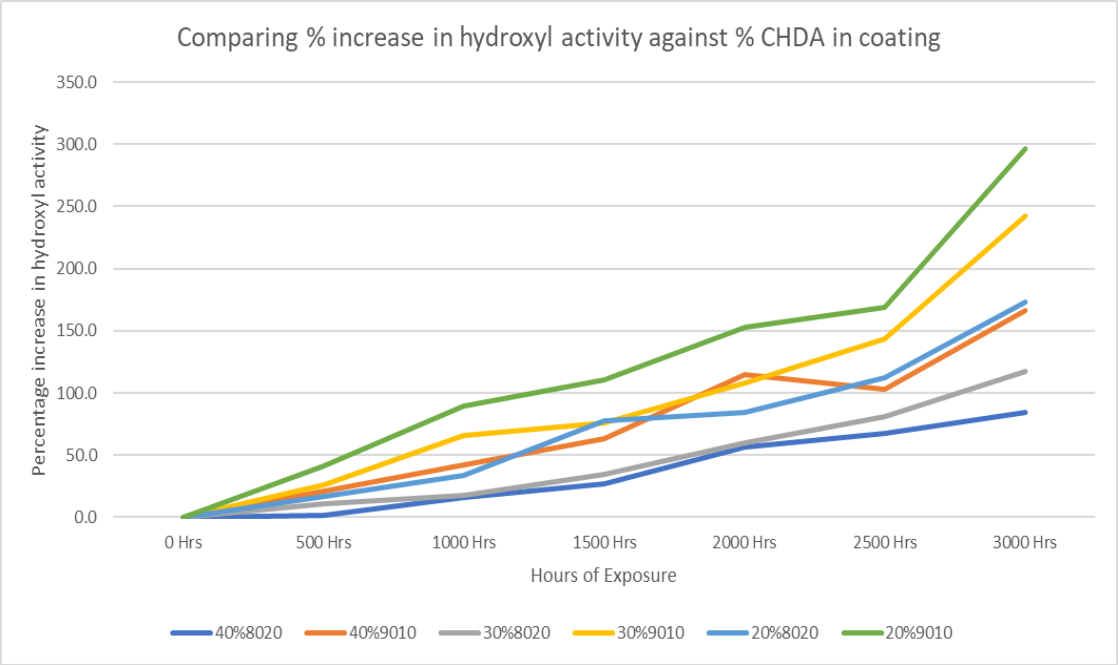

Figure 4.77-*Comparing percentage CHDA against percentage change in hydroxyl activity*

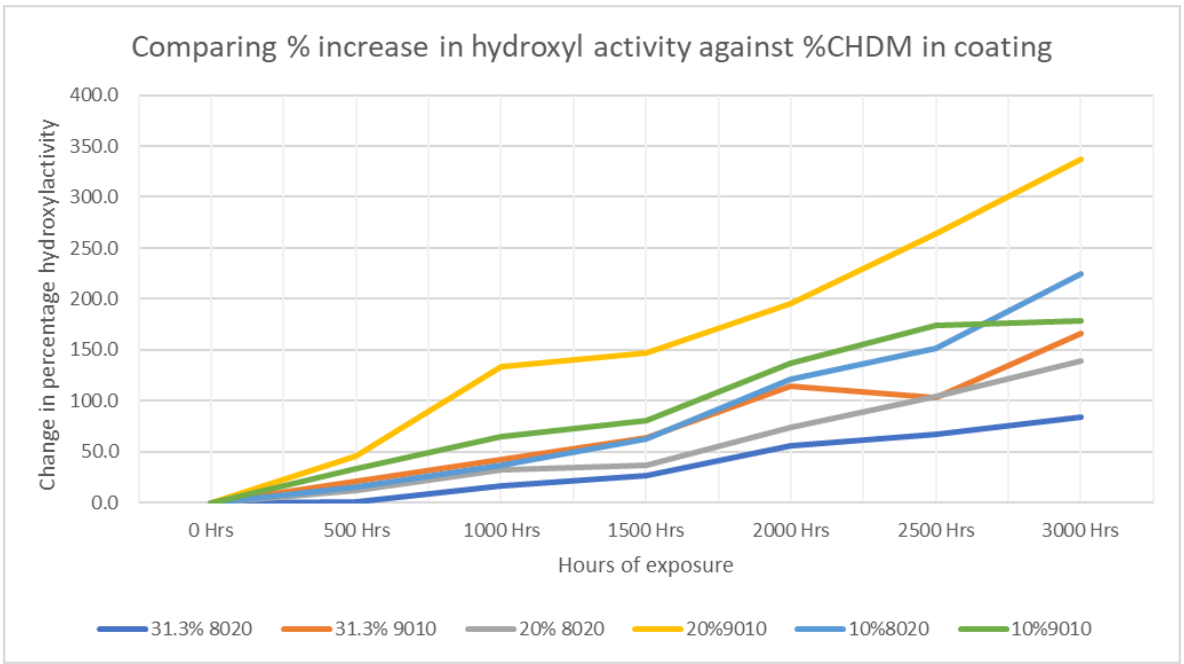

Figure 4.78-*Comparing percentage CHDM against percentage change in hydroxyl activity*

Figure 4.74 highlights that as melamine ratio decreases so does the T_g, this is exhibited by CHDA1.3DM8020Br and CHDA1.3DM9010Br, where the only difference in the coating formulation being the ratio of melamine within the coating system. The pattern was also repeated within all of the other 3rd

generation coatings, with the 80:20 ratio formulations all exhibiting a higher T_g than their respective 90:10 ratio counterparts.

It can also be claimed that the addition of straight chain components (adipic acid and 1,6 hexanediol) has a negative impact on the T_g of coatings. Figure 4.73 shows that as the % of adipic acid or 1,6 hexanediol increases there is a decrease in the T_g of the coating system, it also demonstrates that the coatings with an increase of 1,6 hexanediol shows a larger decrease in T_g compared to the adipic acid additions. This indicates that there is a correlation between increased % of adipic acid or 1,6 hexanediol and lower T_g. However, it is also possible that the lowered T_g is not solely due to the increase in % of adipic acid or 1,6 hexanediol but rather that the lowering of CHDA or CHDM respectively brings about the diminishing of the T_g compared to the reference coating CHDA1.3DM8020/9010Br coatings.

Figure 4.75 compares coatings with different %CHDA against % gloss retention following 1000 hrs of exposure to Hot-UVA up to 3000 hrs. After 1000 hrs exposure CHDA1.3DM8020Br (40% CHDA) shows the highest percentage of gloss retention. However, after 3000 hrs the coating with the greatest % gloss retention was CHDA1.0DM8020Br, which has 30% CHDA. Figure 4.64 also shows that all 80:20 coatings outperformed their 90:10 counterparts in terms of gloss retention.

The 90:10 coating with the poorest % gloss retention is CHDA0.6DM9010Br, which is recorded as showing 0% gloss retention following 1000 hrs of exposure, with CHDA1.0DMBr reaching 0% gloss retention 2250 hrs, and with CHDA1.3DM9010Br reaching 0% gloss retention after 2500 hrs. The poorest performing 80:20 ratio coating is CHDA0.6DM8020Br (20%CHDA) with only 5% gloss retention after 2500 hrs.

Figure 4.76 illustrates the impact that varying the levels of CHDM has on % gloss retention, with CHDA1.3DM8020/9010Br included to act as a standard. It is clear that CHDA1.3DM8020Br shows the highest % gloss retention. The poorest performing 80:20 coating was CHDA4.0DM8020Br, which reaches 0% gloss retention after 2250 hours of exposure. Likewise, the poorest performing 90:10 coating was CHDA4.0DM9010Br, which fell to 0% gloss retention at 1000 hours of exposure.

Comparing the results highlighted in Figures 4.76 and 4.77 indicate that diminishing the level of CHDM within a coating is associated with poorer performance in terms of gloss retention than the corresponding lowering of CHDA percentages. This could indicate that reduction of CHDM presence is more harmful to the coatings, or that the increased percentage presence of 1,6 hexanediol leads to a weaker coating in terms of gloss retention. This could be investigated in further work by replacing 1,6 Hexanediol with NPG as it has a greater level of stability.

Figure 4.77 compares the percentage increase in hydroxyl activity against % CHDA in coatings. All of the 90:10 coating variants show a greater increase in % hydroxyl activity than the corresponding 80:20 coatings. This correlates with the poorer % gloss retention demonstrated by the 9010 coatings.

Figure 4.78 shows the impact that altering the % CHDM within a coating has on the % increase of hydroxyl activity. CHDA4.0DM8020Br is the only 80:20 coating that shows a larger % increase in hydroxyl activity than its 90:10 variant. From observing Figure 4.78 the general observed pattern suggests that as the % CHDM is reduced within the formulation there is an increase in % hydroxyl activity, with the best performing coatings being CHDA1.3DM8020Br (31.3%) and CHDA1.3DM9010Br (31.3%). The only coating which does not follow the observed pattern is CHDA4.0DM9010Br, as levelling off of the hydroxyl value is observed after 2500 hours, however this could be due to the severe degradation observed in the coating, as shown by the low gloss values in Figure 4.63.

Table 4.9 gives a complete breakdown of the final percentage changes in hydroxyl activity for all coatings, alongside their respective rank, with 5 demonstrating the greatest change in activity and 1 the smallest. Comparing the change in hydroxyl activity for naturally weathered samples against those subjected to standard and Hot accelerated weathering tests shows some similarities between the different exposure types. For non-HALS 80:20 coatings CHDA4.0DM8020Br exhibits the greatest increase in percentage hydroxyl activity across all exposure methods. The best performing 80:20 coating in natural weathering was CHDA1.0DM8020Br, while CHDA1.3DM8020Br demonstrated the lowest change in hydroxyl activity in standard and Hot accelerated weathering for an 80:20 coating, with CHDA1.0DM8020Br being the second and best performing coating for each weathering type respectively.

Table 4.9-*Breakdown of percentage change in hydroxyl activity for all coatings under all weathering methods, and performance ranking (1 = Best, 5= Worst)*

Coating code	Natural Weathering %OH change				Standard accelerated weathering %OH				Hot accelerated weathering %OH change			
	Non-HALs	Rank	HALs	Rank	Non-HALs	Rank	HALs	Rank	Non-HALs	Rank	HALs	Rank
CHDA1:3DM8020Br	83%	3	55%	3	84%	1	-23%	1	408%	1	116%	5
CHDA1:0DM8020Br	42%	1	115%	5	118%	2	19%	2	459%	3	88%	2
CHDA0:6DM8020Br	84%	4	39%	2	173%	4	23%	3	526%	4	82%	1
CHDA2:0DM8020Br	56%	2	1%	1	139%	3	34%	4	425%	2	96%	3
CHDA4:0DM8020Br	160%	5	70%	4	225%	5	36%	5	674%	5	104%	4
CHDA1:3DM9010Br	122%	3	5%	1	166%	1	33%	5	506%	3	108%	3
CHDA1:0DM9010Br	97%	2	24%	3	242%	3	16%	3	405%	1	72%	1
CHDA0:6DM9010Br	186%	4	62%	4	297%	4	13%	2	492%	2	137%	5
CHDA2:0DM9010Br	60%	1	12%	2	337%	5	17%	4	597%	4	98%	2
CHDA4:0DM9010Br	299%	5	64%	5	178%	2	7%	1	678%	5	122%	4

In all instances of the exposure of 80:20 non-HALS CHDA4:0DM8020Br was the poorest performing, this indicates that the combination of high ratios of CHDA and 1,6 Hexanediol do not demonstrate high levels

of weathering resistance. CHDA2.0DM9010Br shows the smallest change in hydroxyl activity during natural weathering, but the greatest during standard accelerated weathering as well as the second greatest during Hot accelerated weathering. CHDA1.3DM9010Br exhibits the smallest increase in hydroxyl activity during standard accelerated weathering, while CHDA1.0DM9010Br is the best performing coating when subjected to Hot UV-A weathering. While there is significant variation between how the coatings performed under the different weathering conditions, it is clear that in natural and Hot UV-A accelerated weathering CHDA4.0DM was the poorest performing coating for both 80:20 and 90:10 ratio coatings, suggesting that Hot UV-A weathering may provide the better indicative test to determine the poorest coating.

An interesting note is the degree to which HALS influences the durability of the coating system and to what extent their addition can prolong the work life of the system. There are three instances where the best performing non-HALS coating is the worst performing HALS coating, as demonstrated by CHDA1.0DM8020BrH exposed to natural weathering, CHDA1.3DM9010BrH subjected to standard UV-A accelerated weathering, and CHDA1.3DM8020BrH. This suggests that while the coatings may provide superior weathering resistance without the addition of HALS, there may be issues with the homogenous dispersion of HALS throughout the coating, leading to poorer performance. This could be investigated with further work.

When comparing the data obtained within this section, it becomes clear that reducing the %CHDM within a formulation is associated with poorer properties than a corresponding decrease in % CHDA, implying either that CHDM has more beneficial weathering capabilities than CHDA, or that 1,6 Hexanediol is more susceptible to UV degradation than Adipic Acid.

4.3.4-Conclusions

The control coating is outperformed in every area by the majority of novel coating systems apart from colour retention in which the control coating significantly outperformed all novel coatings. It can be observed in Table 4.8 that the addition of HALS to a coating system generally has a slight negative impact on the T_g value of the coatings. It can also be observed that as the straight chain percentage of the coating systems increase that there is a significant decrease in the T_g value.

Analysis of gloss retention has shown that the 80:20 coatings outperformed their 90:10 counterparts. The poorest performing in both 80:20 and 90:10 was based on the LSBS41 resin, which contained the lowest amount of CHDM of all formulations, the next poorest performing coatings were based on LSBS39, which

contained the lowest amount of CHDA. The fact that lower CHDM ratios within coatings have been shown to result in poorer gloss retention could be indicative of CHDM providing superior weathering resistance to CHDA, or that the addition of the straight chain 1,6 Hexanediol that was used to bolster the hydroxyl values of the resin cause the coating to be more susceptible to degradation. It is also clear to see that as the straight chain percentage increases, the T_g and the ability of the coating to resist degradation decreases.

In terms of colour retention, the best performing coating was CHDA1.0DM8020Br with the worst performing being CHDA4.0DM8020Br. The coating that showed the smallest increase in hydroxyl content was CHDA0.6DM8020Br, with the worst performing once again being CHDA4.0DM8020Br. While there is some variation, it can be stated that the poorer performing novel coatings contain higher relative ratios of CHDA within the resin base. This can be attributed towards several potential reasons, from CHDA being more susceptible to weathering degradation, through to the inclusions of 1,6 Hexanediol introducing areas of weakness within the coatings. This can be taken further by replacing 1,6 Hexanediol in further formulations with NPG, this would make it possible to determine if it was the 1,6 Hexanediol or the greater relative amount of CHDA within the formulation that brought about the lower levels of weathering durability.

In summary, all 80:20 coatings provided superior gloss retention than their 90:10 counterparts, with only one 80:20 coating (CHDA4.0DM8020Br) exhibiting poorer gloss retention than the best performing 90:10 formulation. Colour retention was more complicated, with the 80:20 ratio reference formulation and the two coatings with the largest straight chain percentages showing greater colour change than the comparable 90:10 formulations. However, the 80:20 coatings with low percentages of straight chain components provided superior levels of colour retention.

The 80:20 coatings also showed smaller increases in normalised hydroxyl content than 90:10 coatings, with the exception of CHDA4.0DM8020Br, which exhibited a slightly greater hydroxyl increase than its 90:10 counterpart.

When these findings are viewed alongside the research performed by Persson et al, it suggests that the advantages of a more uniform distribution of melamine throughout the 90:10 coatings are most apparent when the straight chain percentage reaches higher levels and can be clearly observed in terms of colour retention. (5,11)

4.4-Conclusions

The primary focus of this chapter was to compare and contrast the weathering durability capabilities of novel coating systems based on other comparable monomers to that of HHPA, which is commonly held as providing the greatest weathering resistance within the realm of cycloaliphatic monomers.

The analysis of clear coats confirmed the superior weathering resistance of HHPA compared to CHDA. The results also showed that the CHDA:CHDM clear coat also provided superior weathering resistance than the CHDA monomer, indicating that the co-monomer resin would suit further investigation in order to optimise the ratio of monomers within the blend.

It is well known that the addition of pigments to a coating system can exert an influence over the weathering durability of the coating through exacerbating the existing degradation pathways and potentially introducing new ones. Assessment of the data from this investigation showed that HHPA continued to outperform CHDA in all areas with the exception of changes in normalised hydroxyl content, where it closely matched the data obtained from the CHDA based coatings. This can be explained by the fact that CHDA coatings have higher initial hydroxyl values than HHPA coatings, so while the HHPA coatings exhibit normalised changes in hydroxyl content that is in line with that of the CHDA coatings, their actual hydroxyl content levels remain lower than that of CHDA, which results in CHDA hydrolysing at a faster rate.

The investigation into the second generation of pigmented coatings was designed to determine the optimum ratio of CHDA to CHDM coatings. This was due to the superior weathering durability that was exhibited during analysis of the clear coatings earlier within the chapter. It was found that increasing the straight chain to > 20% of the resin formulation by weight facilitated additional degradation pathways, resulting in coatings suffering greatly accelerated rates of degradation. It can also be seen that the coatings with a greater relative weight of CHDA suffered more rapid degradation than those with a larger CHDM ratio.

In all experimental instances, pure CHDA coatings have been shown to offer a lower level of weathering resistance compared to an HHPA counterpart, potentially due to the greater number of instances of carbonyl groups within the repeating units of CHDA monomer. This depends on the energy gap between the non-bonding lone pair and the antibonding pi* orbitals, which is approximately equivalent to UV light below 300nm. The structure of CHDA may push the energy gap to lower values which would push

absorption towards the visible spectrum. It may also be possible that the structure of CHDA containing chains provides less shielding for the carbonyl groups, leaving them more vulnerable to attack.

Investigation of the CHDA:CHDM co-monomer blend based coating systems show that the removal of CHDM from the resin system and replacing it with 1,6 Hexanediol results in a coating with poorer weathering durability than removing CHDA and replacing with adipic acid.

The work performed and recorded in this Chapter in combination with the research performed by Persson et al provide evidence that in certain situations it can be beneficial to have lower melamine ratios within coating systems. The lower melamine ratios reduce the probability of melamine self-condensation reactions from occurring, which in turn prevents the formation of hydrophilic areas across the surface of the coating. A more uniform coating system would, by definition, have fewer instances of lateral inhomogeneities and would likely lead to improved weathering resistance. However, work performed and recorded within this chapter has shown that lower melamine ratios also exert a negative impact over the T_g of the coatings as well as resulting in much poorer levels of percentage gloss retention than their counterparts with higher melamine ratios. (1,5) The poorer percentage gloss retention shown in section 3 between 80:20 and 90:10 coatings is also demonstrated within sections 1 and 2 between the 80:20 and 85:15 coatings.

There are also fears that, if the melamine ratio within a coating system is low, then it can result in a smaller degree of successful crosslinking, weakening the overall coating structure both chemically and mechanically.

Unfortunately, due to time constraints it was not possible to further optimise the CHDA:CHDM ratio due to project time limitations. However, it is hypothesised that further optimisation of the co-monomer ratio and the replacement of CHDA by another cycloaliphatic monomer such as dimethyl malonic acid, or other monomers such as dodecenyl succinic anhydride could result in a coating that is able to surpass the weathering durability of HHPA. As such, further research could investigate the impact of replacing CHDA within the optimum CHDA:CHDM ratio with a range of other cycloaliphatic monomers to determine if the replacement monomers offer any benefits or improvements in terms of weathering durability over HHPA or the CHDA:CHDM co-monomer systems. Future work would be best served by focusing on the coating systems that provided the greatest weathering resistances across the different exposure methods, narrowing tests to investigating CHDA1:3DM, CHDA1:0DM, and CHDA2:0DM, which were the best performing resin systems for 80:20 or 90:10 coatings across all exposure methods.

4.5-References

1. Makki H, Adema KNS, Hendrix MMRM, Peters EAJF, Laven J, Van Der Ven LGJ, et al. Weathering of a polyester-urethane clearcoat: Lateral inhomogeneities. Polymer Degradation and Stability [Internet]. 2015;122:180–6. Available from: http://dx.doi.org/10.1016/j.polymdegradstab.2015.10.022

2. Nguyen T, Gu X, Vanlandingham M, Byrd E, Ryntz R, Martin JW. Degradation modes of crosslinked coatings exposed to photolytic environment. Journal of Coatings Technology and Research. 2013;10(1):1–14.

3. Radičević RZ, Jaroslavak BS. The effects of alkyd/melamine resin ratio and curing temperature on the properties of the coatings. Journal of the Serbian Chemical Society. 2005;70(4):593–9.

4. Sorce FS, Ngo S, Lowe C, Taylor AC. The effect of HMMM crosslinker content on the thermal-mechanical properties of polyester coil coatings. Progress in Organic Coatings [Internet]. 2019;137(August):105338. Available from: https://doi.org/10.1016/j.porgcoat.2019.105338

5. Persson D, Heydari G, Edvinsson C, Sundell PE. Depth-resolved FTIR focal plane array (FPA) spectroscopic imaging of the loss of melamine functionality of polyester melamine coating after accelerated and natural weathering. Polymer Testing [Internet]. 2020;86(March):106500. Available from: https://doi.org/10.1016/j.polymertesting.2020.106500

6. Adar F. Introduction to Interpretation of Raman Spectra Using Database Searching and Functional Group Detection and Identification. Spectroscopy online [Internet]. 2016 [cited 2018 Jul 19];31(7):16–23. Available from: http://www.spectroscopyonline.com/introduction-interpretation-raman-spectra-using-data-base-searching-and-functional-group-detection-a?pageID=1

7. Errandonea D, Muñoz A, Rodríguez-Hernández P, Proctor JE, Sapiña F, Bettinelli M. Theoretical and Experimental Study of the Crystal Structures, Lattice Vibrations, and Band Structures of Monazite-Type PbCrO4, PbSeO4, SrCrO4, and SrSeO4. Inorganic Chemistry. 2015;54(15):7524–35.

8. Hirayama T, Urban M. Distribution of Melamine in melamine polyester coatings.pdf. Progress in Organic Coatings. 1992;20:81–96.

9. Gamage NJW, Hill DJT, Lukey CA, Pomery PJ. Factors affecting the photolysis of polyester-melamine surface coatings. Polymer Degradation and Stability. 2003;81(2):309–26.

10. Zhang WR, Zhu TT, Smith R, Lowe C. An investigation on the melamine self-condensation in polyester/melamine organic coating. Progress in Organic Coatings [Internet]. 2010;69(4):376–83. Available from: http://dx.doi.org/10.1016/j.porgcoat.2010.07.011

11. Zhang WR, Zhu TT, Smith R, Lowe C. A non-destructive study on the degradation of polymer coating II: Modelling of degradation depth profiles. Polymer Testing [Internet]. 2012;31(8):1100–4. Available from: http://dx.doi.org/10.1016/j.polymertesting.2012.08.008

Chapter 5-Influence of Ultraviolet light and hydrolysis on coating longevity

5.1-Introduction

It has been documented within previous chapters (Chapter 4) that HHPA (Hexahydro Phthalic Anhydride) coatings outperform those based on CHDA (cyclohexane dicarboxylic acid) in both natural and accelerated weathering tests (see Chapter 4 for more details.) HHPA and CHDA are cycloaliphatic monomers that are used in the development of resins, which go on to be used in the generation of full coating systems. (8)

This chapter investigates the influence that UV radiation and water have on coatings based on HHPA and CHDA. The aim of which is to improve understanding into why HHPA outperforms CHDA in both accelerated and natural weathering tests.

One of the hypothesised reasons behind the superior weathering performance of HHPA compared to other cycloaliphatic monomers such as CHDA is a smaller absorbance window within the UV-A region. This would be significant because it is well documented that the UV region of the solar spectrum is high energy and causes photo-oxidative degradation, which causes the polymer backbone to breakdown and leads to the generation of self-propagating free radicals. Free radicals are capable of severely damaging the polymer backbone, significantly reducing the life of the polymer. Hydrolysis can also be a significant contributor to coating degradation, more information on both hydrolysis and photodegradation can be found in Chapter 2. (1,9)

5.2-Impact of UV absorption

Clear coat free-film coatings were developed using LSBS-STD and LSBS-33, which are HHPA and CHDA containing resins respectively. An in-depth breakdown of the resin and coating generation methodology can be found within Chapters 3 and 4 and an overview is provided by Table 5.1. The cycloaliphatics had the concentrations modified to ensure that COOH equivalence was maintained. The Mn target was 3400-4200 and the Hydroxyl volume (OHV) was targeted to be between 50-60. The chosen melamine crosslinker was Hexamethoxymethylmelamine (HMMM). Keeping all other pertinent targets within these levels meant that any discrepancies observed during the investigation would be due to the presence of the monomer base.

Table 5.1-*Breakdown of resins utilised within this Chapter*

Resin Code	Main Component(s)	Ratio of contents (if appropriate)
LSBS-STD	HHPA	N/A
LSBS-33	CHDA	N/A

To generate the free films, each coating was applied to a PTFE sheet using a wire-wound bar and then cured in an oven set to 265^{o}C for 35 seconds to reach a Peak Metal Temperature (PMT) of 232^{o}C. Once cooled, the samples were peeled away from the Teflon sheet to produce a free film. A more detailed description into this process has been provided in Chapter 2. A complete breakdown of the coatings is shown in Table 5.2.

Table 5.2-*Breakdown of coatings including film thickness and crosslinker ratio in free films*

Coating code	Resin code	Monomer base	PE:HMMM ratio	Film thickness (µm)
HH*8020	LSBS-STD	HHPA	80:20	27
HH*8515	LSBS-STD	HHPA	85:15	24
HH*9010	LSBS-STD	HHPA	90:10	25
CHDA*8020	LSBS-33	CHDA	80:20	26
CHDA*8515	LSBS-33	CHDA	85:15	27
CHDA*9010	LSBS-33	CHDA	90:10	25

The free films were analysed to determine their Transmission profiles across the Solar Spectrum by measuring every 10nm from 200 to 2500nm, this was performed via a Perkin Elmer Lambda 950 with a 150nm integrating sphere. The primary focus was analysis of absorbance of the free films in the visible and UV-A region (740-380nm and 400-320nm respectively), although the UV-B (315-280nm) and UV-C (280-100nm) region were also investigated as the range of interest was from 780nm to 200nm. The total deviation in film thickness measured for the sample was 3µm. Ensuring that coating thickness was kept as constant as possible allowed for minimal impact on the UV-Vis transmission measurements.

It is important to note that there is a range of 3µm between the thinnest film (24µm) and the thickest films (27µm). This range must be considered when analysing the results, as it can be assumed that a thicker coating would be likely to demonstrate a greater degree of absorbance. The film thicknesses were measured with a micrometer gauge with an error range of 1/200mm (0.005mm).

The transmittance measurements were converted to absorbance through the equation shown by Equation 5.1.

$$Absorbance = 2 - log\%\, Transmittance$$

Equation 5.1-*Conversion of transmittance to Absorbance*

Analysis of the absorbance profiles of HHPA and CHDA based coatings showed that absorbance of UV light decreased as melamine concentration decreased. This indicates that melamine is an important contributor to the total UV absorbance of a coating, as shown in Figures 5.1 and 5.2.

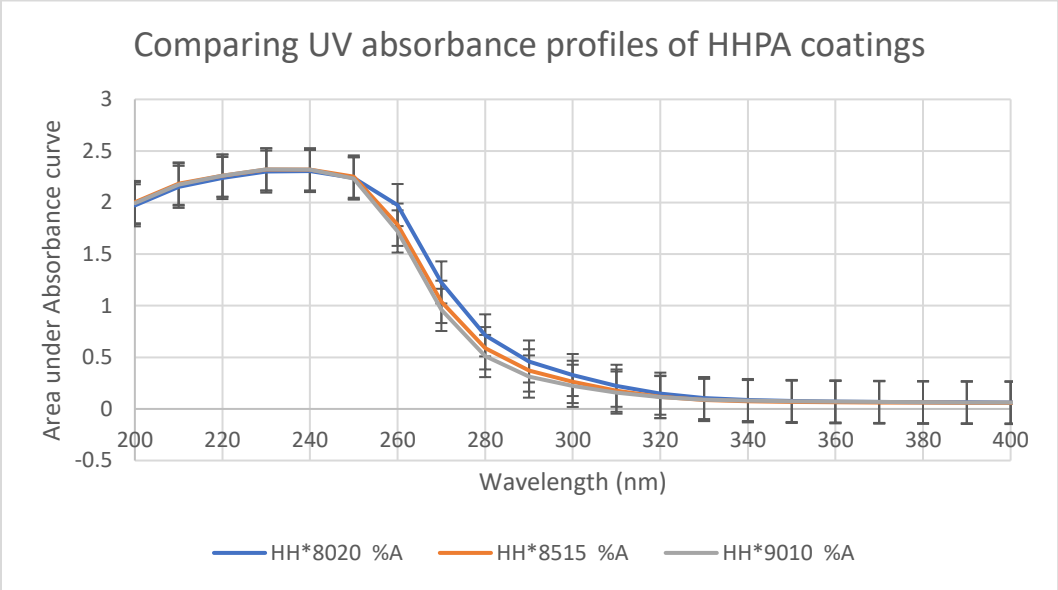

Figure 5.1-*Absorbance profiles for LSBS-STD free-films*

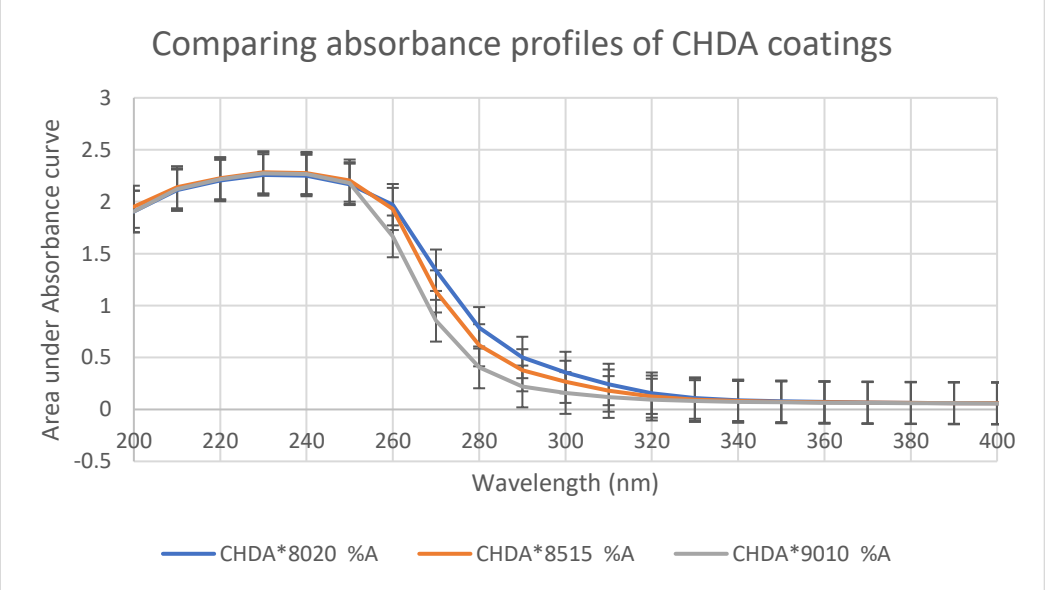

Figure 5.2-*Absorbance profiles for LSBS-33 free-films*

Figure 5.3 shows the comparison between HHPA and CHDA based coatings. At 20% melamine, HH*8020 and CHDA*8020 exhibit extremely similar absorbance pathways, this is replicated with HH*8515 and CHDA*8515. However, CHDA*9010 shows a significantly smaller UV absorbance compared to HH*9010.

Terephthalic acid is an aromatic compound used in the generation of coil coatings (Figure 5.4) and has a significantly larger absorbance profile than its cycloaliphatic counterpart CHDA (Figure 5.2). This higher level of UV absorbance highlights the poorer UV resistance that aromatic monomers generally have compared to cycloaliphatic monomers and can also be seen when comparing HHPA to its aromatic counterpart.

Table 5.3 gives another demonstration of the UV absorbance profiles of the free films across the entire UV area, which has also been sectioned into absorbances for the UV-A, B, and C regions by comparing the area under curve (AUC). It is possible to see that across the entire UV region that CHDA*9010 showed the smallest absorbance, whiles CHDA*8020 and HH*8020 were shown to have the largest absorbance levels. All the coatings demonstrated similar levels of absorbance within the UV-A region, with a total range of 0.84.

Analysis of the AUC of the coating systems shows that the crosslinker concentration exerts an impact on the degree of UV absorbance across the entire spectrum. Table 5.3 also demonstrates that crosslinker concentration has a greater influence over UV absorbance for CHDA coatings than those based on HHPA, which is demonstrated by CHDA*9010 having a smaller UV absorbance than the other CHDA coatings in each UV region. HH*9010 also has a smaller overall UV absorbance as well as lower absorbances in the UV-A and C regions but demonstrates a larger absorbance than HH*8515 within the UV-B region.

The area of greatest absorbance for all coatings was within the UV-C region, which is known to be exceptionally harmful to the majority of coating systems. However, as UV-C is strongly attenuated by atmospheric gases and the bulbs used in accelerated weathering tests are specified to 340nm, it would not have an influence on accelerated or natural weathering tests, and as such would not contribute towards coating degradation on Earth. (3)

Table 5.3-*Breakdown of Area under UV absorbance curves*

Coating code	Full UV area	UV-A (400-320)	UV-B (315-280)	UV-C (280-100)
HH*8020	179.27	7.06	14.43	157.77
HH*8515	172.45	6.24	11.65	154.56
HH*9010	169.09	6.56	10.09	152.43
CHDA*8020	179.24	7.06	15.68	156.49
CHDA*8515	173.34	6.58	11.96	154.80
CHDA*9010	160.85	6.02	7.50	147.33

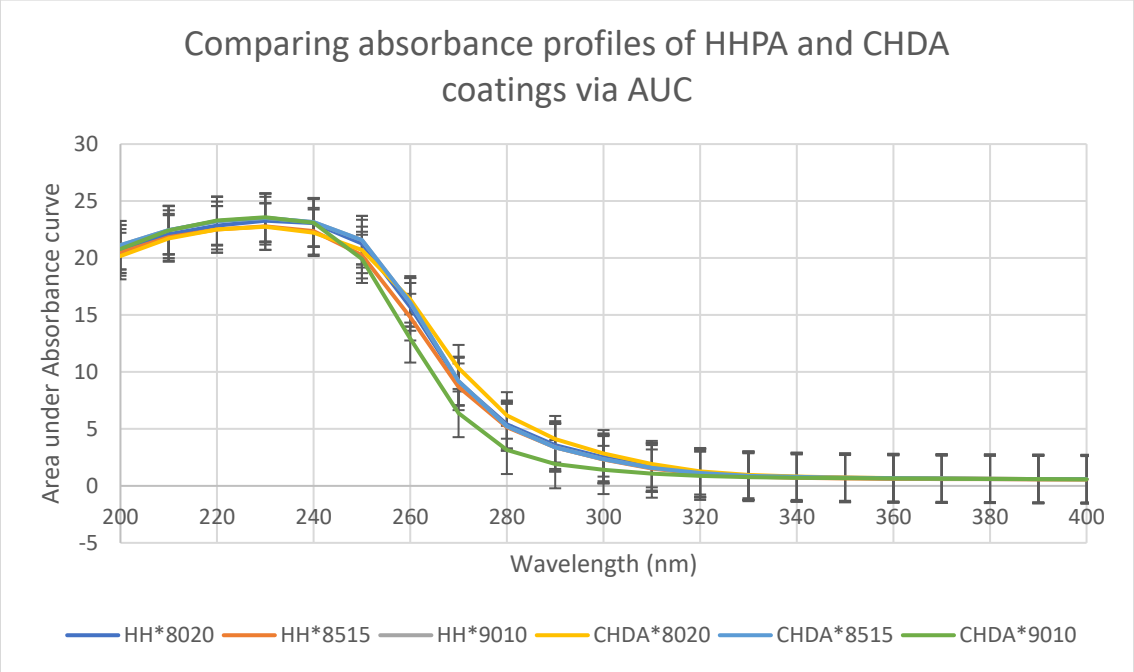

Figure 5.3-*Comparing absorbance profiles of all LSBS-STD and LSBS-33 clearcoat free films*

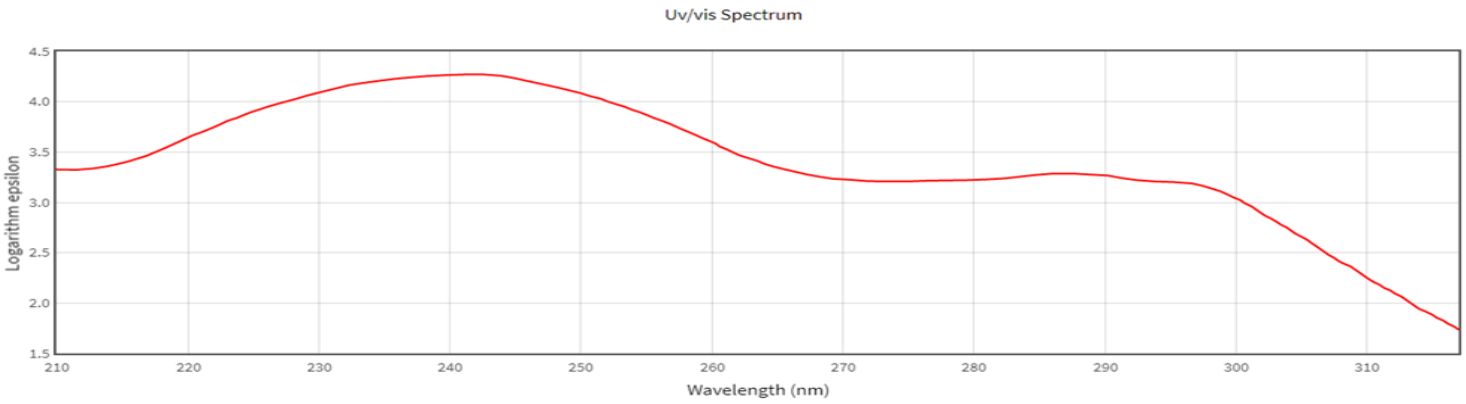

Figure 5.4-*Terephthalic acid Spectra* (10)

If a coatings ability to absorb UV radiation gives an indication of the resistance to photodegradation then it could be assumed that a coating based on CHDA would exhibit UV resistance equivalent to that demonstrated by HHPA coatings, with diminishing UV absorbance recorded alongside lowered crosslinker ratio in CHDA coatings.

However, as the experimental work laid out in Chapter 4 shows, this is not the case as CHDA constantly suffer greater levels of weathering degradation than that of a comparable HHPA coating.

It is known that 290nm is a particularly harmful wavelength that is also the minimum wavelength of UV light on Earth, as such this absorbance point was isolated and investigated for all coatings within this section, the results for which can be seen in Figure 5.5. It can be observed that both the HHPA and HCDA based coatings exhibit a decrease in absorbance at this wavelength as the ratio of crosslinker within the system is lowered. The most significant change in absorbance comes from the CHDA coatings, which demonstrate the greatest absorbance with CHDA*8020, as well as the smallest with CHDA*9010. This further indicates that the absorbance profile of CHDA based coatings are more strongly influenced by the ratio of crosslinker than HHPA coatings, as has been previously suggested above. While the 290nm wavelength is known to be damaging to coatings, combining the evidence within previous chapters and Figure 5.4 highlights that it is not the deciding factor in weathering performance, as it would be anticipated for CHDA*9010 to be one of the better performing coatings, but data in Chapter 4 shows that lower HMMM ratio coatings fail more rapidly compared to those coatings with a larger amount of crosslinker.

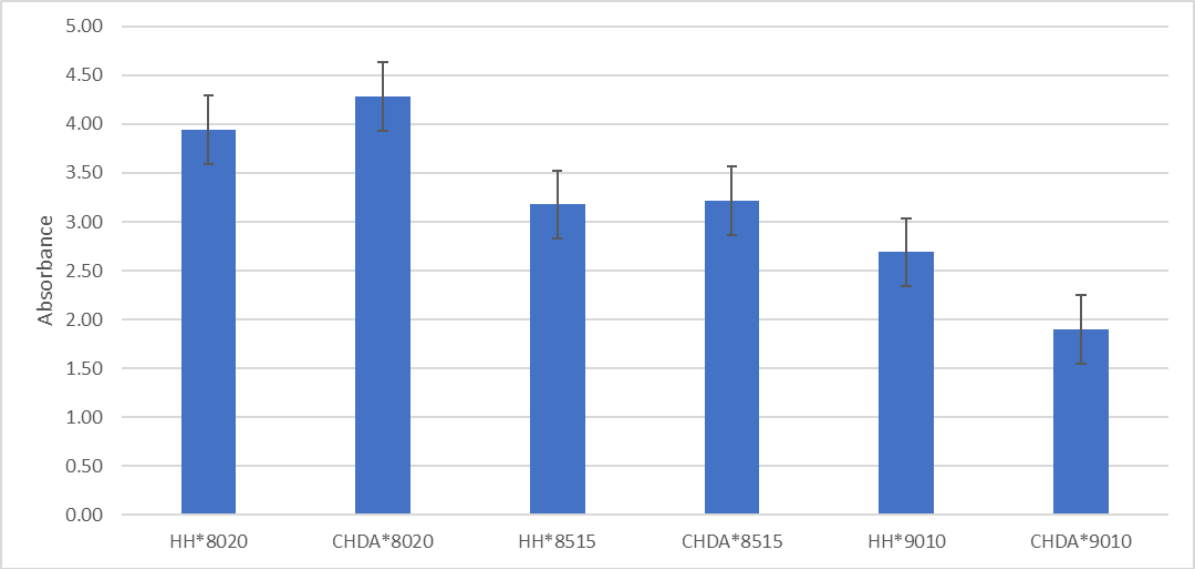

Figure 5.5-*Demonstrating differences in absorbance at 290nm for HHPA and CHDA coating systems*

A typical HOMO/LUMO gap is commonly accepted within the coatings industry to be approximately 333nm which falls within the UV region and is observed in 3,3-di-N-Methylpropylamines (11). Figure 5.6 shows that the CHDA coatings again demonstrate the highest and lowest absorbance levels, with CHDA*8020 giving the greatest and CHDA*9010 the least. As with Figure 5.5, it is shown that the Absorbance profile of CHDA coatings decrease alongside decreasing crosslinker ratio. However, the same is not observed in the HHPA coatings, while HH*8020 again provides the greatest absorbance, the smallest absorbance is demonstrated by HH*8515. This result could be anomalous and brought about by the differences in coating thicknesses, as HH*8020 has the greatest thickness (27µm), followed by HH*9010 (25µm), then HH*8515 (24µm), which could give the appearance of HH*8515 absorbing less within this region than it actually does. It is worth noting that the CHDA containing coatings do not appear to exhibit the same potential error, if they did then it would be anticipated that CHDA*8515 (27µm) would show the greatest levels of absorption, followed by CHDA*8020 (26µm), and CHDA*9010 (25µm).

Combining the results of Figures 5.5 & 5.6 shows that while the wavelengths 290nm and 333nm might be a cause of degradation, HHPA coatings do not exhibit a smaller absorbance within these regions to explain the superior weathering durability that they offer in natural and accelerated weathering tests.

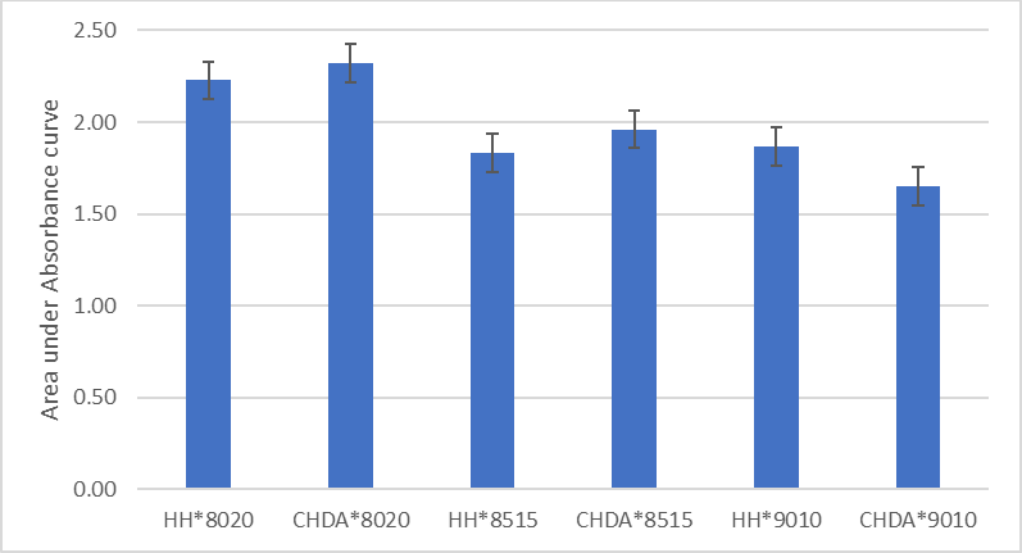

Figure 5.6-*Demonstrating differences in absorbance between 330-340nm for HHPA and CHDA coating systems*

Table 5.4 gives a breakdown of the area under the UV absorbance curves for all coatings and has been utilized to compare the coating systems. Comparing HH*9010 and CHDA*9010 shows that the CHDA coating has a smaller absorbance profile across the entire UV spectrum. CHDA*8515 shows a greater absorbance across the UV-A and UV-B regions, as well as half of UV-C compared to HH*8515, while

HH*8020 shows greater absorbance across the UV-A and UV-C regions, while CHDA*8020 absorbs more strongly within the UV-B region. CHDA*8515 was the only CHDA based coating that exhibited a larger overall UV absorption than its HHPA counterpart.

In order to correct for the small differences in film thickness which may, as previously discussed account for the differences in the observed absorbance profiles, the absorption coefficient was calculated for each free-film using the equation laid out in Equation 5.2 with the results shown in Table 5.4.

$$\alpha = 2.303\ A/t$$

α = Absorption coefficient A=Absorbance t=Film thickness

Equation 5.2-*Calculating Absorption coefficient from Absorbance values*

Table 5.4-*Breakdown of calculated Absorption coefficients*

Coating Code	Absorption coefficient for UV region	Ranking (Highest to lowest)	Absorption coefficient for UV-A region	Ranking (Highest to lowest)	Absorption coefficient for 330nm-340nm	Ranking (Highest to lowest)
HH*8020	152908.27	4	7609.50	2	1517.22	2
HH*8515	165479.65	1	7400.28	3	1463.88	4
HH*9010	155764.38	3	7298.82	4	1486.09	3
CHDA*8020	158763.13	2	8015.86	1	1611.11	1
CHDA*8515	147849.51	6	6911.16	5	1399.38	5
CHDA*9010	148174.53	5	6538.77	6	1360.34	6

Analysis of the results in Table 5.4 show that once the thickness of the coating is taken into account there is a decrease in Absorbance that accompanies the decrease in crosslinker concentration. By comparing the results with Figure 5.6 it shows that even when coating thickness is taken into consideration that HH*8515 demonstrates the lowest absorbance of all HHPA containing coating systems.

5.3-Impact of Hydrolysis

Novel resins were developed using proprietary formulations, utilising either HHPA or CHDA as the sole monomer resin base. Table 5.5 gives a breakdown of the resins.

Table 5.5-*Breakdown of the resins used in this section*

Resin code	Main Component	Ratio of contents	Coatings developed
LSBS-STD	HHPA	N/A	HH*7030Br HH*8020Br HH*8515Br HH*9010Br
LSBS-33	CHDA	N/A	CHDA*7030Br CHDA*8020Br CHDA*8515Br CHDA*9010Br

All resins were developed with two key guidelines in place, a Hydroxyl value (OHV) of 50, and a molecular weight of approximately 2200. All resins were developed using standardised methodologies that are well documented within the literature of resin synthesis. (12)

The resins were then used as the bases for pigmented coating formulations, with each resin being used in the development of 70:30, 80:20, 85:15 and 90:10 ratios with HMMM (HexaMethoxyMethyl Melamine) to develop full Polyester:Melamine coating systems. A detailed description of the development process can be found in Chapter 2.

Table 5.6 shows the coating codes and differences in chemistry relevant to this body of work. Whilst the melamine ratios of 70:30 and 90:10 ratio coatings are less commonly seen within external coating systems than 80:20 and 85:15 ratio coatings, they were included in the investigation in order to gain greater understanding on a wider range of melamine ratios impact the ability of a coating to resist the influence of hydrolysis. All experiments within this section were carried out as dark hydrolysis, which means that they took place while shielded from UV radiation to prevent it from influencing the investigation.

Table 5.6-*Overview of coatings used in Hydrolysis investigation*

Coating code	Monomer Base	Polyester: Melamine Ratio	Glass Transition temperature (T_g)
HH*7030Br	HHPA	70:30	31
HH*8020Br	HHPA	80:20	32
HH*8515Br	HHPA	85:15	29
HH*9010Br	HHPA	90:10	30
CHDA*8020Br	CHDA	80:20	29
CHDA*8515Br	CHDA	85:15	29
CHDA*7030Br	CHDA	70:30	28
CHDA*9010Br	CHDA	90:10	27

A total of 2 environments were chosen for analysis. Immersion in room temperature water and immersion in water at 40°C. Room temperature water was chosen to provide a source of water below the T_g of all the coatings. A 40°C water bath was utilised to provide an environment which subjected the samples to water above their T_g levels, 40°C was chosen as that is the temperature at which condensation cycles are performed under STD UV-A weathering (as explained by BS EN ISO 11507:2007).

Two samples of each coating were placed into each environment and were removed following each of 1, 3, and 7 days of immersion, after which they were allowed to air dry and were analysed before being returned to the respective water baths.

Samples were air dried in a fume hood before being analysed. Air drying was performed as wiping the samples dry would have potentially caused damage to the coatings through removal of coating layers. Once dry, the coatings were analysed via IR spectroscopy, colour and gloss tests.

IR spectroscopy was performed using a Spectrum 100 FT-IR using UATR (Universal Attenuated Total Reflectance Crystal) giving 8 scans over a wavelength range of 4000nm-400nm. There were three wavelength ranges of interest, as shown in Table 5.7.

Table 5.7-S*howing initial areas of interest in band areas from IR analysis*

Band wavenumber (nm):	**Corresponds to:**
3600-3100	OH stretch
3000-2800	CH_2 and CH_3 Stretch
3600-2400	Combination of above

Gloss measurements were obtained using a hand-held glossmeter that utilised a 60° contact angle. 3 gloss measurements, a more in-depth description of the gloss measurement process and calculations can be found in Chapter 2.

Figure 5.9 illustrates the changes in average percentage hydroxyl activity over time during immersion in a room temperature water bath. Figure 5.9 shows that the poorest performing coating overall was CHDA*8020Br and the poorest performing HHPA containing coating was HH*8020Br, while the best performing coatings following 7 days of immersion were CHDA*9010Br and HH*8515Br. The general pattern that can be observed in Figure 5.7 is that the coatings with lower crosslinker concentration tend to have a lower change in hydroxyl activity than the higher ratio counterparts. The spectra for CHDA*8020Br before and after dark hydrolysis is shown in Figure 5.7, while Figure 5.8 demonstrates the changes in HH*8515Br spectra over the same time.

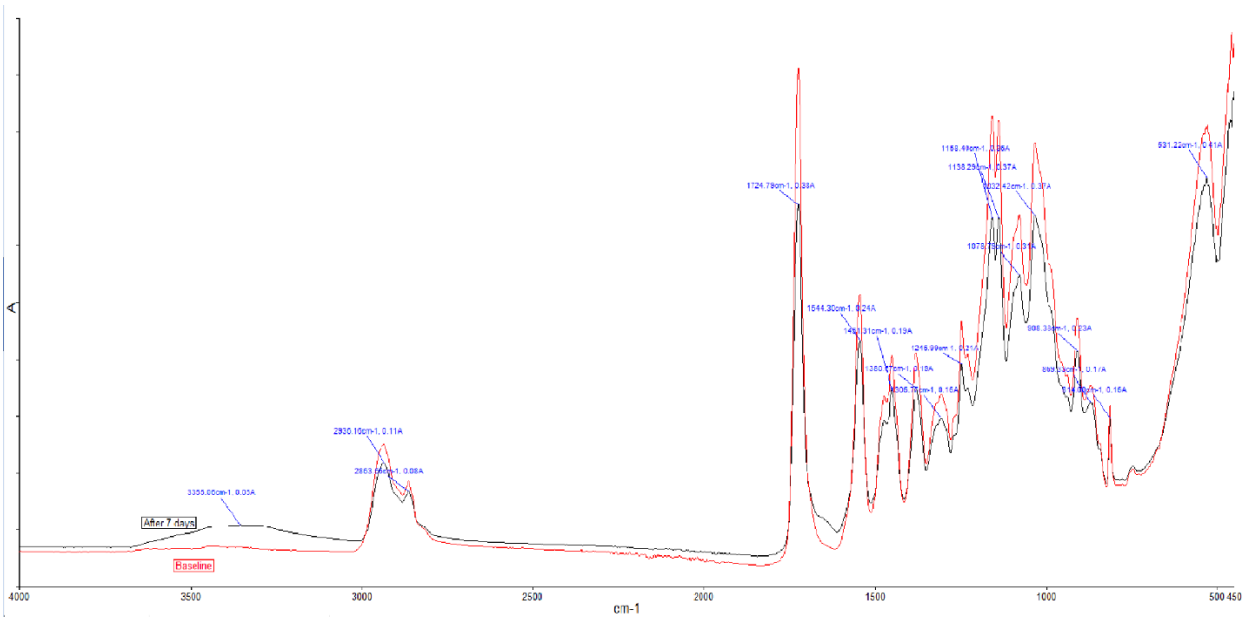

Figure 5.7-*Change in IR spectra of CHDA*8020Br, poorest performing coating during dark hydrolysis*

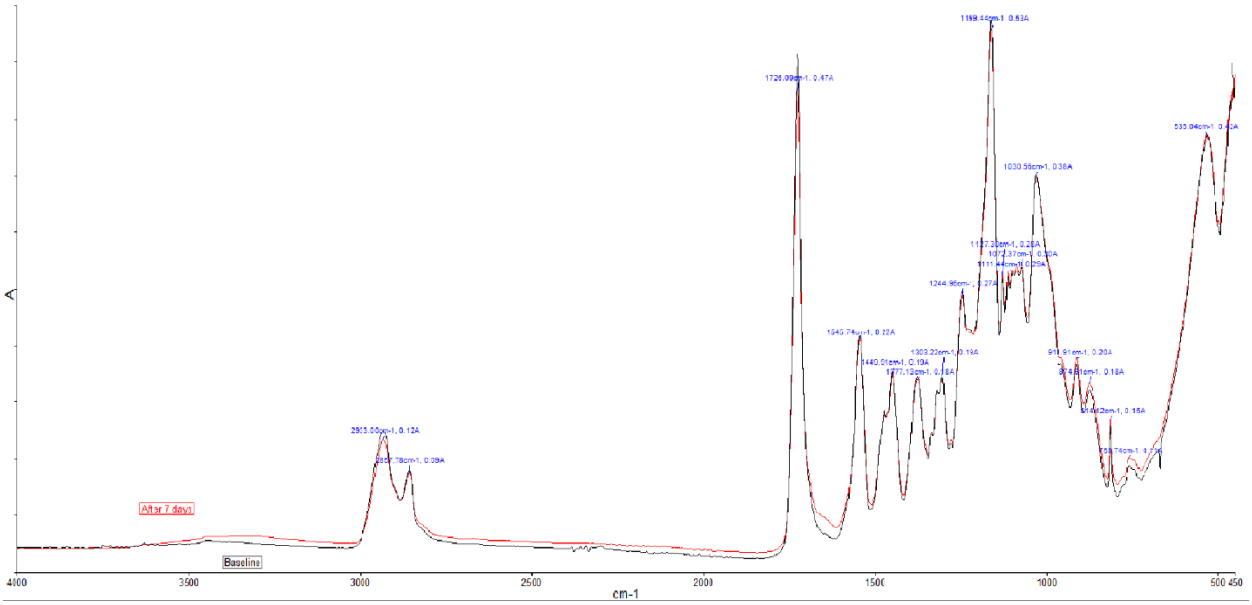

Figure 5.8-*Change in IR spectra of HH*8515Br, best performing coating during dark hydrolysis*

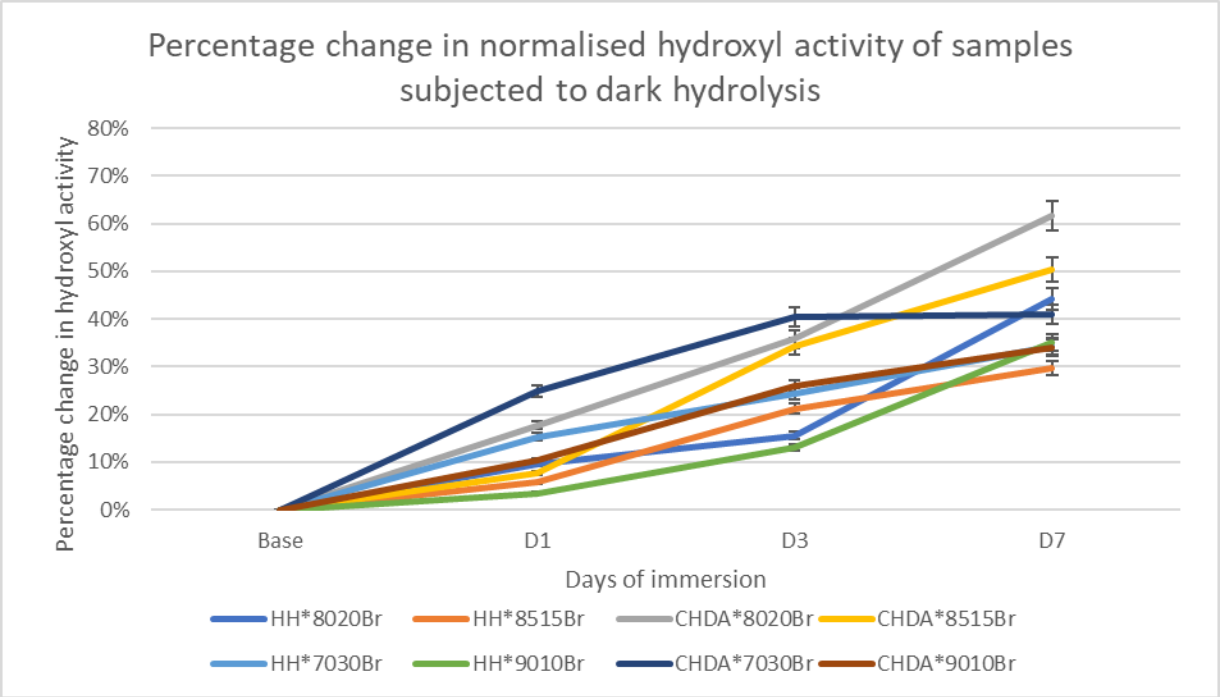

Figure 5.9-*Change in percentage hydroxyl activity of samples subjected to room temperature dark hydrolysis*

Figure 5.10 shows the change in average hydroxyl activity of coating samples that were immersed in a water bath at 40°C. The poorest performing coating was again CHDA*8020Br, followed by HH*8020Br, while CHDA*9010Br was the best performing CHDA containing coating and HH*8515Br was the best performing coating overall in terms of increases in hydroxyl activity.

Comparing Figures 5.9 and 5.10 shows some similarities in the form of the best and worst performing coatings, with CHDA*8020Br showing the greatest increase in percentage hydroxyl activity and HH*8515Br demonstrating the smallest increase during immersion.

While in all instances the coatings immersed in 40°C dark hydrolysis show a greater increase in hydroxyl activity than the room temperature counterparts, some coatings demonstrated greater increases than others. The largest difference in percentage hydroxyl activity was 19% from HH*8020Br, which was a 10% greater increase than the next largest difference.

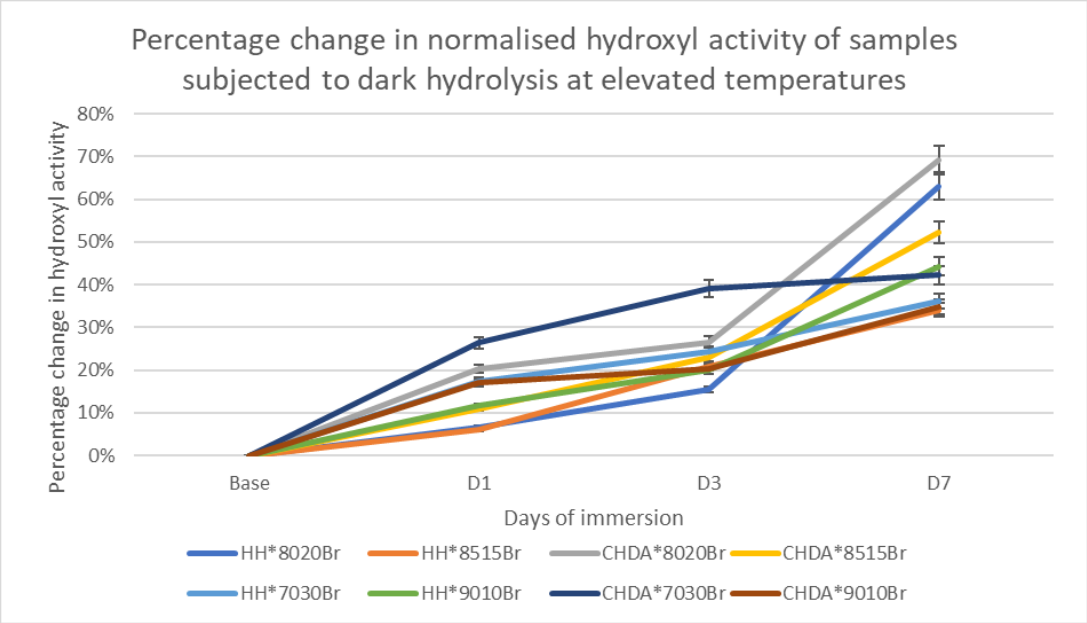

Figure 5.10-*Change in percentage hydroxyl activity of samples subjected to dark hydrolysis at 40°C*

Figures 5.11 and 5.12 show the colour change of samples immersed in room temperature dark hydrolysis and 40°C dark hydrolysis respectively, with the colour change represented through calculation of ΔE periodically during the investigation. The poorest colour retention in Figure 5.11 was demonstrated by CHDA*7030Br, followed closely by HH*8020Br, with the greatest colour retention shown by HH*8515Br followed by HH*9010Br.

The greatest colour change for samples subjected to dark hydrolysis in a warm water bath was exhibited by CHDA*9010Br, with the smallest colour change demonstrated by CHDA*8515Br. Comparing Figures 5.11 and 5.12 show that all of the coatings suffered a greater measured colour change from immersion in a warm water bath, indicating that the combination of raising the coatings above their glass transition temperatures and long term immersion in water exerts a greater influence over colour retention than dark hydrolysis by itself.

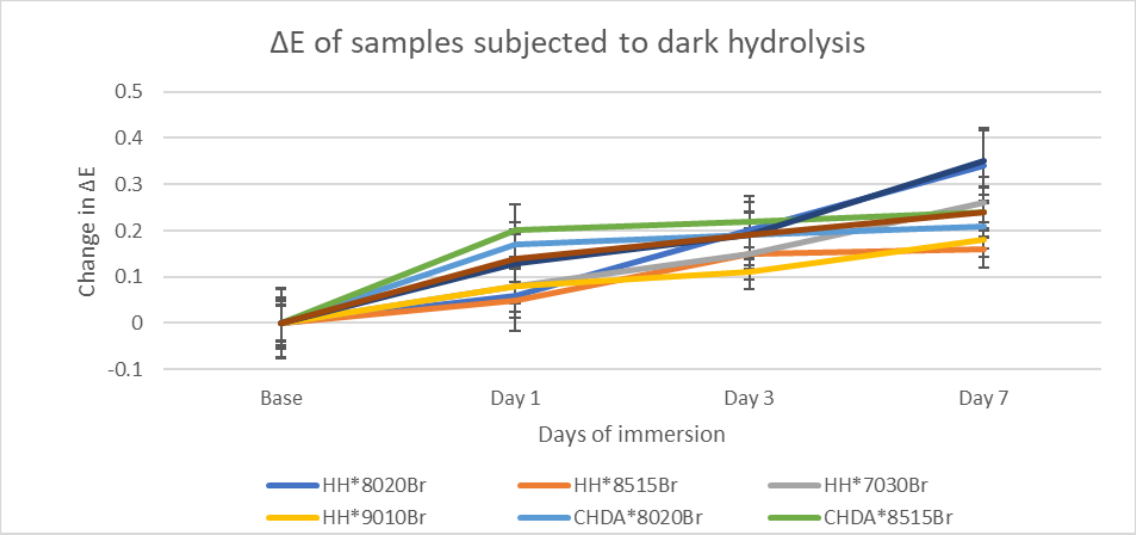

Figure 5.11-*Change in ΔE of samples subjected to room temperature dark hydrolysis*

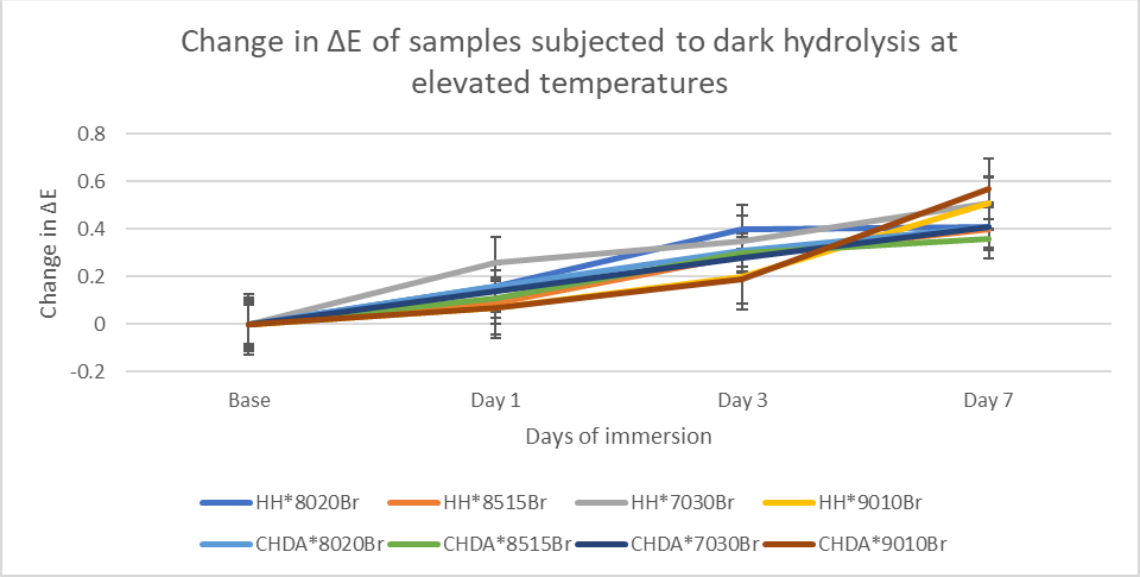

Figure 5.12-*Change in ΔE of samples subjected to dark hydrolysis at 40°C*

As mentioned previously, gloss measurements were obtained following 1,3, and 7 days of dark hydrolysis, with 3 measurements taken and an average value calculated. Figure 5.13 shows the impact that dark hydrolysis at room temperature had on the percentage retained gloss values. It can be seen that HH*8515Br exhibits the greatest retained gloss after 7 days immersion in a water bath, with HH*7030Br and HH*9010Br were the second and third best gloss retaining coatings, indicating that in general HHPA coatings exert a greater ability to retain gloss during dark hydrolysis than the CHDA containing counterparts.

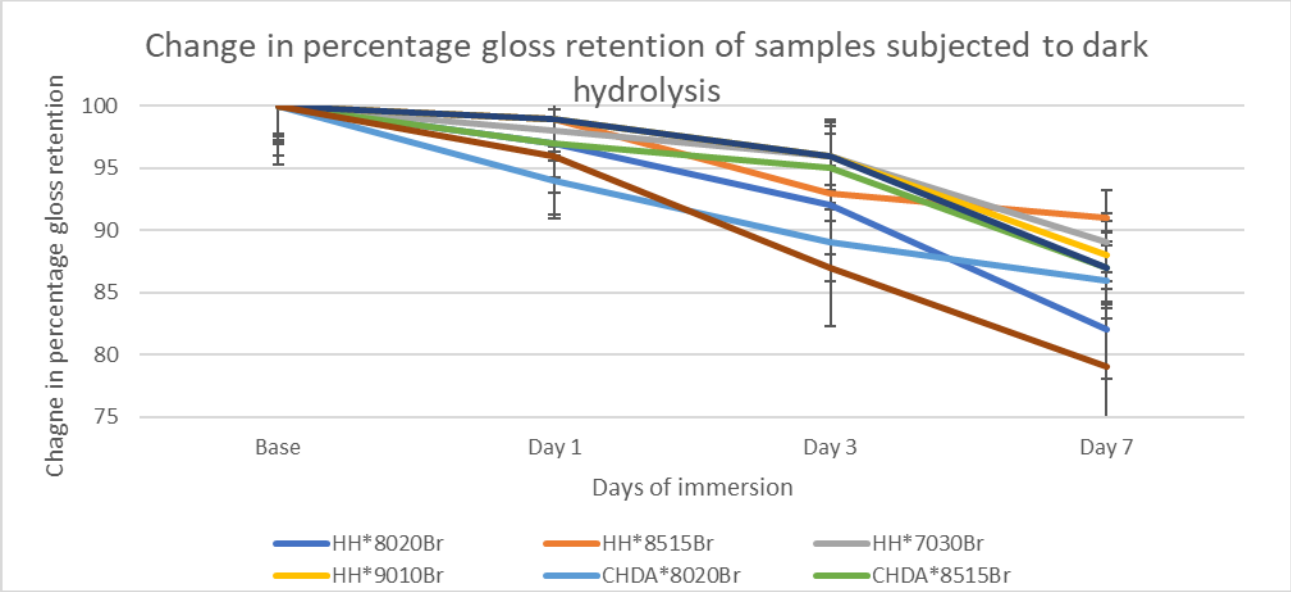

Figure 5.13-*Change in percentage retained gloss values of samples subjected to room temperature dark hydrolysis*

Figure 5.14 shows the average percentage gloss retention of coating samples that were subjected to dark hydrolysis in a 40°C water bath. The three coatings that demonstrate the highest levels of gloss retention are CHDA*7030Br, CHDA*9010Br, and CHDA*8020Br respectively, while the three coatings with the poorest gloss retention were HH*8020Br, HH*7030Br, and CHDA*8515Br. This indicates that CHDA containing coatings are generally better able to resist gloss loss through hydrolytic interactions than HHPA containing coatings.

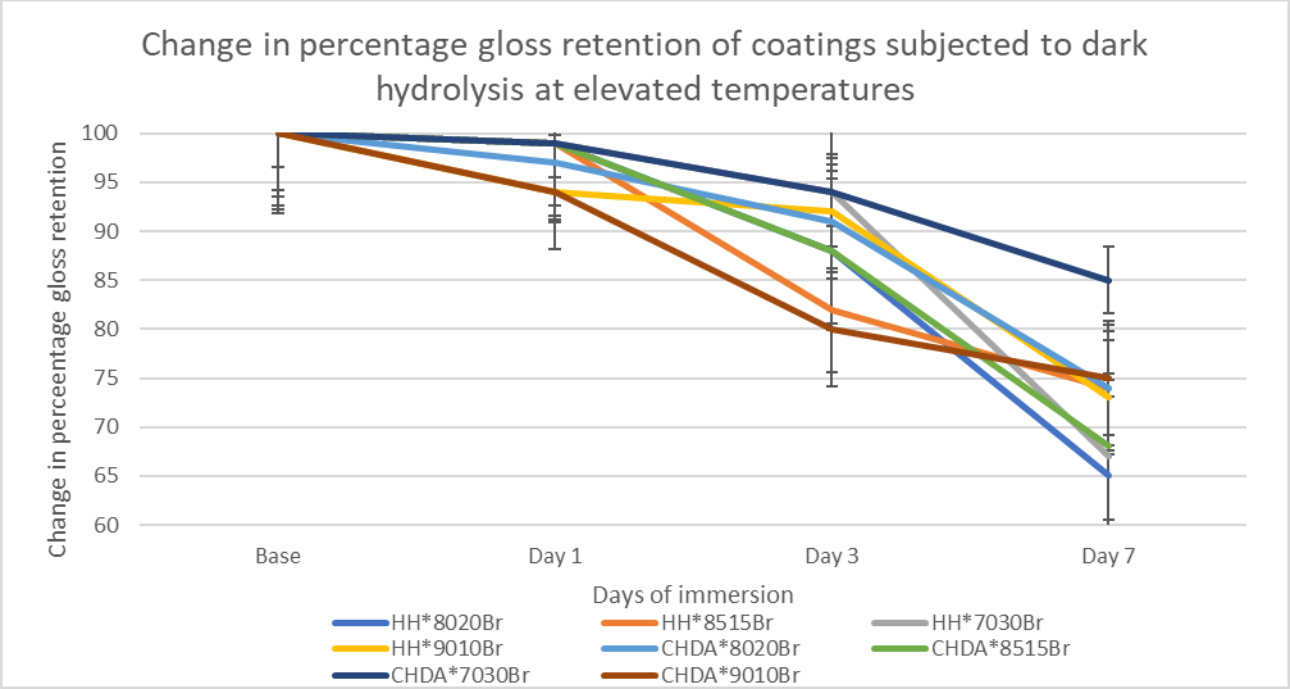

Figure 5.14-*Change in percentage retained gloss values of samples subjected to 40°C dark hydrolysis*

Table 5.8-*Ranking of coating systems from best to worst performing (1-8) in terms of % change hydroxyl activity, % gloss retention, and ΔE for dak hydrolysis and 40°C dark hydrolysis*

Coating code	% Hydroxyl change		Gloss retention		ΔE		Overall rank	HHPA/CHDA Specific Group Rank
	Dark	Dark (40°C)	Dark	Dark (40°C)	Dark	Dark (40°C)		
HH*8020Br	5	7	6	7	6	3	7	4
HH*8515Br	1	1	1	3	1	2	1	1
HH*7030Br	2	3	2	6	5	4	3	3
HH*9010Br	3	5	3	4	2	4	2	2
CHDA*8020Br	7	8	5	3	3	3	6	4
CHDA*8515Br	6	6	4	5	4	1	5	3
CHDA*7030Br	4	4	4	1	7	3	4	1
CHDA*9010Br	2	2	7	2	4	5	3	2

Table 5.8 gives a breakdown of how well the coatings performed in each test area, with the best and worst ranking coloured green and red respectively. By assigning points to each coating based on performance in each area and totalling them, the overall performance rankings can be obtained, as shown within the tables. It makes it clear that HH*8515Br was the overall best performing coating, with the best performance in 4 areas and highly ranked in the other 2 areas, while HH*8020Br can be seen to be the

poorest overall performing coating, as while it was only the poorest performing coating in one area, it was consistently one of the poorest performing coatings in each area.

Table 5.8 also illustrates the influence that varying the crosslinker concentration has on the overall coating systems, HH*7030Br is shown to be one of the poorest performing coatings, demonstrating the greatest change in hydroxyl activity at room temperature and 40^{o}C and some of the poorest rankings in 3 of the other 4 areas. Table 5.8 also provides a demonstration of where the coatings rank when split into HHPA or CHDA containing groups. The relationship between coating performance and crosslinker concentration is not linear, however a pattern can be observed that differs depending on the main monomer of choice within the base resin system. When considering HHPA containing coatings it can be seen that the two coating systems with lower crosslinker concentration provide overall superior results, with HH*9010Br demonstrating the greatest performance. It is interesting to note that HH*8020Br is outperformed by HH*7030Br, potentially indicating that lower and higher crosslinker concentrations can exhibit beneficial properties in combating hydrolytic degradation. The behaviour of HH*7030Br can be explained by a greater dispersion of melamine rich areas across the coating surface as a product of a greater number of melamine agglomerations, which would result in a more uniform degradation across the coating surface compared to HH*8020Br.

CHDA containing coatings show a different pattern, with CHDA*7030Br exhibiting the best overall performance, followed by CHDA*9010Br, indicating that both high and low crosslinker concentrations can provide a benefit in resisting the impact of hydrolytic degradation compared to CHDA*8020Br.

It is known that the HMMM crosslinker has a tendency to self-condensate, resulting in the formation of melamine rich areas throughout the coating. Regarding HHPA containing coatings it can be seen that the lower crosslinker ratios are superior, potentially due to the decreased likelihood of melamine rich areas throughout the coating system. The poorer performance of HH*9010Br can be explained by a lower degree of crosslink occurring throughout the coating due to the lower concentration. The superior performance of HH*7030Br over HH*8020Br can be explained by the more uniform dispersion of melamine rich areas throughout the coating system, meaning that while there are more areas susceptible to hydrolytic interactions, their dispersal throughout the system means that the degradation is more evenly dispersed across the coating surface.

The CHDA containing coatings exhibit a different pattern, with CHDA*7030Br giving the best overall performance, indicating that the more uniform dispersion of melamine self-condensates throughout the

coating system provides a benefit through potentially providing a more uniform coating system that is actually better able to resist degradation than coatings with lower ratios. The second best performing CHDA coating was CHDA*9010Br, by limiting the crosslinker ratio to a low level it lowers the crosslinker excess meaning that the majority of the crosslinker reacted in its desired role rather than in self-condensation reactions, which in turn limited the production of hydrophilic areas at the coating surface.

In both HHPA and CHDA containing coating systems, the poorest performing was the *8020Br variant, this is potentially due to the crosslinker ratio, which being at excess allows for the development of the hydrophilic melamine rich areas, which are then particularly susceptible to removal via hydrolytic interactions during long term dark hydrolysis.

5.4-How do the results compare to accelerated weathering and real-world exposure tests

The data obtained from the UV absorbance and hydrolysis investigations was compared against the accelerated and natural weathering data that were previously presented in Chapter 4. Figures 5.15 and 5.16 illustrate the percentage change in hydroxyl activity of coatings subjected to STD accelerated QUV weathering and natural weathering.

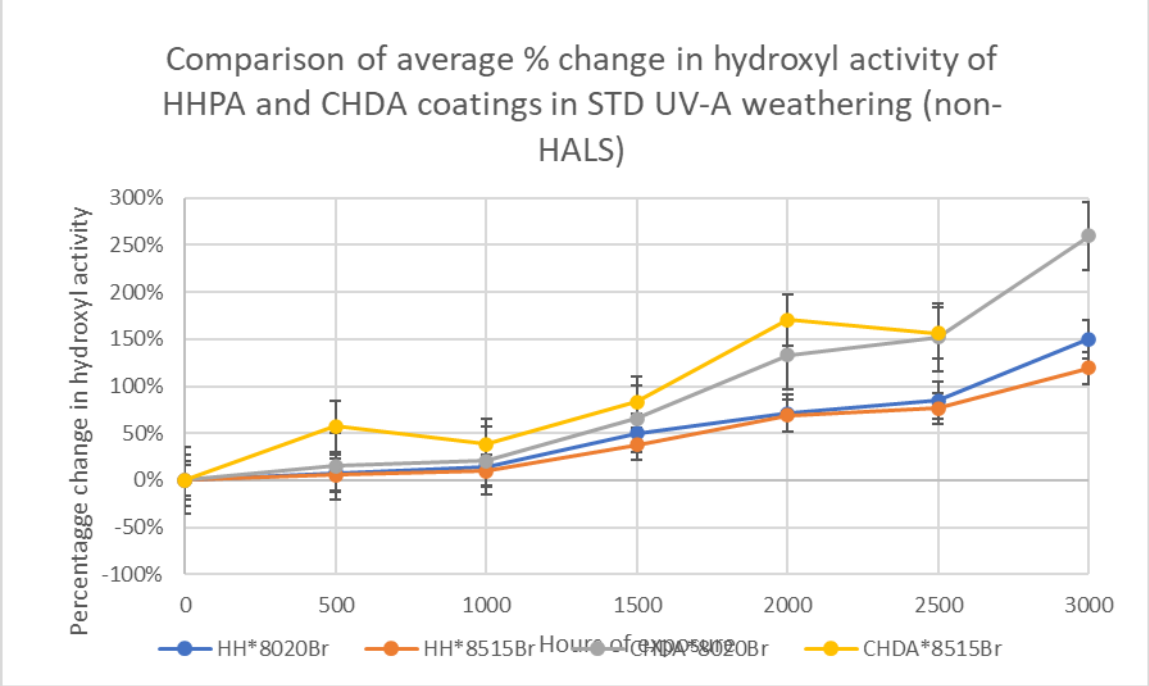

Figure 5.15-*Percentage change of hydroxyl activity of coatings subjected to STD UV-A weathering*

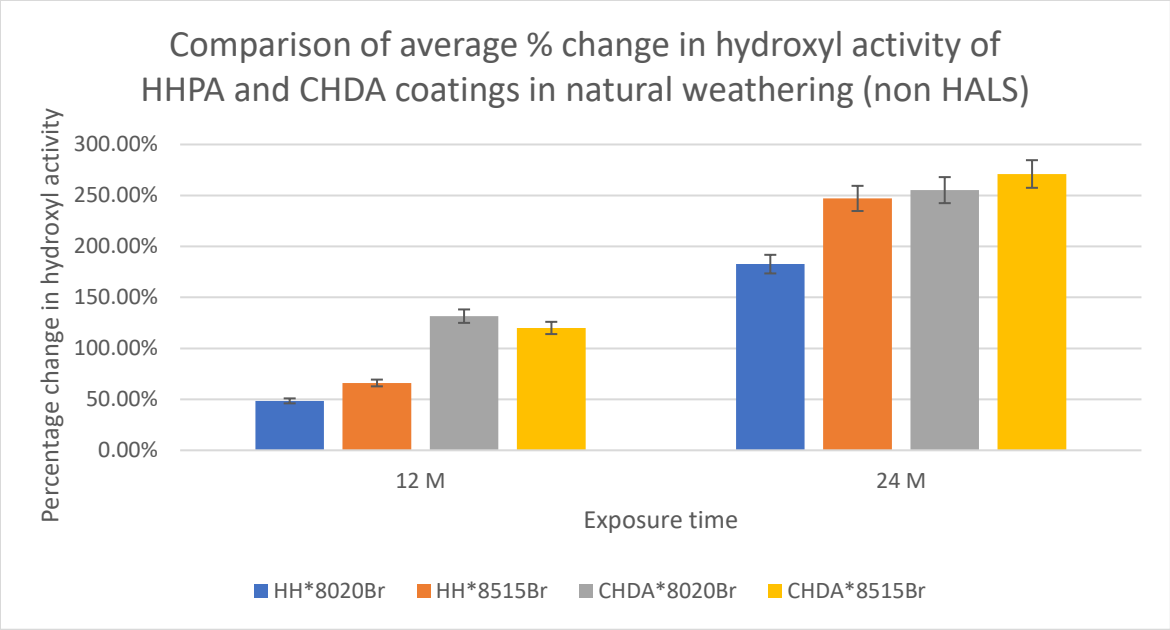

Figure 5.16-*Percentage change of hydroxyl activity of coatings subjected to natural weathering over 12 and 24 months*

As mentioned previously within the chapter, the UV absorbance profiles of CHDA and HHPA based coatings were extremely similar, so if the UV absorbance of the coatings was of critical importance it would be anticipated that CHDA and HHPA coatings would exhibit similar rates of degradation. However, as shown in Figures 5.15 and 5.16, CHDA*8020Br and CHDA*8515Br exhibit greater increases in hydroxyl activity compared to the HHPA alternatives. Figures 5.17-5.20 show the gloss and colour retention of accelerated and naturally weathered coatings. The CHDA coatings show significantly poorer gloss retention and higher instances of colour change than the comparable HHPA coatings. This significant difference between the gloss and colour retention between CHDA and HHPA coatings could be due to a variety of reasons, such as the fluctuations in temperatures between UV and condensation cycles, but is most probably caused by the repeated switching between UV and condensation cycles every 4 hours, which allowed for regular instances of moisture enhanced photodegradation to occur, which is known to be the most harmful type of weathering. (6,13)

Table 5.9-*Summary of changes of coatings during dark hydrolysis and dark hydrolysis at elevated temperatures.*

Sample code	Final change in % hydroxyl activity		Final % gloss retention		Final ΔE		T_g (midpoint)
	Water	Warm water	Water	Warm water	Water	Warm water	
HH*8020Br	44	63	82	65	0.34	0.41	32
HH*8515Br	30	34	91	74	0.16	0.4	29
HH*7030Br	34	36	89	67	0.26	0.51	31
HH*9010Br	35	44	88	73	0.18	0.51	30
CHDA*8020Br	62	69	86	74	0.21	0.41	29
CHDA*8515Br	50	52	87	68	0.24	0.36	29
CHDA*7030Br	41	42	87	85	0.35	0.41	28
CHDA*9010Br	34	35	79	75	0.24	0.57	27

By comparing Figures 5.15-5.16 with the performance summary of the coatings subjected to dark Hydrolysis provided in Table 5.9 it is possible to see that in terms of hydrolytic activity, neither of the dark hydrolysis investigations match up with what has been observed during weathering tests. There are some observed similarities between the changes in hydroxyl value recorded in samples exposed to dark hydrolysis and those subjected to accelerated and natural weathering. It can be observed that CHDA*8020Br shows a final change of hydroxyl activity of 69% following dark hydrolysis at 40^{o}C, 66% following 1500 hours of STD accelerated weathering cycles, and 132% following 12 months of natural weathering. While there is no correlation between the results of natural weathering and dark hydrolysis experiments, similarities can be observed between accelerated weathering tests and dark hydrolysis. Another equivalence can be seen from the 1500 hours measurement for HH*8515Br of 38% and the 34% observed following 7 days immersion at 40^{o}C. These were the only similarities between the percentage change in hydroxyl activity observed between the different exposure methods.

Comparing the percentage retained gloss values from Table 5.9 with those from accelerated and natural weathering exposure illustrated in Figures 5.15-5.16 shows multiple instances where the values overlap. HH*8020Br had 5 instances of approximate overlap, where the final retained gloss value from dark hydrolysis matched within 5% for 3 measurements obtained from accelerated weathering (1500 Hrs, 1750Hrs, 2000Hrs) and 12 months of natural weathering, while the final measurement from 40^{o}C dark hydrolysis matched the retained gloss following 24 months of natural weathering. HH*8515Br matched dark hydrolysis after 1250 hours of accelerated testing and after 12 months of natural exposure. After 750

hours of accelerated weathering CHDA*8020Br matched the final retained gloss value of 40°C dark hydrolysis, while CHDA*8515Br matched the final retained gloss after 500 hours of accelerated testing. The wide range at which the values matched, as well as the matching occurring over multiple exposure methods in different places, indicate that it was coincidental in nature and that no pattern was discernible.

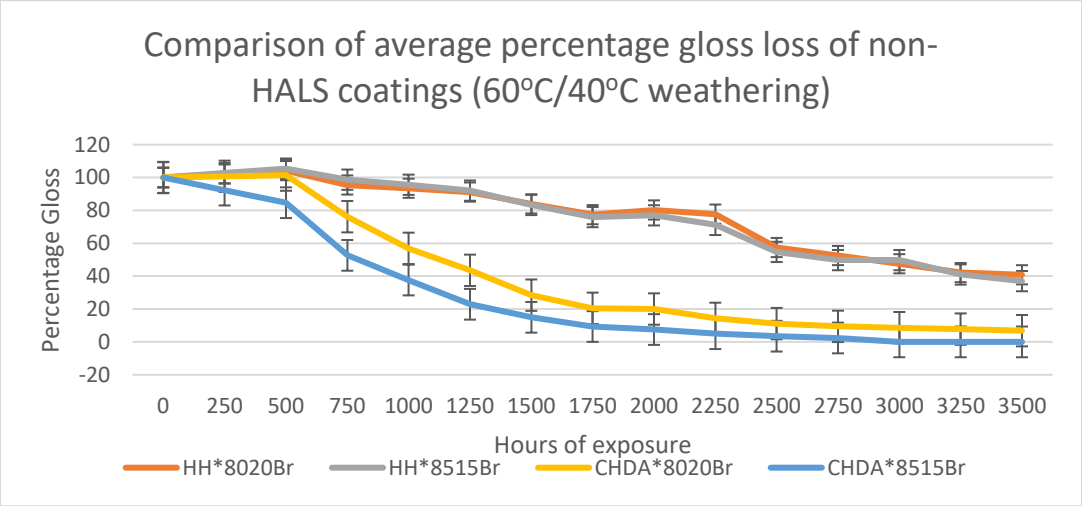

Figure 5.17-*Percentage change in gloss of coatings subjected to STD UV-A weathering*

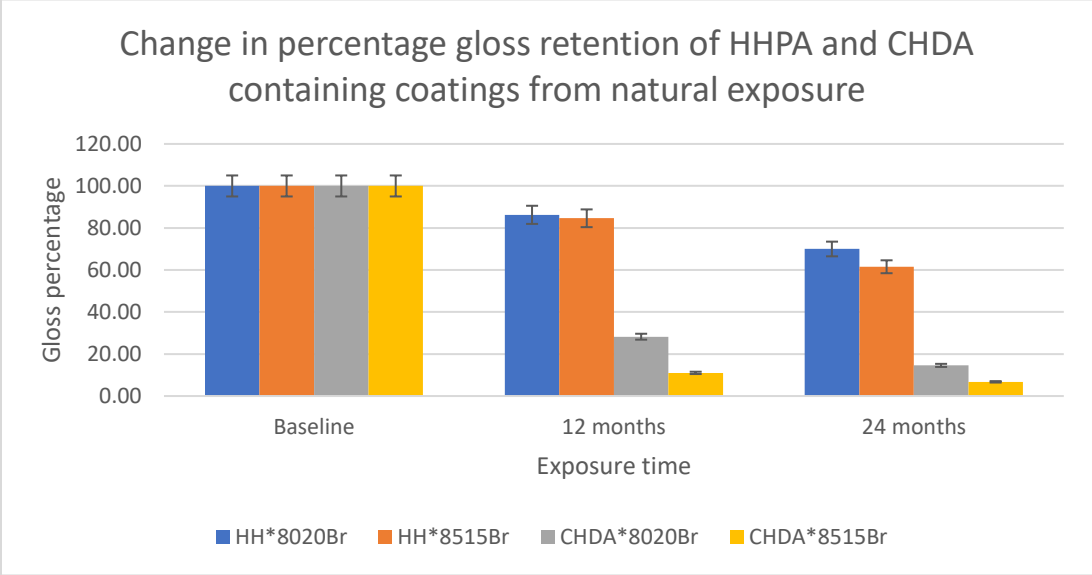

Figure 5.18-*Percentage change in gloss of coatings subjected to natural weathering*

Figures 5.19-5.20 were compared against Table 5.9 to determine if the final observed ΔE values from the dark hydrolysis investigation matched with the values obtained during accelerated and natural weathering. It was found that the final dark hydrolysis value for HH*8020Br matched that obtained via

1500Hrs of accelerated weathering, while the HH*8515Br ΔE from 40°C dark hydrolysis matched 1000 hours of accelerated weathering. Neither of the CHDA containing coatings had any matching measurements to those from accelerated weathering. No significant similarities were observed between the ΔE values obtained from the dark hydrolysis investigation and those from natural weathering for any of the samples in terms of raw values or trends. This highlights that dark hydrolysis investigations cannot be used to predict ΔE for accelerated and natural weathering tests, as it fails to take into account other factors such as UV exposure and pollution.

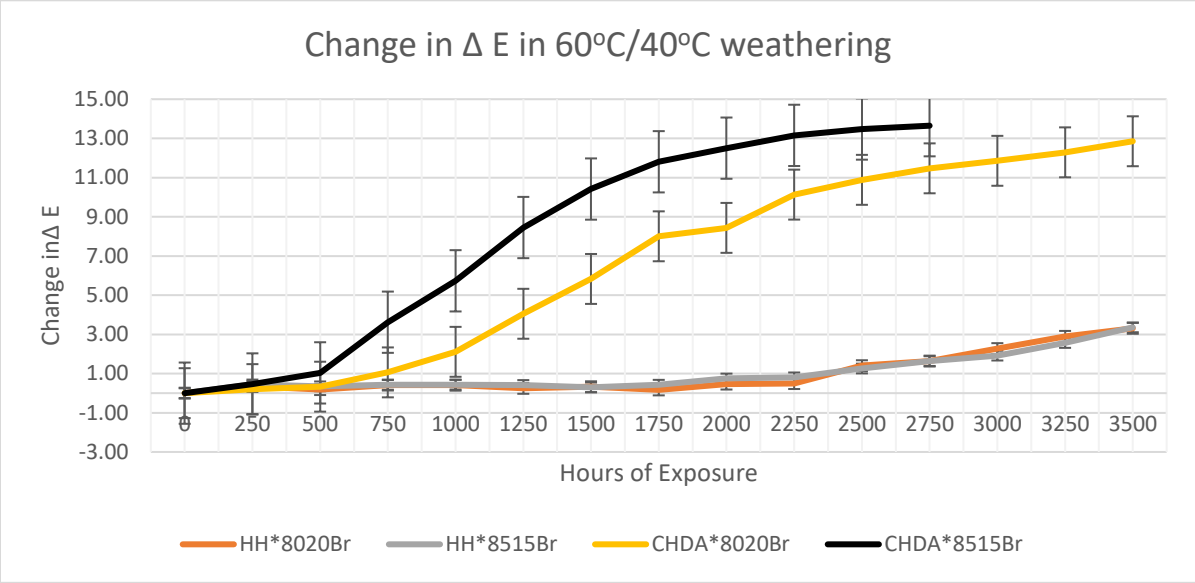

Figure 5.19-*Change in Δ E of coatings subjected to STD UV-A weathering*

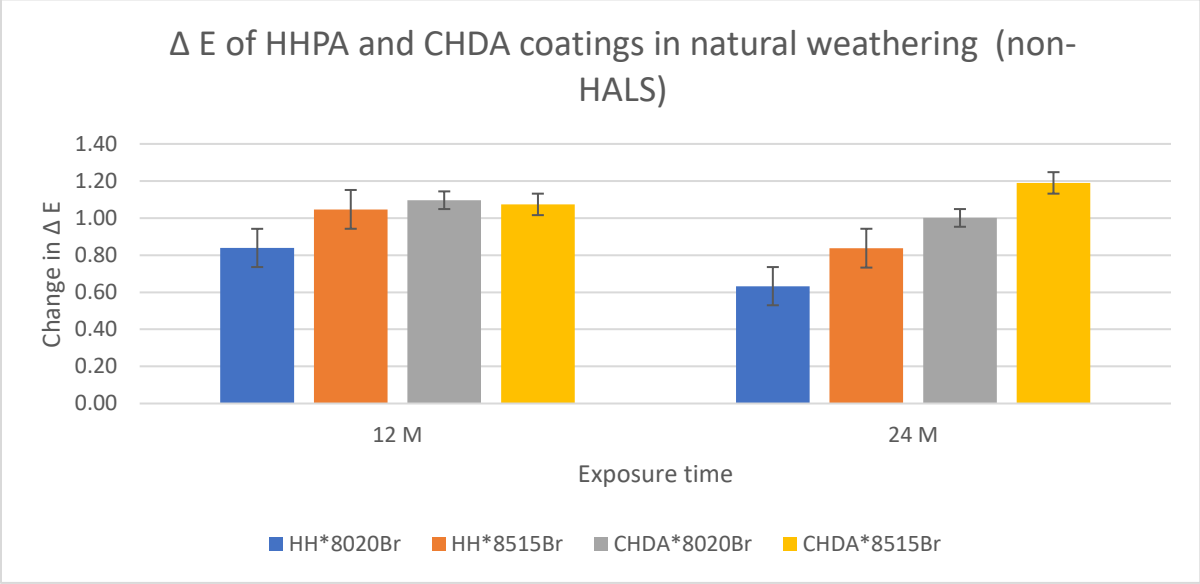

Figure 5.20-*Change in Δ E of coatings subjected to natural weathering*

Previous comparisons within this chapter made it clear that it would not be possible to draw a comparison from the individual results, but the purpose of Table 5.10 was to determine if the order of performance observed from the coatings subjected to dark hydrolysis and those subjected to weathering tests were similar, if so then it would allow short term hydrolysis investigations to act as predictors of future coating performance. Table 5.10 suggests that it may be possible to utilise dark hydrolysis investigations to predict the best performing coating in terms of increased hydroxyl activity, but that it would not be possible to use short term dark hydrolysis investigations to predict the order of performance for multiple coating systems for hydroxyl activity, gloss retention, or colour change.

Table 5.10-*Ranking of coatings from best to worst for changes in Hydroxyl, gloss and colour tests under all conditions*

Hydroxyl STD	HH*8515Br	HH*8020Br	CHDA*8020Br	CHDA*8515Br
Hydroxyl Nat	HH*8020Br	HH*8515Br	CHDA*8020Br	CHDA*8515Br
Hydroxyl dark	HH*8515Br	CHDA*8515Br	CHDA*8020Br	HH*8020Br
Hydroxyl dark 40°C	HH*8515Br	CHDA*8515Br	CHDA*8020Br	HH*8020Br
Gloss STD	HH*8020Br	HH*8515Br	CHDA*8020Br	CHDA*8515Br
Gloss Nat	HH*8020Br	HH*8515Br	CHDA*8020Br	CHDA*8515Br
Gloss dark	HH*8515Br	CHDA*8515Br	CHDA*8020Br	HH*8020Br
Gloss dark 40°C	HH*8515Br	CHDA*8020Br	CHDA*8515Br	HH*8020Br
Colour STD	HH*8515Br	HH*8020Br	CHDA*8020Br	CHDA*8515Br
Colour Nat	HH*8020Br	HH*8515Br	CHDA*8020Br	CHDA*8515Br
Colour dark	HH*8515Br	CHDA*8020Br	CHDA*8515Br	HH*8020Br
Colour dark 40°C	CHDA*8515Br	HH*8515Br	CHDA*8020Br	HH*8020Br

Figures 5.21-5.23 compare hydroxyl activity, percentage gloss retention, and colour change when normalised against the best performing coating for each area. It can be seen that HH*8515Br was the best performing coating in terms of hydroxyl activity during dark hydrolysis, with CHDA*8020Br the worst performing in both instances and offering in excess of 30% additional increase in hydroxyl activity compared to HH*8515Br.

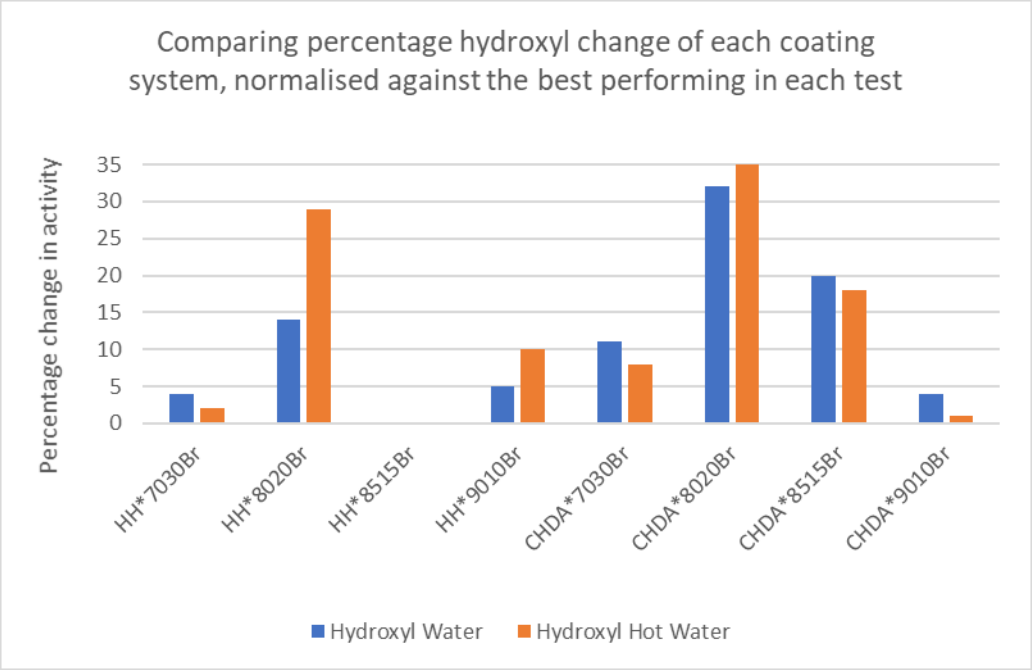

Figure 5.21-*Comparing final percentage change in hydroxyl activity (normalised against the best performing coating from each test) for coatings subjected to dark hydrolysis, dark hydrolysis at elevated temperatures, and dark acid catalysed hydrolysis*

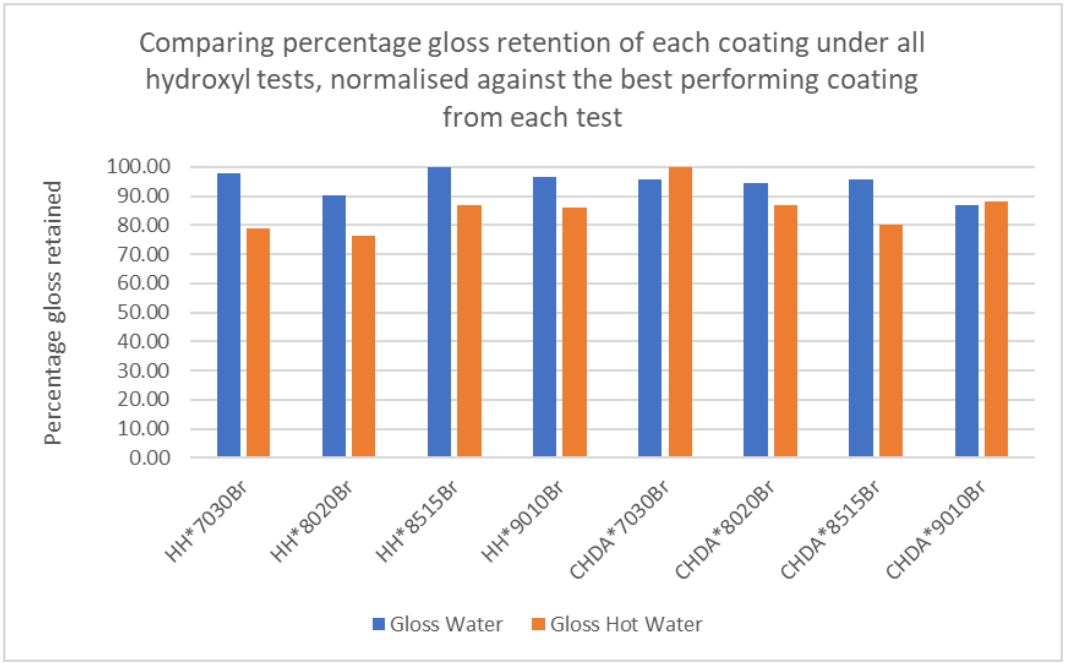

Figure 5.22-*Comparing final percentage gloss retention (normalised against the best performing coating from each test) for coatings subjected to dark hydrolysis, dark hydrolysis at elevated temperatures, and dark acid catalysed hydrolysis*

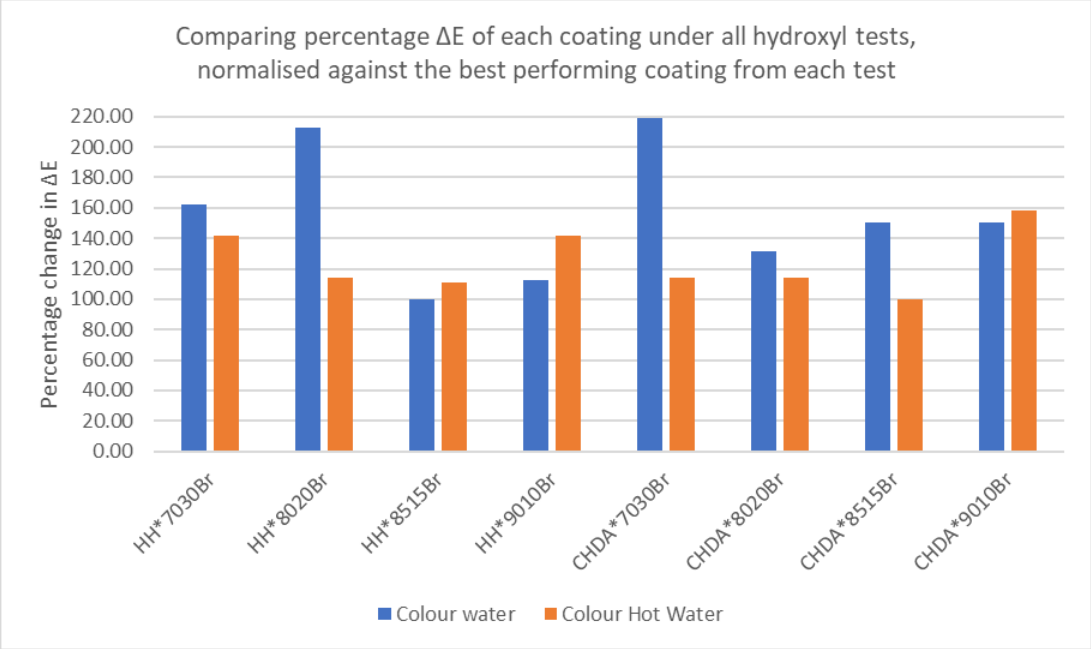

Figure 5.23-*Comparing final percentage increase in ΔE (normalised against the best performing coating from each test) for coatings subjected to dark hydrolysis, dark hydrolysis at elevated temperatures, and dark acid catalysed hydrolysis*

5.5-Conclusions

While the UV absorbance profile of a coating is important, it is not the most significant factor to be considered during the coating development process when choosing between different cycloaliphatic acids. This was confirmed through the natural and accelerated weathering of CHDA and HHPA based coatings, where the HHPA coatings significantly outperformed the CHDA variants in both colour and gloss retention, as well as through a lower average percentage increase in hydroxyl activity. If the UV absorbance profiles were the most significant factor, then it would have been anticipated that the coatings would fail at a similar rate. However, this was not the case as CHDA coatings failed significantly faster in both real world and accelerated weathering tests. This higher rate of failure is most probably due to a greater susceptibility to moisture enhanced photodegradation in addition to a greater susceptibility to pigment removal through coating interactions between lateral inhomogeneities across the coating surface and moisture.

The results of the dark hydrolysis investigation showed that the optimum coating in the majority of instances was HH*8515Br, while the poorest performing overall coating was HH*8020Br. The fact that HH*8020Br was the poorest performing coating during the hydrolysis investigation shows that short term dark hydrolysis experiments cannot be used as predictors of the performance of several different coating

systems exposed to accelerated or natural weathering degradation by the fact that accelerated and natural weathering tests show that HH*8020Br outperforms CHDA*8020Br and CHDA*8515Br during weathering tests and was the best overall coating during the weathering tests. This suggests that the HH*8020Br coating is more susceptible to hydrolytic degradation than the other coating formulations, the same can also be suggested of CHDA*8020Br as it was the second poorest overall performing coating investigated and the worst performing CHDA containing coating. It can be suggested that the poor resistance to hydrolytic degradation exhibited by HH*8020Br and CHDA*8020Br is a consequence of the Polyester to Crosslinker ratio. As mentioned previously it is known that melamine can undergo a self-condensation reaction which results in the formation of melamine rich areas within the coating, which are hydrophilic in nature. Lowering the ratio of the melamine crosslinker would reduce the excess within the formulation and therefore theoretically reduce the number of hydrophilic areas within the coating system. However, this can have other impacts on the coating, potentially reducing performance in other areas as shown in natural and accelerated weathering tests where the 85:15 ratio coatings suffer degradation at a higher rate compared to the 80:20 coatings.

Increasing the ratio of crosslinker can also provide beneficial effects as shown in Figure 5.21 where HH*7030Br showed the second smallest increase in hydroxyl activity after HH*8515Br for HHPA containing coatings. The same benefit can be observed in CHDA containing coatings, where CHDA*7030Br showed the second smallest increase in hydroxyl activity after CHDA*9010Br.

To conclude, this chapter has found that short term hydrolysis investigations cannot be used as indicators of how well different coating systems will perform relative to each other in accelerated and natural weathering tests. Also, it can be confirmed that while a lower crosslinker ratio can prove to be beneficial in the resistance of hydrolytic degradation this does not necessarily carry over to improved resistance to either accelerated or natural weathering degradation.

Finally, while UV absorbance is known to be an important characteristic for coatings, investigating HHPA and CHDA containing free-films has indicated that the UV absorbance is very similar, with CHDA coatings demonstrating equivalent UV absorbances, or ones slightly smaller than those of the HHPA containing coatings. The dark hydrolysis investigation has shown that for the most part the HHPA coatings are better able to minimise the impact of hydrolytic degradation, as evidenced by the higher ranks that the coatings obtained (with the exception of HH*8020Br) in Table 5.10.

If HHPA coatings are better able to resist hydrolytic interactions than CHDA coatings, then it could explain how they are able to provide greater levels of resistance to weathering degradation as they may be less susceptible to moisture enhanced photodegradation than CHDA containing coatings. The failure of the coatings may be influenced by the degree to which they are susceptible to electrophilic attack, as such an attack by H+ would lead to the generation of a cabocation which would then be vulnerable to interactions with water. (14)

Future research in this area should explore accelerated weathering tests on HH*7030Br, HH*9010Br, CHDA*7030Br, and CHDA*9010Br coating systems in order to gain a more well-rounded understanding into their weathering performance and compare against the information contained within this chapter. Unfortunately, due to time constraints and matters outside of our control, it has not yet been possible to perform this research.

5.6-References

1. Cakić SM, Bošković LB. Ftir analysis and the effects of alkyd/melamine resin ratio on the properties of the coatings. Hem Ind. 2009;63(6):637–43.

2. Yousif E, Haddad R. Photodegradation and photostabilization of polymers, especially polystyrene: review. Springerplus. 2013;2(1):398.

3. Wypych G. Uv Degradation & Stabilization of Industrial Products. In: Handbook of UV Degradation and Stabilization. 2015. p. 293–347.

4. Wypych G. Uv Degradation & Stabilization of Polymers & Rubbers. In: Handbook of UV Degradation and Stabilization. 2015. p. 177–292.

5. Talrose V, Yermakov A, Usov A, Goncharove A, Leskin A, Messineva N, et al. NIST Webbook Terephthalic acid. NIST. 2017.

6. Salih KSM. Synthesis, characterization, surface analysis, optical activity and solvent effects on the electronic absorptions of Schiff base-functionalized amino thiophene derivatives: Experimental and TD-DFT investigations. J Mol Struct [Internet]. 2021;1244:131267. Available from: https://doi.org/10.1016/j.molstruc.2021.131267

7. Amoco. How to Process Better Coating Resins with Amoco PIA and TMA. 1992.

8. Tan KT, White CC, Benatti DJ, Hunston DL. Effects of ultraviolet radiation, temperature and moisture on aging of coatings and sealants - A chemical and rheological study. Polym Degrad Stab [Internet]. 2010;95(9):1551–6. Available from: http://dx.doi.org/10.1016/j.polymdegradstab.2010.06.008

9. Nguyen T, Gu X, Vanlandingham M, Byrd E, Ryntz R, Martin JW. Degradation modes of crosslinked coatings exposed to photolytic environment. J Coatings Technol Res. 2013;10(1):1–14.

10. McMichael K (Washington SU. Electrophillic additions. Chemistry LibreTexts.

Chapter 6-Computational Chemical Modelling

6.1-Introduction

Computational chemical modelling has seen use since the 1950's, but the continued technological development and increased prevalence of computers within society has enabled computational modelling to become more widely used in recent years. While simple calculations can be performed using personal computers, more complex calculations are more computationally expensive and as such generally require access to high powered computers or Super-Computer networks.

Computational modelling can offer an insight into the interactions and properties of molecules and will be utilised within this chapter to investigate the interactions of monomers such as CHDA (CycloHexaneDicarboxylic Acid), HHPA (Hexahydrophthalic Anhydride), and DDSA (Dodecenyl Succinic Anhydride) with other resin components. The purpose of this chapter is to identify the areas within the structures that are more susceptible to harm and degradation to determine if weaknesses within the structures differ to better understand the differences in weathering performance exhibited in the coatings analysed within other chapters of this thesis.

The computational calculations will focus around DFT (Density Functional Theory) which is a versatile calculation method useful for improving understanding of the molecular and electronic structure of atoms, molecules, clusters, and solids. It can calculate the molecular properties of the species of interest and provides a better understanding of the chemical reactivities of the investigated models, with ORCA being the program of choice. (1–4)

6.2-Method

An in-depth breakdown of the computational method used can be found in Chapter 2, section 2.5.

To summarise, monomers were investigated by themselves and as extended structures bonded to other coating components. Models were developed and optimised for 3D space in Avogadro before an ORCA input was generated. (5)

Following initial ORCA calculations output files were generated, from these it was possible to identify the HOMO and LUMO energies, from which the Mulliken electronegativity was calculated to determine the rough chemical hardness of the models. The chemical hardness of a structure is an indicator of their inherent reactivity. Cube files were then generated and used to highlight the areas vulnerable to electrophilic and nucleophilic attack via visualisation software.

6.3-Results

Reactivity of the compounds were determined as a factor of their chemical hardness, with the results laid out in Table 6.1, along with the rankings of each structure from least reactive to most reactive. From the results shown in Table 6.1, it can be seen that of the base monomers that CHDA is the least reactive, which could potentially result in longer resin processing times or increased potential for unreacted components within the resin system. It can be seen that there is no pattern in the results within this table, demonstrating that the poorer weathering durability exhibited by CHDA containing coatings cannot be explained through analysis of the calculated chemical reactivity alone.

Table 6.1-*Highlighting HOMO, LUMO, and calculated chemical hardness for modelled structures.*

Structure name	HOMO (eV)	LUMO (eV)	Mulliken Electronegativity (eV)	Ranking (1=Least reactive, 12 =Most)
HHPA	7.9053	1.0681	4.4867	1
HHPA-NPG	7.2518	-0.617	3.3174	11
HHPA-TMP	7.0157	0.2514	3.63355	8
HHPA-BEPD	6.6814	-0.3527	3.16435	12
CHDA	7.3915	0.2405	3.816	4
CHDA-NPG	7.3295	0.393	3.86125	3
CHDA-TMP	7.2177	0.1597	3.6887	6
CHDA-BEPD	7.2497	0.3451	3.7974	5
DDSA	7.3728	1.0084	4.1906	2
DDSA-NPG	6.8657	-0.0727	3.3965	10
DDSA-TMP	6.9038	0.3798	3.6418	7
DDSA-BEPD	6.841	0.2763	3.55865	9

Analysis of Table 6.1 shows that CHDA is slightly more reactive than either HHPA or DDSA. Comparing the different HHPA containing structures with the CHDA containing ones suggests that the HHPA models are more reactive, this could suggest that a greater degree of crosslinking can occur during curing which results in a more durable coating system.

Further computational modelling can be used to generate .cube files of the molecular structures, from this it becomes possible to identify areas that are susceptible to electrophilic and nucleophilic attack within the different structures. All areas susceptible to electrophilic attack are highlighted in yellow, while those vulnerable to nucleophilic attack are purple. These areas were identified with isovalues of 0.01 and -0.01 respectively. The isovalues control the wireframe representation of the areas vulnerable to electrophilic and nucleophilic attack.

As shown in Figure 6.1, HHPA by itself has multiple areas that are susceptible to both electrophilic and nucleophilic attacks, primarily around the carbonyl groups. When combined with NPG (as shown in Figure 6.2), the number of areas susceptible to nucleophilic attack and electrophilic attack remain the same. The areas that are susceptible to attack in Figure 6.2 are the Oxygens that join the HHPA to the NPG, suggesting that attack could sever this bond and impact the performance of the coating system.

Figure 6.3 shows that HHPA and TMP is susceptible to electrophilic attack in 4 areas and nucleophilic in 6 others. The nucleophilic areas remain primarily around the Oxygens that join the two structures together, however, in three-dimensional space the larger structure of TMP may provide steric hinderance to protect this area that is not present within Figure 6.2. This may also explain why the attack sites are concentrated on one side of the model.

Figure 6.4 provides a 3D structure of HHPA and BEPD, this structure has the fewest sites susceptible to attack for any of the HHPA containing models. While many of the areas susceptible to electrophilic attack remain around the Oxygen joining the HHPA to the BEPD, only 1 of these binding sites is targeted, with the oxygen on the left of the structure being left alone. This suggests that the size and structure of the BEPD provides a shielding effect to protect parts of the structure.

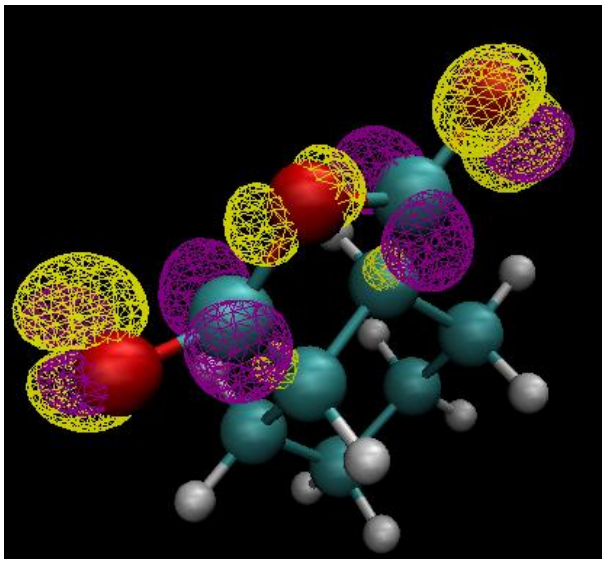

Figure 6.1-*Highlighting areas susceptible to electrophilic and nucleophilic attack to HHPA*

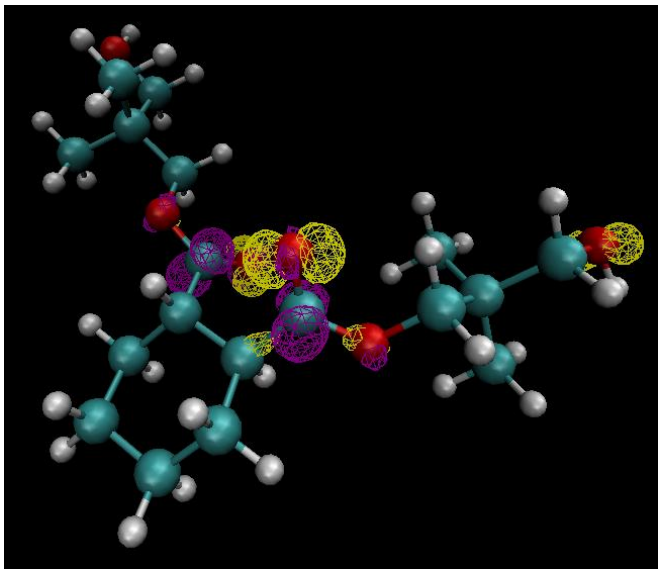

Figure 6.2-*Highlighting areas susceptible to electrophilic and nucleophilic attack to HHPA and NPG*

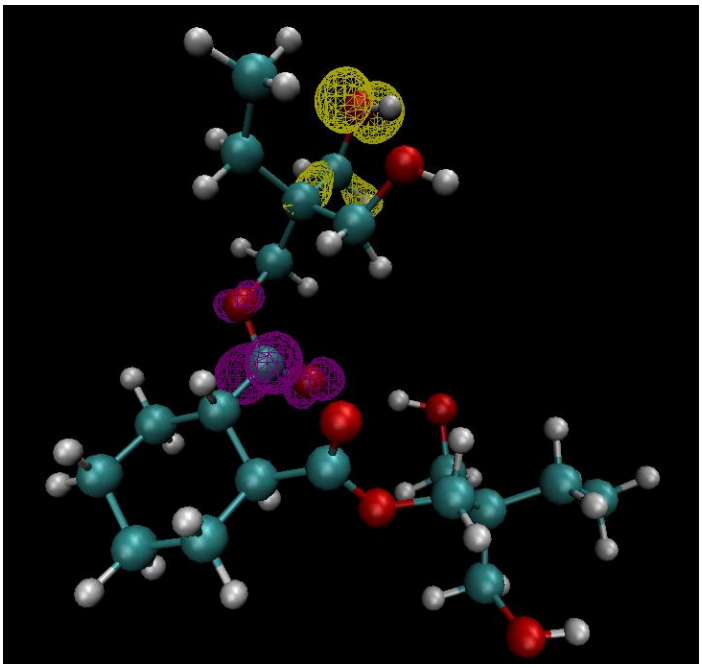

Figure 6.3-*Highlighting areas susceptible to electrophilic and nucleophilic attack to HHPA and TMP*

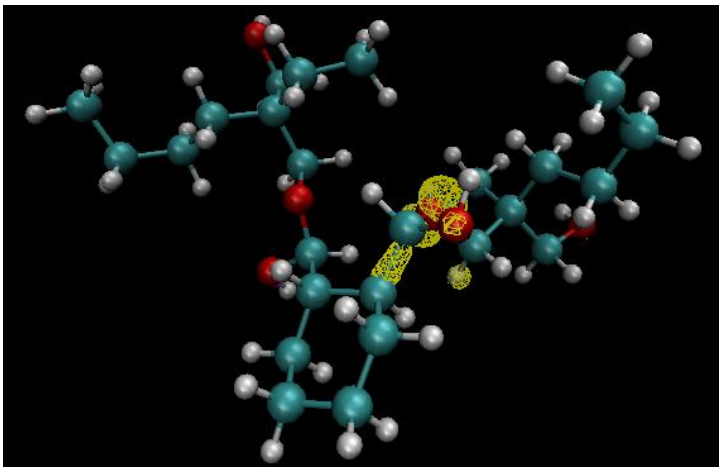

Figure 6.4-*Highlighting areas susceptible to electrophilic and nucleophilic attack to HHPA and BEPD*

Figures 6.5-6.8 show the models of CHDA as a stand-alone compound, as well as when reacted with NPG, TMP, and BEPD respectively. CHDA as a stand-alone structure has 8 sites susceptible to electrophilic attack, and another 12 that are vulnerable to nucleophilic attack. The carboxylic acid groups are the primary targets for both forms of attack.

The areas of susceptibility for CHDA and NPG can be found in Figure 6.6. There are 12 areas of the model that are vulnerable to electrophilic attack, primarily around the bridge Oxygen between CHDA and NPG.

In the model of CHDA and TMP (Figure 6.7), there are 7 sites of electrophilic attack and 6 of nucleophilic at one end of the model, it is possible that the orientation of the structure within 3D space provides a measure of protection for portions of the model. All areas of potential attack centre around the Carboxylic acid groups within the structure.

Figure 6.8 illustrates the points where the structure of CHDA combined with BEPD is vulnerable to attack. There are 8 areas susceptible to electrophilic attack, and a further 12 sites where nucleophilic attack can occur.

Of the CHDA containing models, CHDA+BEPD is the most reactive, followed by CHDA+NPG, CHDA+TMP, and finally CHDA. CHDA+BEPD is the only combined CHDA based model where all active sites focus at the carboxylic acid groups, whereas other models have additional areas of potential attack.

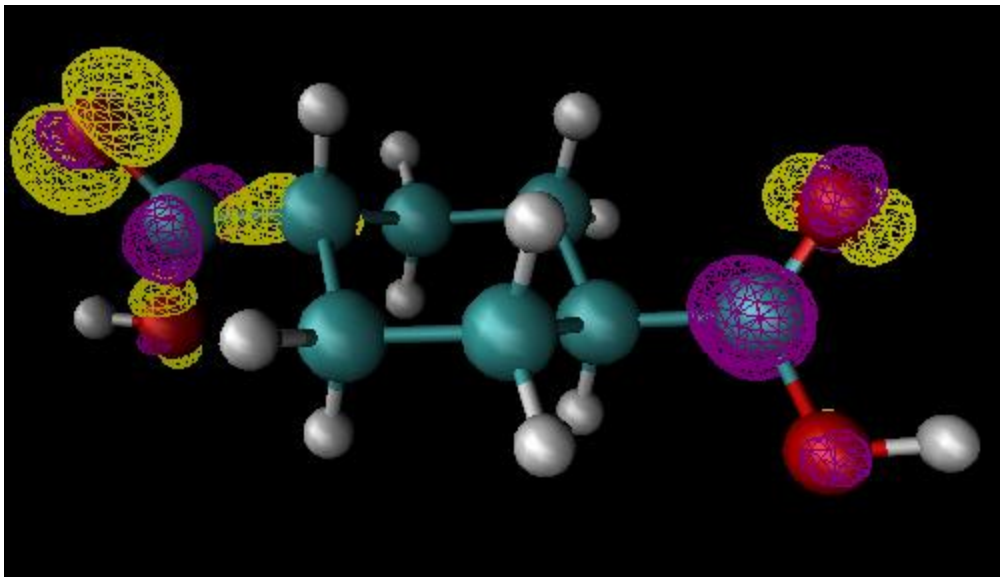

Figure 6.5-*Highlighting areas susceptible to electrophilic and nucleophilic attack to CHDA*

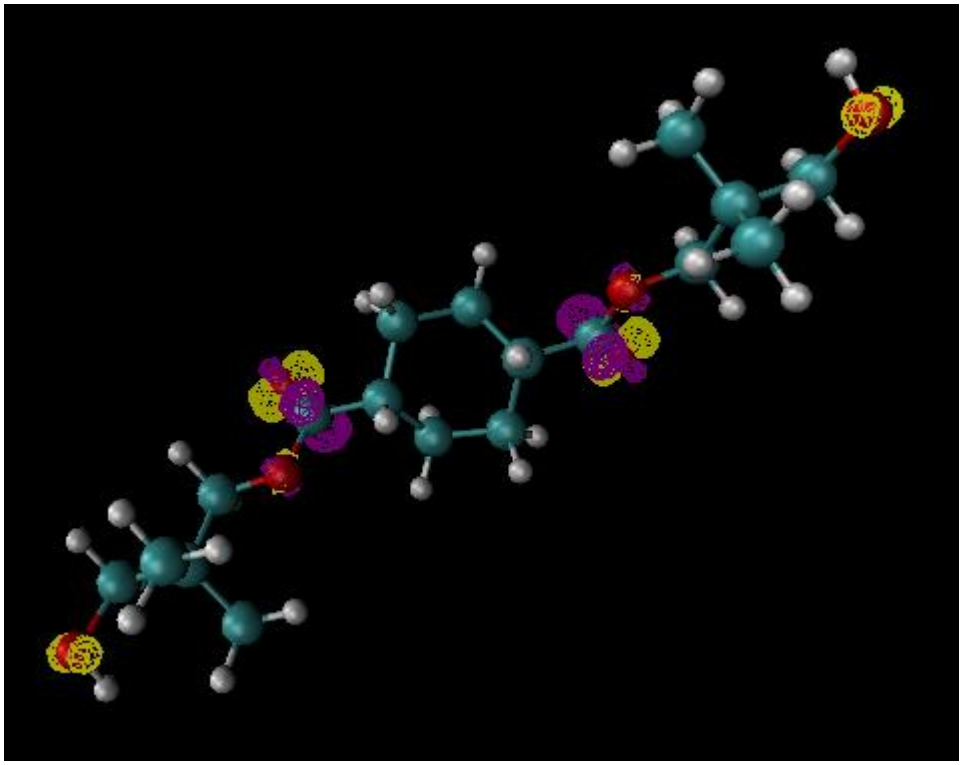

Figure 6.6-*Highlighting areas susceptible to electrophilic and nucleophilic attack to CHDA and NPG*

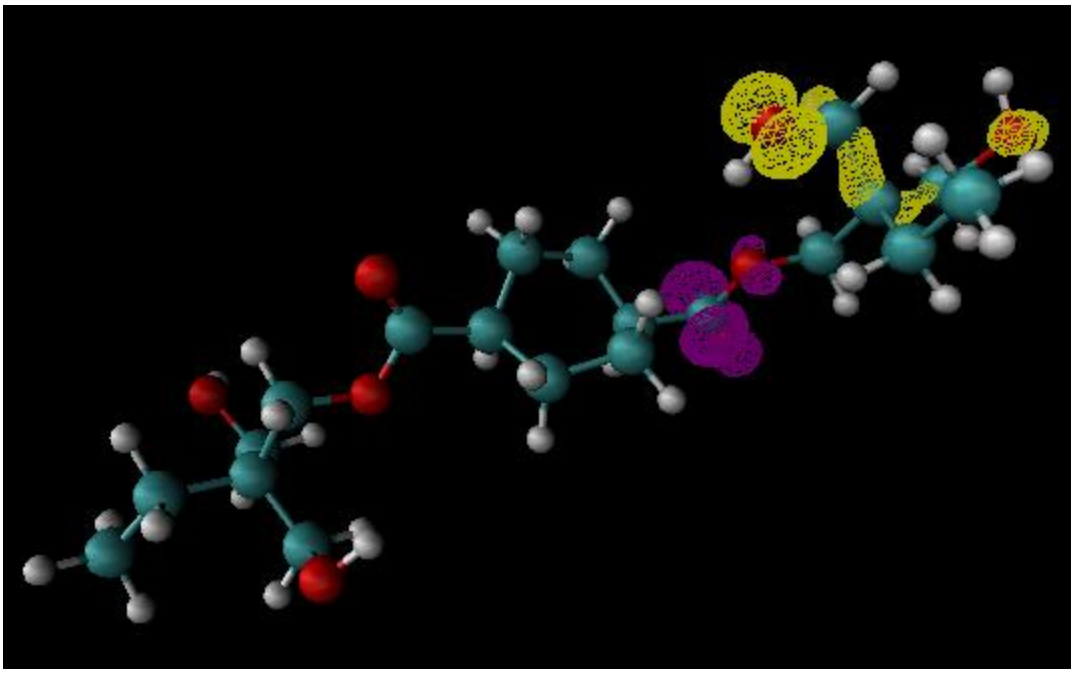

Figure 6.7-*Highlighting areas susceptible to electrophilic and nucleophilic attack to CHDA and TMP*

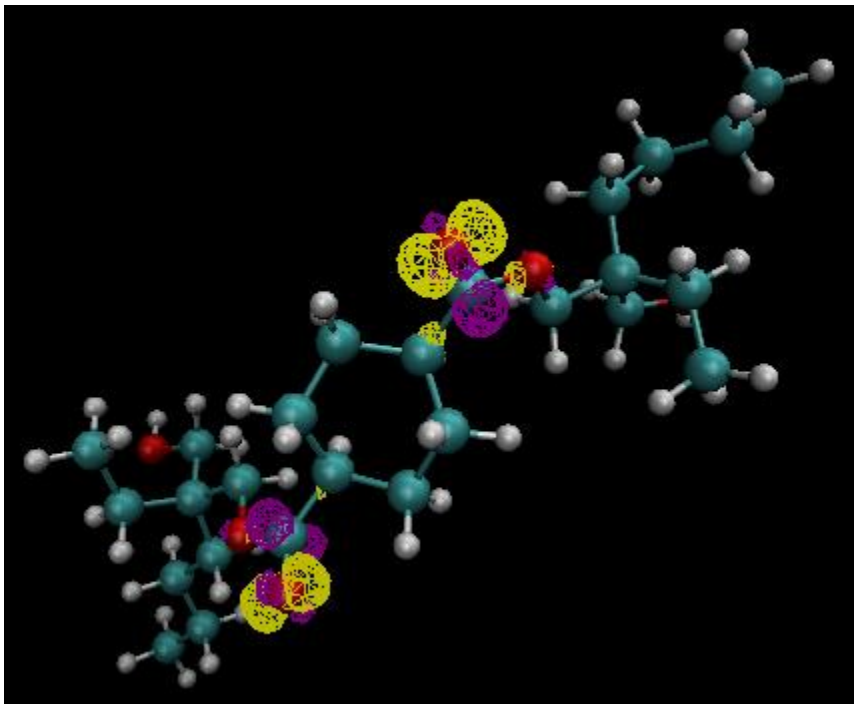

Figure 6.8-*Highlighting areas susceptible to electrophilic and nucleophilic attack to CHDA and BEPD*

Figure 6.9 shows what areas are susceptible to attack in a model of DDSA. DDSA has more areas where nucleophilic attack is probable than electrophilic. This low level of electrophilic susceptibility may be due

to the structure and orientation of the model, where the ring structure offers protection to the straight chain tail.

Figure 6.10 shows the areas susceptible to harm for DDSA and NPG. There are more regions where nucleophilic attack is probable and that they are primarily located around oxygen atoms. There is only one area of the straight chain tail that is recognised to be susceptible to attack, which is at the base in the same location as in Figure 6.9.

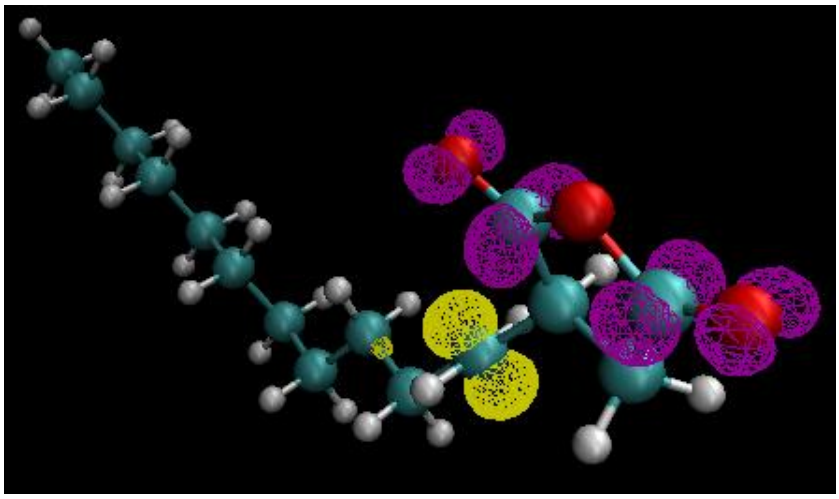

Figure 6.9-*Highlighting areas susceptible to electrophilic and nucleophilic attack to DDSA*

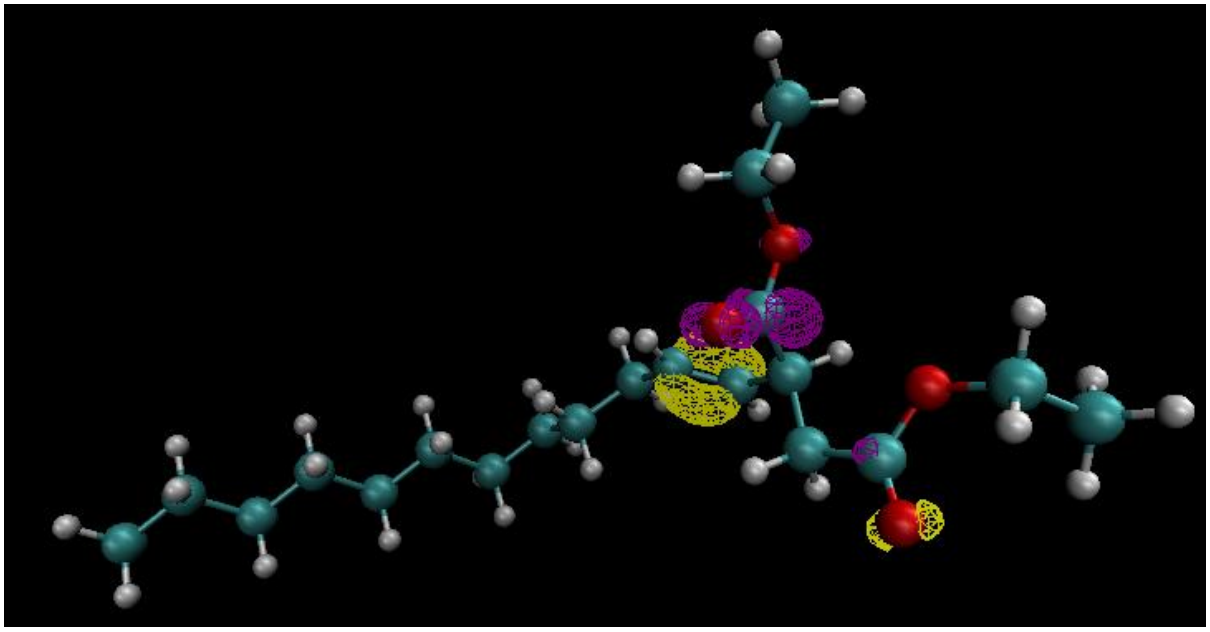

Figure 6.10-*Highlighting areas susceptible to electrophilic and nucleophilic attack to DDSA and NPG*

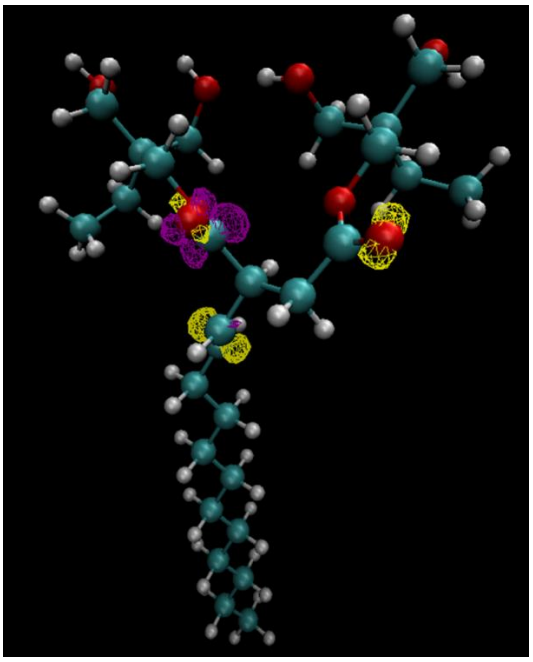

Figure 6.11-*Highlighting areas susceptible to electrophilic and nucleophilic attack to DDSA and TMP*

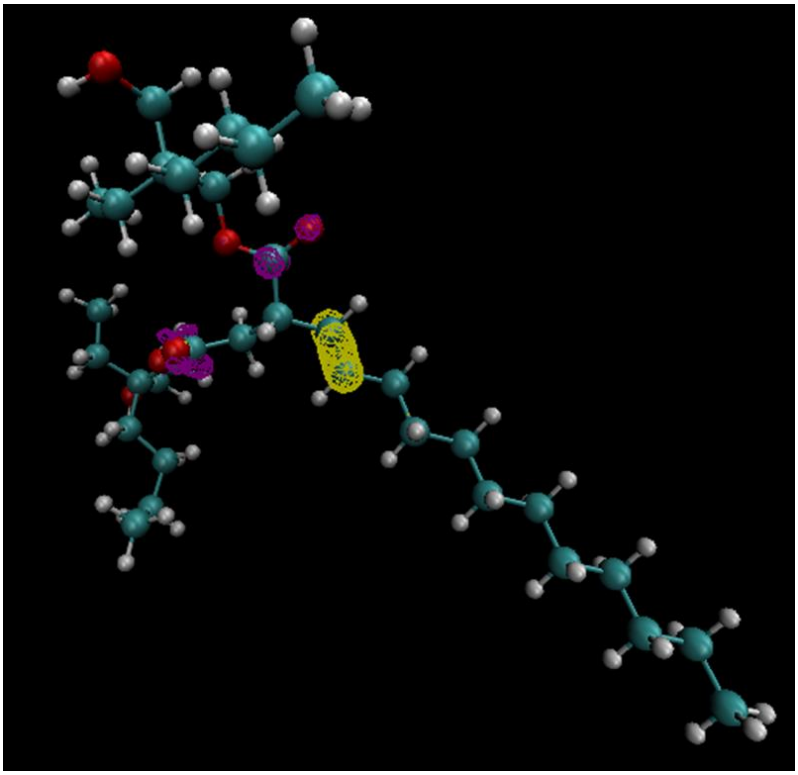

Figure 6.12-*Highlighting areas susceptible to electrophilic and nucleophilic attack to DDSA and BEPD*

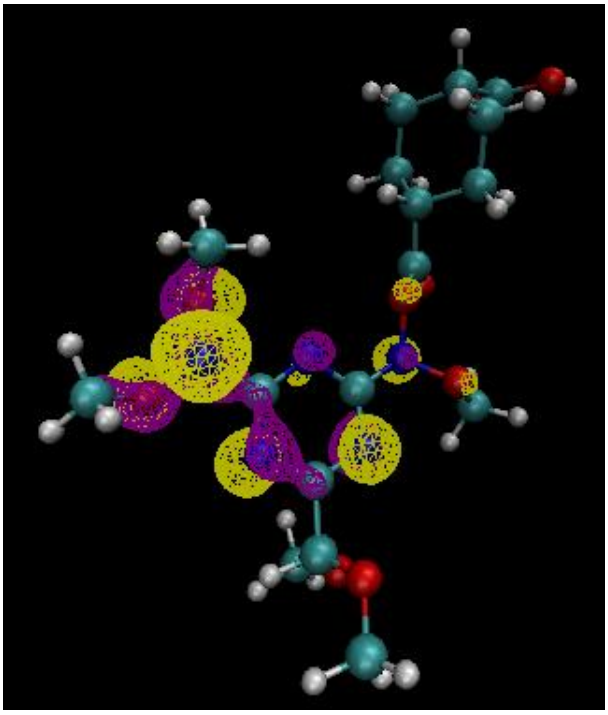

Figure 6.13-*Highlighting areas susceptible to electrophilic and nucleophilic attack to HMMM and HHPA*

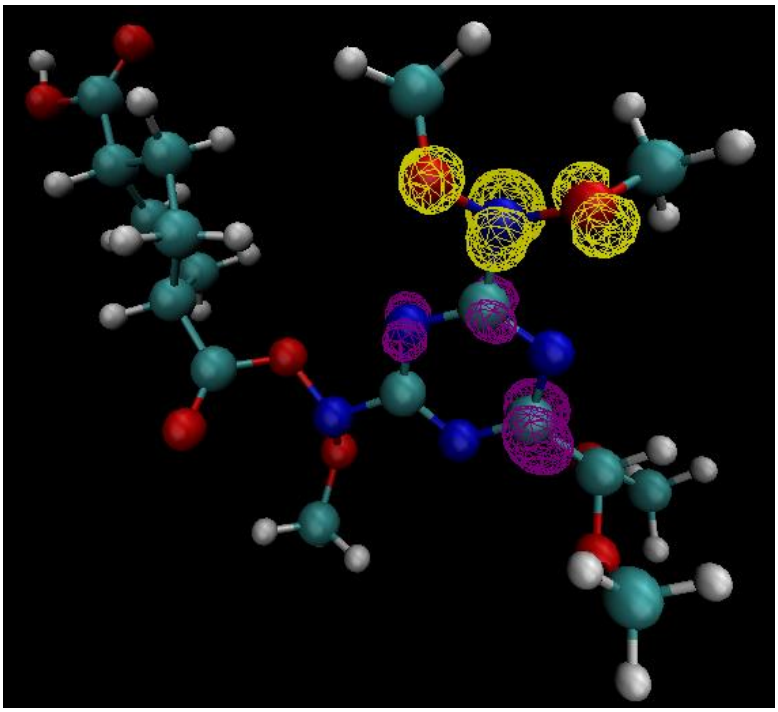

Figure 6.14-*Highlighting areas susceptible to electrophilic and nucleophilic attack to HMMM and CHDA*

Table 6.2 gives a breakdown of the sites on each model that are susceptible to electrophilic and nucleophilic attack, in addition to the total number of sites. All of the CHDA containing models

demonstrate a significantly greater number of sites vulnerable to nucleophilic attack, which is most likely water or potentially OH ions. This susceptibility to attack may explain why CHDA containing coatings generally performed worse than their HHPA containing counterparts in the dark hydrolysis tests carried out in Chapter 5, where all CHDA coatings ranked 7-4 while HHPA ranked 1-3 with one further HHPA coating receiving the worst overall rank, as well as demonstrating poorer overall weathering resistance during accelerated and natural weathering exposure in Chapter 4.

The greater susceptibility towards nucleophilic attack demonstrated by CHDA and CHDA containing models is indicative of a more pronounced weakness to interactions with water, which would be significantly exacerbated when moisture is on the coating, which is then exposed to UV light. The location of many of the areas of nucleophilic attack susceptibility in the CHDA containing models are also primarily located at key points within the model which, if attacked, would cause chain scission and provide opportunities for free radical generation and propagation.

Table 6.2-*Identifying and comparing sites susceptible to electrophilic and nucleophilic attack.*

Model	Number of electrophilic sites	Number of nucleophilic sites	Total
HHPA	8	8	16
HHPA NPG	8	2	10
HHPA TMP	4	6	10
HHPA BEPD	7	1	8
HHPA HMMM	12	10	22
CHDA	8	12	20
CHDA NPG	12	10	22
CHDA TMP	7	6	13
CHDA BEPD	8	12	20
CHDA HMMM	6	6	12
DDSA	3	8	11
DDSA NPG	4	7	11
DDSA TMP	6	7	13
DDSA BEPD	4	8	12

Figures 6.13 and 6.14 show the areas susceptible to electrophilic and nucleophilic attack in the models of HMMM joined to HHPA and CHDA respectively. HHPA+HMMM demonstrates a greater total number of vulnerable sites compared to the CHDA model. This indicates that the weakest link in a HHPA containing coating is the bond to the crosslinker of choice, whereas the CHDA and HMMM model (Fig 6.14) suggests that this structure is the most stable part of a CHDA containing coating in terms of the number of potential attack sites.

The data within Table 6.2 is contradictory to Table 6.1, where it appeared that HHPA containing models would be more reactive than their CHDA counterparts. However, Table 6.1 uses the energy difference between the HOMO and the LUMO to provide a rough estimate of latent reactivity, but Table 6.2 looks deeper into the model structures and identifies areas of weakness. It can be assumed that structures with greater numbers of vulnerable areas would degrade at an accelerated rate due to the presence of these weaknesses within an optimised 3-D structure, meaning that they exist with shielding taken into account.

6.3.1-Summary of results

The number of reactive sites does not influence the outcome of how likely the compounds are to react as calculated through chemical hardness. However, a correlation can be observed between the number of sites within the models vulnerable to attack and how rapidly they fail, with CHDA containing coatings exhibiting significantly greater rates of degradation compared to their HHPA containing counterparts.

The CHDA model exhibits the lowest reactivity of all CHDA containing models, while CHDA+BEPD demonstrated the greatest reactivity, despite both models containing the same number of active sites in the same ratio (8 electrophilic sites, 12 nucleophilic sites). The CHDA model shows the lowest degree of reactivity of all base monomer models, which could be problematic and lead to increased reaction times or overall fewer reactions occurring during coating generation.

6.4-Conclusion

Calculated chemical hardness indicates that CHDA containing structures are less reactive and as such may be less inclined to react during curing, resulting in fewer crosslinks and a weaker coating system. However, there is more evidence to suggest that there is a connection between the number of electrophilic and nucleophilic attack sites and how quickly as coating system degrades during natural and accelerated weathering tests.

HHPA was shown to have a greater calculated reactivity than CHDA when investigating HOMO and LUMO energy levels, which could have led to a greater degree of crosslinking during curing, which would result in a stronger coating system. It may be possible to test this experimentally through further experimentation to produce coatings containing HHPA or CHDA with a wide range of crosslinker concentrations. The HHPA containing models demonstrated within this chapter show that there are significantly less areas susceptible to nucleophilic attack located at key points of the structures where attack would result in chain scission when compared to CHDA models.

While it is not possible to claim that DDSA would be a viable alternative to CHDA based on data shown in this chapter alone, the smaller number of sites vulnerable to attack suggests that it would provide a performance superior to CHDA coating systems based upon the number of nucleophilic attack sites within the different models. Many of the nucleophilic attack sites in the DDSA models also focus on key areas of the systems, which would have the potential to bring about chain scission.

The research within this Chapter goes some way to explain the behaviour of the coating systems observed in Chapters 4 and 5. As shown in Table 6.2, CHDA and CHDA containing models demonstrate significantly greater total areas susceptible to attack, particularly those areas vulnerable to nucleophilic attack, which would mean that the coating systems would be more vulnerable to interactions with water, this in turn would means that the coating systems would fail more rapidly in accelerated and natural weathering tests thanks to the impact of moisture enhanced photodegradation attacking key sites in the CHDA model structures and bringing about chain scission.

Further work should include multiple computational chemical calculations of common coating components and monomers in combination, with the aim towards determining if it is possible to predict the rank by which different coating formulations will fail during accelerated and natural weathering testing. If this can be achieved, then it has the potential to save wastage of materials and to greatly expedite the production of new and superior coating systems in the future. Unfortunately, due to resource limitations, it was not possible to model larger, more complex models. This was problematic as the larger chain models would have provided a deeper understanding into the behaviour of the coating systems as they would have been a more accurate representation. As such, it is recommended that further research is carried out that investigates performing longer term computational calculations that are more computationally expensive, with the aim of adding to the novel work carried out within this chapter.

6.5-References

1. Craig B, Skylaris CK, Schoetz T, de León CP. A computational chemistry approach to modelling conducting polymers in ionic liquids for next generation batteries. Energy Reports [Internet]. 2020;6:198–208. Available from: https://doi.org/10.1016/j.egyr.2020.03.025

2. U Von Barth Ã. Basic Density-Functional Theory — an Overview. Physica Scripta. 2004;T109:9–39.

3. Neese F. Software update: the ORCA program system, version 4.0. WIREs Computational Molecular Science [Internet]. 2018 Jan 17;8(1). Available from: https://onlinelibrary.wiley.com/doi/10.1002/wcms.1327

4. Geerlings P, De Proft F, Langenaeker W. Conceptual density functional theory. Chemical Reviews. 2003;103(5):1793–873.

5. Avogadro [Internet]. 2018. Available from: https://avogadro.cc/docs/

6. Supercomputing Wales [Internet]. 2021. Available from: https://portal.supercomputing.wales/

Chapter 7-Conclusions and Further Work

7.1-Conclusions to current research

The aims of this body of work were to determine if a viable alternative to HHPA that is non-hazardous and capable of producing coating systems with comparable properties could be identified. This was to be performed by producing a series of polyester-melamine coatings and testing for their efficacy. Computational modelling was also utilised to improve understanding of the degradation pathways of the evaluated coatings in order to improve further research.

The work reported in Chapter 3 showed that not all cycloaliphatic monomers are suitable for inclusion to resin systems without significant time spent within the formulation stage, as indicated by the failure of Perhydro Bisphenol S to form a resin that would melt below 41^{o}C, which would cause glycol loss and alter the chemistry of the resin system. Investigation into CHDA and CHDM co-monomer resin systems showed that they have the potential to be accompanied by significant issues, such as unpredictability regarding rates of reactions and a tendency to solidify at room temperature. While this was not an issue during small scale coating development, it could become a problem when considering large scale coating generation processes, as additional steps or time spent to ‘‘melt out’’ the base resin will slow production and incur additional costs to the process.

Analysis of clear coating systems as reported in Chapter 4 indicates the superiority of HHPA coating systems over CHDA and CHDA+CHDM based coatings. This trend is replicated within the analysis of the first generation of pigmented coating systems, where the CHDA containing coatings were significantly outperformed by the HHPA containing counterparts in all investigations.

In terms of colour change, CHDA1.0DM8020Br was the best performing coating, which was comprised of 30% CHDA, 31.3% CHDM, and 8.6% Adipic acid to compensate for the decrease in CHDA. Colour retention shows that a lower amount of CHDA with a small Adipic acid addition in conjunction with CHDM can provide a superior degree of colour retention compared to a coating that contains a greater amount of CHDA, further indicating that CHDA would be the component of concern in a co-monomer coating system. It was also shown that the crosslinker ratio exerts a small influence over the final T_g of a coating system, with the 90:10 ratio coatings reported within Chapter 4.3 exhibiting lower midpoint T_g values compared to the 80:20 ratio variants.

CHDA1.3DM8020Br is the best performing coating in terms of gloss retention when exposed to STD UV-A weathering, which indicates that the addition of straight chain components has a greater influence over the coatings in terms of gloss retention through the presence of components that are more vulnerable to photo-oxidative degradation. This is shown to be the case as both the CHDA and CHDM majority coatings with the greatest straight chain percentage demonstrated the poorest gloss retention. During HOT UV-A accelerated weathering CHDA1.0DM8020Br retains the most gloss, with all other coating systems performing in the same trend as with STD UV-A weathering. While there were some fluctuations in performance of the coating systems for the different tests, CHDA1:0DM was consistently one of the top performing coating ratios, while CHDA4.0DM was the worst. This indicates that the combination of lowering the CHDM ratio within the coating and replacing it with 1,6 Hexanediol produces a significantly poorer coating system. This can be explained in multiple ways, either 1,6 Hexanediol is more susceptible to degradation, or CHDM demonstrates superior weathering resistance compared the CHDA.

Investigation into UV absorbance and the influence of dark hydrolysis has been reported in Chapter 5. The purpose of investigating the UV absorbance of HHPA and CHDA containing coating systems was to begin identifying the cause of the poorer weathering performance that it offered compared to HHPA. It was found that within the UV region HHPA and CHDA containing coatings demonstrated extremely similar absorbance profiles. It was also found that lowering the crosslinker ratio within the system brought about a decrease in the UV absorbance for all coatings but more significantly for those containing CHDA. Particular points of the UV spectrum were also of interest, 290nm and 330-340nm. The conclusions that can be made from investigating the UV absorbance of HHPA and CHDA containing free-films is that the melamine crosslinker exerts a greater influence over the absorbance of CHDA coatings and that the UV absorbance window is not the cause of the poor performance demonstrated by CHDA containing coatings in natural and accelerated weathering tests.

Dark hydrolysis and dark hydrolysis at elevated temperatures (reported in Chapter 5) showed that CHDA containing coatings were generally poorer performing than their HHPA counterparts when immersed in water in the absence of UV light. This suggests that CHDA containing coatings have a greater weakness to the interactions with water than HHPA coatings do. This would suggest that the most harmful time of accelerated weathering for CHDA containing coatings would be during condensation cycles or following these cycles when exposed to UV light and the coating remains wet.

Computational Chemical Modelling was carried out as reported in Chapter 6 to shed more light on the monomers and how reactive they were alone and when bonded to other common coating components.

It was found that CHDA was calculated to be less reactive than HHPA as a stand-alone monomer, indicating a potential for longer resin processing times and a possibility for more incomplete reactions, which was also observed during the synthesis of the novel CHDA containing resins. Calculation of areas of susceptibility indicated that CHDA and CHDA containing models illustrated significantly more areas susceptible to nucleophilic degradation compared to HHPA models, which corresponded with the generally poorer performance shown during dark hydrolysis as well as the poorer weathering resistance in accelerated and real-world tests. This vulnerability to nucleophilic attack makes the structures more susceptible to degradation through interactions with water, couple this with the fact that the majority of these sites surround the bridging oxygen that links the CHDA to the other components shows that chain scission would not just be possible, but likely in the event of moisture enhanced photodegradation.

To conclude, the research contained within this thesis shows that HHPA based coatings continue to exhibit superior weathering compared to other popular cycloaliphatics, that co-monomer base resin systems should be the basis of future work and that the poor weathering resistance offered by CHDA is brought about by a greater susceptibility to nucleophilic attack via interactions with water and moisture enhanced photodegradation through electrophilic attack via H^+ ions. CHDA based coatings have been shown to generally exhibit poorer degradation resistance compared to HHPA coatings when undergoing dark hydrolysis at room temperatures and elevated temperatures. The improved understanding of the behaviour of CHDA and the interactions that it undergoes during contact with water obtained from the research reported in Chapter 5 indicated that knowledge of the sites of potential electrophilic and nucleophilic attacks on the structures was of great importance. Chapter 6 showed that, in all instances, the structures that included the CHDA monomer exhibited a greater total number of attack sites, and that these were primarily sites of nucleophilic attack. There was no clear correlation between the number of these active sites and how reactive the structures were as a function of chemical hardness. The vulnerability to nucleophilic attack goes towards explaining the poor performance when in contact with water, which is a weak nucleophile.

The most harmful aspect of accelerated weathering for CHDA containing coatings is likely to be moisture enhanced photodegradation, followed by condensation and finally UV exposure. This is because of the additional energy that the UV provides, accelerated the rate and instances of interactions with water, leading to free radical generation, with the condensation stage then providing the opportunity for numerous nucleophilic attacks to occur to structures within the coating system, and finally UV

photoinitiation of self-propagating free radicals enabling degradation by attack throughout the coating system.

To conclude, the research carried out in this body of work has shown that, of the investigated monomers, a suitable replacement for HHPA cannot be identified. While it may still be possible to find a viable alternative to HHPA, it will require additional research.

7.2-Proposed Further work

Co-monomer resin systems would benefit from further research, with a focus on replacing CHDA in CHDA:CHDM resins with other monomers of interest, such as dodecenyl succinic anhydride. These resins would then be made into pigmented coating systems covering a range of polyester: melamine ratios. It would be beneficial for further research to investigate different colouration systems, particularly red, yellow, blue, black, grey, and white as they are popular colours for coil coated steels. The impacts of the chemistry of different pigments on the behaviours of the coating systems that result from the physical chemical interactions between the pigments and the polymers may also be studied. Investigating different polyester: melamine ratios for the various co-monomer systems can show if different ratios exert an influence over the mechanical and chemical characteristics of the final coating as well as highlighting which is the optimum ratio for the different systems. It is proposed that initial tests investigate 60:40, 70:30, 80:20, and 90:10 PE:HMMM ratios, these ratios will cover those that regularly see use within coil coatings as well as less typical higher melamine coatings. The work carried out in section Chapter 4 suggests that straight chain components should be kept to a minimum or omitted entirely if the formulations allow as there is a correlation between straight chain additions and poor weatherability. Additives should also not be included in the coatings, as the natural weatherability should be determined first, and additives would extend this time.

The dark hydrolysis investigation caried out in Chapter 5 indicated that coatings with lower crosslinker ratios could exhibit greater resistance to interactions with water than some higher ratio coatings. The investigation also showed a correlation between immersion in water maintained at higher temperature and more significant degradation of the coatings. As the investigation was carried out over the short term, it would be beneficial to extend the time frame of the immersion to investigate the longer-term impact. Further investigations should also weigh the samples after each period of immersion, this would allow the water uptake of the samples to be measured and compared against the IR specta.

The investigation could be further improved by expanding the range of testing to include more acidic environments. This would benefit the overall investigation as acid rain is a known contributor to coating

degradation. A potential starting point would be to immerse the samples in a relatively weak acid (pH 4) at room temperature and at 40°C, this would allow a direct comparison between the performance of samples immersed in acidic and neutral environments.

The work carried out into computational chemical modelling shows that it can be utilised to highlight areas in chemical structures that are vulnerable to electrophilic or nucleophilic attack. Additionally, a correlation was observed between the number of attack sites in the models and the degree of weathering durability exhibited by the real-world coating system, with a greater number of attack sites corresponding to poorer resistance. There are multiple areas of the computational modelling work that would benefit from further research, such as investigating the potential differences between the approximate chemical hardness and the true chemical hardness. Due to time constraints, it was only possible to calculate the approximate chemical hardness for the investigated models and there was no observed correlation between the approximate chemical hardness and real world weathering performance. However, as true chemical hardness is determined through more dedicated calculations it is possible for the results to differ from the approximate values.

Another avenue of computational modelling that would benefit from further research is to investigate the correlation between the data obtained from computational modelling and the results of natural and accelerated weathering exposure. The focus should be on if computational modelling accurately predicts the performance rankings of coatings subjected to weathering, the initial focus should be on idealised polyester: melamine coatings of various formulations and polyester: crosslinker ratios under accelerated and natural weathering conditions. Natural weathering can also be expanded to also compare sites across the world, such as North America, Europe, India, Australia, and South-East Asia to determine if there are environments that the computational models do not match. This would then need to be repeated with other coating systems such as polyurethane, epoxy, and acrylic coatings. This would build up a detailed picture of the range and potential benefits of comparing computational modelling data to real-world weathering results. This would be a long-term investigation and would benefit from industrial involvement to facilitate the coatings and sample generation that is required.

It would be prudent for the proposed computational chemical modelling work to be carried out alongside the design and development of additional novel co-monomer coating systems. This would allow the expansion of the existing knowledge base for the computational work, while also providing indications for if a monomer would be suitable for further work. It would be beneficial to perform computational modelling on longer, more complex molecular structures as these would more accurately reflect the real-

world chemistry of the coating systems. An example of such a system would be CHDM, 2,2-dimethyl malonic acid and HMMM, that would provide a suitable molecular chain to model as it would require more computational resources in addition to potentially providing a further avenue of research regarding the development of novel resin systems.